



REACTIVITY AND COORDINATION STUDIES OF DIPHOSPHACYCLOBUTADIENE SANDWICH ANIONS

Dissertation zur Erlangung des
Doktorgrades der Naturwissenschaften

DR. RER. NAT.

am Institut für Anorganische Chemie
der Fakultät für Chemie und Pharmazie
der Universität Regensburg

vorgelegt von

CHRISTIAN RÖDL

aus Vilsbiburg

Regensburg 2019

Der experimentelle Teil der vorliegenden Arbeit wurde von Januar 2015 bis November 2018 unter Anleitung von Prof. Dr. Robert Wolf am Institut für Anorganische Chemie der Universität Regensburg angefertigt.

Diese Arbeit wurde angeleitet von:		Prof. Dr. Robert Wolf
Promotionsgesuch eingereicht am:		02.05.2019
Tag der mündlichen Prüfung:		03.07.2019
Promotionsausschuss:	Vorsitz:	Prof. Dr. Alkwin Slenczka
	Erstgutachter:	Prof. Dr. Robert Wolf
	Zweitgutachter:	Prof. Dr. Manfred Scheer
	Dritter Prüfer:	Prof. Dr. Frank-Michael Matysik

PROLOGUE

This thesis reports on the synthesis and characterization of mono-, di-, and oligonuclear cobalt complexes with diphosphacyclobutadiene and diphosphacyclobutene ligands. Chapter 1 reviews the chemistry of transition metal phosphalkyne and diphosphacyclobutadiene complexes. Besides the synthesis and structural motifs of diphosphacyclobutadiene complexes, this chapter also deals with the coordination properties of such species. In chapters 2 and 3, the functionalization of the diphosphacyclobutadiene ligand is discussed. Chapters 4 and 5 describe coordination studies, which have resulted in the synthesis and characterization of numerous new di- and oligonuclear complexes with diphosphacyclobutadiene ligands. Chapter 6 reports on the thermal properties as well as the potential application of complexes with diphosphacyclobutadienes and other phosphorus containing ligands in atomic layer deposition. The final chapter 7 summarizes the results of this thesis and gives a brief outlook.

TABLE OF CONTENTS

1	THE CHEMISTRY OF PHOSPHAALKYNE AND DIPHOSPHACYCLOBUTADIENE COMPLEXES	1
1.1	Introduction	1
1.1.1	Historical Development of Phosphaalkyne Chemistry	1
1.1.2	The Coordination Chemistry of Phosphaalkynes	2
1.2	Transition Metal-Mediated Oligomerization	3
1.2.1	Dimerization and Trimerization.....	3
1.2.2	Access to further Phosphaorganometallic Ligands by Phosphaalkyne Oligomerization.....	6
1.2.3	Coordination Compounds and Metal Aggregates	7
1.3	Conclusion	10
1.4	References	12
2	FUNCTIONALIZATION OF 1,3-DIPHOSPHACYCLOBUTADIENE COBALT COMPLEXES VIA SI-P BOND INSERTION	15
2.1	Introduction	17
2.2	Results and Discussion	19
2.2.1	Synthesis and Structural and Spectroscopic Characterization of Silylated 1,3-Diphosphacyclobutadiene Complexes	19
2.2.2	Functionalization Reactions by Insertion into the Phosphorus-Silicon Bond.....	22
2.3	Conclusion	28
2.4	Supporting Information	29
2.4.1	General Procedures.....	29
2.4.2	Synthesis and Characterization	29
2.4.3	$^{31}\text{P}\{^1\text{H}\}$ NMR Spectra of 6-8	38
2.4.4	UV/Vis and IR Spectroscopy	40
2.4.5	X-ray Crystallography	46
2.5	References	52
3	1,3-DIPHOSPHACYCLOBUTENE COBALT COMPLEXES.....	55

3.1	Introduction	57
3.2	Results and Discussion.....	59
3.2.1	Reaction of [Co(P ₂ C ₂ tBu ₂)H] with Lithium Organyls	59
3.2.2	Reaction of [Co(P ₂ C ₂ tBu ₂)H] with Grignard Reagents.....	65
3.2.3	Computational Studies	65
3.2.4	Synthesis of 5 by Trimethylsilylation of 1	67
3.3	Conclusion	69
3.4	Supporting Information	70
3.4.1	General Procedures	70
3.4.2	Synthesis and Characterization	70
3.4.3	Reaction of [Co(P ₂ C ₂ tBu ₂) ₂ H] with Grignard Reagents	73
3.4.4	³¹ P{ ¹ H} NMR Spectra of 1-3 , and 5	74
3.4.5	Variable Temperature and 2D Correlation NMR Spectroscopy.....	78
3.4.6	Cyclic Voltammetry.....	84
3.4.7	X-ray Crystallography.....	85
3.4.8	Theoretical Investigations	88
3.5	References.....	91
4	FLEXIDENTATE COORDINATION BEHAVIOR AND CHEMICAL NON-INNOCENCE OF A BIS(1,3-DIPHOSPHACYCLOBUTADIENE) SANDWICH ANION.....	95
4.1	Introduction	97
4.2	Results and Discussion.....	100
4.2.1	Reaction of [K(thf) ₂ {Co(P ₂ C ₂ tBu ₂) ₂ }] with [Ni ₂ Cp ₃]BF ₄	100
4.2.2	Reaction of [K(thf) ₂ {Co(P ₂ C ₂ tBu ₂) ₂ }] with [Cp* ⁺ RuCl] ₄	104
4.2.3	Reaction of [K(thf) ₂ {Co(P ₂ C ₂ tBu ₂) ₂ }] with [RhCl(cod)] ₂	107
4.2.5	Reaction of [K(thf) ₂ {Co(P ₂ C ₂ tBu ₂) ₂ }] with <i>cis</i> -PdCl ₂ (PPh ₃) ₂	109
4.2.6	Reaction of [K(thf) ₂ {Co(P ₂ C ₂ tBu ₂) ₂ }] with HgCl ₂	113
4.3	Conclusion	117
4.4	Supporting Information	118
4.4.1	General Procedures	118
4.4.2	Optimized Synthesis of [K(thf) _{1.75} {Co(P ₂ C ₂ tBu ₂) ₂ }] (A)	118
4.4.3	Synthesis of [CpNi{Co(P ₂ C ₂ tBu ₂) ₂ }(thf)] (2)	118
4.4.4	Synthesis of [Co(η ⁴ -CpNi{1,3-P ₂ C ₂ tBu ₂ -κP,κC})(η ⁴ -1,3-P ₂ C ₂ tBu ₂)] (3).....	119

4.4.5	Synthesis of $[\text{Co}(\eta^4\text{-CpNi}\{1,4\text{-P}_2\text{C}_2\text{tBu}_2\text{-}\kappa^2\text{P,P}\})(\eta^4\text{-1,3-P}_2\text{C}_2\text{tBu}_2)]$ (4)	119
4.4.6	Synthesis of $[(\text{Cp}^*\text{Ru})_3(\mu\text{-Cl})_2\{\text{Co}(\text{P}_2\text{C}_2\text{tBu}_2)_2\}]$ (5)	120
4.4.7	Synthesis of $[(\text{Cp}^*\text{Ru})_2(\mu,\eta^2\text{-P}_2)(\mu,\eta^2\text{-C}_2\text{tBu}_2)]$ (6)	120
4.4.8	Synthesis of $[\text{Rh}(\text{cod})\{\text{Co}(\text{P}_2\text{C}_2\text{tBu}_2)_2\}]$ (7)	120
4.4.9	Synthesis of $[\text{Rh}(\text{cod})\{\text{Co}(\text{P}_2\text{C}_2\text{Ad}_2)_2\}]$ (8)	121
4.4.10	Synthesis of 9 by Reaction of 8 with Adamantyl-Phosphaalkyne (AdCP)	121
4.4.11	Synthesis of $[\text{Pd}_3(\text{PPh}_3)_2\{\text{Co}(\text{P}_2\text{C}_2\text{tBu}_2)_2\}_2]$ (10)	122
4.4.12	Synthesis of $[\text{Hg}\{\text{Co}(\text{P}_2\text{C}_2\text{tBu}_2)_2\}_2]$ (11,12)	122
4.4.13	X-ray Crystallography	123
4.4.14	Variable Temperature NMR Monitoring	128
4.4.15	UV/Vis Spectra	134
4.4.16	Cyclic Voltammetry	138
4.4.17	Theoretical Calculations	139
4.5	References	156
5	A HOMOLEPTIC 1,3-DIPHOSPHACYCLOBUTADIENE TRIPLEDECKER COMPLEX	161
5.1	Introduction	163
5.2	Results and Discussion	165
5.3	Conclusion	169
5.4	Supporting Information	170
5.4.1	General Procedures	170
5.4.2	Synthesis and Characterization	170
5.4.3	NMR Data of 1	171
5.4.4	X-ray Crystallography	173
5.4.5	UV/Vis Spectrum	175
5.4.6	Cyclic Voltammetry	176
5.4.7	Theoretical Calculations	176
5.5	References	178
6	PHOSPHAORGANOMETALLIC COBALT COMPLEXES AS POTENTIAL PRECURSORS FOR THE GENERATION OF THIN INORGANIC FILMS	181
6.1	Introduction	183
6.2	Results and Discussion	186

6.2.1	Synthesis, Characterization and Thermal Properties of Monophosphane Complexes	186
6.2.2	Synthesis, Characterization and Thermal Properties of Phosphaalkyne Complexes.....	187
6.2.3	Synthesis, Characterization and Thermal Properties of 1,3-Diphosphacyclobutadiene Complexes	188
6.2.4	Synthesis, Characterization and Thermal Properties of Phosphole Complexes	189
6.3	Conclusion	190
6.4	Supporting Information	191
6.4.1	General Procedures	191
6.4.2	Synthesis and Characterization of Phosphane Complexes 1–5	191
6.4.3	Synthesis and Characterization of Phosphaalkyne Complexes 6 and 7	192
6.4.4	Synthesis and Characterization of 1,3-Diphosphacyclobutadiene Complexes 8–11	192
6.4.5	Synthesis and Characterization of Phosphole Complex 12	193
6.4.6	Long-Term Stability Tests	194
6.4.7	Vapor Pressure Measurements	197
6.4.8	Thermogravimetric Analysis	200
6.5	References.....	203
7	SUMMARY.....	207
8	ACKNOWLEDGEMENT.....	215
9	CURRICULUM VITAE	217
10	LIST OF PUBLICATIONS	218

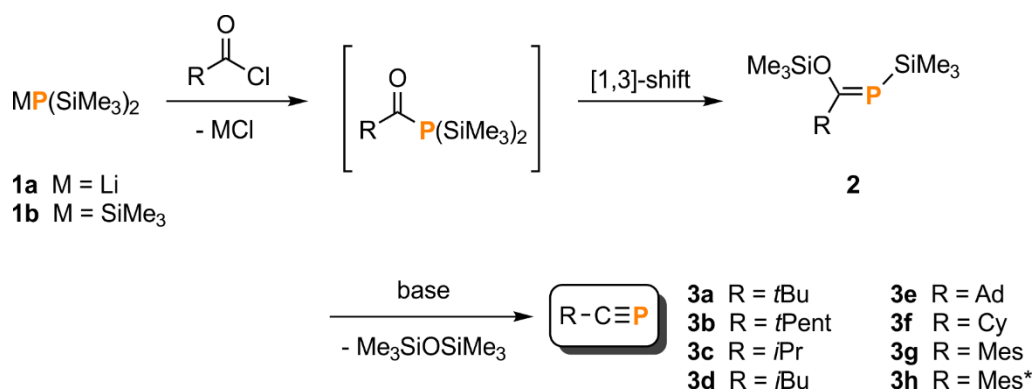
1 THE CHEMISTRY OF PHOSPHAALKYNE AND DIPHOSPHACYCLOBUTADIENE COMPLEXES

1.1 Introduction

1.1.1 Historical Development of Phosphaalkyne Chemistry

Phosphaalkynes and their oligomerization products (in particular diphosphacyclobutadienes and triphosphaabenzenes) have attracted much attention in the past three decades due to their versatile coordination properties.^{1,2} Several synthetic routes to a wide range of phosphaalkynes have been described.^{2a,c} Phosphaacetylene, $\text{HC}\equiv\text{P}$, the simplest phosphaalkyne, and, according to the isolobal concept, the phosphorus-containing counterpart of acetylene, was initially proposed by Albers in 1950 and characterized by Gier in 1961.³ Nevertheless, Becker and co-workers were able to isolate $t\text{BuC}\equiv\text{P}$ only 20 years later.⁴ $t\text{BuC}\equiv\text{P}$ is kinetically stabilized by a *tert*-butyl substituent. To date, it remains the most commonly used phosphaalkyne. Subsequently, numerous related phosphaalkynes were synthesized and their reaction chemistry was explored in detail.⁵ Apart from serving as starting materials for a wide range of new phosphoorganic compounds, these investigations opened a new field in coordination chemistry.^{2,6,7}

The original synthesis of phosphaalkynes devised by Becker and subsequently developed further by Regitz and co-workers is shown in Scheme 1.⁷ Phosphide **1a** or phosphane **1b** is treated with the corresponding acyl chloride to give a phosphaalkene **2**, followed by base-catalyzed β -elimination of hexamethyldisiloxane.⁷ This procedure is most common for the synthesis of phosphaalkynes **3**, however, there are also other protocols describing the elimination of hydrogen halides, chlorotrimethylsilanes, or lithium trimethylsilylanolates.^{2c} The scope of phosphaalkynes synthesized by this approach is limited by the stabilities of the corresponding precursor and the product.^{2a}



Scheme 1. Synthetic route toward common phosphaalkynes.⁷ (*t*Bu = *tert*-butyl, *t*Pent = *tert*-pentyl, *i*Pr = *iso*-propyl, *i*Bu = *iso*-butyl, Ad = adamantyl, Cy = cyclohexyl, Mes = 2,4,6-Me₃-C₆H₂, Mes* = 2,4,6-(*t*Bu)₃-C₆H₂)

1.1.2 The Coordination Chemistry of Phosphaalkynes

Phosphaalkynes are versatile ligands to transition metal atoms and ions which display a wide range of coordination modes including both side-on (**A**) and end-on (**B**) as well as diverse bridging modes (e.g. **C–E**, Figure 1).⁸ Furthermore, they can act as ligands donating a total of two, four or six electrons as demonstrated by prominent examples. The first complex featuring a phosphaalkyne in its structural framework was reported by Nixon and co-workers. This complex exhibits *t*BuCP side-on (type **A**) coordinated to Pt⁰ acting as 2e⁻ donating ligand (**4**, Figure 1).⁹ In the same publication, the authors also described the 4e⁻ bridging mode **D**, which is exemplified by the dicobalt complex [Co₂(CO)₆(*t*BuCP)] (**7**), which is prepared by adding *t*BuCP to a THF solution of Co₂(CO)₈ and isolated as light-sensitive, red oil. While the crystal structure of this compound was not obtained due to its being an oil, addition of [W(CO)₅(THF)] afforded [Co₂(CO)₆(*t*BuCP)W(CO)₅] (**8**), in which a new Lewis-acidic W(CO)₅ moiety is also bound to the *t*BuCP ligand, now displaying the 6e⁻ donating mode **E**.¹⁰ In comparison with side-on binding, η¹-type coordination **B** is usually unfavored and thus only accessible with sterically demanding phosphaalkynes such as AdCP (**5**) or bulky ligands such as dppe (= 1,2-bis(diphenylphosphano)ethane) in order to avoid competing η²-type coordination¹¹ or in combination with the side-on η²-fashion (mode **C**) demonstrated by [Pt(dppe)(*t*BuCP)W(CO)₅] (**6**).¹² This competing ligation can be explained by the nature of the orbitals centered at the carbon and the phosphorus atom of the phosphaalkyne. Photoelectron spectroscopy revealed that the HOMO is essentially centered at the C≡P triple bond, while the HOMO–1 is located at the phosphorus lone pair.¹³

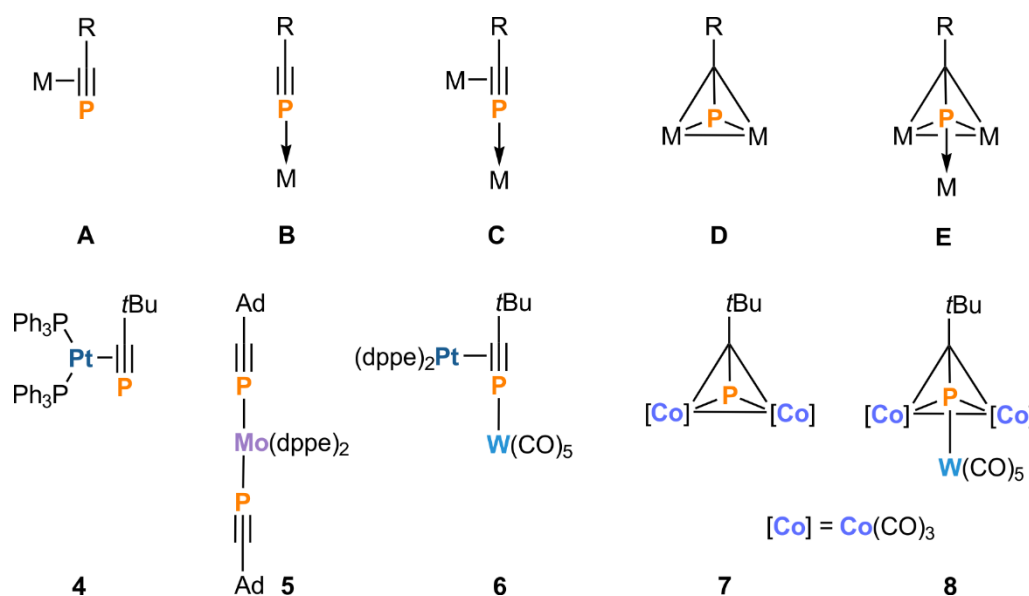
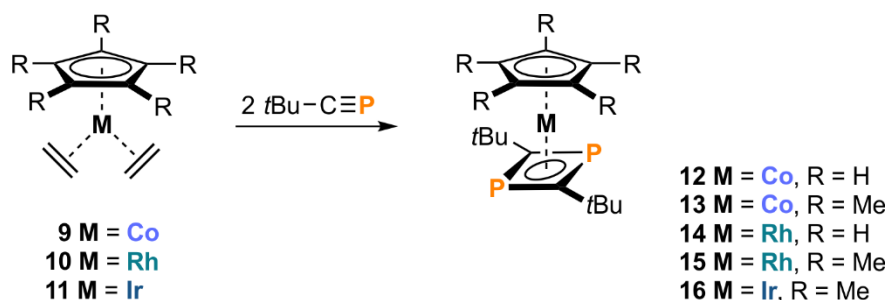


Figure 1. Coordination modes of phosphaalkynes (A–E).

1.2 Transition Metal-Mediated Oligomerization

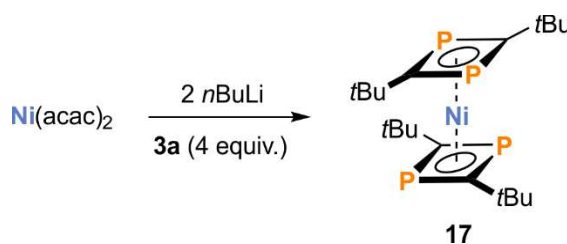
1.2.1 Dimerization and Trimerization

The first examples for the cyclodimerization of phosphalkynes in the coordination sphere of transition metal centers were independently reported by Nixon and co-workers and the group of Binger and Regitz.¹⁴ $t\text{BuC}\equiv\text{P}$ undergoes metal-mediated [2+2]-cycloaddition to give η^4 -coordinated 1,3-diphosphacyclobutadiene ligands (Scheme 2).



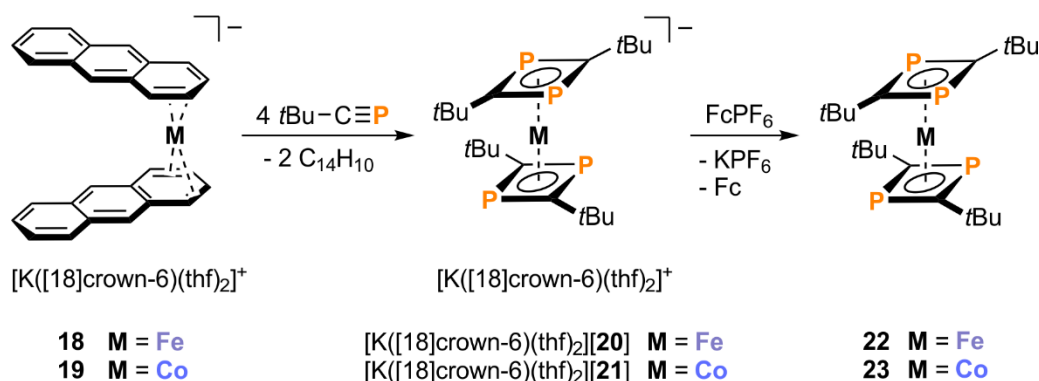
Scheme 2. The first examples of 1,3-diphosphacyclobutadiene complexes obtained by cyclodimerization of phosphalkynes.¹⁴

Subsequently, it was shown that iron(0), titanium(0), and molybdenum(0) also mediate the cyclodimerization of phosphalkynes.¹⁵ Treatment of the Ni(II) precursor $\text{Ni}(\text{acac})_2$ (acac = acetyl acetonate) with two equivalents of $n\text{BuLi}$ at low temperature and subsequent addition of four equivalents of **3a** afforded the bis(1,3-diphosphacyclobutadiene)nickel (**17**, Scheme 3).¹⁶ Alternatively, this complex can be obtained by reacting $[\text{Ni}(\text{cod})_2]$ with four equivalents of phosphalkyne.¹⁷ Remarkably, this was the first homoleptic 1,3-diphosphacyclobutadiene complex.



Scheme 3. The first example of a homoleptic bis(1,3-diphosphacyclobutadiene) complex.¹⁶

Wolf, Lammertsma and co-workers later found that the reaction of the anthracene metalates **18** and **19**¹⁸ afforded homoleptic P_2C_2 complexes $[\text{K}([\text{18}]\text{crown-6})(\text{thf})_2][\text{20}]$ and $[\text{K}([\text{18}]\text{crown-6})(\text{thf})_2][\text{21}]$, respectively (Scheme 4).^{19a,b} Cyclic voltammetry studies showed that the $[\text{M}(\eta^4\text{-P}_2\text{C}_2t\text{Bu}_2)_2]^-$ anions (**20** and **21**) can be reversibly oxidized to the neutral species **22** and **23**, which was achieved chemically by treatment with ferrocenium hexafluorophosphate (FcPF_6).^{19c}



Scheme 4. Synthesis of anionic bis(1,3-diphosphacyclobutadiene) complexes $[K([18]\text{crown-6})(\text{thf})_2][\mathbf{20}]$ and $[K([18]\text{crown-6})(\text{thf})_2][\mathbf{21}]$ and oxidation to the neutral compounds **22** and **23** (Fc = Ferrocene).

Although most diphosphacyclobutadiene complexes reported in the literature incorporate the 1,3-isomer, some 1,2-derivatives have also been described, including titanium(0) complexes **24a** and **24b**,²⁰ the iron(0) complex **25**,²¹ the tantalum(III) complex **26**,²² and the tungsten(0) complex **27**, in which the diphosphacyclobutadiene ligand is stabilized by coordination of two $\text{W}(\text{CO})_5$ fragments²³ (Figure 2).

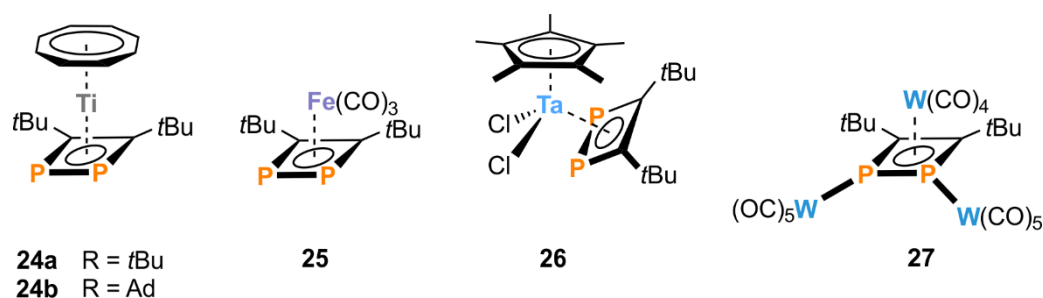
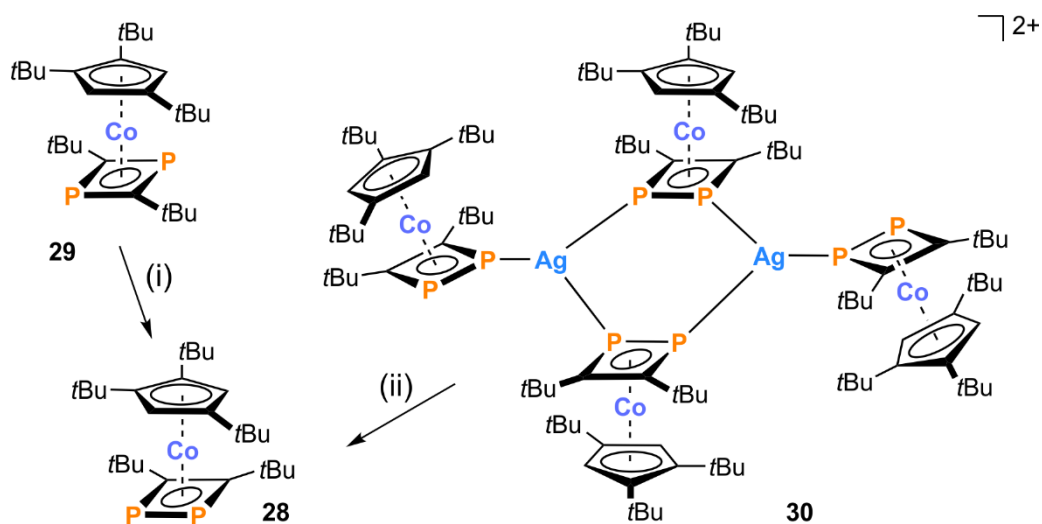


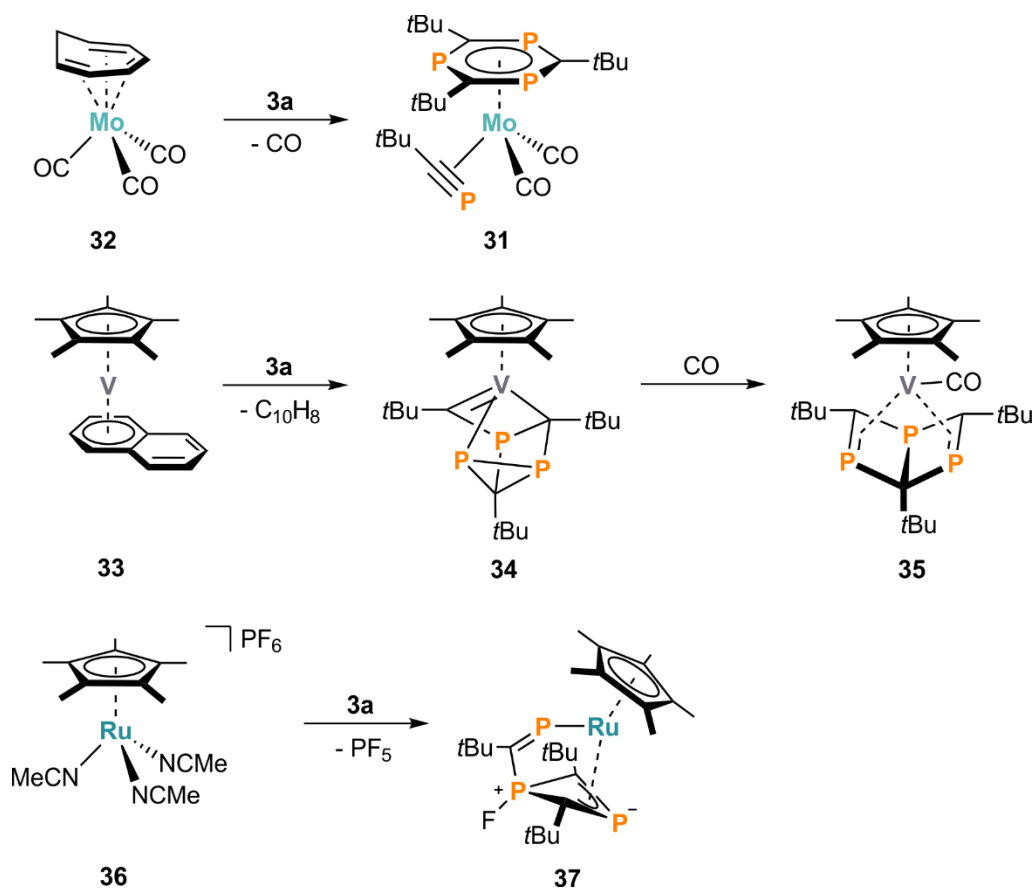
Figure 2. Illustration of examples of 1,2-diphosphacyclobutadiene complexes.

Very recently, Scheer and co-workers reported the synthesis of $[\text{Cp}^{\text{III}}\text{Co}(\eta^4\text{-1,2-P}_2\text{C}_2\text{tBu}_2)]$ (**28**, $\text{Cp}^{\text{III}} = \text{C}_5\text{tBu}_3\text{H}_2$). This 1,2-diphosphacyclobutadiene complex can be obtained either by thermolysis of the 1,3-derivative **29** or by release from the corresponding Ag(I) coordination compound **30** (Scheme 5), which was prepared by treating $[\text{Cp}^{\text{III}}\text{Co}(\eta^4\text{-1,3-P}_2\text{C}_2\text{tBu}_2)]$ (**29**) with $[\text{Ag}(\text{pftb})]$ ($\text{pftb} = \text{Al}(\text{OC}(\text{CF}_3)_3)_4$).²⁴



Scheme 5. Synthesis of **28** by either (i) thermolysis of **29** or (ii) treatment of **30** with pyridine at room temperature.

While examples of phosphalkynes cyclodimerizing in the coordination sphere of transition metals are far more numerous,²⁵ a few examples have nevertheless demonstrated that phosphalkynes can also cyclotrimerize forming 1,3,5-triphosphabenzenes in a manner analogous to alkyne trimerization reactions. The first such trimerization was reported for the molybdenum(0) complex **31** by Barron and Cowley.^{26a} Refluxing the cycloheptatriene-carbonyl molybdenum complex **32** with **3a** in THF gave **31** in moderate yield (Scheme 6). At the same time, Binger and co-workers described the formation of valence isomers of 1,3,5-triphosphabenzene mediated by vanadium (**34** and **35**, Scheme 6).^{26b} Nixon has also reported the ruthenium(II)-mediated trimerization of **3a**.²⁷ The structural motif in this case is different, featuring a metallaphosphaalkene fragment bound to a bent, fluoro-substituted, four-membered P₂C₂ ring that exhibits a novel 2-phosphaallylic unit (**37**).



Scheme 6. Cyclotrimerization of phosphalkynes in the coordination sphere of molybdenum(0), vanadium(I), and ruthenium(II).

1.2.2 Access to further Phosphaorganometallic Ligands by Phosphaalkyne Oligomerization

1,2- and 1,3-Diphosphacyclobutadienes are the most common products of phosphalkyne oligomerization. However, other ligand types can also be accessible through co-condensation or high temperature approaches such as metal vapor synthesis. Nixon reported that the co-condensation of electron-beam generated molybdenum atoms with $t\text{BuC}\equiv\text{P}$ (**3a**) affords the tris(1,3-diphosphacyclobutadiene)molybdenum complex **38** (Figure 3).^{28a} The same compound can be obtained as side product when a THF solution of *fac*- $[\text{Mo}(\text{CH}_3\text{CN})_3(\text{CO})_3]$ and **3a** (four equivalents) is heated to reflux for eight hours, while the main product is $[\text{Mo}(\text{P}_2\text{C}_2t\text{Bu}_2)_2(\text{CO})_2]$ (**39**).^{28b}

In contrast, reaction of cobalt atoms generated through a metal vapor approach with **3a** gave three heteroleptic compounds featuring a combination of a 1,3-diphosphacyclobutadiene ligand and a second ligand, i.e. 1,2,4-triphosphacyclopentadienyl (**40**), 1,3-diphosphacyclopentadienyl (**41**), and 1,3,5,7-tetraphosphabarrelene (**42**) (Figure 3).²⁹

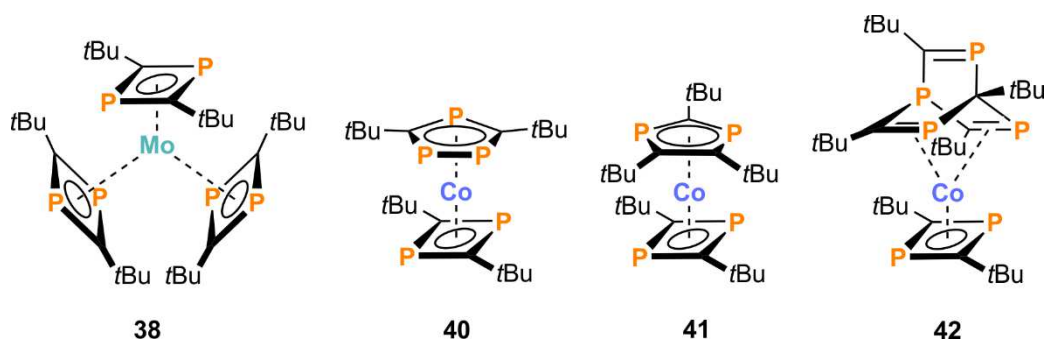


Figure 3. Complexes obtained via co-condensation of *t*BuCP (**3a**) with metal atoms generated by electron beam or metal-vapor synthesis methods.

Meanwhile, treatment of iron, chromium or vanadium atoms generated by metal vapor techniques with **3a** afforded pentaphosphametalloenes **43–45**.³⁰ By contrast, treatment of nickel atoms obtained by the same approach with **3a** yielded two compounds of which one was identified as the known homoleptic $[\text{Ni}(\eta^4\text{-P}_2\text{C}_2\text{tBu}_2)_2]$ (**17**). The second species (**46**) was characterized by X-ray crystallographic studies on the $\text{W}(\text{CO})_5$ adduct. These studies confirmed that this complex features a phosphirenyl cation (PC_2tBu_2)⁺ (Figure 4).³¹

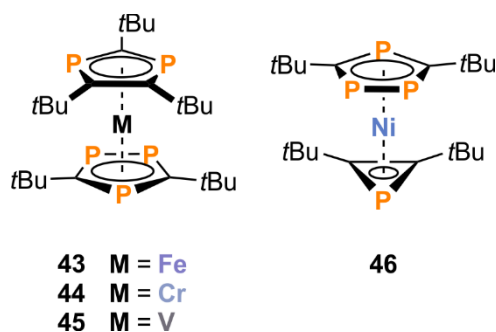
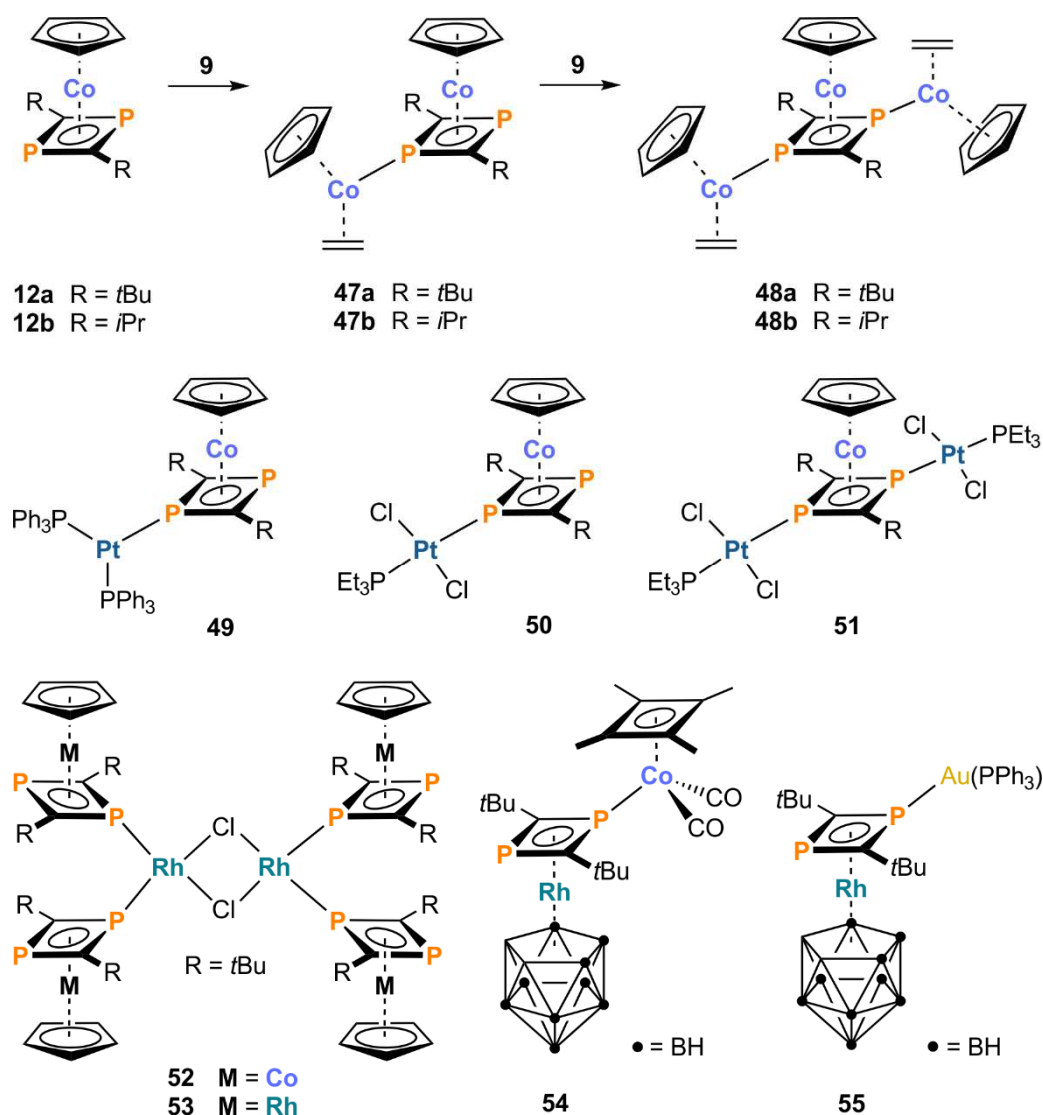


Figure 4. Different structural motifs obtained by co-condensation reactions of V, Cr, Fe, and Ni atoms with $\text{tBuC}\equiv\text{P}$.

1.2.3 Coordination Compounds and Metal Aggregates

The phosphorus atoms in the structural framework of diphosphacyclobutadiene complexes can be used to coordinate further metal atoms, leading to oligonuclear coordination compounds.^{14b,c} The first examples of such oligonuclear species, compounds **47** and **48** (Figure 5, top), were prepared by treating mononuclear $[\text{CpCo}(\eta^4\text{-P}_2\text{C}_2\text{R}_2)]$ (**12a,b**) with one and two equivalents of $[\text{CpCo}(\eta^2\text{-C}_2\text{H}_4)_2]$ (**9**), respectively. Subsequently, the coordination behavior of diphosphacyclobutadiene complexes was investigated in detail by several groups.³² Nixon and co-workers described the coordination of **12** to one or two platinum centers (**49–51**).^{32d} The same authors reported the remarkable hexanuclear complexes **52** and **53**, in which four molecules of **12** and **14**, respectively, are coordinated to a Rh_2Cl_2 fragment.^{32a,d} Complexes **54** and **55** (Figure 5, bottom), reported by Stone and co-workers, show the anionic $[\text{Rh}(\eta^4\text{-P}_2\text{C}_2\text{tBu}_2)(\eta^5\text{-C}_2\text{B}_9\text{H}_{11})]^-$ fragment coordinated to $[(\eta^4\text{-C}_4\text{Me}_4)\text{Co}(\text{CO})_2]^+$ in **54** and $[\text{Au}(\text{PPh}_3)]^+$ in **55**, respectively.^{32b,c}

Figure 5. First σ -coordination compounds of 1,3-diphosphacyclobutadiene complexes.

It is in this context that Wolf and co-workers have been investigating the coordination behavior of the $[\text{Co}(\eta^4\text{-P}_2\text{C}_2\text{tBu}_2)_2]^-$ sandwich anion (**21**), which exhibits four phosphorus atoms in its structural framework. Reactions with coinage metal halides afforded various oligonuclear compounds (Figure 6).³³ Di- and trinuclear structures **56–62** were formed when $[\text{K}(\text{thf})_2\{\text{Co}(\eta^4\text{-P}_2\text{C}_2\text{R}_2)_2\}]$ (R = *t*Bu, *t*Pent, Ad) was reacted with $[\{\text{CuCl}(\text{PPh}_3)\}_4]$, AgCl, or AuCl(tht) in a 1:1 ratio and in the presence of tertiary phosphanes. Complex **63** was obtained by reacting $[\text{K}(\text{thf})_3\{\text{Co}(\eta^4\text{-P}_2\text{C}_2\text{tPent}_2)_2\}]$ with two equivalents of AgSbF₆ and an excess amount of PMe₃. In the absence of phosphanes, polymeric compounds **64** and **65** formed, which were characterized by solid-state NMR spectroscopy and elemental analysis. Treatment of **60** with four equivalents of $[\text{AuCl}(\text{PPh}_3)]$ afforded the unprecedented molecular square $[\text{Au}\{\text{Co}(\text{P}_2\text{C}_2\text{tBu}_2)_2\}]_4$ (**66**), which consists of four units of anion **21** connected by four gold cations (Figure 6, bottom).³⁴

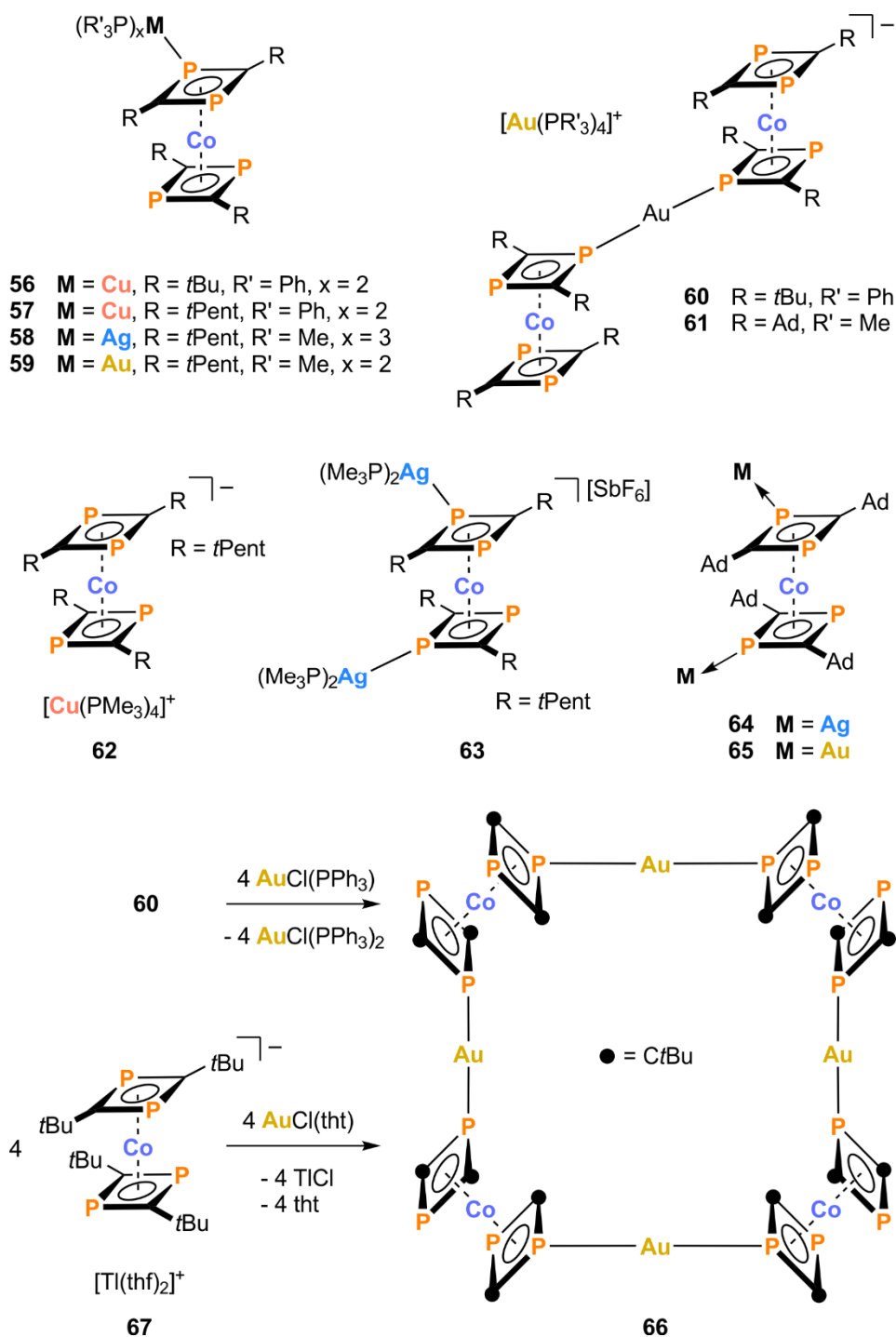


Figure 6. Coordination compounds with coinage metals obtained by our group.

A second synthetic pathway to **66** is the 1:1 reaction of [Tl(thf)₂{Co(η⁴-P₂C₂tBu₂)₂}] (**67**) with AuCl(tht). Reaction of **67** with [(η⁴-C₄Me₄)Co(CO)₂I] and [CpNi(PPh₃)Br] afforded dinuclear compounds **68** and **69** (Figure 7).³⁵ Similar to the coinage metal complexes shown in Figure 6 and the earlier examples reported by Binger, Nixon, and Stone, the molecular structures of **68** and **69** show σ-coordinated diphosphacyclobutadiene ligands.^{14b,c,32}

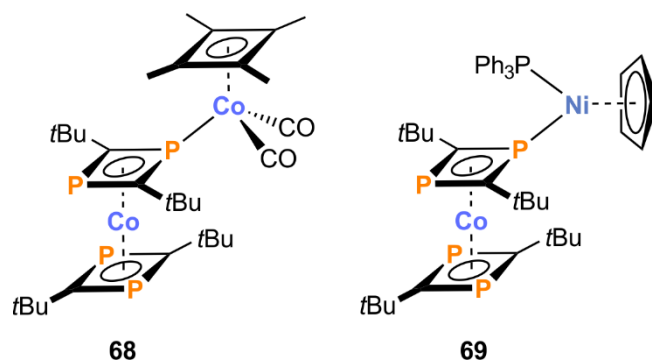


Figure 7. First examples of the homoleptic bis(diphosphacyclobutadiene)cobaltate coordinated to 3d transition metals.

1.3 Conclusion

Phosphaalkynes show a wide variety of coordination modes which have been investigated by several groups. These studies revealed that phosphaalkynes can act as two, four or six electron donating ligands. Moreover, they undergo cyclization reactions to form low-coordinate phosphorus heterocycles such as diphosphacyclobutadienes (dimerization), triphospha benzenes (trimerization) as well as other cyclic oligomers like di- or triphospholides and phosphinines.

In particular, the metal-mediated [2+2]-cyclodimerization in the coordination sphere of transition metal atoms has turned out to be a facile route to form metal-complexed diphosphacyclobutadienes which are unstable in their free, uncoordinated form. Depending on the steric demand of the substituents on the phosphaalkyne, 1,2- as well as 1,3-diphosphacyclobutadienes are accessible, however, due to the wide use of sterically encumbered *tert*-butylphosphaalkyne most reported complexes feature the 1,3-derivative. The chemistry of such diphosphacyclobutadiene complexes has been substantially explored in the past 30 years with the main focus being on the investigation of the coordination behavior. Most of the reported coordination compounds feature coordination of the diphosphacyclobutadiene ligand to coinage metal cations and precious metal cations of rhodium, palladium, and platinum. Notably, the formation of σ -complexes has been exclusively observed with such metal cations.

Wolf and co-workers contributed to this area by developing homoleptic bis(1,3-diphosphacyclobutadiene) sandwich anions which afforded new coordination compounds. The most striking example is the octanuclear $[\text{Au}\{\text{Co}(\text{P}_2\text{C}_2\text{tBu}_2)_2\}]_4$ (**66**) macrocycle. Expanding the investigations to 3d metal atoms afforded two novel dinuclear compounds **68** and **69**, where the $[\text{Co}(\text{P}_2\text{C}_2\text{tBu}_2)_2]^-$ anion (**21**) coordinates to $[(\eta^4\text{-C}_4\text{Me}_4)\text{Co}(\text{CO})_2]^+$ and $[\text{CpNi}(\text{PPh}_3)]^+$. Further investigations into the coordination behavior of **21** toward 3d and 4d metal cations was one of the main goals of this thesis. In this course, we wished to explore the ability of **21** to act as a π ligand to another metal cation forming a tripledecker or a tripledecker-like complex. Therefore, a suitable precursor was essential to enable this rare coordination mode.

Furthermore, functionalization of the diphosphacyclobutadiene ligand was also a fascinating goal which might give access to novel P-containing ligands. This could be realized by introducing reactive groups³⁶ (e.g. electrophiles) followed by addition of suitable, organic substrates. Reactivity toward nucleophiles might also give access to diverse new complexes bearing one or even two functionalized ligand moieties. While the reactivity of diphosphacyclobutadiene complexes toward electrophilic transition metal complexes has been extensively explored, reports on the reactivity of diphosphacyclobutadiene complexes toward nucleophiles are scarce.^{28b,37}

1.4 References

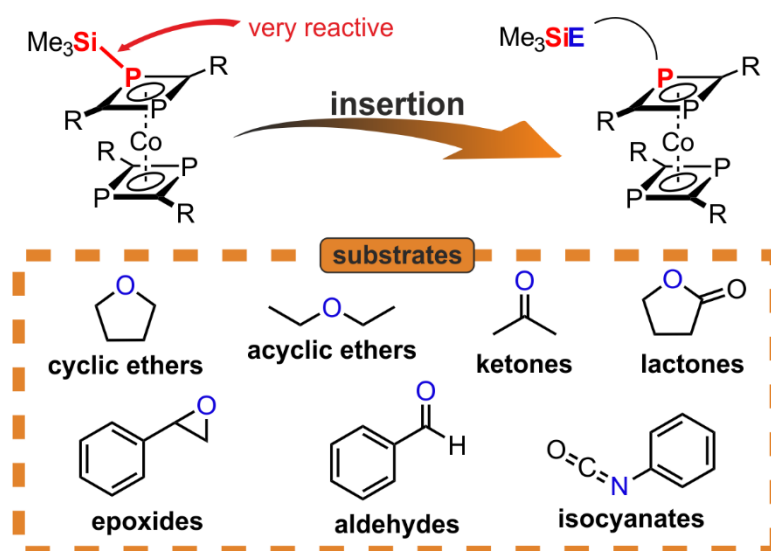
- 1 Book chapters: a) M. Regitz, P. Binger, *Multiple Bonds and Low Coordination in Phosphorus Chemistry*, Thieme, Stuttgart **1990**; b) K. B. Dillon, F. Mathey, J. F. Nixon, *Phosphorus: The Carbon Copy*, Wiley, Chichester **1998**.
- 2 Reviews: a) M. Regitz, P. Binger, *Angew. Chem.* **1988**, *100*, 1541; *Angew. Chem. Int. Ed. Engl.* **1988**, *27*, 1484; b) J. F. Nixon, *Chem. Rev.* **1988**, *88*, 1327; c) M. Regitz, *Chem. Rev.* **1990**, *90*, 191; d) J. F. Nixon, *Endeavour* **1991**, *15*, 49; e) J. F. Nixon, *Coord. Chem. Rev.* **1995**, *145*, 201; f) A. Chirila, R. Wolf, J. C. Sloatweg, K. Lammertsma, *Coord. Chem. Rev.* **2014**, *270–271*, 57.
- 3 a) H. Albers, *Angew. Chem.* **1950**, *62*, 451; b) T. E. Gier, *J. Am. Chem. Soc.* **1961**, *83*, 1769.
- 4 G. Becker, G. Gresser, W. Uhl, *Z. Naturforsch. B* **1981**, *36*, 16.
- 5 a) K. S. Pitzer, *J. Am. Chem. Soc.* **1948**, *70*, 2140; b) R. S. Mulliken, *J. Am. Chem. Soc.* **1950**, *72*, 4493.
- 6 a) L. D. Markovski, V. D. Romanenko, *Tetrahedron* **1989**, *45*, 6019; b) F. Mathey, *Angew. Chem.* **2003**, *115*, 1616; *Angew. Chem. Int. Ed.* **2003**, *42*, 1578; c) M. Yoshifuji, *Pure Appl. Chem.* **2005**, *77*, 2011; d) J. M. Lynam, *Organomet. Chem.* **2007**, *33*, 170.
- 7 a) T. Allspach, M. Regitz, G. Becker, W. Becker, *Synthesis* **1986**, *1986*, 31; b) M. Regitz, *Chem. Rev.* **1990**, *90*, 191; c) A. C. Gaumont, J. Denis, *Chem. Rev.* **1994**, *94*, 1413.
- 8 J. F. Nixon, *Chem. Soc. Rev.* **1995**, *24*, 319.
- 9 J. C. T. R. B.-S. Laurent, P. B. Hitchcock, H. W. Kroto, J. F. Nixon, *J. Chem. Soc., Chem. Commun.* **1981**, 1141.
- 10 J. C. T. R. B.-S. Laurent, P. B. Hitchcock, H. W. Kroto, M. F. Meidine, J. F. Nixon, *J. Organomet. Chem.* **1982**, *238*, C82.
- 11 a) P. B. Hitchcock, M. J. Maah, J. F. Nixon, J. A. Zora, G. J. Leigh, M. A. Bakar, *Angew. Chem. Int. Ed. Engl.* **1987**, *26*, 474; b) S. M. Mansell, M. Green, C. A. Russell, *Dalton Trans.* **2012**, *41*, 14360.
- 12 D. Carmichael, S. I. Al-Resayes, J. F. Nixon, *J. Organomet. Chem.* **1993**, *453*, 207.
- 13 J. C. T. R. B.-S. Laurent, M. A. King, H. W. Kroto, J. F. Nixon, R. J. Suffolk, *J. Chem. Soc. Dalton Trans.* **1983**, 755.
- 14 a) P. B. Hitchcock, M. J. Maah, J. F. Nixon, *J. Chem. Soc., Chem. Commun.* **1986**, 737; b) P. Binger, R. Milczarek, R. Mynott, M. Regitz, W. Rösch, *Angew. Chem.* **1986**, *98*, 645; *Angew. Chem. Int. Ed. Engl.* **1986**, *25*, 644; c) P. Binger, R. Milczarek, K. Mynott, C. Kruger, Y. H. Tsay, E. Raabe, M. Regitz, *Chem. Ber.* **1988**, *121*, 637.
- 15 a) M. Driess, D. Hu, H. Pritzkow, H. Schäufele, U. Zenneck, M. Regitz, W. Rösch, *J. Organomet. Chem.* **1987**, *334*, C35; b) P. Binger, B. Biedenbach, R. Schneider, M. Regitz, *Synthesis* **1989**, *1989*, 960; c) D. Böhm, F. Knoch, S. Kummer, U. Schmidt, U. Zenneck, *Angew. Chem. Int. Ed. Engl.* **1995**, *34*, 198; d) P. Binger, G. Glaser, S. Albus, C. Krüger,

- Chem. Ber.* **1995**, 128, 1261; d) G. Brauers, M. Green, C. Jones, J. F. Nixon, *J. Chem. Soc., Chem. Commun.* **1995**, 1125; e) M. Scheer, J. Krug, *Z. anorg. allg. Chem.* **1998**, 624, 399.
- 16 a) T. Wettling, G. Wolmershäuser, P. Binger, M. Regitz, *J. Chem. Soc., Chem. Commun.* **1990**, 1541; b) D. Himmel, M. Seitz, M. Scheer, *Z. anorg. allg. Chem.* **2004**, 630, 1220.
- 17 D. Himmel, M. Seitz, M. Scheer, *Z. anorg. allg. Chem.* **2004**, 630, 1220–1228.
- 18 a) W. W. Brennessel, V. G. Young, J. E. Ellis, *Angew. Chem. Int. Ed.* **2002**, 41, 1211; b) W. W. Brennessel, R. E. Jilek, J. E. Ellis, *Angew. Chem. Int. Ed.* **2007**, 46, 6132.
- 19 a) R. Wolf, A. W. Ehlers, J. C. Slootweg, M. Lutz, D. Gudat, M. Hunger, A. L. Spek, K. Lammertsma, *Angew. Chem. Int. Ed.* **2008**, 47, 4584; b) R. Wolf, J. C. Slootweg, A. W. Ehlers, F. Hartl, B. de Bruin, M. Lutz, A. L. Spek, K. Lammertsma, *Angew. Chem. Int. Ed.* **2009**, 48, 3104; c) R. Wolf, A. W. Ehlers, M. M. Khusniyarov, F. Hartl, B. de Bruin, G. J. Long, F. Grandjean, F. M. Schappacher, R. Pöttgen, J. C. Slootweg, M. Lutz, A. L. Spek, K. Lammertsma, *Chem. Eur. J.* **2010**, 16, 14322.
- 20 P. Binger, G. Glaser, S. Albus, C. Krüger, *Chem. Ber.* **1995**, 128, 1261.
- 21 F. W. Heinemann, S. Kummer, U. Seiss-Brandl, U. Zenneck, *Organometallics* **1999**, 18, 2021.
- 22 A. D. Burrows, A. Dransfeld, M. Green, J. C. Jeffery, C. Jones, J. M. Lynam, M. T. Nguyen, *Angew. Chem. Int. Ed.* **2001**, 40, 3221.
- 23 C. Jones, C. Schulten, A. Stasch, *Dalton Trans.* **2006**, 3733.
- 24 E.-M. Rummel, G. Balázs, V. Heintl, M. Scheer, *Angew. Chem. Int. Ed.* **2017**, 56, 9592.
- 25 a) S. Creve, M. T. Nguyen, L. G. Vanquickenborne, *Eur. J. Inorg. Chem.* **1999**, 1999, 1281–1289; b) R. Wolf, N. Ghavtadze, K. Weber, E.-M. Schnöckelborg, B. de Bruin, A. W. Ehlers, K. Lammertsma, *Dalton Trans.* **2010**, 39, 1453–1456.
- 26 a) A. R. Barron, A. H. Cowley, *Angew. Chem. Int. Ed. Engl.* **2003**, 26, 907; b) R. Milczarek, W. Rüsseler, P. Binger, K. Jonas, K. Angermund, C. Krüger, M. Regitz, *Angew. Chem.* **1987**, 99, 957.
- 27 P. B. Hitchcock, C. Jones, J. F. Nixon, *Angew. Chem. Int. Ed. Engl.* **1994**, 33, 463.
- 28 a) F. G. N. Cloke, K. R. Flower, P. B. Hitchcock, J. F. Nixon, *J. Chem. Soc., Chem. Commun.* **1994**, 489; b) C. Topf, T. Clark, F. W. Heinemann, M. Hennemann, S. Kummer, H. Pritzkow, U. Zenneck, *Angew. Chem. Int. Ed.* **2002**, 41, 4047.
- 29 F. G. N. Cloke, P. B. Hitchcock, J. F. Nixon, D. M. Vickers, *J. Organomet. Chem.* **2001**, 635, 212.
- 30 a) R. Bartsch, P. B. Hitchcock, J. F. Nixon, *J. Chem. Soc., Chem. Commun.* **1987**, 0, 1146; b) J. F. Nixon, *Phosphorus, Sulfur Silicon Relat. Elem.* **1994**, 93, 87; c) F. G. N. Cloke, K. R. Flower, P. B. Hitchcock, J. F. Nixon, *J. Chem. Soc., Chem. Commun.* **1995**, 0, 1659.
- 31 A. G. Avent, F. G. N. Cloke, K. R. Flower, P. B. Hitchcock, J. F. Nixon, D. M. Vickers, *Angew. Chem. Int. Ed. Engl.* **1994**, 33, 2330.

- 32 a) P. B. Hitchcock, M. J. Maah, J. F. Nixon, C. Woodward, *J. Chem. Soc., Chem. Commun.* **1987**, 844; b) H. F. Dare, J. A. K. Howard, M. U. Pilotti, F. G. A. Stone, J. Szameitat, *J. Chem. Soc., Chem. Commun.* **1989**, 1409; c) H. F. Dare, J. A. K. Howard, M. U. Pilotti, F. G. A. Stone, J. Szameitat, *J. Chem. Soc., Dalton Trans.* **1990**, 2263; d) P. B. Hitchcock, M. J. Maah, J. F. Nixon, *Heteroatom Chem.* **1991**, 2, 253.
- 33 a) J. Malberg, T. Wiegand, H. Eckert, M. Bodensteiner, R. Wolf, *Chem. Eur. J.* **2013**, 19, 2356; b) J. Malberg, T. Wiegand, H. Eckert, M. Bodensteiner, R. Wolf, *Eur. J. Inorg. Chem.* **2014**, 2014, 1638.
- 34 J. Malberg, M. Bodensteiner, D. Paul, T. Wiegand, H. Eckert, R. Wolf, *Angew. Chem. Int. Ed.* **2014**, 53, 2771.
- 35 C. Rödl, R. Wolf, *Eur. J. Inorg. Chem.* **2016**, 2016, 736.
- 36 Initial work on this topic was reported in: J. Malberg, *Dissertation* **2013**, University of Regensburg.
- 37 a) P. B. Hitchcock, M. J. Maah, J. F. Nixon, *J. Organomet. Chem.* **1994**, 466, 153; b) A. S. Weller, C. D. Andrews, A. D. Burrows, M. Green, J. M. Lynam, M. F. Mahon, C. Jones, *Chem. Commun.* **1999**, 2147.

2 FUNCTIONALIZATION OF 1,3-DIPHOSPHACYCLOBUTADIENE COBALT COMPLEXES VIA Si–P BOND INSERTION^[a,b]

CHRISTIAN RÖDL, JENNIFER BISSMEYER NEÉ MALBERG, AND ROBERT WOLF



[a] Reproduced with permission from C. Rödl, J. Bissmeyer, R. Wolf, *Z. Naturforsch. B* **2018**, 73, 895–909. Copyright 2019 *de Gruyter*, License number: 4562380106166.

[b] C. Rödl synthesized and characterized compounds **[K(tol)₂][1a]**, **2a**, and **4-12**. J. Bissmeyer née Malberg synthesized and characterized compounds **[K(tol)₂][1b]**, **2b**, and **3a-c**, see J. Malberg, *Dissertation* **2013**, University of Regensburg. C. Rödl prepared all schemes and figures and wrote the manuscript. R. Wolf supervised the project and commented on the manuscript.

2.1 Introduction

The synthesis of *tert*-butyl-phosphaalkyne $t\text{BuC}\equiv\text{P}$ by Becker and co-workers was a milestone in organophosphorus chemistry.¹ Since then, the chemistry of phosphoalkynes has been extensively developed, including their coordination behavior toward transition metals where σ - and π -coordination as well as the cyclization of phosphoalkynes in the coordination sphere have been observed.^{2,3} Numerous contributions have shown that cyclodimerizations in the coordination sphere of transition metal cations may result in 1,2- and 1,3-diphosphacyclobutadiene complexes.^{4,5} The preferred formation of the 1,2- vs. the 1,3-isomer depends on the steric demand of the substituent on the phosphoalkyne. 1,3-Diphosphacyclobutadiene complexes are much more prevalent in the literature due to the sterically encumbering nature of the most commonly used phosphoalkynes such as $t\text{BuC}\equiv\text{P}$.

We have shown that the sandwich complex anion $[\text{Co}(\eta^4\text{-P}_2\text{C}_2t\text{Bu}_2)_2]^-$ (**1a**, Figure 1) is readily accessible on a multigram scale by reaction of $[\text{Co}(\eta^4\text{-C}_{14}\text{H}_{10})_2]^-$ ($\text{C}_{14}\text{H}_{10}$ = anthracene) and $t\text{BuC}\equiv\text{P}$.⁶ This complex exhibits a C_{2v} symmetrical structure with two η^4 -coordinated 1,3-diphosphacyclobutadiene ligands. Preliminary reactivity studies have shown that anion **1a** reacts with $\text{HCl}\cdot\text{Et}_2\text{O}$, MeI , and Ph_2PCl to afford neutral sandwich complexes **A–C** (Figure 1).^{6a} The structural diversity of these new sandwich compounds was intriguing to us, however, this approach is limited by the redox activity and the basicity of **1a**.⁷

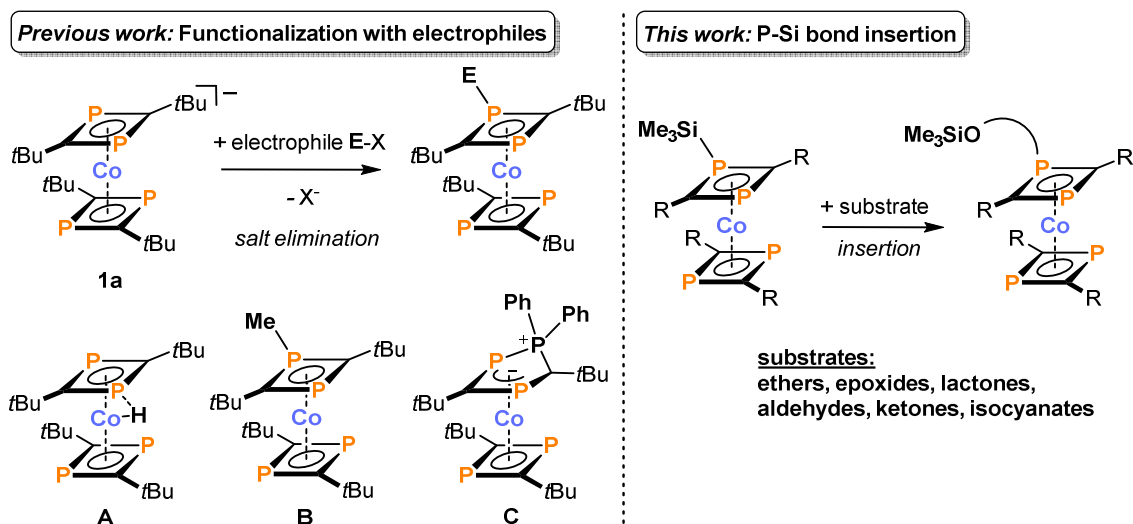


Figure 1. Functionalization of 1,3-diphosphacyclobutadiene complexes by P-Si bond insertions.

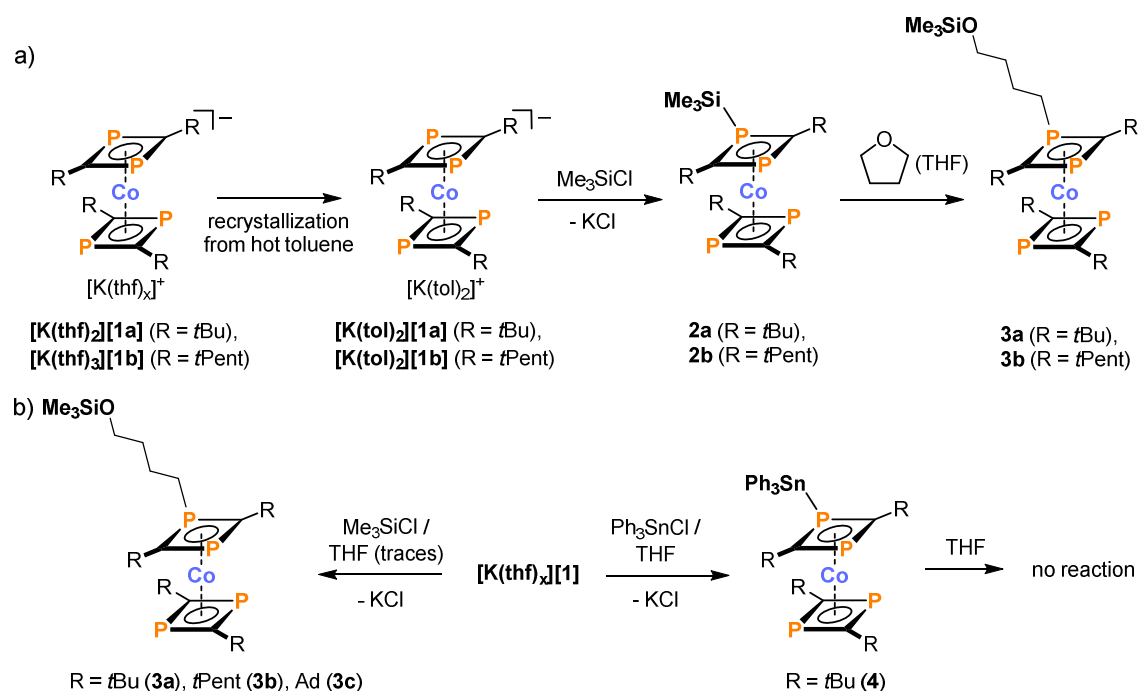
Here, we report a new approach to access functionalized bis(1,3-diphosphacyclobutadiene) cobalt complexes (Figure 1). This new method is based on the observation that the carbon-oxygen bonds of epoxides and carbonyl compounds readily insert into the phosphorus-silicon bond of silylated 1,3-diphosphacyclobutadiene compounds. We describe the synthesis of the reactive silylated sandwich compounds $[\text{Co}(\eta^4\text{-P}_2\text{C}_2\text{R}_2\text{SiMe}_3)(\eta^4\text{-P}_2\text{C}_2\text{R}_2)]$ (**2a, b**, $\text{R} = t\text{Bu}, t\text{Pent}$). In addition, we report the synthesis of a stannylated derivative $[\text{Co}(\eta^4\text{-P}_2\text{C}_2t\text{Bu}_2\text{SnPh}_3)(\eta^4\text{-P}_2\text{C}_2t\text{Bu}_2)]$ (**4**). The

utility and the limitations of P–Si bond insertion are demonstrated by a series of reactions of **2a** with epoxides and ethers (styrene oxide, 1,2-epoxy-2-methylpropane, 1,2-epoxyoctane, diethyl ether and 1,2-dimethoxyethane), γ -butyrolactone, aldehydes (benzaldehydes and cinnamaldehyde), ketones (acetone, 3-pentanone, acetophenone, dibenzylketone, and α,α,α -trifluoroacetophenone), and phenyl isocyanate. From these reactions, several new complexes **5–12** have been identified. We describe our attempts to isolate and characterize these complexes, including the crystallographic characterization of **[K(tol)₂][1b]**, **2a**, **2b**, **3c**, **4**, **5**, and **9-12**.

2.2 Results and Discussion

2.2.1 Synthesis and Structural and Spectroscopic Characterization of Silylated 1,3-Diphosphacyclobutadiene Complexes

In order to access trimethylsilylated derivatives, the synthesis of the THF-free salt $[\text{K}(\text{tol})_2\{\text{Co}(\text{P}_2\text{C}_2\text{tBu}_2)_2\}]$ ($[\text{K}(\text{tol})_2][\mathbf{1a}]$, $\text{tol} = \text{toluene}$) was necessary. Deep-orange $[\text{K}(\text{tol})_2][\mathbf{1a}]$ is readily obtained by recrystallization of the known THF solvate $[\text{K}(\text{thf})_2\{\text{Co}(\text{P}_2\text{C}_2\text{tBu}_2)_2\}]$ ($[\text{K}(\text{thf})_2][\mathbf{1a}]$)^{8a-c} in hot toluene (Scheme 1a). The closely related *tert*-pentyl-substituted complex $[\text{K}(\text{tol})_2\{\text{Co}(\text{P}_2\text{C}_2\text{tPent}_2)_2\}]$ ($[\text{K}(\text{tol})_2][\mathbf{1b}]$, *tPent* = *tert*-pentyl) is accessible in a completely analogous manner. The latter complex was also structurally characterized by X-ray crystallography.



Scheme 1. Synthesis of complexes **2a**, **2b**, **3a-c**, and **4**.

Crystals of $[\text{K}(\text{tol})_2][\mathbf{1b}]$ were obtained at $-18\text{ }^\circ\text{C}$ from a concentrated toluene solution. The molecular structure (Figure 2, left) is closely related to that of $[\text{K}(\text{thf})_4\{\text{Co}(\text{P}_2\text{C}_2\text{Ad}_2)_2\}]$ ($[\text{K}(\text{thf})_4][\mathbf{1c}]$).^{8a} The potassium cation interacts with one 1,3-diphosphacyclobutadiene ring of the cobaltate anion in an η^4 fashion. The coordination sphere of the potassium atom is completed by two toluene molecules that coordinate to K1 in an η^6 fashion (K1–C_{tol} 3.148(4)–3.270(4) Å). The remaining structural parameters are unexceptional and very close to those of previously reported structures of anion **1a**.^{6a,c} In comparison with some of the structures discussed below, the Co–P distances in $[\text{K}(\text{tol})_2][\mathbf{1b}]$ are in a very similar range (2.2452(9)–2.256(1) Å).

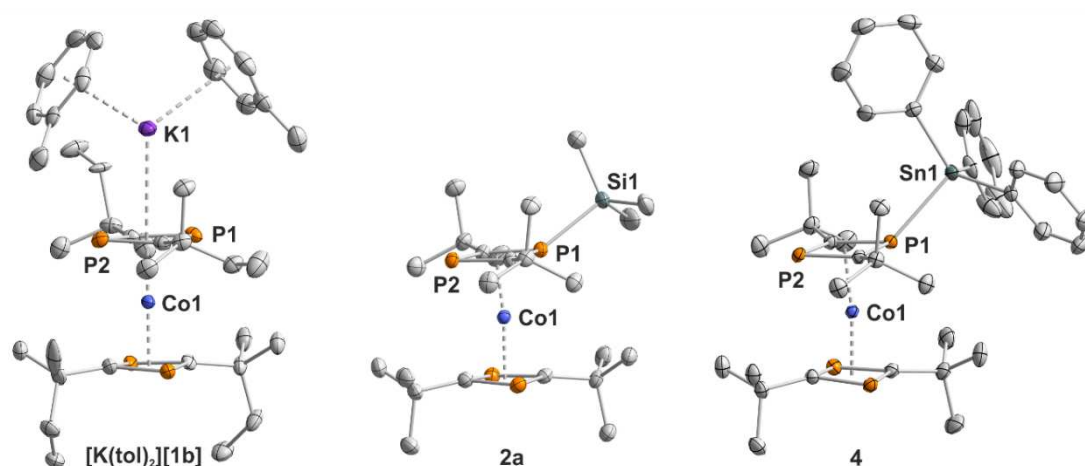


Figure 2. Solid-state molecular structures of $[\text{K}(\text{tol})_2\{\text{Co}(\eta^4\text{-P}_2\text{C}_2\text{tPent}_2)_2\}]$ ($[\text{K}(\text{tol})_2][\mathbf{1b}]$, left), $[\text{Co}(\eta^4\text{-P}_2\text{C}_2\text{tBu}_2\text{SiMe}_3)(\eta^4\text{-P}_2\text{C}_2\text{tBu}_2)]$ ($\mathbf{2a}$, center), and $[\text{Co}(\eta^4\text{-P}_2\text{C}_2\text{tBu}_2\text{SnPh}_3)(\eta^4\text{-P}_2\text{C}_2\text{tBu}_2)]$ ($\mathbf{4}$, right). The hydrogen atoms are omitted for clarity. Displacement ellipsoids are drawn at the 40% (for $\mathbf{2a}$) and 50% (for $[\text{K}(\text{tol})_2][\mathbf{1b}]$ and $\mathbf{4}$) probability level. Selected bond lengths (Å) and angles (°) for $[\text{K}(\text{tol})_2][\mathbf{1b}]$: P1–K1 3.272(1), P1–Co1 2.2452(9), P1–C1 1.812(3), P1–C2 1.808(4), C2–P1–C1 80.4(2); $\mathbf{2a}$: P1–Si1 2.2895(9), P1–Co1 2.1685(7), P1–C1 1.785(3), P1–C2 1.782(3); C2–P1–C1 84.4(1); $\mathbf{4}$: P1–Sn1 2.5347(4), P1–Co1 2.1824(4), P1–C1 1.789(1), P1–C2 1.787(1); C2–P1–C1 83.62(6).

Reaction of $[\text{K}(\text{tol})_2][\mathbf{1a}]$ and $[\text{K}(\text{tol})_2][\mathbf{1b}]$ with one equivalent of Me_3SiCl in toluene afforded the desired silylated complexes $[\text{Co}(\eta^4\text{-P}_2\text{C}_2\text{R}_2\text{SiMe}_3)(\eta^4\text{-P}_2\text{C}_2\text{R}_2)]$ ($\mathbf{2a}$: R = *t*Bu, $\mathbf{2b}$: R = *t*Pent, Scheme 1a). The reaction is quantitative according to ^{31}P NMR monitoring. Deep-red $\mathbf{2a}$ and $\mathbf{2b}$ were isolated in 77% and 72% yield, respectively, by crystallization from *n*-pentane. It is important to note that the reactions must be performed in strictly THF- and water-free solvent, otherwise the THF insertion products $\mathbf{3a}$ and $\mathbf{3b}$ (*vide infra*) or the hydride complexes $[\text{Co}(\eta^4\text{-P}_2\text{C}_2\text{R}_2)_2\text{H}]$ \mathbf{A} and \mathbf{A}' (\mathbf{A} : R = *t*Bu, \mathbf{A}' : R = *t*Pent) are formed as side products. In solution, $\mathbf{2a}$ and $\mathbf{2b}$ even react with traces of THF contaminant (even THF contamination present in a glovebox atmosphere).

The composition of $\mathbf{2a}$ and $\mathbf{2b}$ was unequivocally confirmed by multinuclear NMR spectroscopy and single-crystal X-ray structure determinations. Crystals of $\mathbf{2a}$ suitable for single-crystal X-ray diffraction were grown from a concentrated *n*-pentane solution at -35 °C. Compound $\mathbf{2a}$ crystallizes in the monoclinic space group $P2_1/n$ with four formula units per unit cell. The structure of $\mathbf{2a}$ (Figure 2, center) comprises one Me_3Si fragment connected to a phosphorus atom of a $\text{Co}(\text{P}_2\text{C}_2\text{tBu}_2)_2$ unit with a P1–Si1 bond length of 2.2895(9) Å. This results in a tetrahedral environment for the silicon atom Si1. The P1–Si1 distance is in the range of typical phosphorus–silicon single bonds.⁹ As a consequence of the coordination to Si1, the Co1–P1 distance (2.1685(7) Å) is shorter than the other Co1–P distances (2.2560(8)–2.2706(7) Å). Compound $\mathbf{2b}$ is isostructural with $\mathbf{2a}$ (see the Supporting Information, Figure S17 and Table S1). The $^{31}\text{P}\{^1\text{H}\}$ NMR spectrum of $\mathbf{2a}$ in C_6D_6 features three signals in an intensity ratio of 1:1:2. A singlet at $\delta = -1.7$ ppm is assigned to the silylated phosphorus atom. No P–H coupling was

observed. The second phosphorus atom of the silylated 1,3-diphosphacyclobutadiene resonates at $\delta = 19.2$ ppm. The phosphorus atoms of the remaining 1,3-diphosphacyclobutadiene ligand resonate at $\delta = 21.7$ ppm. The ^1H and the $^{13}\text{C}\{^1\text{H}\}$ NMR data are likewise consistent with the proposed molecular structure, showing three distinct *tert*-butyl environments. The trimethylsilyl group gives rise to a signal at $\delta = 0.28$ ppm in the ^1H NMR spectrum with ^{29}Si satellites [$^2J(^{29}\text{Si}, ^1\text{H}) = 6.5$ Hz]. No ^1H – ^{31}P coupling was observed for this signal in the ^1H NMR spectrum. The ^{29}Si NMR spectrum shows a doublet of doublets at $\delta = 12.0$ ppm with $^1J(^{29}\text{Si}, ^{31}\text{P}) = 26.0$ Hz and $^3J(^{29}\text{Si}, ^{31}\text{P}) = 3.2$ Hz. The NMR spectroscopic data of **2b** are very similar to those of **2a** (see the Supporting Information) and will therefore not be discussed in further detail.

Isolated samples of **2a** and **2b** were contaminated with small amounts of the hydride complexes $[\text{Co}(\eta^4\text{-P}_2\text{C}_2\text{R}_2)_2\text{H}]$ (**A**: R = *t*Bu, **A'**: R = *t*Pent).^{6a} This is presumably caused by the presence of traces of moisture in the solvent or traces of HCl in the Me_3SiCl solution. The amount of hydride by-product varied from 3% to 23% in the samples investigated by us (as shown by ^1H NMR spectroscopy). Attempts to separate these products by recrystallization or sublimation were thwarted by the very similar solubility and sublimation properties. Nonetheless, the isolated samples **2a**, **b** can be successfully used in subsequent reactivity studies even when contaminated with **A** or **A'**, because the hydride complexes are rather unreactive.

$[\text{K}(\text{thf})_2\{\text{Co}(\text{P}_2\text{C}_2\text{tBu}_2)_2\}]$ ($[\text{K}(\text{thf})_2][\mathbf{1a}]$) reacts cleanly with Ph_3SnCl affording $[\text{Co}(\eta^4\text{-P}_2\text{C}_2\text{tBu}_2\text{SnPh}_3)(\eta^4\text{-P}_2\text{C}_2\text{tBu}_2)]$ (**4**) in 78% yield (Scheme 1b). Note that THF insertion was not observed even though the reaction was performed in THF solvent. Orange crystals of **4** suitable for single-crystal X-ray diffraction were obtained from a saturated diethyl ether solution at room temperature. Compound **4** crystallizes in the space group $P\bar{1}$ with two formula units per unit cell. Similar to **2a**, the molecular structure of **4** (Figure 2, right) features the Ph_3Sn group attached to one phosphorus atom of the sandwich molecule. The P1–Sn1 bond length of 2.5347(4) Å is in the usual range of phosphorus(III)–tin(IV) single bonds.⁹ As in **2a**, the Co1–P1 distance (2.1824(4) Å) is shorter than the other Co1–P distances (2.2505(4)–2.2797(4) Å) due to the coordination to Sn1.

The $^{31}\text{P}\{^1\text{H}\}$ NMR spectrum of **4** in C_6D_6 shows three signals at $\delta = -14.5$, 22.9, and 24.6 ppm. The spectrum is similar to that of **2a**. The signal at $\delta = -14.5$ ppm features ^{119}Sn satellites [$^1J(^{31}\text{P}, ^{119}\text{Sn}) = 1000$ Hz] and therefore can be assigned to phosphorus atom P1 attached to tin. The singlet at $\delta = 22.9$ ppm also features ^{119}Sn satellites with a smaller coupling constant [$^3J(^{31}\text{P}, ^{119}\text{Sn}) = 30$ Hz]. Hence, this signal can be assigned to P2 in the same P_2C_2 ring, while the second 1,3-diphosphacyclobutadiene ligand in **4**, which is not coordinated to tin, gives rise to the signal at $\delta = 24.6$ ppm. In accord with this, the $^{119}\text{Sn}\{^1\text{H}\}$ spectrum of **4** displays a doublet of doublets at $\delta = -120.0$ ppm with coupling constants of $^1J(^{119}\text{Sn}, ^{31}\text{P}) = 1000$ Hz and $^3J(^{119}\text{Sn}, ^{31}\text{P}) = 30$ Hz, respectively.

2.2.2 Functionalization Reactions by Insertion into the Phosphorus-Silicon Bond

2.2.2.1 Reaction of $[\text{Co}(\eta^4\text{-P}_2\text{C}_2t\text{Bu}_2\text{SiMe}_3)(\eta^4\text{-P}_2\text{C}_2t\text{Bu}_2)]$ (**2a**) with epoxides and ethers

Attempts to synthesize the silylated target compounds $[\text{Co}(\eta^4\text{-P}_2\text{C}_2\text{R}_2\text{SiMe}_3)(\eta^4\text{-P}_2\text{C}_2\text{R}_2)]$ (**2a**: R = *t*Bu, **2b**: R = *t*Pent, **2c**: R = Ad) by reacting $[\text{K}(\text{thf})_x\{\text{Co}(\text{P}_2\text{C}_2\text{R}_2)_2\}]$ ($[\text{K}(\text{thf})_x][\mathbf{1a-c}]$) ($x = 2-4$) with Me_3SiCl in THF were unsuccessful. Instead, NMR monitoring revealed the quantitative formation of $[\text{Co}(\eta^4\text{-P}_2\text{C}_2\text{R}_2(\text{CH}_2)_4\text{OSiMe}_3)(\eta^4\text{-P}_2\text{C}_2\text{R}_2)]$ (**3a-c**) via C–O bond cleavage of THF.¹⁰ **3a, b** were even obtained from $[\text{K}(\text{thf})_2\{\text{Co}(\text{P}_2\text{C}_2t\text{Bu}_2)_2\}]$ ($[\text{K}(\text{thf})_2][\mathbf{1a}]$) and $[\text{K}(\text{thf})_3\{\text{Co}(\text{P}_2\text{C}_2t\text{Pent}_2)_2\}]$ ($[\text{K}(\text{thf})_3][\mathbf{1b}]$) in toluene solvent via reaction of the THF solvate molecules coordinated to the potassium cations. They may also be synthesized via reaction of **2a, b** (*vide supra*) with THF (Scheme 1a). Compounds **3a-c** were isolated in 37% to 56% yield from *n*-hexane or *n*-pentane. These relatively modest yields can presumably be attributed to the high solubility of **3a-c** in apolar solvents; the reactions are essentially quantitative according to ³¹P NMR spectroscopy. **3a, b** were isolated as orange oils. Attempts to crystallize **3a, b** were hampered by their remarkably high solubility in apolar solvents. **3c** was obtained as orange X-ray quality crystals from a concentrated toluene solution at -18°C . The molecular structure (Figure 4, left) confirms that the $(\text{CH}_2)_4\text{OSiMe}_3$ fragment is bound to one phosphorus atom (P1) of one 1,3-diphosphacyclobutadiene ligand (P1–C45 1.813(4) Å). The structure is related to that of $[\text{Co}(\eta^4\text{-P}_2\text{C}_2t\text{Bu}_2\text{Me})(\eta^4\text{-P}_2\text{C}_2t\text{Bu}_2)]$ (**B**, Figure 1).^{6a}

Multinuclear NMR spectroscopy has unequivocally supported the proposed molecular structures of **3a-c**. The ¹H and ¹³C{¹H} NMR spectra each feature one signal for an SiMe₃ moiety as well as four multiplets for the CH₂ groups of the $(\text{CH}_2)_4\text{OSiMe}_3$ fragment. The *tert*-butyl, *tert*-pentyl or adamantyl substituents give rise to a set of three signals in the NMR spectra in a ratio of 1:1:2. In accord with these details, the ³¹P{¹H} NMR spectra (Table 1) show three signals in a ratio of 1:2:1 with a pattern similar to that observed for the methylated complex **B** (Figure 1).^{6a}

Table 1. Comparison of the assignment of the ³¹P{¹H} resonances of **3a-c** with the resonances of $[\text{Co}(\text{P}_2\text{C}_2t\text{Bu}_2\text{Me})(\text{P}_2\text{C}_2t\text{Bu}_2)]$ (**B**). Chemical shifts are given in ppm, the multiplicity and the ²*J*(³¹P,³¹P) coupling constants are given in parentheses. The general labeling scheme is shown in Figure 3.

Assignment	3a	3b	3c	B ²⁸
P1	55.5 (d, 15 Hz)	55.4 (d, 15 Hz)	55.5 (d, 16 Hz)	41.7 (br)
P2	-50.0 (d, 15 Hz)	-45.5 (d, 15 Hz)	-57.3 (d, 16 Hz)	-50.5 (d, 14 Hz)
P3 and P4	25.8 (s)	29.4 (s)	19.1 (s)	25.5 (s)

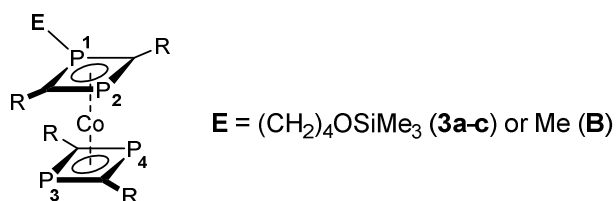


Figure 3. Labeling scheme for the insertion products **3a-c** and the methylated complex **B**.

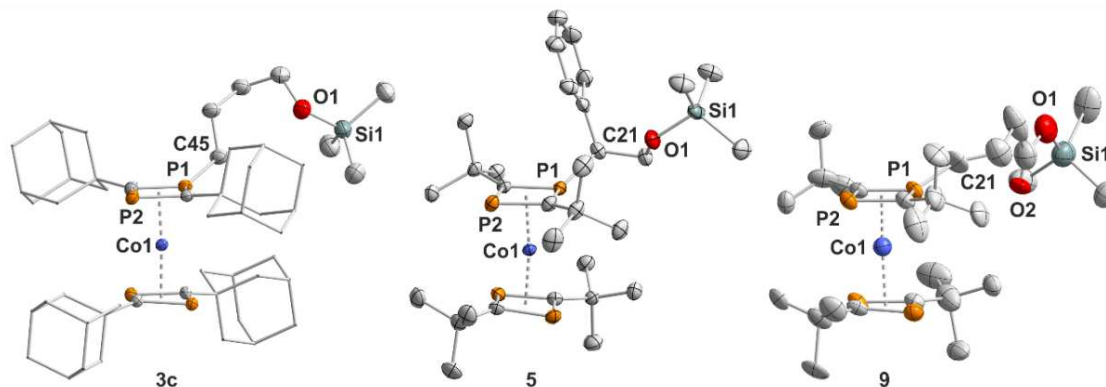
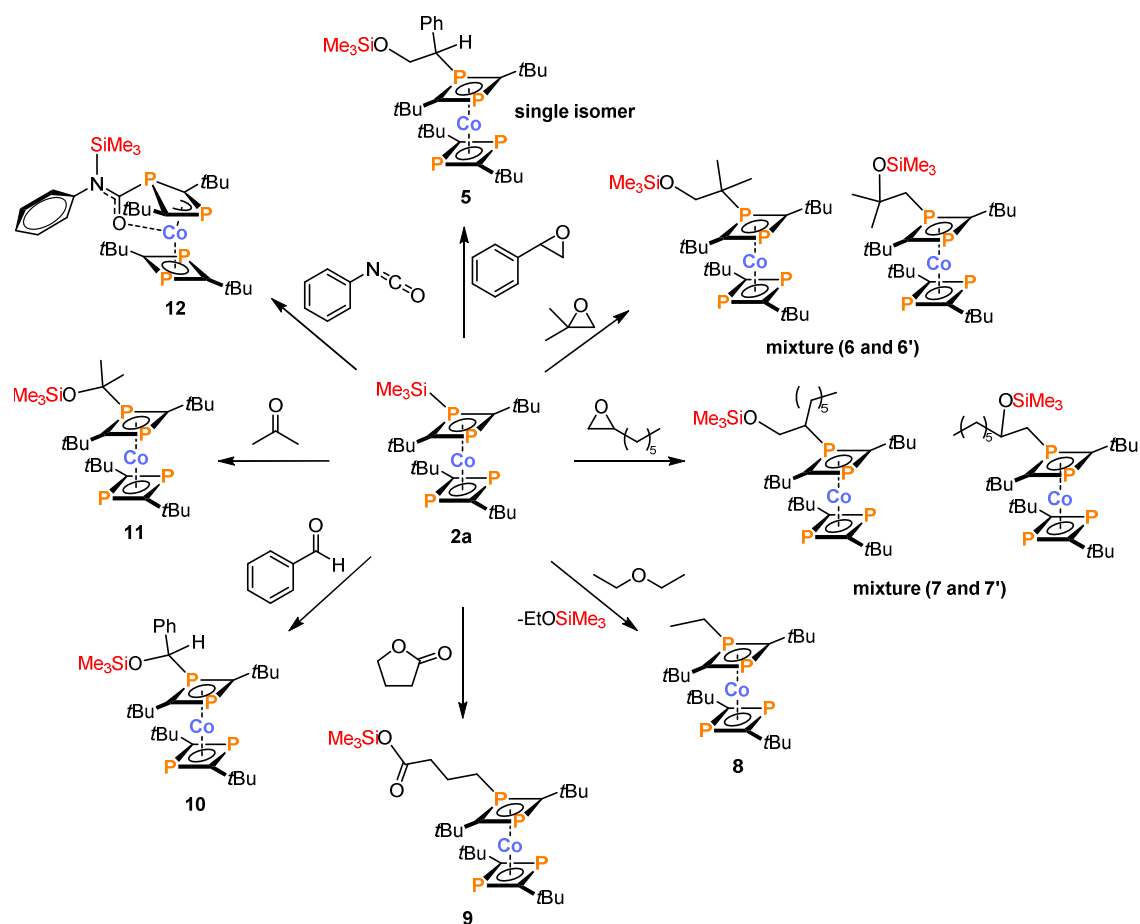


Figure 4. Solid state molecular structure of $[\text{Co}(\eta^4\text{-P}_2\text{C}_2\text{Ad}_2(\text{CH}_2)_4\text{OSiMe}_3)(\eta^4\text{-P}_2\text{C}_2\text{Ad}_2)]$ (**3c**, left), $[\text{Co}(\eta^4\text{-P}_2\text{C}_2\text{tBu}_2\text{PhC}_2\text{H}_3\text{OSiMe}_3)(\eta^4\text{-P}_2\text{C}_2\text{tBu}_2)]$ (**5**, center), and $[\text{Co}(\eta^4\text{-P}_2\text{C}_2\text{tBu}_2(\text{CH}_2)_3\text{C}(\text{O})\text{OSiMe}_3)(\eta^4\text{-P}_2\text{C}_2\text{tBu}_2)]$ (**9**, right). Thermal ellipsoids are drawn at the 40% probability level. H-atoms and the toluene solvate molecule of **3c** are omitted for clarity. Selected bond lengths [Å] and angles [°] for **3c**: P1–C45 1.813(4), O1–Si1 1.646(3), P1–C1–P2–C2/P3–C3–P4–C4 1.38; **5**: P1–C21 1.853(2), O1–Si1 1.662(2), P1–C1–P2–C2/P3–C3–P4–C4 4.76; **9**: P1–C21 1.867(4), O1–Si1 1.652(7), P1–C1–P2–C2/P3–C3–P4–C4 2.60.

The extremely facile insertion of even traces of THF into the P–Si bonds of **2a**, **b** inspired us to study insertion reactions of other organic substrates containing C–O and C=O bonds (Scheme 2). Initial investigations focused on the reaction of epoxides with **2a**. Addition of styrene oxide to an *n*-hexane solution of **2a** afforded the insertion product $[\text{Co}(\eta^4\text{-P}_2\text{C}_2\text{tBu}_2\text{PhC}_2\text{H}_3\text{OSiMe}_3)(\eta^4\text{-P}_2\text{C}_2\text{tBu}_2)]$ (**5**, Figure 4, center), which was observed as the sole product by ^{31}P NMR spectroscopy and was isolated in 80% yield. The ^1H and $^{13}\text{C}\{^1\text{H}\}$ NMR spectra of **5** in C_6D_6 feature similar patterns as found for **2a** with one signal for the SiMe_3 group and three sets of signals in a 1:1:2 ratio assigned to chemically inequivalent *tert*-butyl substituents. The $^{31}\text{P}\{^1\text{H}\}$ NMR spectrum of **5** features two doublets at $\delta = -26.0$ ppm [$^2J(^{31}\text{P}, ^{31}\text{P}) = 13.7$ Hz] and $\delta = 60.8$ ppm [$^2J(^{31}\text{P}, ^{31}\text{P}) = 13.7$ Hz] assigned to the functionalized 1,3-diphosphacyclobutadiene ligand, while the unfunctionalized 1,3-diphosphacyclobutadiene ligand gives rise to a singlet at $\delta = 25.5$ ppm.



Scheme 2. Synthesis of complexes 5–12.

In contrast to the reaction with styrene oxide, reactions of **2a** with 1,2-epoxy-2-methylpropane and 1,2-epoxyoctane afforded isomers **6/6'** (observed in a ratio of 63:37 by ^{31}P NMR, Table 2) and **7/7'** (74:26 ratio), respectively, according to the $^{31}\text{P}\{^1\text{H}\}$ NMR spectra (see the Supporting Information for more detailed data). Presumably, these species are regioisomers arising from the insertion of one or the other of the two C–O bonds of the epoxides into the P–Si bond. So far, we could not obtain crystals of these complexes, which are highly soluble in *n*-pentane and other apolar solvents. **6/6'** and **7/7'** are difficult to separate as they form red oils in apolar solvents such as *n*-hexane.

Table 2. Comparison of the assignment of the $^{31}\text{P}\{^1\text{H}\}$ NMR resonances of **5**–**7**. Chemical shifts are given in ppm, the multiplicity and the $^2J(^{31}\text{P},^{31}\text{P})$ coupling constants are given in parantheses. The general labeling scheme is shown in Figure 5.

Assignment	5	6/6'	7/7'
<i>major isomer</i>			
P1	60.8 (d, 13.7 Hz)	81.8 (d, 17.5 Hz)	72.0 (d, 14.0 Hz)
P2	–26.0 (d, 13.7 Hz)	–22.4 (d, 17.5 Hz)	–29.6 (d, 14.0 Hz)
P3 and P4	25.5 (s)	24.7 (s)	23.7 (s), 25.2 (s)
<i>minor isomer</i>			
P1	–	–35.4 (d, 33.7 Hz)	29.8 (d, 16.2 Hz)
P2	–	–46.2 (d, 33.7 Hz)	–57.8 (d, 16.2 Hz)
P3 and P4	–	24.6 (s)	25.9 (s), 26.5 (s)

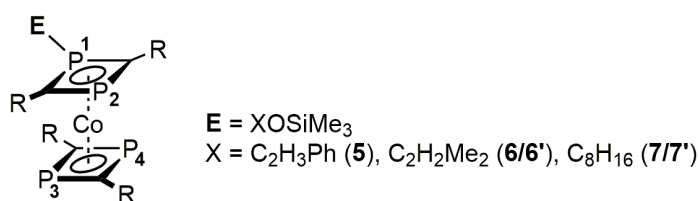


Figure 5. Labeling scheme for the insertion products **5**–**7**.

Reactions of **2a** with acyclic ethers were also examined (Scheme 2). With 1,2-dimethoxyethane and *tert*-butylmethyl ether, this resulted in the cleavage of the C–O bond as evidenced by the formation of $[\text{Co}(\eta^4\text{-P}_2\text{C}_2\text{tBu}_2\text{Me})(\eta^4\text{-P}_2\text{C}_2\text{tBu}_2)]$ (**B**, Figure 1) observed by ^{31}P NMR spectroscopy. By contrast, reaction of **2b** with diethyl ether (two hours at 60 °C) afforded the ethyl-substituted complex $[\text{Co}(\eta^4\text{-P}_2\text{C}_2\text{tBu}_2\text{Et})(\eta^4\text{-P}_2\text{C}_2\text{tBu}_2)]$ (**8**) according to $^{31}\text{P}\{^1\text{H}\}$ NMR spectroscopy (see the Supporting Information, Figures S2–S4).

2.2.2.2 Reaction of $[\text{Co}(\eta^4\text{-P}_2\text{C}_2\text{tBu}_2\text{SiMe}_3)(\eta^4\text{-P}_2\text{C}_2\text{tBu}_2)]$ (**2a**) with carbonyl compounds

We also studied the reactivity of **2a** towards carbonyl compounds. Reaction of γ -butyrolactone with **2a** in *n*-hexane afforded $[\text{Co}(\eta^4\text{-P}_2\text{C}_2\text{tBu}_2(\text{CH}_2)_3\text{C}(\text{O})\text{OSiMe}_3)(\eta^4\text{-P}_2\text{C}_2\text{tBu}_2)]$ (**9**, Figure 4, right), which was isolated in 56% yield from *n*-hexane. The very similar ^{31}P NMR data compared to **3a** indicates that the C–O single bond of the lactone is cleaved. This is also confirmed by a single-crystal X-ray structure analysis of the dark orange crystals of **9** (space group $P2_1/n$ with four formula units per unit cell) obtained upon storing a concentrated *n*-hexane solution of **9** at –35 °C overnight. The molecular structure (Figure 4, right) shows that the insertion of a C–O single bond of the lactone resulted in the formation of a silyl ester moiety connected to the $\text{Co}(\text{P}_2\text{C}_2\text{R}_2)_2$ sandwich via a spacer of three methylene units (P1–C21 1.867(4) Å).

The $^{31}\text{P}\{^1\text{H}\}$ NMR spectrum of **9** features two doublets at $\delta = -48.7$ [$^2J(^{31}\text{P},^{31}\text{P}) = 15$ Hz] and 54.0 ppm [$^2J(^{31}\text{P},^{31}\text{P}) = 15$ Hz] which are assigned to a functionalized 1,3-diphosphacyclobutadiene ligand. The unfunctionalized P_2C_2 ring gives rise to a singlet at $\delta = 26.1$ ppm. The ^1H and $^{13}\text{C}\{^1\text{H}\}$ NMR spectra of **9** feature similar patterns as **3a–c**. According to the ^1H NMR spectrum, compound **9** is contaminated with approximately 20% of the hydride complex $[\text{Co}(\eta^4\text{-P}_2\text{C}_2\text{tBu}_2)\text{H}]$ (**A**).

Reaction of **2a** with benzaldehyde in *n*-hexane at room temperature afforded $[\text{Co}(\eta^4\text{-P}_2\text{C}_2\text{tBu}_2\text{CH(Ph)OSiMe}_3)(\eta^4\text{-P}_2\text{C}_2\text{tBu}_2)]$ (**10**) via the insertion of the C=O bond of the aldehyde into the P–Si bond of **2a**. A single-crystal X-ray structure determination of red crystals of **10** (space group $P2_1/m$ with four formula units per unit cell) showed that the former carbonyl carbon atom is bound to a P atom of one of the 1,3-diphosphacyclobutadiene ligands (P1–C21 1.88(1) Å), while the Me_3Si is attached to the oxygen atom. The $^{31}\text{P}\{^1\text{H}\}$ NMR spectrum of **10** in C_6D_6 shows two doublets at $\delta = -39.9$ [$^2J(^{31}\text{P},^{31}\text{P}) = 18.5$ Hz] and 75.2 ppm [$^2J(^{31}\text{P},^{31}\text{P}) = 18.5$ Hz] assigned to the functionalized P_2C_2 ring, while the unfunctionalized diphosphacyclobutadiene ligand gives rise to two singlets at $\delta = 25.0$ and 28.0 ppm. The observation of two NMR signals for the unfunctionalized P_2C_2 unit is likely due to the diastereotopic nature of the P atoms that arises from slow rotation of this ring around the cobalt– P_2C_2 ring axis. In accord with this, the $^{13}\text{C}\{^1\text{H}\}$ NMR spectrum of **10** reveals four sets of resonances for the *tert*-butyl substituents, indicating that the *t*Bu groups on the unfunctionalized P_2C_2 ring are also diastereotopic. Similar $^{31}\text{P}\{^1\text{H}\}$ NMR spectra were obtained when **2a** was reacted with *p*-methylbenzaldehyde and *p-tert*-butylbenzaldehyde. By contrast, reaction of **2a** with cinnamaldehyde yielded two isomers in a ratio of 3:1 as evidenced by the observation of two sets of signals in the $^{31}\text{P}\{^1\text{H}\}$ NMR spectrum in C_6D_6 at $\delta = -34.5, 24.6, 25.4,$ and 77.6 ppm, and at $\delta = -38.2, 24.2, 27.0,$ and 75.4 ppm, respectively.

We furthermore used ketones as substrates. Acetone reacted quantitatively with **2a**, affording the insertion product $[\text{Co}(\eta^4\text{-P}_2\text{C}_2\text{tBu}_2\text{CMe}_2\text{OSiMe}_3)(\eta^4\text{-P}_2\text{C}_2\text{tBu}_2)]$ (**11**), which was characterized by X-ray crystallography. Red crystalline **11** precipitated from a concentrated *n*-hexane solution at -35 °C. The molecular structure (Figure 6, center) is very similar to that of **10** as is the $^{31}\text{P}\{^1\text{H}\}$ NMR spectrum in C_6D_6 , which features two doublets at $\delta = -27.0$ [$^2J(^{31}\text{P},^{31}\text{P}) = 20$ Hz] and 90.4 ppm [$^2J(^{31}\text{P},^{31}\text{P}) = 20$ Hz] for the functionalized 1,3-diphosphacyclobutadiene ligand and a singlet at $\delta = 25.7$ ppm for the unfunctionalized 1,3-diphosphacyclobutadiene unit.

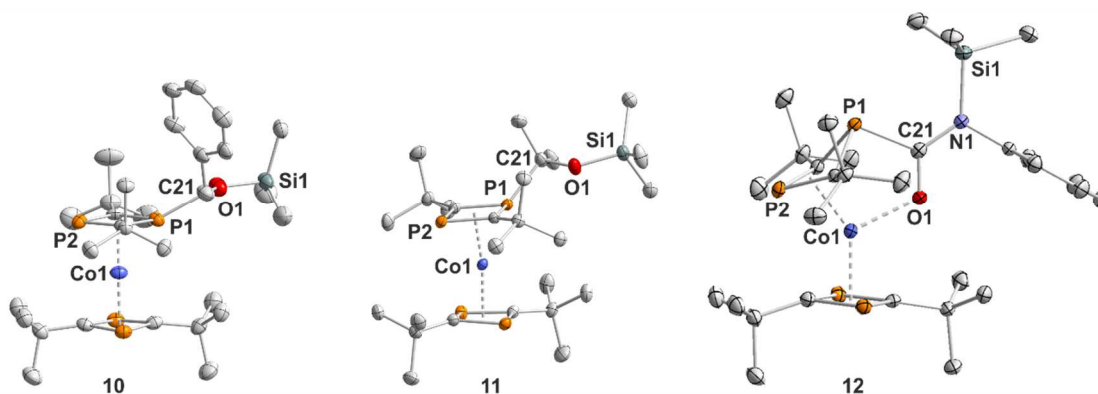


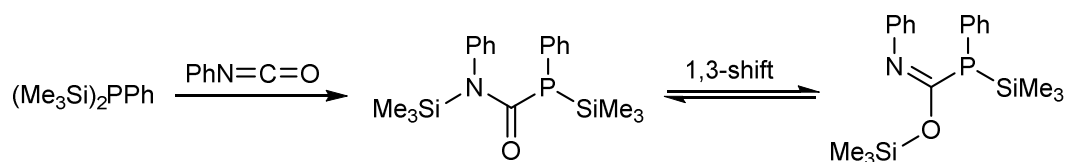
Figure 6. Solid-state molecular structures of $[\text{Co}(\eta^4\text{-P}_2\text{C}_2\text{tBu}_2\text{CH(Ph)OSiMe}_3)(\eta^4\text{-P}_2\text{C}_2\text{tBu}_2)]$ (**10**, left), $[\text{Co}(\eta^4\text{-P}_2\text{C}_2\text{tBu}_2\text{CHMe}_2\text{OSiMe}_3)(\eta^4\text{-P}_2\text{C}_2\text{tBu}_2)]$ (**11**, center), and $[\text{Co}(\eta^4\text{-P}_2\text{C}_2\text{tBu}_2\text{CON(Ph)SiMe}_3)(\eta^4\text{-P}_2\text{C}_2\text{tBu}_2)]$ (**12**, right). Displacement ellipsoids are drawn at the 50% probability level. H atoms and the *n*-hexane solvate molecule of **12** are omitted for clarity. Selected bond lengths (Å) and dihedral angles (°) for **10**: P1–C21 1.88(1), C21–O1 1.39(1), O1–Si1 1.672(7); **11**: P1–C21 1.902(2)(1), C21–O1 1.414(2), O1–Si1 1.662(2); **12**: P1–C21 1.865(1), C21–O1 1.249(2), C21–N1 1.350(2), N1–Si1 1.804(1), Co1–O1 2.037(1), Co1–P1 2.8241(4), P1–C1 1.844(1), P1–C2 1.847(2), P2–C1 1.790(1), P2–C2 1.794(1); C2–P1–C1/C1–P2–C2 38.3.

Samples of **11** were found to be contaminated with ca. 18% of **A** according to their ^1H NMR spectra. **11** and **A** could not be separated by recrystallization or by sublimation due to very similar solubility and sublimation properties. Reactions of **2a** with the sterically more demanding ketones 3-pentanone and acetophenone selectively yielded **A** according to ^1H and $^{31}\text{P}\{^1\text{H}\}$ NMR spectroscopy. Dibenzylketone afforded a minor amount of the desired insertion product, but **A** was the major product (ca. 88% of the P content determined by integration of the $^{31}\text{P}\{^1\text{H}\}$ NMR spectrum in C_6D_6). Interestingly, α,α,α -trifluoroacetophenone did not react with **2a**.

An unusual $^{31}\text{P}\{^1\text{H}\}$ NMR signal pattern was detected when we reacted **2a** with phenyl isocyanate (PhNCO) in *n*-hexane at 50 °C overnight. Orange crystals (space group $P2_1/n$, four formula units in the unit cell) suitable for single-crystal X-ray diffraction were obtained from a concentrated *n*-hexane solution at room temperature. Remarkably, the molecular structure shows that the C=N bond of the isocyanate molecule became inserted into the phosphorus–silicon bond of the starting complex **2a**. This leads to an elongation of the C–N bond (1.350(2) Å; C=N reported for PhNCO 1.21 Å¹¹). Furthermore, an interaction between the isocyanate oxygen atom and the cobalt atom is observed (Co–O 2.037(1) Å). This results in a severely tilted η^3 -coordinated 1,3-diphosphacyclobutene-2-yl ligand showing a dihedral angle between the C1–P2–C2/C2–P1–C1 planes of 38.34°. The C21–O1 bond, however, is not affected by this interaction as shown by the bond length of 1.249(2) Å (sum of covalent radii 1.24 Å⁹). An IR (ATR) spectrum of **12** shows three characteristic bands at 1516, 1487, and 1454 cm^{-1} which are assigned to the C–O and C–N vibrations, respectively. The bands at 1487 and 1454 cm^{-1} confirm the weakening of the C–N bond compared to the spectrum of free PhNCO ($\nu_{\text{as}}(\text{N}=\text{C}=\text{O}) = 2260 \text{ cm}^{-1}$, $\nu_{\text{s}}(\text{N}=\text{C}=\text{O}) = 1445 \text{ cm}^{-1}$).¹²

The $^{31}\text{P}\{^1\text{H}\}$ NMR spectrum of **12** in C_6D_6 features two doublets at $\delta = 77.0$ [$^2J(^{31}\text{P}, ^{31}\text{P}) = 33$ Hz] and 140.0 ppm [$^2J(^{31}\text{P}, ^{31}\text{P}) = 33$ Hz] which are assigned to a functionalized 1,3-diphosphacyclobutene-2-yl moiety. Two overlapping signals are observed for the P atoms of the unfunctionalized 1,3-diphosphacyclobutadiene ring at $\delta = 21.55$ and 21.60 ppm. This could be due to partially restricted rotation of the $\text{N}(\text{SiMe}_3)\text{Ph}$ moiety around the C–N bond. The amido group gives rise to a set of five signals in the $^{13}\text{C}\{^1\text{H}\}$ NMR spectrum. The most downfield shifted signal was detected at $\delta = 140.0$ ppm and is assigned to the *ipso*-carbon atom of the phenyl substituent. The signal for the carbon atom of the amido moiety was detected at $\delta = 124.3$ ppm.

Regarding the synthesis of **12**, the work of Itoh and co-workers should be noted, who previously studied reactions of PhNCO with $(\text{Me}_3\text{Si})_2\text{PPh}$ and $\text{Me}_3\text{SiPPh}_2$.¹³ $\text{Me}_3\text{SiPPh}_2$ was found to be an effective catalyst for the cyclization of phenyl isocyanate to the cyclic dimer and trimer, while $(\text{Me}_3\text{Si})_2\text{PPh}$ gave a mixture of the two different insertion products shown in Scheme 3, which are in equilibrium.



Scheme 3. Reactivity of $(\text{Me}_3\text{Si})_2\text{PPh}$ with PhNCO reported by Itoh and co-workers.¹³

2.3 Conclusion

In extension of our previous investigations on the synthesis and characterization of 1,3-diphosphacyclobutadiene sandwich complexes,^{6,8} this study has shown that trimethylsilated complexes **2a**, **b** are readily accessible by salt metathesis of the previously known potassium salts **1a**, **b** with trimethylchlorosilane. Interestingly, we have found that the P–Si bond in these complexes is very reactive: Complex **2a** reacts with a range of ethers, including epoxides, as well as aldehydes, ketones, esters and phenyl isocyanate to afford functionalized 1,3-diphosphacyclobutadiene complexes. In particular, the reaction with cyclic ethers, cyclic esters and with the isocyanate indicates that this approach is a promising avenue to introduce functional groups and generate interesting new structures. The unselective nature of the insertion reaction of certain epoxides and aldehydes, and the sluggish reactivity of larger ketones represent limitations of this methodology. Nevertheless, these P–Si bond insertion reactions are a viable alternative to the previously established salt metathesis approach.^{6a} The insertion of other element-element bonds and an investigation of the subsequent reactivity of some of the new complexes such as **9** and **12** prepared in this study appear to be worthwhile targets for future investigations.

2.4 Supporting Information

2.4.1 General Procedures

All experiments were performed under an atmosphere of dry argon using standard Schlenk techniques or a MBraun UniLab glovebox. Solvents were dried and degassed with a MBraun SPS800 solvent purification system. Tetrahydrofuran, toluene, and diethyl ether were stored over molecular sieves (3 Å). *n*-Hexane was stored over a potassium mirror. NMR spectra were recorded on Bruker Avance 300 and Avance 400 spectrometers at 300 K and internally referenced to residual solvent resonances. Melting points were measured on samples in sealed capillaries on a Stuart SMP10 melting point apparatus and are uncorrected. UV/Vis spectra were recorded on an Ocean Optics Flame Spectrometer. Infrared spectra were recorded with an Agilent Cary 670 FTIR spectrometer equipped with a diamond ATR unit. Elemental analyses were determined by the analytical department of Regensburg University. Me₃SiCl was purchased from Sigma Aldrich and stored over molecular sieves (3 Å) prior to use. Ph₃SnCl was purchased from TCI and used as received. Styrene oxide, isobutylene oxide, 1,2-epoxyoctane, γ -butyrolactone, benzaldehyde, acetone, and PhNCO were purchased from Sigma Aldrich and distilled prior to use.

2.4.2 Synthesis and Characterization

2.4.2.1 Synthesis of [K(tol)₂{Co(η^4 -P₂C₂tBu₂)₂}] ([K(tol)₂][1a])

[K(tol)₂][1a] was obtained as a light red crystalline solid by recrystallization of [K(thf)₂{Co(P₂C₂tBu₂)₂}] ([K(thf)₂][1a], 9.65 g, 15.0 mmol) in hot toluene (ca. 350 mL) and storage at -18 °C overnight. The dried solid contains a variable amount of toluene molecules. The number of toluene molecules present per formula unit was determined by ¹H NMR spectroscopy individually on each sample. Yield 8.20 g (80%, *x* = 1.0); ¹H NMR (400.13 MHz, 300 K, [D₈]THF) δ /ppm = 1.06 (s, 36H, *t*Bu), 2.10 (s, 3H, toluene), 6.98–7.14 (m, 5H, toluene); ¹³C{¹H} NMR (100.61 MHz, 300 K, [D₈]THF) δ /ppm = 21.3 (s, toluene), 32.8 (s, C(CH₃)₃), 35.1 (s, C(CH₃)₃), 101.9 (t, ¹J_{C,P} = 55.8 Hz, P₂C₂), 125.8 (s, 4-C of toluene), 128.7 (s, 3,5-C of toluene), 129.5 (s, 2,6-C of toluene); The ipso-C_{tol} was not detected; ³¹P{¹H} NMR (161.98 MHz, 300 K, [D₈]THF) δ /ppm = 3.2 (s).

2.4.2.2 Synthesis of [K(tol)₂{Co(η^4 -P₂C₂tPent₂)₂}] ([K(tol)₂][1b])

[K(tol)₂][1b] was obtained as a light red crystalline solid by recrystallization of [K(thf)_{2.5}{Co(P₂C₂tPent₂)₂}] ([K(thf)₃][1b], 0.86 g, 1.17 mmol) in hot toluene (ca. 180 mL) and storage at -18 °C overnight. X-ray quality crystals were obtained from a concentrated toluene solution at -18 °C. The dried solid contains a variable amount of toluene molecules. The number of toluene molecules present per formula unit was determined by ¹H NMR spectroscopy individually on each sample. Yield 0.69 g (88%, *x* = 1.25); m.p. 180 °C; ¹H NMR (400.13 MHz,

300 K, [D₈]THF) δ = 0.90–0.94 (overlapping s and t, 36 H; C(CH₃)₂CH₂CH₃ and C(CH₃)₂CH₂CH₃), 1.45 (q, 8 H; C(CH₃)₂CH₂CH₃), 2.30 (s, 3.75 H; CH₃ of toluene); 7.06–7.17 (m, 6.25 H; CH of toluene). ¹³C{¹H} NMR (100.61 MHz, 300 K, [D₈]THF/C₇D₈ ca. 1:1) δ = 10.6 (s; C(CH₃)₂CH₂CH₃), 21.2 (s; CH₃ of toluene), 29.3 (s; C(CH₃)₂CH₂CH₃), 38.4 (s; C(CH₃)₂CH₂CH₃), 40.1 (s; C(CH₃)₂CH₂CH₃), 101.2 (t, ¹J_{C,P} = 51.93 Hz; P₂C₂ ring), 125.8 (s; 4-C of toluene), 129.5 (s; 3,5-C of toluene), 138.2 (s; 2,6-C of toluene). ³¹P{¹H} NMR (161.98 MHz, 300 K, [D₈]THF) δ = 9.6 (s); elemental analysis calcd. for C₂₄H₄₄CoKP₄ · 1.5 C₇H₈ (*M* = 692.76, calculated for a sample which contains 1.5 molecules toluene): C 59.82, H 8.12; found: C 59.97, H 8.12.

2.4.2.3 Synthesis of [Co(η⁴-P₂C₂tBu₂SiMe₃)(η⁴-P₂C₂tBu₂)] (2a)

A solution of Me₃SiCl in toluene (0.15 M, 5.7 mL, 0.87 mmol) was added to a solution of [K(tol)₂{Co(η⁴-P₂C₂tBu₂)₂}] ([K(tol)₂][**1a**], 0.43 g, 0.79 mmol) in toluene (30 mL). After stirring the reaction mixture overnight, the solvent was removed *in vacuo*. The residue was extracted with *n*-pentane (20 mL). The filtrate was concentrated to ca. 10 mL and stored at –35 °C. Red crystals of **2a** formed upon storage over two days. Complex **2a** is contaminated with variable amounts (3% to 23%) of the protonated compound [Co(C₂P₂tBu₂)₂H] (**A**). Attempts to remove the impurity by recrystallization or sublimation (1·10^{–3} mbar / 80 °C) failed due to the very similar solubility and sublimation properties of both compounds. The content of **A** was determined for each sample individually by ¹H NMR spectroscopy. Yield 0.32 g (77%); m.p. >135 °C (decomp. to a black oil); ¹H NMR (400.13 MHz, 300 K, C₆D₆) δ /ppm = 0.28 (d, ³J_{H,P} = 7 Hz, 9H, SiMe₃), 1.24 (s, 18H, *t*Bu), 1.30 (s, 18H, *t*Bu); ¹³C{¹H} NMR (100.61 MHz, 300 K, C₆D₆) δ /ppm = 1.0 (d, ²J_{C,P} = 12.4 Hz, SiMe₃), 32.6 (d, ³J_{C,P} = 3.4 Hz, C(CH₃)₃), 33.4 (d, ³J_{C,P} = 3.4 Hz, C(CH₃)₃), 33.6 (d, ³J_{C,P} = 4.1 Hz, C(CH₃)₃), 34.5 (dd, ²J_{C,P} = 2.8 Hz, ²J_{C,P} = 7.4 Hz, C(CH₃)₃), 35.7 (t, ²J_{C,P} = 7.4 Hz, C(CH₃)₃), 36.2 (t, ²J_{C,P} = 7.4 Hz, C(CH₃)₃), 86.0 (dd, ¹J_{C,P} = 10.5 Hz, ¹J_{C,P} = 62.5 Hz, P₂C₂), 113.8 (t, ¹J_{C,P} = 53.3 Hz, P₂C₂), 124.0 (t, ¹J_{C,P} = 56.0 Hz, P₂C₂); ³¹P{¹H} NMR (161.98 MHz, 300 K, C₆D₆) δ /ppm = –1.7 (s, 1P; P1), 19.2 (s, 1P; P2), 21.7 (s, 2P; P3 and P4); ²⁹Si DEPT NMR (79.49 MHz, 300 K, C₆D₆): δ = 12.0; UV/Vis (*n*-hexane, λ_{\max} /nm, (ϵ_{\max} /L·mol^{–1}·cm^{–1}): 277 (shoulder, 15200), 318 (10000), 370 (2600); the sample which was submitted for elemental analysis was contaminated with 5% of [Co(P₂C₂tBu₂)₂H] (**A**): elemental analysis calcd. for C₂₃H₄₅CoP₄Si · 0.05**A** (*M* = 555.54): C 51.89, H 8.50, found: C 52.12, H 8.53.

2.4.2.4 Synthesis of [Co(η⁴-P₂C₂tPent₂SiMe₃)(η⁴-P₂C₂tPent₂)] (2b)

A solution of Me₃SiCl in toluene (0.39 M, 1.45 mmol, ca. 3.7 mL) was added to a suspension of [K(tol)_{1.5}{Co(P₂C₂tPent₂)₂}] ([K(tol)₂][**1b**], 0.91 g, 1.32 mmol) in toluene (60 mL) at room temperature. The reaction mixture was stirred overnight whereupon a dark red solution was formed. The solvent was then removed *in vacuo* and the deep red residue was dissolved in ca. 50 mL *n*-pentane. The dark red solution was filtered and concentrated to ca. 10 mL. Dark reddish

brown crystals of complex **2b** were isolated after storage at $-78\text{ }^{\circ}\text{C}$ for three days. Compound **2b** is contaminated with ca. 7% $[\text{CoH}(\text{P}_2\text{C}_2\text{tPent}_2)_2]$ (**A'**) according to the ^1H NMR spectrum and elemental analysis and with small amounts of an unidentified silicon containing species ($\delta(^{29}\text{Si}) = 7.5$ and -21.4 ppm) according to the ^{29}Si NMR spectrum. The isolated compound still contains traces (0.13 molecules per formulat unit) of *n*-pentane after drying in *vacuo* for 45 min according to the ^1H -NMR spectrum. X-ray quality crystals of **2b** were obtained by storing a concentrated *n*-pentane solution at $-78\text{ }^{\circ}\text{C}$ for three days. Yield 0.56 g (72%); m.p. $170\text{ }^{\circ}\text{C}$ (decomp.). ^1H NMR (400.13 MHz, 300 K, C_6D_6) δ /ppm = 0.28 (d, $^3J_{\text{P,H}} = 7.9$ Hz, 9H; SiMe_3), 0.86 (t, 0.8 H; CH_3 of *n*-pentane), 1.00–1.34 (overlapping s, t and q, 42 H; $\text{C}(\text{CH}_3)_3\text{CH}_2\text{CH}_3$ and $\text{C}(\text{CH}_3)_3\text{CH}_2\text{CH}_3$ and $\text{C}(\text{CH}_3)_3\text{CH}_2\text{CH}_3$ of **2b** and **A'**, CH_2 of *n*-pentane), 1.46–1.73 (overlapping q, 7H; $\text{C}(\text{CH}_3)_3\text{CH}_2\text{CH}_3$ of **2b** and **A'**). $^{13}\text{C}\{^1\text{H}\}$ NMR (100.61 MHz, 300 K, C_6D_6) δ /ppm = -1.0 (d, $^2J_{\text{C,P}} = 8.3$ Hz; SiMe_3), 10.0–10.4 (br. overlapping s; $\text{C}(\text{CH}_3)_3\text{CH}_2\text{CH}_3$), 14.2 (s; CH_3 of *n*-pentane), 22.7 (s; 2,4- CH_2 of *n*-pentane), 27.4 (s; $\text{C}(\text{CH}_3)_2\text{CH}_2\text{CH}_3$), 29.1 (s; $\text{C}(\text{CH}_3)_2\text{CH}_2\text{CH}_3$), 29.9 (s; $\text{C}(\text{CH}_3)_2\text{CH}_2\text{CH}_3$), 32.2 (s; $\text{C}(\text{CH}_3)_2\text{CH}_2\text{CH}_3$), 34.4 (s; 3- CH_2 of *n*-pentane), 37.2 (s; $\text{C}(\text{CH}_3)_2\text{CH}_2\text{CH}_3$), 38.3 (s; $\text{C}(\text{CH}_3)_2\text{CH}_2\text{CH}_3$), 38.9–39.3 (overlapping s; $\text{C}(\text{CH}_3)_2\text{CH}_2\text{CH}_3$). The signals for the C_2P_2 rings were not observed. ^{31}P NMR (161.98 MHz, 300 K, C_6D_6) δ /ppm = 25.5 (s, $\nu_{\text{FWHM}} = 12.9$ Hz, 2P; P3 and P4), 23.1 (s, $\nu_{\text{FWHM}} = 17.2$ Hz, 1P; P2), -2.6 (br s, $\nu_{\text{FWHM}} = 40.9$ Hz, 1P; P1). $^{31}\text{P}\{^1\text{H}\}$ NMR (161.98 MHz, 300 K, C_6D_6): δ /ppm = 25.6 (s, 2P; P3 and P4), 23.1 (s, 1P; P2), -2.6 (s, 1P; P1). ^{29}Si DEPT NMR (79.49 MHz, 300 K, C_6D_6): δ /ppm = 11.8 (dd, $^1J_{\text{Si,P}} = 28.6$ Hz, $^3J_{\text{Si,P}} = 23.8$ Hz), 7.5 (impurity), -21.4 (impurity). UV/Vis (*n*-hexane, $\lambda_{\text{max}}/\text{nm}$ ($\epsilon_{\text{max}}/\text{dm}^3\text{mol}^{-1}\text{cm}^{-1}$): 251 (26500); 281 (shoulder); 326 (13500); elemental analysis calcd. for $0.93(\text{C}_{27}\text{H}_{53}\text{CoP}_4\text{Si}) \cdot 0.07(\text{C}_{24}\text{H}_{45}\text{CoP}_4) \cdot 0.13\text{C}_5\text{H}_{12}$ ($M = 592.96$): C 55.58, H 9.18; found: C 55.41, H 8.70.

2.4.2.5 Synthesis of $[\text{Co}(\eta^4\text{-P}_2\text{C}_2\text{tBu}_2(\text{CH}_2)_4\text{OSiMe}_3)(\eta^4\text{-P}_2\text{C}_2\text{tBu}_2)]$ (**3a**)

Compound **3a** was prepared by adding a solution of Me_3SiCl in toluene (0.39 M, 0.39 mmol, ca. 1.0 mL) to a suspension of $[\text{K}(\text{thf})_{1.75}\{\text{Co}(\text{P}_2\text{C}_2\text{tBu}_2)_2\}]$ ($[\text{K}(\text{thf})_2][\mathbf{1a}]$, 0.20 g, 0.35 mmol) in toluene (ca. 35 mL) at room temperature. The reaction mixture was stirred overnight at room temperature whereupon a light red solution was formed. The solvent was then removed in *vacuo*, and the dark red residue was dissolved in ca. 25 mL *n*-hexane. After filtration the solution was concentrated to ca. 10 mL. Complex **3a** precipitated as a red oily solid after storage at $-18\text{ }^{\circ}\text{C}$ for ten days. Yield: 79 mg (37%). An elemental analysis could not be performed due to the oily consistence of the isolated compound. ^1H NMR (400.13 MHz, 300 K, C_6D_6) δ /ppm = 0.06 (s with ^{29}Si satellites, $^2J_{\text{Si,H}} = 6.5$ Hz, 9H; SiMe_3), 1.23 (s, 18 H; *t*Bu), 1.28 (s, 9H; *t*Bu), 1.32 (s, 9H; *t*Bu), 1.42 (m, 2H; $\text{PCH}_2\text{CH}_2\text{CH}_2\text{CH}_2\text{O}$), 2.04 (m, 2H; $\text{PCH}_2\text{CH}_2\text{CH}_2\text{CH}_2\text{O}$), 2.33 (m, 2H; $\text{PCH}_2\text{CH}_2\text{CH}_2\text{CH}_2\text{O}$), 3.37 (t, $^3J_{\text{H,H}} = 5.64$ Hz, 2H; $\text{PCH}_2\text{CH}_2\text{CH}_2\text{CH}_2\text{O}$). $^{13}\text{C}\{^1\text{H}\}$ NMR (100.61 MHz, 300 K, C_6D_6) δ /ppm = -0.6 (s; SiMe_3), 25.2 (d, $^2J_{\text{C,P}} = 7.7$ Hz;

PCH₂CH₂CH₂CH₂O), 27.8 (dd, ¹J_{C,P} = 19.6 Hz, ³J_{C,P} = 6.8 Hz; PCH₂CH₂CH₂CH₂O), 32.3 (very br s; PCH₂CH₂CH₂CH₂O), 33.0–33.9 (br overlapping s; C(CH₃)₃ of *t*Bu), 35.8–36.2 (very br overlapping s; C(CH₃)₃ of *t*Bu), 61.3 (s; PCH₂CH₂CH₂CH₂O), 77.8 (dd, ¹J_{C,P} = 66.5 Hz, ³J_{C,P} = 3.3 Hz; substituted P₂C₂ ring), 114.4 (t, ¹J_{C,P} = 51.4 Hz; free P₂C₂ ring), 122.2 (d, ¹J_{C,P} = 54.6 Hz; free P₂C₂ ring). ³¹P{¹H} NMR (161.98 MHz, 300 K, C₆D₆, labeling scheme analogous to **2a**) δ /ppm = –50.0 (d, ²J_{P,P} = 15 Hz, 1P; P2), 25.8 (s, 2P; P3 and P4), 55.5 (d, ²J_{P,P} = 15 Hz, 1P; P1). ²⁹Si DEPT NMR (79.49 MHz, 300 K, C₆D₆) δ / ppm = 17.2.

2.4.2.6 Synthesis of [Co(η⁴-P₂C₂*t*Pent₂(CH₂)₄OSiMe₃)(η⁴-P₂C₂*t*Pent₂)] (**3b**)

Compound **3b** was prepared by two synthetic routes:

Method A: A solution of Me₃SiCl in toluene (0.39 M, 0.35 mmol, ca 0.9 mL) was added to a light red solution of [K(thf)_{1.25}{Co(P₂C₂*t*Pent₂)₂}] ([K(thf)₃][**1b**], 0.21 g; 0.31 mmol) in THF (ca. 40 mL) at room temperature. After the reaction mixture had been stirred overnight the solvent was removed in *vacuo*, and the red residue was dissolved in ca. 30 mL *n*-pentane. The mixture was filtered, and the solvent was evaporated to dryness. Complex **3b** was obtained as a dark red oil. Complex **3b** is contaminated with the protonated compound [CoH(C₂P₂*t*Pent₂)₂] (**A'**) (ca. 16% according to ¹H NMR spectroscopy). Attempts to remove the impurity by recrystallization failed due to the similar solubility of both compounds. Yield: 0.12 g (56%); ¹H NMR (400.13 MHz, 300 K, C₆D₆) δ /ppm = 0.06 (s with ²⁹Si satellites, ²J_{Si,H} = 6.5 Hz, 9H; SiMe₃), 0.96–1.18 (overlapping s, and t, 40 H; C(CH₃)₂CH₂CH₃ and C(CH₃)₂CH₂CH₃ of **3b** and **A'**), 1.35–1.50 (overlapping q and m, 5H; C(CH₃)₂CH₂CH₃ of **3b** and **A'** and PCH₂CH₂CH₂CH₂O), 1.62–1.69 (overlapping q, 6H; C(CH₃)₂CH₂CH₃ of **3b** and **A'**), 2.01 (m, 2H; PCH₂CH₂CH₂CH₂O), 2.38 (m, 2H; PCH₂CH₂CH₂CH₂O), 3.36 (t, ³J_{H,H} = 5.77 Hz, 2H; PCH₂CH₂CH₂CH₂O). ¹³C{¹H} NMR (100.61 MHz, 300 K, C₆D₆) δ /ppm = –0.6 (s; SiMe₃), 10.0 (s; C(CH₃)₃CH₂CH₃), 10.3 (s; C(CH₃)₃CH₂CH₃), 10.4 (s; C(CH₃)₃CH₂CH₃), 25.2 (d, ¹J_{C,H} = 7.1 Hz; PCH₂CH₂CH₂CH₂O), 27.8–29.7 (overlapping s; C(CH₃)₂CH₂CH₃), 33.5 (d, ¹J_{C,P} = 12.9 Hz; PCH₂CH₂CH₂CH₂O), 36.7 (d, ¹J_{C,H} = 5.6 Hz; PCH₂CH₂CH₂CH₂O), 38.4–38.7 (br overlapping s; C(CH₃)₃CH₂CH₃), 38.9 (br s; C(CH₃)₃CH₂CH₃), 39.2 (br s; C(CH₃)₃CH₂CH₃), 39.6 (br s; C(CH₃)₃CH₂CH₃), 61.3 (s; PCH₂CH₂CH₂CH₂O), 77.0 (d, ¹J_{C,P} = 66.1 Hz; substituted P₂C₂ ring), 113.2 (t, ¹J_{C,P} = 54.3 Hz; free P₂C₂ ring), 120.4 (t, ¹J_{C,P} = 54.8 Hz; free P₂C₂ ring). ³¹P{¹H} NMR (161.98 MHz, 300 K, C₆D₆) δ /ppm = –45.5 (d, ²J_{P,P} = 15 Hz, 1P; P2), 29.4 (s, 2P; P3 and P4), 55.4 (d, ²J_{P,P} = 15 Hz, 1P; P1). ²⁹Si DEPT NMR (79.49 MHz, 300 K, C₆D₆): δ / ppm = 17.2.

Method B: Complex **2b** (69 mg; 0.12 mmol) was dissolved in ca. 1 mL THF at room temperature and stirred overnight. The deep red solution was then filtered and evaporated to dryness giving complex **3b** as red oil in 59% yield (46 mg). The isolated compound was contaminated with ca. 7% [CoH(P₂C₂*t*Pent₂)₂] (**A'**) (according to the ¹H-NMR spectrum) due to presence of **A'** in the

starting material **2b**. The spectroscopic properties for this sample are identical within experimental error to that of the sample prepared by method A.

2.4.2.7 Synthesis of $[\text{Co}(\eta^4\text{-P}_2\text{C}_2\text{Ad}_2(\text{CH}_2)_4\text{OSiMe}_3)(\eta^4\text{-P}_2\text{C}_2\text{Ad}_2)]$ (**3c**)

Me_3SiCl (0.13 mL, 1.0 mmol) was added to a light red solution of $[\text{K}(\text{thf})_4\{\text{Co}(\text{P}_2\text{C}_2\text{Ad}_2)_2\}]$ ($[\text{K}(\text{thf})_4][\mathbf{1c}]$, 1.1 g, 1.0 mmol) in THF (ca. 45 mL) at room temperature, and the reaction mixture was stirred overnight. The solvent was then removed in *vacuo*, and the deep red residue was dissolved in ca 30 mL *n*-hexane, filtered, and concentrated to ca. 15 mL. Complex **3c** precipitates as a red solid after storage at $-18\text{ }^\circ\text{C}$ for two days. Crystals suitable for X-ray crystallography were obtained from a concentrated toluene solution at $-18\text{ }^\circ\text{C}$. The isolated compound still contains one *n*-hexane molecule per formula unit after drying in *vacuo* for 30 min according to the ^1H NMR spectrum. Complex **3c** is contaminated with the protonated compound $[\text{Co}(\text{P}_2\text{C}_2\text{Ad}_2)_2\text{H}]$ (**A''**) (ca. 12% according to ^1H NMR spectroscopy). Attempts to remove the impurity by recrystallization failed due to the similar solubility of both compounds. Yield: 0.35 g (38%); m.p. $235\text{ }^\circ\text{C}$ (decomp.). ^1H NMR (400.13 MHz, 300 K, C_6D_6) δ /ppm = 0.09 (s with ^{29}Si satellites, $^2J_{\text{Si,H}} = 6.5\text{ Hz}$, 9H; SiMe_3), 0.89 (t, 6 H; CH_3 of *n*-hexane), 1.24 (br m, 8H; CH_2 of *n*-hexane), 1.49–2.24 (overlapping m, 69 H; Ad-H of **3c**, Ad-H of **A''**, $\text{PCH}_2\text{CH}_2\text{CH}_2\text{CH}_2\text{O}$), 2.21 (m, 2H; $\text{PCH}_2\text{CH}_2\text{CH}_2\text{CH}_2\text{O}$), 2.59 (m, 2H; $\text{PCH}_2\text{CH}_2\text{CH}_2\text{CH}_2\text{O}$), 3.44 (t, $^3J_{\text{H,H}} = 5.64\text{ Hz}$, 2H; $\text{PCH}_2\text{CH}_2\text{CH}_2\text{CH}_2\text{O}$). $^{13}\text{C}\{^1\text{H}\}$ NMR (100.61 MHz, 300 K, C_6D_6 , see Figure S1 for the labeling scheme) δ /ppm = -0.6 (s; SiMe_3), 14.3 (s; CH_3 of *n*-hexane), 23.1 (s; 2- CH_2 and of *n*-hexane), 26.2 (d, $^2J_{\text{C,P}} = 7.7\text{ Hz}$; $\text{PCH}_2\text{CH}_2\text{CH}_2\text{CH}_2\text{O}$), 29.3 (br s; C-3, C-5 and C-7 of Ad), 29.5 (br s; C-3, C-5 and C-7 of Ad), 29.6 (br s; C-3, C-5 and C-7 of Ad), 31.9 (s; 3- CH_2 of *n*-hexane), 33.7 (d, $^1J_{\text{C,P}} = 12.4\text{ Hz}$; $\text{PCH}_2\text{CH}_2\text{CH}_2\text{CH}_2\text{O}$), 35.3 (d, $^3J_{\text{C,P}} = 6.9\text{ Hz}$; $\text{PCH}_2\text{CH}_2\text{CH}_2\text{CH}_2\text{O}$), 36.7 (br s; C-1 of Ad), 36.9 (br s; C-4, C-6 and C-10 of Ad), 37.1 (br s; C-4, C-6 and C-10 of Ad), 37.1 (br s; C-4, C-6 and C-10 of Ad), 46.0 (br s; C-2, C-3 and C-9 of Ad), 46.4 (br s; C-2, C-3 and C-9 of Ad), 47.1 (br s; C-2, C-3 and C-9 of Ad), 61.6 (s; $\text{PCH}_2\text{CH}_2\text{CH}_2\text{CH}_2\text{O}$). The signals for the P_2C_2 rings were not observed. $^{31}\text{P}\{^1\text{H}\}$ NMR (161.98 MHz, 300 K, C_6D_6) δ /ppm = -57.3 (d, $^2J_{\text{P,P}} = 16\text{ Hz}$, 1P; P2), 19.1 (s, 2P; P3 and P4), 55.5 (d, $^2J_{\text{P,P}} = 16\text{ Hz}$, 1P; P1). ^{29}Si DEPT NMR (79.49 MHz, 300 K, C_6D_6) δ /ppm = 16.8.

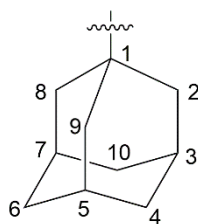


Figure S1. Labeling scheme adamantyl substituent.

2.4.2.8 Synthesis of $[\text{Co}(\eta^4\text{-P}_2\text{C}_2\text{tBu}_2\text{PhC}_2\text{H}_3\text{OSiMe}_3)(\eta^4\text{-P}_2\text{C}_2\text{tBu}_2)]$ (**5**)

Styrene oxide (16 mg, 0.13 mmol) was added to a solution of **2a** (84 mg, 0.13 mmol) in *n*-hexane. After stirring the reaction mixture for 60 min the solvent was removed *in vacuo*. In order to remove the hydride compound $[\text{Co}(\eta^4\text{-P}_2\text{C}_2\text{R}_2)_2\text{H}]$ (**A**) present from the contaminated starting material (ca. 23%) the residue was redissolved in THF (1.5 mL) and treated with NaH (1 mg, 0.04 mmol). After stirring the reaction mixture for further 60 min the solvent was removed *in vacuo*. The residue was extracted with *n*-hexane (4 mL). Dark orange crystals formed upon storage over two days. Yield 69 mg (80%); m.p. >178 °C (decomp. to a black oil); ^1H NMR (400.13 MHz, 300 K, C_6D_6) δ /ppm = 0.25 (br, 9H, SiMe₃), 1.15 (s, 18H, *t*Bu), 1.28 (s, 9H, *t*Bu), 1.42 (s, 9H, *t*Bu), 1.54 (br, 1H, Ph-CH-CH₂), 5.88 (d, $^3J_{\text{H,H}} = 51.7$ Hz, 1H, Ph-CH-CHH), 6.25 (d, $^3J_{\text{H,H}} = 23.2$ Hz, 1H, Ph-CH-CHH), 7.01–7.13 (m, 3H, m-/p-H_{Ar}), 7.61 (d, $^3J_{\text{H,H}} = 7.9$ Hz, 2H, o-H_{Ar}); $^{13}\text{C}\{^1\text{H}\}$ NMR (100.61 MHz, 300 K, C_6D_6) δ /ppm = 4.7 (br, SiMe₃), 32.4 (br, C(CH₃)₃), 32.9 (br, C(CH₃)₃), 33.2 (br, C(CH₃)₃), 34.2 (dd, $^2J_{\text{C,P}} = 7.4$ Hz, $^2J_{\text{C,P}} = 2.1$ Hz, C(CH₃)₃), 36.0 (t, $^2J_{\text{C,P}} = 7.2$ Hz, C(CH₃)₃), 36.1 (t, $^2J_{\text{C,P}} = 7.2$ Hz, C(CH₃)₃), 77.3 (d, $^1J_{\text{C,P}} = 65.7$ Hz, C₂P₂), 113.6 (t, $^1J_{\text{C,P}} = 53.8$ Hz, C₂P₂), 127.7 (overlapping with solvent signal, o-C_{Ar}), 128.6 (s, p-C_{Ar}), 129.0 (d, $^1J_{\text{C,P}} = 4.7$ Hz, C₂P₂), 129.3 (s, m-C_{Ar}), 130.5 (d, $^2J_{\text{C,P}} = 21.6$ Hz, PCH(Ph)CH₂OSiMe₃), 137.5 (dd, $^1J_{\text{C,P}} = 13.7$ Hz, $^3J_{\text{C,P}} = 4.7$ Hz, PCH(Ph)CH₂OSiMe₃), 138.2 (d, $^2J_{\text{C,P}} = 2.9$ Hz, ipso-C_{Ar}); $^{31}\text{P}\{^1\text{H}\}$ NMR (161.98 MHz, 300 K, C_6D_6) δ /ppm = -26.0 (d, $^2J_{\text{P,P}} = 13.7$ Hz, 1P; P2), 25.5 (s, 2P; P3 and P4), 60.8 (d, $^2J_{\text{P,P}} = 13.7$ Hz, 1P; P1); UV/Vis (*n*-hexane, λ_{max} /nm, (ϵ_{max} /L·mol⁻¹·cm⁻¹): 280 (10800), 344 (shoulder, 4200); IR(ATR) ($\tilde{\nu}$ / cm⁻¹): 2944(s), 2921(w), 2892(w), 2856(w), 1452(s); elemental analysis calcd. for C₃₁H₅₃CoOP₄Si (M = 652.68): C 57.05, H 8.19, found: C 57.32, H 7.98.

2.4.2.9 Synthesis of 6/6' and 7/7' (NMR experiments)

Isobutylene oxide (8 mg, 0.1 mmol) or 1,2-epoxyoctane (13 mg, 0.1 mmol) were added to solutions of **2a** (24 mg, 0.05 mmol) in C_6D_6 (0.5 mL). The NMR samples were submitted for measurements after one, seven, and 27 hours. No changes in ratios were observed for the different reaction times. $^{31}\text{P}\{^1\text{H}\}$ NMR (161.98 MHz, 300 K, C_6D_6) of **6**: δ /ppm = -22.4 (d, $^2J_{\text{P,P}} = 17.5$ Hz, 1P; P2), 24.7 (s, 2P; P3 and P4), 81.8 (d, $^2J_{\text{P,P}} = 17.5$ Hz, 1P; P1); **6'**: δ /ppm = -46.2 (d, $^2J_{\text{P,P}} = 33.7$ Hz, 1P; P2), -35.4 (d, $^2J_{\text{P,P}} = 33.7$ Hz, 1P; P1), 81.8 (s, 2P; P3 and P4); **7**: δ /ppm = -57.8 (d, $^2J_{\text{P,P}} = 16.2$ Hz, 1P; P2), 25.9 (s, 1P; P3 or P4), 26.5 (s, 1P; P4 or P3), 29.8 (d, $^2J_{\text{P,P}} = 16.2$ Hz, 1P; P1); **7'**: δ /ppm = -29.6 (d, $^2J_{\text{P,P}} = 15.0$ Hz, 1P; P2), 23.7 (s, 1P; P3 or P4), 25.2 (s, 1P; P4 or P3), 72.0 (d, $^2J_{\text{P,P}} = 15.0$ Hz, 1P; P1).

2.4.2.10 Synthesis of $[\text{Co}(\eta^4\text{-P}_2\text{C}_2\text{tBu}_2\text{Et})(\eta^4\text{-P}_2\text{C}_2\text{tBu}_2)]$ (**8**, NMR experiment)

Diethyl ether (13 mg, 0.18 mmol) was added to a solution of **2a** (37 mg, 0.06 mmol) in C_6D_6 . Subsequently, the reaction mixture was heated to 60 °C for two hours. $^{31}\text{P}\{^1\text{H}\}$ NMR

(161.98 MHz, 300 K, C₆D₆) δ / ppm = -47.9 (d, $^2J_{P,P}$ = 14.6 Hz, 1P; P2), 25.6 (s, 2P; P3 and P4), 60.9 (d, $^2J_{P,P}$ = 14.6 Hz, 1P; P1).

2.4.2.11 Synthesis of [Co(η^4 -P₂C₂tBu₂(CH₂)₃COOSiMe₃)(η^4 -P₂C₂tBu₂)] (9)

γ -Butyrolactone (30 mg, 0.35 mmol) was added to a solution of **2a** (0.12 g, 0.17 mmol) in *n*-hexane. After stirring the reaction mixture for 30 min the solvent and volatiles were removed *in vacuo*. The residue was redissolved in *n*-hexane (2 mL). Dark orange crystals formed upon storage over one day at -35 °C. According to the ¹H NMR spectrum **9** was contaminated with 18% of [Co(η^4 -P₂C₂R₂)₂H] (**A**). Yield 67 mg (56%); m.p. >176 °C (decomp. to a black oil); ¹H NMR (400.13 MHz, 300 K, C₆D₆) δ / ppm = 0.21 (s, with ²⁹Si satellites, $^2J_{Si,H}$ = 7.0 Hz, 9H, SiMe₃), 1.22 (s, 18H, *t*Bu), 1.26 (s, 9H, *t*Bu), 1.32 (s, 18H, *t*Bu), 2.03–2.14 (m, 4H, lactone), 2.31–2.41 (m, 2H, lactone); ¹³C{¹H} NMR (100.61 MHz, 300 K, C₆D₆) δ / ppm = -0.4 (s, SiMe₃), 23.8 (d, $^2J_{C,P}$ = 6.8 Hz, PCH₂CH₂CH₂COO), 27.0 (dd, $^3J_{C,P}$ = 6.0 Hz, $^1J_{C,P}$ = 20.7 Hz, PCH₂CH₂CH₂COO), 33.0 (br d, $^3J_{C,P}$ = 4.1 Hz, C(CH₃)₃), 33.2 (br d, $^3J_{C,P}$ = 3.0 Hz, C(CH₃)₃), 33.9 (m, C(CH₃)₃), 35.7 (d, $^2J_{C,P}$ = 13.3 Hz C(CH₃)₃), 35.8 (t, $^2J_{C,P}$ = 7.3 Hz, C(CH₃)₃), 36.1 (t, $^2J_{C,P}$ = 7.2 Hz, C(CH₃)₃), 36.2 (overlapping with *t*Bu signals, PCH₂CH₂CH₂COO), 78.1 (dd, $^1J_{C,P}$ = 2.6 Hz, 67.2 Hz, C₂P₂) 114.6 (t, $^1J_{C,P}$ = 58.0 Hz, C₂P₂), 122.8 (t, $^1J_{C,P}$ = 55.0 Hz, C₂P₂), 172.1 (s, PCH₂CH₂CH₂COO); ³¹P{¹H} NMR (161.98 MHz, 300 K, C₆D₆) δ / ppm = -48.7 (d, $^2J_{P,P}$ = 14.9 Hz, 1P; P2), 26.1 (s, 2P; P3 and P4), 54.0 (d, $^2J_{P,P}$ = 14.9 Hz, 1P; P1); UV/Vis (THF, λ_{max} /nm, (ϵ_{max} /L·mol⁻¹·cm⁻¹): 274 (79800), 302 (shoulder, 46700), 333 (shoulder, 26700); elemental analysis calcd. for C₂₇H₅₁P₄CoO₂Si · 0.18A (M = 701.48): C 52.39, H 8.29, found: C 53.10, H 7.85.

2.4.2.12 Synthesis of [Co(η^4 -P₂C₂tBu₂CH(Ph)OSiMe₃)(η^4 -P₂C₂tBu₂)] (10)

Benzaldehyde (21 mg, 0.20 mmol) was added to a solution of **2a** (0.11 g, 0.20 mmol) in toluene (3 mL). After stirring the reaction mixture for 30 min the solvent and volatiles were removed *in vacuo*. The residue was sublimed (10⁻² mbar / 80 °C) to remove [Co(η^4 -P₂C₂R₂)₂H] (**A**). Red crystals formed after redissolving in *n*-hexane upon storage over one day at -35 °C. Yield 92 mg (72%); m.p. >172 °C (decomp. to a black oil); ¹H NMR (400.13 MHz, 300 K, C₆D₆) δ / ppm = -0.09 (s, 9H, SiMe₃), 1.08 (s, 9H, *t*Bu), 1.29 (s, 9H, *t*Bu), 1.30 (s, 9H, *t*Bu), 1.40 (s, 9H, *t*Bu), 5.95 (d, $^2J_{H,P}$ = 5.8 Hz, 1H, CH(Ph)), 6.97–7.10 (m, 3H, *o*-/*p*-H_{Ar}), 7.40–7.47 (m, 2H, *m*-H_{Ar}); ¹³C{¹H} NMR (100.61 MHz, 300 K, C₆D₆) δ / ppm = 0.0 (s, with ²⁹Si satellites, $^1J_{C,Si}$ = 59 Hz, SiMe₃), 32.9 (br d, $^3J_{C,P}$ = 4.0 Hz, C(CH₃)₃), 33.3 (br, C(CH₃)₃), 33.4 (br, C(CH₃)₃), 33.8 (br, C(CH₃)₃), 34.1 (dd, $^2J_{C,P}$ = 1.5 Hz, 7.4 Hz, C(CH₃)₃), 36.1 (t, $^2J_{C,P}$ = 7.3 Hz, C(CH₃)₃), 36.2 (t, $^2J_{C,P}$ = 7.6 Hz, C(CH₃)₃), 76.4 (dd, $^1J_{C,P}$ = 10.4 Hz, $^3J_{C,P}$ = 5.4 Hz, PCH(Ph)), 77.4 (dd, $^1J_{C,P}$ = 5.2 Hz, 65.3 Hz, C₂P₂), 78.5 (dd, $^1J_{C,P}$ = 9.1 Hz, 65.1 Hz, C₂P₂), 113.6 (t, $^1J_{C,P}$ = 53.3 Hz, C₂P₂), 128 (overlapping with solvent signal, *p*-C_{Ar}), 129.1 (d, $^4J_{C,P}$ = 1.3 Hz, *m*-C_{Ar}), 129.6 (d, $^3J_{C,P}$ = 2.4 Hz, *o*-C_{Ar}), 139.4 (s, *ipso*-C_{Ar}); ³¹P{¹H} NMR (161.98 MHz, 300 K, C₆D₆)

δ /ppm = –39.9 (d, $^2J_{P,P}$ = 18.5 Hz, 1P; P2), 25.0 (s, 1P; P3 or P4), 28.0 (s, 1P; P3 or P4), 75.2 (d, $^2J_{P,P}$ = 18.5 Hz, 1P; P1); IR(ATR) ($\tilde{\nu}$ / cm^{-1}): 2951(s), 2918(w), 2892(w), 2855(w), 1452(s); UV/Vis (*n*-hexane, λ_{max} /nm, (ϵ_{max} / $\text{L}\cdot\text{mol}^{-1}\cdot\text{cm}^{-1}$): 304 (34500), 346 (shoulder, 17800), 420 (shoulder, 4500); elemental analysis calcd. for $\text{C}_{30}\text{H}_{51}\text{CoOP}_4\text{Si}$ (M = 638.60): C 56.42, H 8.05, found: C 56.62, H 7.59.

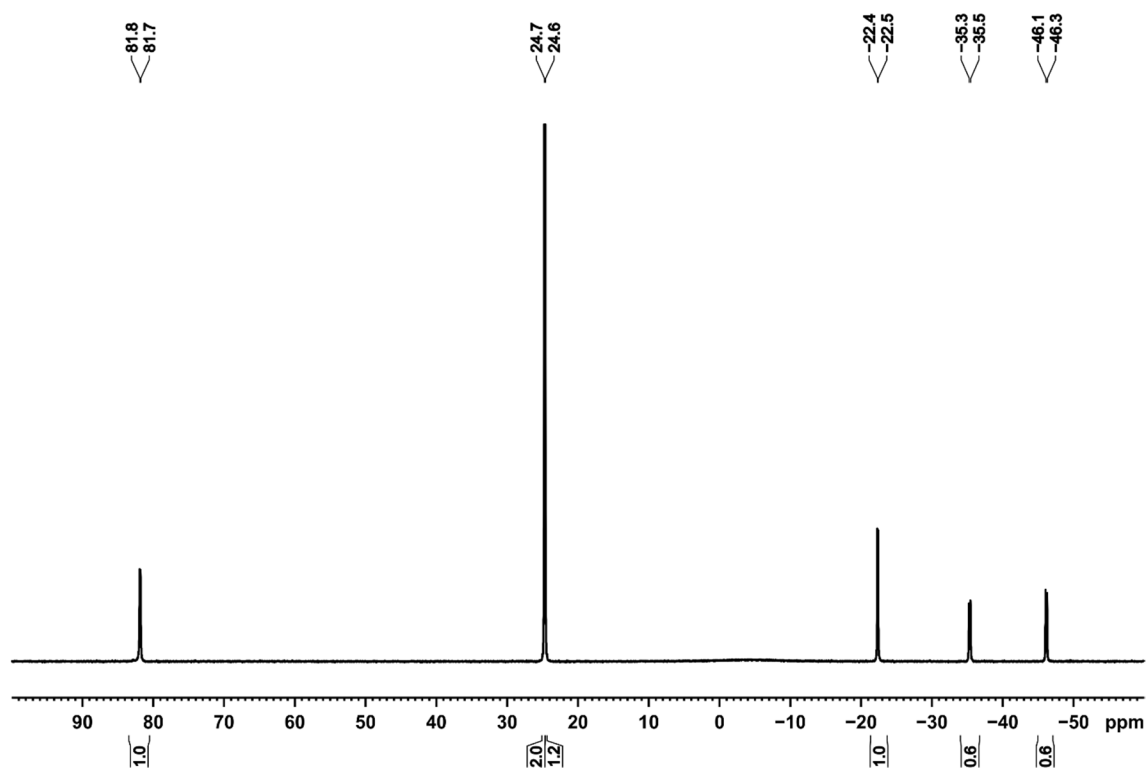
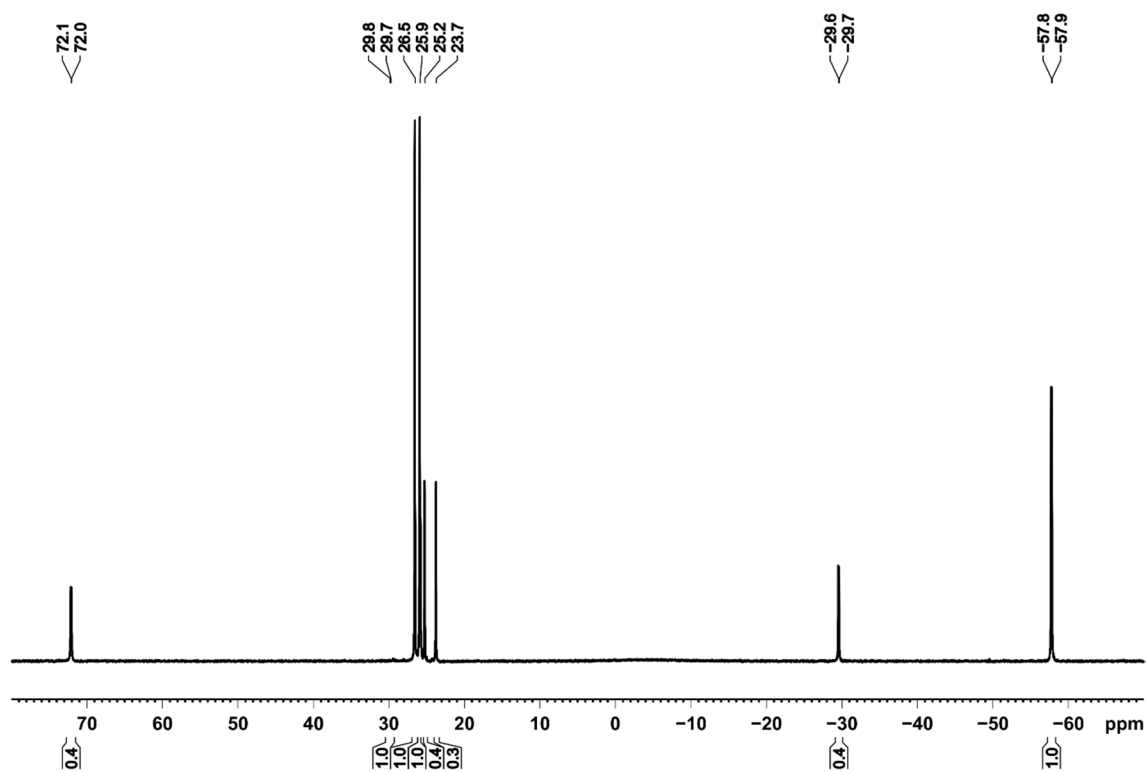
2.4.2.13 Synthesis of $[\text{Co}(\eta^4\text{-P}_2\text{C}_2\text{tBu}_2\text{CHMe}_2\text{OSiMe}_3)(\eta^4\text{-P}_2\text{C}_2\text{tBu}_2)]$ (11)

Acetone (7 mg, 0.12 mmol) was added to a solution of **2a** (67 mg, 0.10 mmol) in *n*-hexane (2 mL). After stirring the reaction mixture for 30 min the solvent and volatiles were removed *in vacuo*. The residue was redissolved in a minimum amount of *n*-hexane (1 mL). Dark orange crystals formed upon storage over one day at –35 °C. According to the ^1H NMR spectrum **11** is contaminated with 18% of **A**. Yield 55 mg (82%); m.p. >118 °C (decomp. to a black oil); ^1H NMR (400.13 MHz, 300 K, C_6D_6) δ /ppm = 0.02 (s, with ^{29}Si satellites, $^2J_{\text{Si,H}}$ = 6.5 Hz, 9H, SiMe_3), 1.30 (br, 27H, *t*Bu), 1.37 (s, 9H, *t*Bu), 1.66 (s, 3H, CH_3), 1.70 (s, 3H, CH_3); $^{13}\text{C}\{^1\text{H}\}$ NMR (100.61 MHz, 300 K, C_6D_6) δ /ppm = 2.4 (s, SiMe_3), 31.6 (s, $-\text{OC}(\text{CH}_3)_2$), 31.7 (s, $-\text{OC}(\text{CH}_3)_2$), 32.9 (br, $\text{C}(\text{CH}_3)_3$), 33.5 (br, $\text{C}(\text{CH}_3)_3$), 33.9 (m, $\text{C}(\text{CH}_3)_3$), 35.8 (t, $^2J_{\text{C,P}}$ = 7.2 Hz, $\text{C}(\text{CH}_3)_3$), 36.2 (t, $^2J_{\text{C,P}}$ = 7.0 Hz, $\text{C}(\text{CH}_3)_3$), 74.9 (dd, $^1J_{\text{C,P}}$ = 64.3 Hz, $^3J_{\text{C,P}}$ = 10.6 Hz, C_2P_2), 80.0 (d, $^1J_{\text{C,P}}$ = 4.7 Hz, $-\text{C}(\text{O})(\text{CH}_3)_2$), 128.0 (overlapping with solvent signal, C_2P_2); $^{31}\text{P}\{^1\text{H}\}$ NMR (161.98 MHz, 300 K, C_6D_6) δ /ppm = –27.0 (d, $^2J_{\text{P,P}}$ = 20.4 Hz, 1P; P2), 25.8 (s, 1P; P3 and P4), 90.5 (d, $^2J_{\text{P,P}}$ = 20.4 Hz, 1P; P1); UV/Vis (*n*-hexane, λ_{max} /nm, (ϵ_{max} / $\text{L}\cdot\text{mol}^{-1}\cdot\text{cm}^{-1}$): 282 (39500), 340 (shoulder, 15900), 408 (shoulder, 3700); IR(ATR) ($\tilde{\nu}$ / cm^{-1}): 2943(s), 2920(w), 2893(w), 2856(w), 1452(s); elemental analysis calcd. for $\text{C}_{26}\text{H}_{51}\text{CoOP}_4\text{Si} \cdot 0.18\text{A}$ (M = 673.47): C 52.88, H 8.70, found: C 52.82, H 8.10.

2.4.2.14 Synthesis of $[\text{Co}(\eta^3\text{-P}_2\text{C}_2\text{tBu}_2\text{CON}(\text{Ph})\text{SiMe}_3)(\eta^4\text{-P}_2\text{C}_2\text{tBu}_2)]$ (12)

PhNCO (17 mg, 0.15 mmol) was added to a solution of **2a** (60 mg, 0.12 mmol) in *n*-hexane. Subsequently, the reaction mixture was heated up to 50 °C overnight. The solvent and volatiles were removed *in vacuo*. The residue was redissolved in *n*-hexane (2 mL). Dark orange crystals formed upon storage over three days at –35 °C. Yield 55 mg (67%); m.p. >143 °C (decomp. to a black oil); ^1H NMR (400.13 MHz, 300 K, C_6D_6) δ /ppm = 0.08 (s, 9H, SiMe_3), 0.89 (s, 9H, *t*Bu), 0.93 (s, 9H, *t*Bu), 1.74 (s, 18H, *t*Bu), 6.49 (d, $^2J_{\text{H,H}}$ = 7.1 Hz, 2H, *o*- H_{Ar}), 6.81–6.93 (m, 3H, *m/p*- H_{Ar}); $^{13}\text{C}\{^1\text{H}\}$ NMR (100.61 MHz, 300 K, C_6D_6) δ /ppm = 0.3 (d, $^2J_{\text{C,P}}$ = 10.8 Hz, SiMe_3), 27.9 (br, $\text{C}(\text{CH}_3)_3$), 28.0 (br, $\text{C}(\text{CH}_3)_3$), 31.5 (m, $\text{C}(\text{CH}_3)_3$), 35.9 (t, $^2J_{\text{C,P}}$ = 7.5 Hz, $\text{C}(\text{CH}_3)_3$), 37.2 (dd, $^2J_{\text{C,P}}$ = 6.3 Hz, 7.8 Hz, $\text{C}(\text{CH}_3)_3$), 37.5 (t, $^2J_{\text{C,P}}$ = 7.5 Hz, $\text{C}(\text{CH}_3)_3$), 96.5 (s, C_2P_2), 107.5 (s, C_2P_2), 124.3 (s, NCO), 126.0 (s, *p*- C_{Ar}), 126.7 (overlapping with solvent signal, *o*- C_{Ar}), 128.1 (s, *m*- C_{Ar}), 140.0 (s, *ipso*- C_{Ar}); $^{31}\text{P}\{^1\text{H}\}$ NMR (161.98 MHz, 300 K, C_6D_6) δ /ppm = 21.6 (s, 2P), 77.0 (d, $^2J_{\text{P,P}}$ = 34 Hz, 1P), 141.0 (d, $^2J_{\text{P,P}}$ = 34 Hz, 1P); UV/Vis (THF, λ_{max} /nm, (ϵ_{max} / $\text{L}\cdot\text{mol}^{-1}\cdot\text{cm}^{-1}$): 276 (45300), 308 (35200), 375 (12900); IR(ATR) ($\tilde{\nu}$ / cm^{-1}): 2954(s), 2892(w), 2855(w),

1516(vs), 1487(s), 1454(s); elemental analysis calcd. for $C_{30}H_{50}P_4CoONSi$ ($M = 651.65$): C 55.30, H 7.73, N 2.15 found: C 55.94, H 7.42, N 2.02.

2.4.3 $^{31}\text{P}\{^1\text{H}\}$ NMR Spectra of 6–8Figure S2. $^{31}\text{P}\{^1\text{H}\}$ NMR spectrum (161.49 Mhz, C_6D_6 , 300 K) of 6/6'.Figure S3. $^{31}\text{P}\{^1\text{H}\}$ NMR spectrum (161.49 Mhz, C_6D_6 , 300 K) of 7/7'.

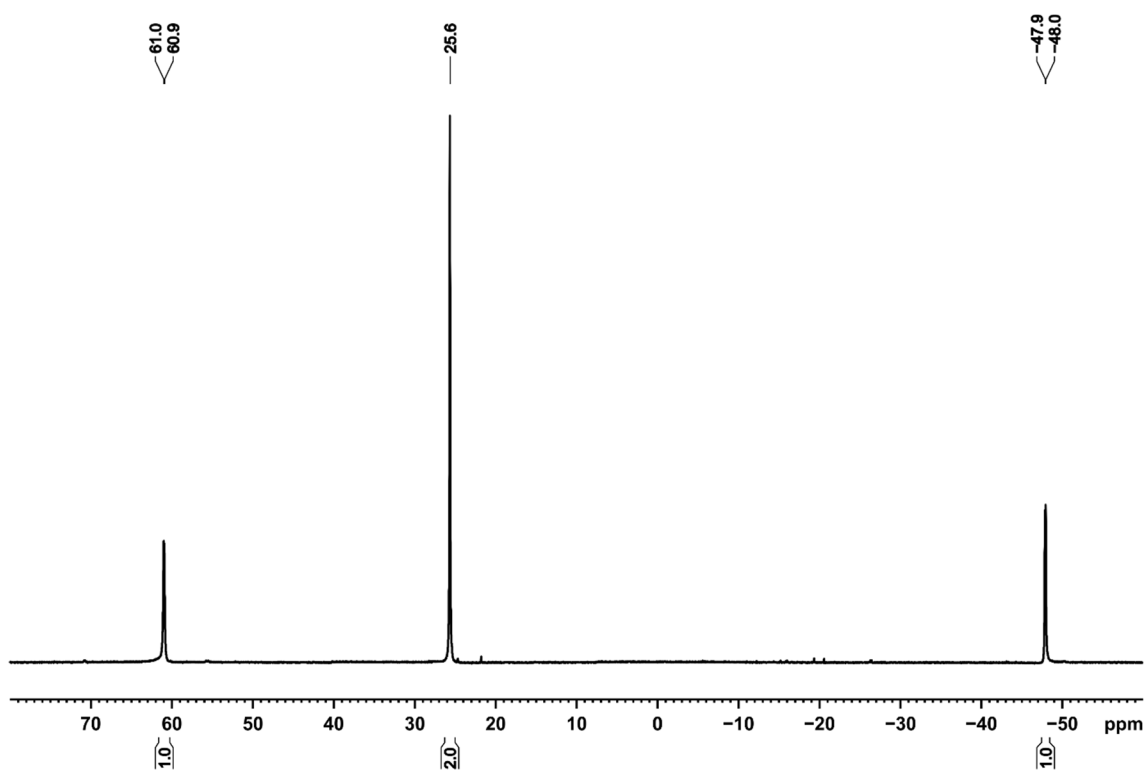
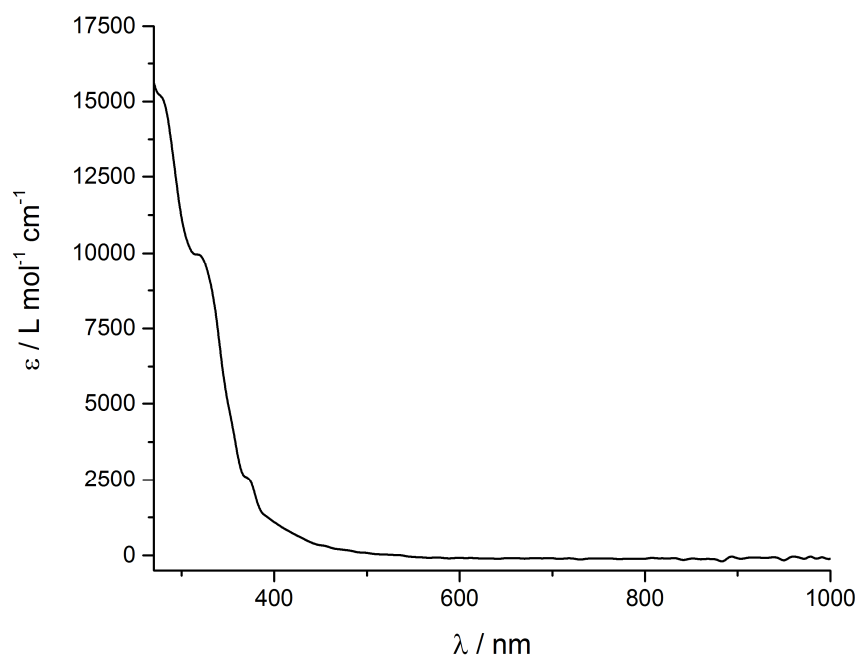
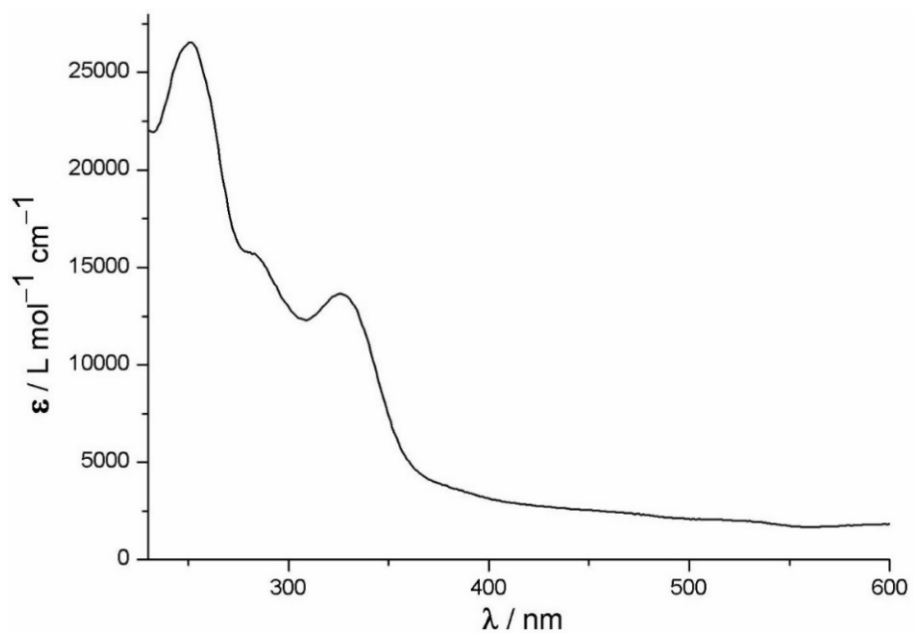


Figure S4. $^{31}\text{P}\{^1\text{H}\}$ NMR spectrum (161.49 Mhz, C_6D_6 , 300 K) of **8**.

2.4.4 UV/Vis and IR Spectroscopy

Figure S5. UV/Vis spectrum of **2a** in *n*-hexane.Figure S6. UV/Vis spectrum of **2b** in *n*-hexane.

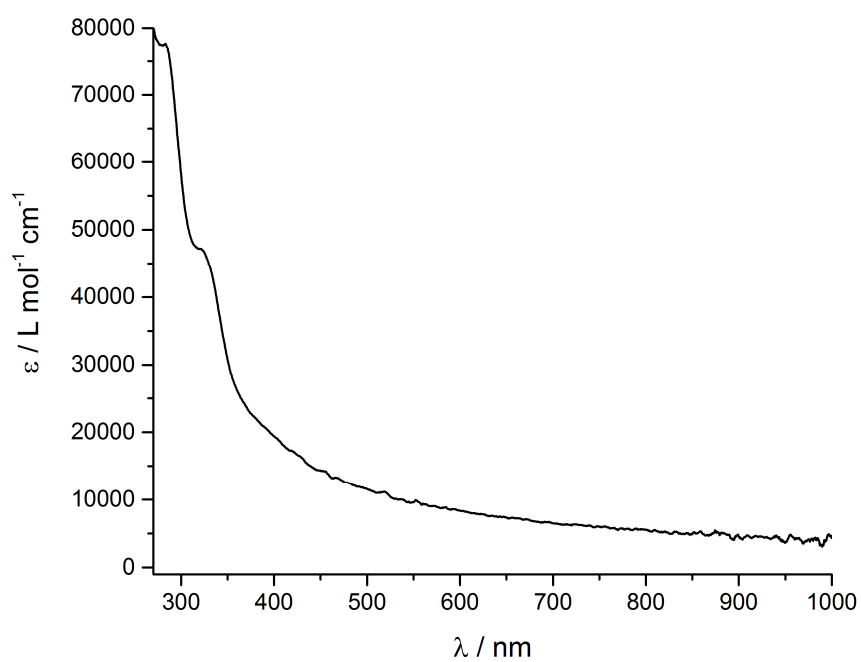


Figure S7. UV/Vis spectrum of **4** in THF.

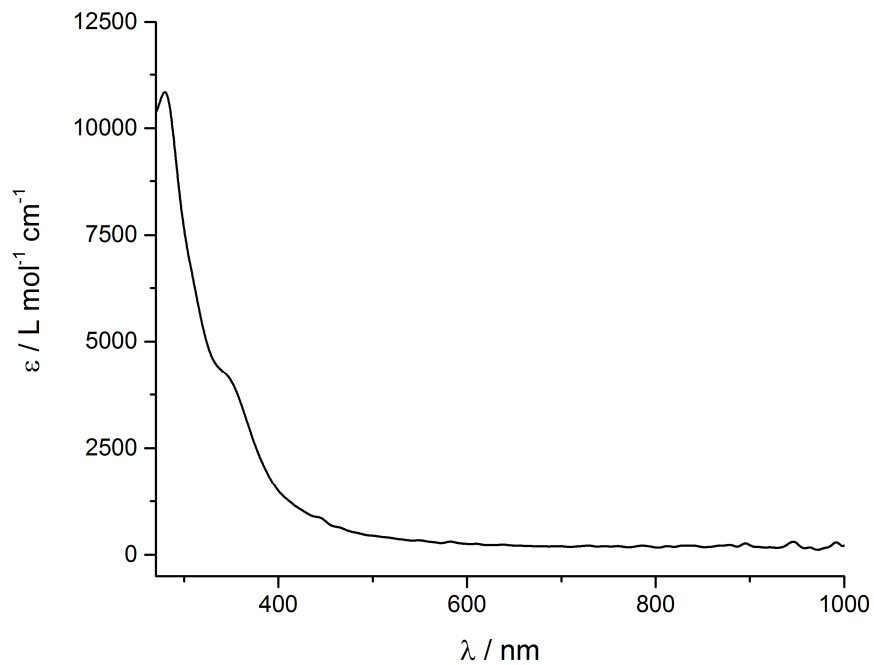


Figure S8. UV/Vis spectrum of **5** in *n*-hexane.

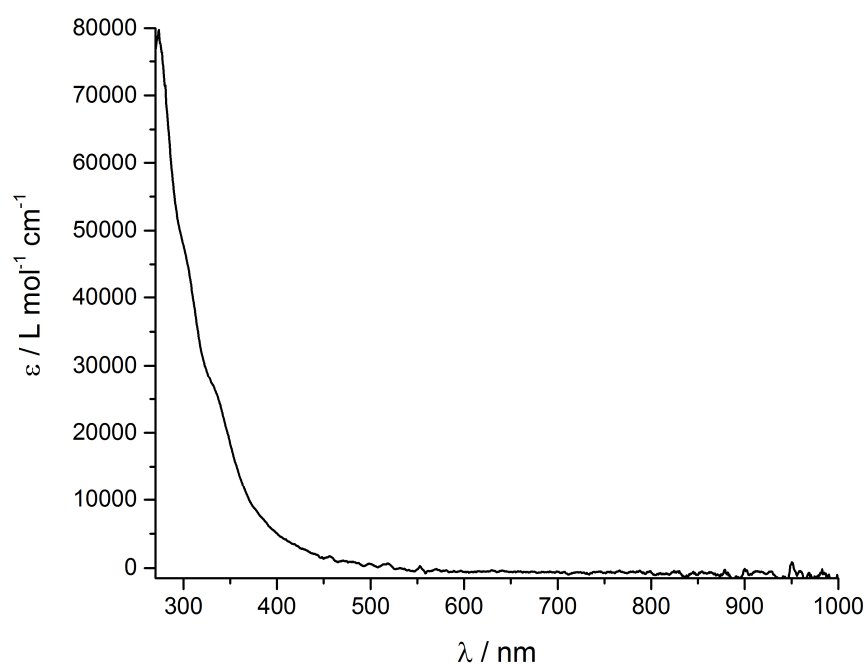


Figure S9. UV/Vis spectrum of **9** in *n*-hexane.

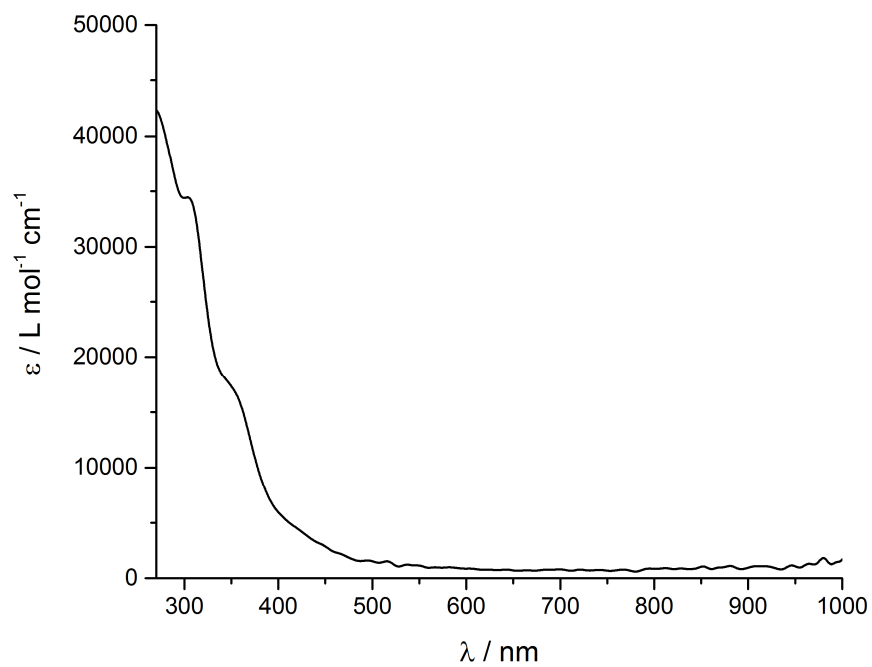


Figure S10. UV/Vis spectrum of **10** in *n*-hexane.

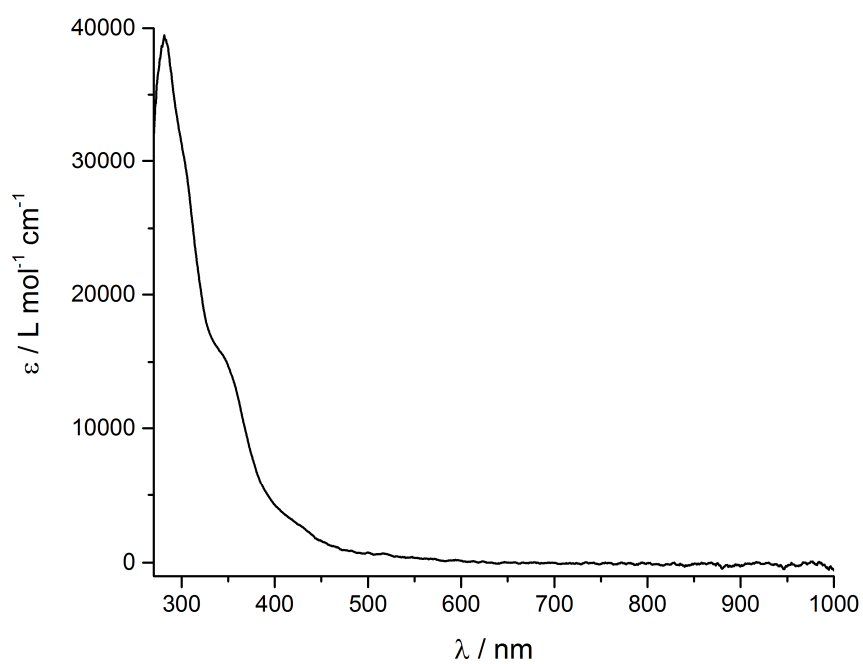


Figure S11. UV/Vis spectrum of **11** in *n*-hexane.

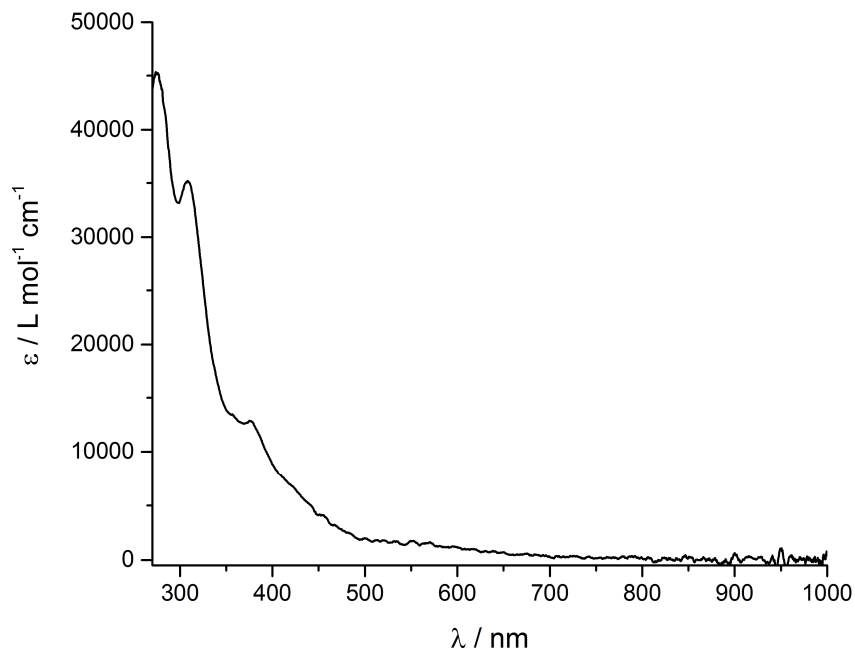


Figure S12. UV/Vis spectrum of **12** in *n*-hexane.

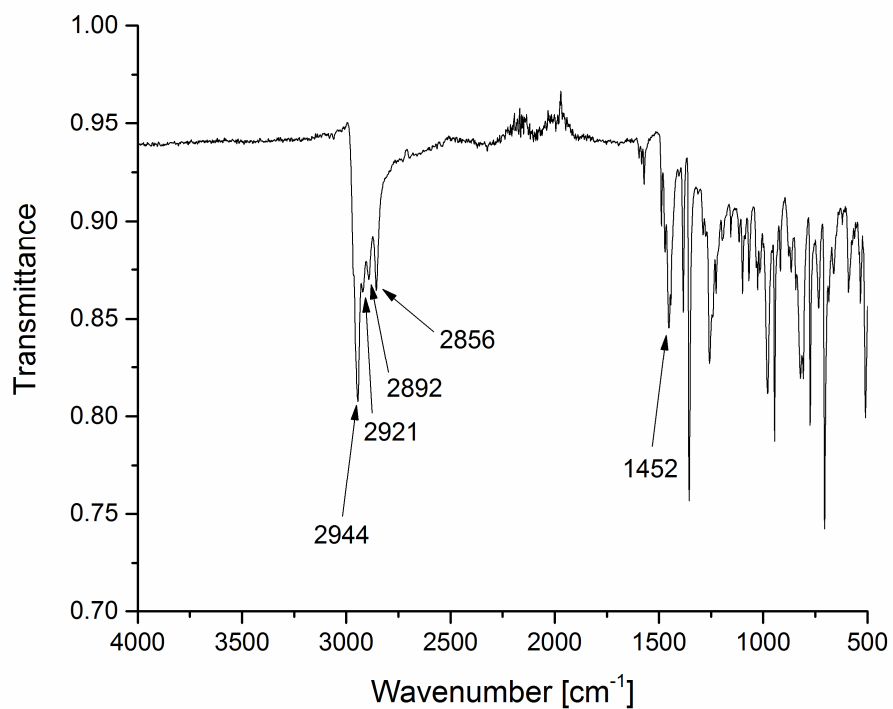


Figure S13. IR(ATR) spectrum of **5**.

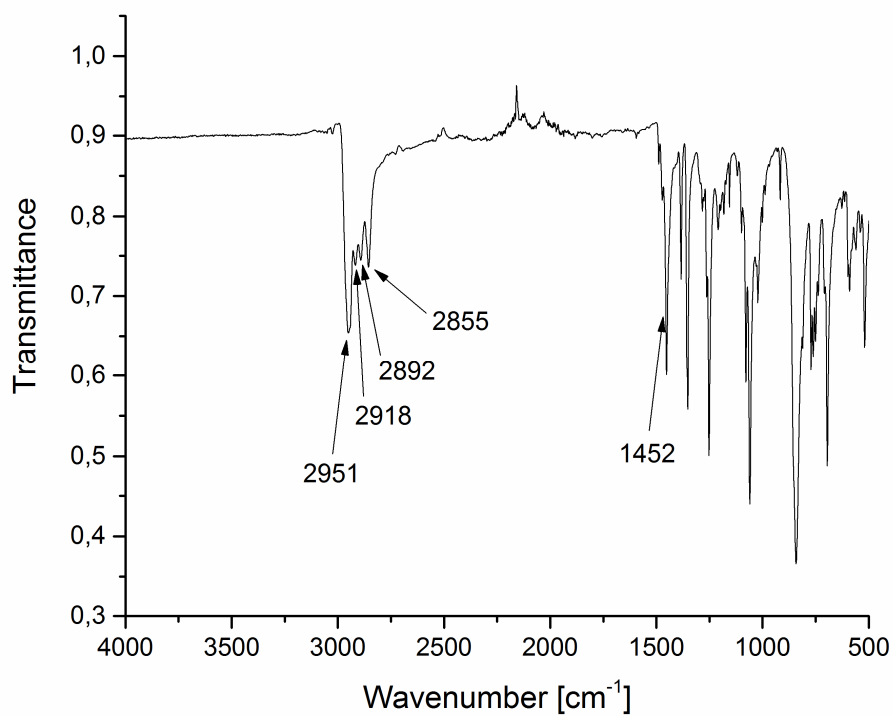


Figure S14. IR(ATR) spectrum of **10**.

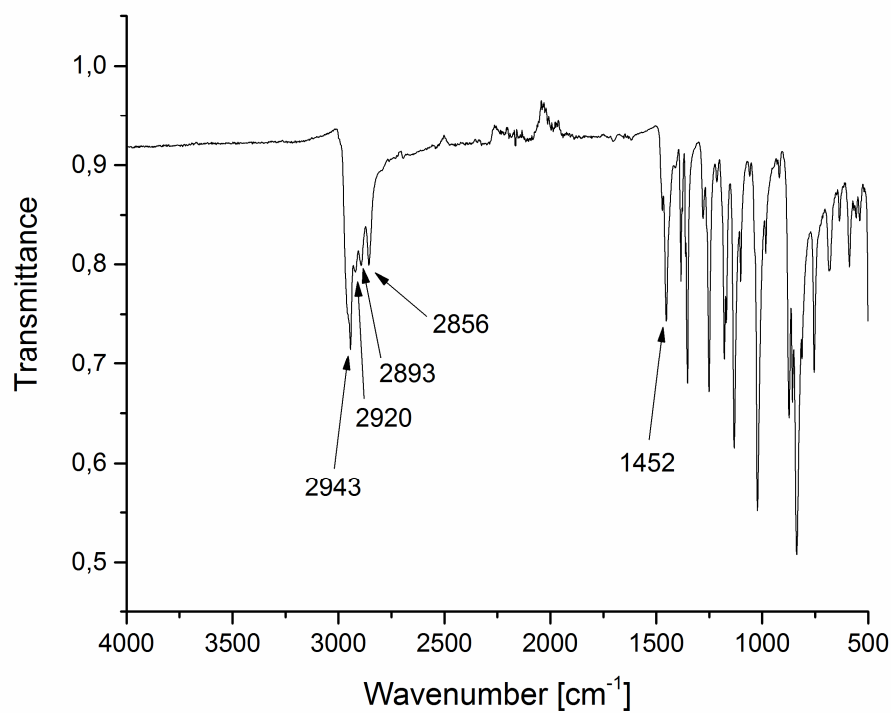


Figure S15. IR(ATR) spectrum of **11**.

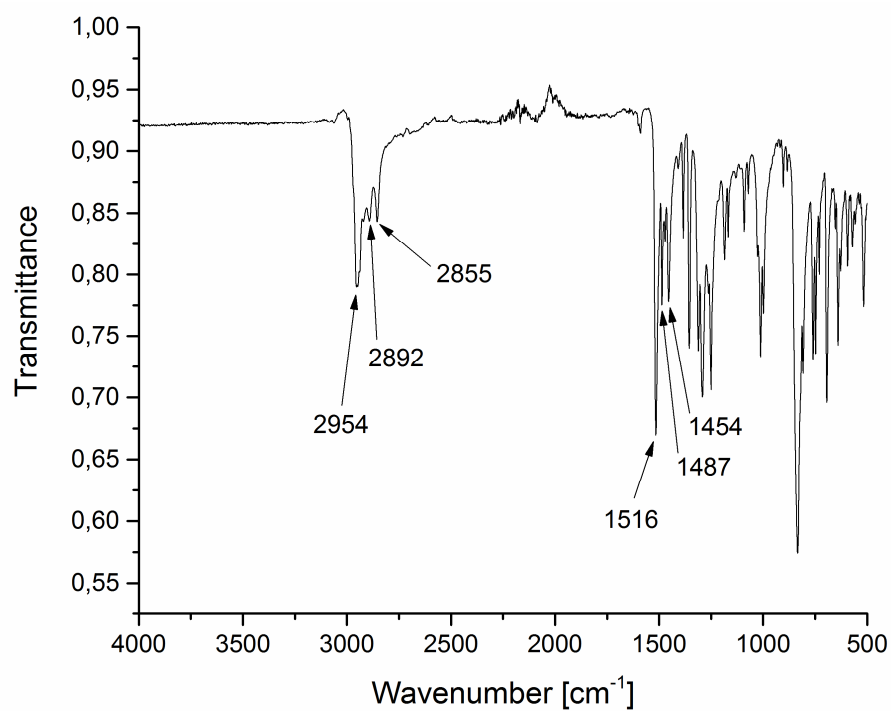


Figure S16. IR(ATR) spectrum of **12**.

2.4.5 X-ray Crystallography

The single crystal X-ray diffraction data were recorded on Agilent Technologies Gemini R Ultra (**2a**), GV1000 (**10**), SuperNova ([**K(tol)**]₂)[**1b**], **2b**, **4**, **5**, **9**, **11**, **12**), and devices and on a Bruker AXS APEX II (**3c**) diffractometer with Cu K α radiation ($\lambda = 1.54184 \text{ \AA}$). Semi-empirical multiscan¹⁴ and analytical absorption¹⁵ corrections were applied to the data. Using Olex2, the structures were solved with SIR2004¹⁶ ([**K(tol)**]₂)[**1b**]), SHELXS¹⁷ (**2b**, **3c**) or SHELXT¹⁸ (**4**, **5**, **9–12**), and least-square refinements on F^2 were carried out with SHELXL¹⁹.

CCDC 1849347-1849356 contain supplementary crystallographic data for this paper. These data can be obtained free of charge from the Cambridge Crystallographic Date Center via www.ccdc.cam.ac.uk/data_request/cif.

Table S1. Crystallographic data of $[\text{K}(\text{tol})_2][\mathbf{1b}]$, $\mathbf{2a}$, and $\mathbf{2b}$.

Compound	$[\text{K}(\text{tol})_2][\mathbf{1b}]$	$\mathbf{2a}$	$\mathbf{2b}$
Empirical formula	$\text{C}_{38}\text{H}_{60}\text{CoP}_4\text{K}$	$\text{C}_{23}\text{H}_{45}\text{CoP}_4\text{Si}$	$\text{C}_{27}\text{H}_{53}\text{CoP}_4\text{Si}$
Formula weight	738.77	532.49	588.59
Temperature [K]	123(1)	123(1)	123(1)
Crystal system	monoclinic	monoclinic	orthorhombic
Space group	$P2_1/n$	$P2_1/n$	$Pnma$
a [Å]	11.3548(2)	9.8500(2)	16.9382(3)
b [Å]	20.4325(3)	17.8576(2)	11.0030(2)
c [Å]	17.0180(3)	16.4002(2)	17.2884(2)
α [°]	90	90	90
β [°]	90.789(2)	90.846(2)	90
γ [°]	90	90	90
Volume [Å ³]	3947.9(1)	2884.45(8)	3222.06(9)
Z	4	4	4
ρ_{calc} [g/cm ³]	1.243	1.226	1.213
μ [mm ⁻¹]	6.056	7.209	6.499
F(000)	1576.0	1136.0	1264.0
Crystal size [mm ³]	0.3 × 0.3 × 0.2	0.4 × 0.15 × 0.1	0.2067 × 0.1618 × 0.1027
Radiation	$\text{CuK}\alpha$ ($\lambda = 1.54184$)	$\text{CuK}\alpha$ ($\lambda = 1.54184$)	$\text{CuK}\alpha$ ($\lambda = 1.54184$)
2 θ range for data collection [°]	6.76 to 119.988	7.318 to 133.366	7.306 to 147.16
Index ranges	$-12 \leq h \leq 11, -22 \leq k \leq 19, -14 \leq l \leq 19$	$-9 \leq h \leq 11, -21 \leq k \leq 21, -19 \leq l \leq 18$	$-20 \leq h \leq 20, -13 \leq k \leq 13, -21 \leq l \leq 21$
Reflections collected	10610	26223	17036
Independent reflections	5250 [$R_{\text{int}} = 0.0304$, $R_{\text{sigma}} = 0.0382$]	5083 [$R_{\text{int}} = 0.0599$, $R_{\text{sigma}} = 0.0335$]	3321 [$R_{\text{int}} = 0.0332$, $R_{\text{sigma}} = 0.0224$]
Data / restraints / parameters	5250 / 1 / 445	5083 / 0 / 277	3321 / 0 / 176
Goodness-of-fit on F^2	1.093	1.049	1.037
Final R indexes [$I \geq 2\sigma(I)$]	$R_1 = 0.0458$, $wR_2 = 0.1159$	$R_1 = 0.0435$, $wR_2 = 0.1146$	$R_1 = 0.0272$, $wR_2 = 0.0640$
Final R indexes [all data]	$R_1 = 0.0494$, $wR_2 = 0.1182$	$R_1 = 0.0458$, $wR_2 = 0.1204$	$R_1 = 0.0310$, $wR_2 = 0.0659$
Largest diff. peak/hole [$e \text{ \AA}^{-3}$]	0.73/−0.47	0.83/−0.35	0.28/−0.25
CCDC	1849356	1849350	1849351

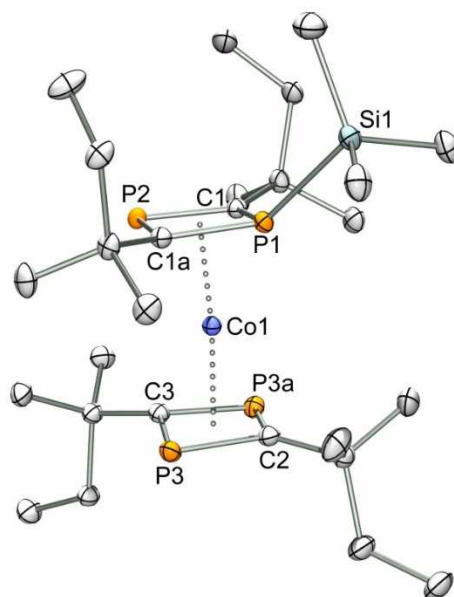


Figure S17. Solid-state molecular structure of $[\text{Co}(\eta^4\text{-P}_2\text{C}_2\text{tPent}_2\text{SiMe}_3)(\eta^4\text{-P}_2\text{C}_2\text{tPent}_2)]$ (**2b**). Displacement ellipsoids are drawn at the 40% probability level. Hydrogen atoms are omitted for clarity. Selected bond lengths (Å) and angles (°): C1–P1 1.784(2), C1–P2 1.794(2), C1a–P1 1.784(2), C1a–P2 1.794(2), C2–P3 1.796(2), C3–P3 1.801(2), Co1–P1 2.1866(6), Co1–P2 2.2651(6), Co1–P3 2.2570(6), Co1–P3a 2.2570(6); Co1–C1 2.118(2), Co1–C1a 2.118(2), Co1–C2 2.080(2), Co1–C3 2.073(2), Co1–C4 2.070(3), P1–Si1 2.2893(8), C1–P1–C1a 84.42(7), C1–P2–C1a 83.84(7), Si1–P1–C1 127.20(5), Si1–P1–C1a 127.20(5), P1–C1–P2 95.81(7), P1–C1a–P2 95.81(7), C2–P3–C3 80.71(8), C2–P3a–C3 80.71(8), P3–C2–P3a 99.3(1), P3–C3–P3a 98.9(1).

Table S2. Crystallographic data of **3c**, **4**, **5**, and **9-12**.

Compound	3c	4	5
Empirical formula	C ₅₈ H ₈₅ CoP ₄ SiO	C ₃₈ H ₅₁ CoP ₄ Sn	C ₃₁ H ₅₃ CoP ₄ SiO
Formula weight	1009.15	809.28	652.63
Temperature [K]	153(1)	123(1)	123(1)
Crystal system	monoclinic	triclinic	monoclinic
Space group	<i>P</i> 2 ₁ / <i>n</i>	<i>P</i> –1	<i>P</i> 2 ₁ / <i>n</i>
a [Å]	13.4814(2)	9.9926(2)	12.1773(3)
b [Å]	20.6464(3)	11.7420(3)	20.2536(5)
c [Å]	19.7044(2)	17.0948(3)	15.3016(4)
α [°]	90	87.129(2)	90
β [°]	103.521(1)	87.346(2)	107.107(2)
γ [°]	90	76.381(2)	90
Volume [Å ³]	5332.6(1)	1945.71(7)	3606.9(2)
Z	4	2	4
ρ _{calc} [g/cm ³]	1.257	1.381	1.202
μ [mm ⁻¹]	4.160	10.173	5.879
F(000)	2168.0	832.0	1544.0
Crystal size [mm ³]	0.24 × 0.18 × 0.1	0.166 × 0.148 × 0.117	0.192 × 0.132 × 0.09
Radiation	CuK _α (λ = 1.54184)	CuK _α (λ = 1.54184)	CuK _α (λ = 1.54184)
2θ range for data collection [°]	6.294 to 143.492	7.754 to 153.148	7.456 to 152.76
Index ranges	–16 ≤ h ≤ 14, –25 ≤ k ≤ 24, –23 ≤ l ≤ 24	–12 ≤ h ≤ 12, –14 ≤ k ≤ 13, –21 ≤ l ≤ 21	–15 ≤ h ≤ 15, –25 ≤ k ≤ 25, –18 ≤ l ≤ 19
Reflections collected	31033	31277	42123
Independent reflections	10038 [R _{int} = 0.0503, R _{sigma} = 0.0494]	8078 [R _{int} = 0.0197, R _{sigma} = 0.0149]	7478 [R _{int} = 0.0519, R _{sigma} = 0.0333]
Data / restraints / parameters	10038 / 27 / 585	8078 / 0 / 409	7478 / 0 / 358
Goodness-of-fit on F ²	1.063	1.035	1.059
Final R indexes [I >= 2σ (I)]	R ₁ = 0.0556, wR ₂ = 0.1592	R ₁ = 0.0184, wR ₂ = 0.0446	R ₁ = 0.0387, wR ₂ = 0.0921
Final R indexes [all data]	R ₁ = 0.0762, wR ₂ = 0.1691	R ₁ = 0.0191, wR ₂ = 0.0449	R ₁ = 0.0412, wR ₂ = 0.0936
Largest diff. peak/hole [e Å ⁻³]	1.09/–0.64	0.44/–0.49	0.97/–0.29
CCDC	1849352	1849353	1849354

Compound	9c	10	11
Empirical formula	C ₂₇ H ₅₁ CoP ₄ SiO ₂	C ₃₀ H ₅₁ CoP ₄ SiO	C ₂₆ H ₅₁ CoP ₄ SiO
Formula weight	617.06	638.60	590.56
Temperature [K]	153(1)	123(1)	123(1)
Crystal system	monoclinic	triclinic	monoclinic
Space group	<i>P</i> ₂ ₁ / <i>n</i>	<i>P</i> ₂ ₁ / <i>m</i>	<i>P</i> ₂ ₁ / <i>c</i>
a [Å]	14.1563(3)	9.8471(3)	15.1113(2)
b [Å]	15.3883(3)	11.6134(4)	13.7665(2)
c [Å]	15.2556(3)	15.0022(4)	17.1160(2)
α [°]	90	90	90
β [°]	93.378(2)	91.971(3)	116.100(2)
γ [°]	90	90	90
Volume [Å ³]	3317.5(1)	1714.62(8)	3197.54(8)
Z	4	2	4
ρ _{calc} [g/cm ³]	1.235	1.237	1.227
μ [mm ⁻¹]	6.385	6.173	6.576
F(000)	1314.0	680.0	1264.0
Crystal size [mm ³]	0.208 × 0.178 × 0.162	0.1991 × 0.1199 × 0.0674	0.1422 × 0.1229 × 0.0848
Radiation	CuK _α (λ = 1.54184)	CuK _α (λ = 1.54184)	CuK _α (λ = 1.54184)
2θ range for data collection [°]	8.168 to 147.388	8.986 to 146.994	6.514 to 146.94
Index ranges	-17 ≤ h ≤ 17, -18 ≤ k ≤ 18, -18 ≤ l ≤ 18	-12 ≤ h ≤ 9, -14 ≤ k ≤ 13, -17 ≤ l ≤ 18	-18 ≤ h ≤ 18, -17 ≤ k ≤ 15, -21 ≤ l ≤ 21
Reflections collected	38917	8221	44720
Independent reflections	6619 [R _{int} = 0.0691, R _{sigma} = 0.0374]	3498 [R _{int} = 0.0342, R _{sigma} = 0.0359]	6365 [R _{int} = 0.0363, R _{sigma} = 0.0198]
Data / restraints / parameters	6619 / 28 / 547	3498 / 0 / 248	6365 / 0 / 502
Goodness-of-fit on F ²	1.068	1.136	1.091
Final R indexes [I >= 2σ (I)]	R ₁ = 0.0594, wR ₂ = 0.1496	R ₁ = 0.0634, wR ₂ = 0.1700	R ₁ = 0.0254, wR ₂ = 0.0670
Final R indexes [all data]	R ₁ = 0.0682, wR ₂ = 0.1556	R ₁ = 0.0668, wR ₂ = 0.1718	R ₁ = 0.0287, wR ₂ = 0.0688
Largest diff. peak/hole [e Å ⁻³]	0.43/-0.43	1.15/-0.50	0.48/-0.36
CCDC	1849355	1849347	1849348

Compound	12c
Empirical formula	C ₃₃ H ₅₇ CoP ₄ SiNO
Formula weight	694.69
Temperature [K]	123(1)
Crystal system	monoclinic
Space group	<i>P</i> 2 ₁ / <i>n</i>
a [Å]	10.2866(1)
b [Å]	16.1496(2)
c [Å]	23.1576(3)
α [°]	90
β [°]	98.966(1)
γ [°]	90
Volume [Å ³]	3800.04(8)
Z	4
ρ _{calc} [g/cm ³]	1.214
μ [mm ⁻¹]	5.618
F(000)	1484.0
Crystal size [mm ³]	0.145 × 0.095 × 0.058
Radiation	CuK _α (λ = 1.54184)
2θ range for data collection [°]	6.7 to 147.092
Index ranges	-12 ≤ h ≤ 12, -19 ≤ k ≤ 20, -28 ≤ l ≤ 25
Reflections collected	31398
Independent reflections	7554 [R _{int} = 0.0279, R _{sigma} = 0.0217]
Data / restraints / parameters	7554 / 0 / 386
Goodness-of-fit on F ²	1.033
Final R indexes [I >= 2σ (I)]	R ₁ = 0.0258, wR ₂ = 0.0618
Final R indexes [all data]	R ₁ = 0.0287, wR ₂ = 0.0632
Largest diff. peak/hole [e Å ⁻³]	0.31/-0.23
CCDC	1849349

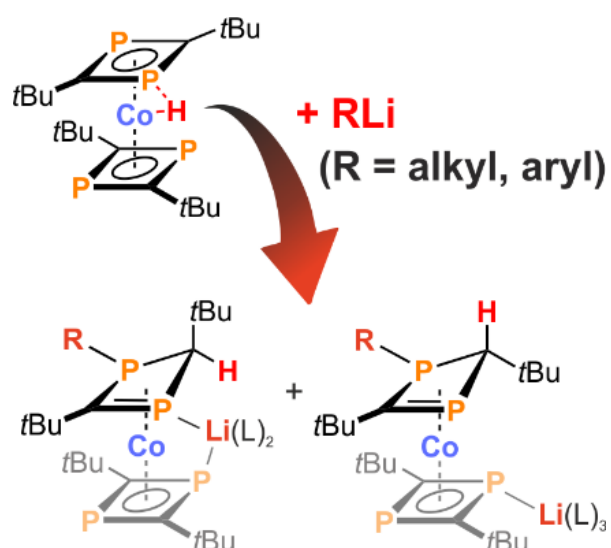
2.5 References

- 1 G. Becker, G. Gresser, W. Uhl, *Z. Naturforsch. B* **1981**, *36*, 16–19.
- 2 K. B. Dillon, F. Mathey, J. F. Nixon, *Phosphorus: The Carbon Copy*, Wiley, Chichester, **1998**.
- 3 Reviews: a) A. Chirila, R. Wolf, J. C. Slootweg, K. Lammertsma, *Coord. Chem. Rev.* **2014**, *270–271*, 57; b) F. Mathey, *Angew. Chem. Int. Ed.* **2003**, *42*, 1578–1604; c) M. Regitz, *Chem. Rev.* **1990**, *90*, 191–213; d) M. Regitz, P. Binger, *Angew. Chem. Int. Ed. Engl.* **1988**, *27*, 1484–1508; e) J. F. Nixon, *Chem. Rev.* **1988**, *88*, 1327–1362.
- 4 1,2-diphosphacyclobutadiene compounds: a) P. Binger, G. Glaser, S. Albus, C. Krüger, *Chem. Ber.* **1995**, *128*, 1261–1265; b) F. W. Heinemann, S. Kummer, U. Seiss-Brandl, U. Zenneck, *Organometallics* **1999**, *18*, 2021–2029; c) P. Kramkowski, M. Scheer, *Eur. J. Inorg. Chem.* **2000**, 1869–1876; d) C. Jones, C. Schulten, A. Stasch, *Dalton Trans.* **2006**, 3733–3735; e) E.-M. Rummel, G. Balazs, V. Heintl, M. Scheer, *Angew. Chem.* **2017**, *129*, 9720–9725; *Angew. Chem. Int. Ed.* **2017**, *56*, 9592–9596.
- 5 Selected examples of 1,3-diphosphacyclobutadiene complexes: a) P. Binger, R. Milczarek, R. Mynott, M. Regitz, W. Rösch, *Angew. Chem.* **1986**, *98*, 645–646; *Angew. Chem. Int. Ed. Engl.* **1986**, *25*, 644–645; b) P. B. Hitchcock, M. J. Maah, J. F. Nixon, *J. Chem. Soc., Chem. Commun.* **1986**, 737–738; c) P. Binger, R. Milczarek, R. Mynott, C. Krüger, Y. H. Tsay, E. Raabe, M. Regitz, *Chem. Ber.* **1988**, *121*, 637–645; d) P. Binger, B. Biedenbach, R. Schneider, M. Regitz, *Synthesis* **1989**, *12*, 960–961; e) analogous rhodium(I) and iridium(I) compounds [CpM(η^4 -P₂C₂tBu₂)] (M = Rh, Ir) and coordination compounds of [CpCo(η^4 -P₂C₂tBu₂)]: P. B. Hitchcock, M. J. Maah, J. F. Nixon, *Heteroatom. Chem.* **1991**, *2*, 253–264; f) A. G. Avent, F. G. N. Cloke, K. R. Flower, P. B. Hitchcock, J. F. Nixon, D. M. Vickers, *Angew. Chem.* **1994**, *106*, 2406–2408; *Angew. Chem. Int. Ed. Engl.* **1994**, *33*, 2330–2332; g) D. Böhm, F. Knoch, S. Kummer, U. Schmidt, U. Zenneck, *Angew. Chem.* **1995**, *107*, 251–254; *Angew. Chem. Int. Ed. Engl.* **1995**, *34*, 198–201; h) P. A. Arnold, F. G. N. Cloke, P. B. Hitchcock, J. F. Nixon, *J. Am. Chem. Soc.* **1996**, *118*, 7630–7631; i) M. Scheer, J. Krug, *Z. Anorg. Allg. Chem.* **1998**, *624*, 399–405; j) F. W. Heinemann, S. Kummer, U. Seiss-Brandl, U. Zenneck, *Organometallics* **1999**, *18*, 2021–2029; k) F. G. N. Cloke, P. B. Hitchcock, J. F. Nixon, D. M. Vickers, *J. Organomet. Chem.* **2001**, *635*, 212–221; l) A. D. Burrows, A. Dransfeld, M. Green, J. C. Jeffery, C. Jones, J. M. Lyman, M. T. Nguyen, *Angew. Chem.* **2001**, *113*, 3321–3324; *Angew. Chem. Int. Ed.* **2001**, *40*, 3221–3224; m) C. Topf, T. Clark, F. W. Heinemann, M. Hennemann, S. Kummer, H. Pritzkow, U. Zenneck, *Angew. Chem.* **2002**, *114*, 4221–4226; *Angew. Chem. Int. Ed.* **2002**, *41*, 4047–4052; n) D. Himmel, M. Seitz, M. Scheer, *Z. Anorg. Allg. Chem.* **2004**, *630*, 1220–1228; o) E.-M. Rummel, M. Eckhardt, M. Bodensteiner, E.V. Peresyphkina, W. Kremer, C. Gröger, M. Scheer, *Eur. J. Inorg. Chem.* **2014**, 1625–1637.
- 6 a) R. Wolf, A. W. Ehlers, J. C. Slootweg, M. Lutz, D. Gudat, M. Hunger, A. L. Spek, K. Lammertsma, *Angew. Chem.* **2008**, *120*, 4660–4663; *Angew. Chem. Int. Ed.* **2008**, *47*, 4584–4587; b) R. Wolf, J. C. Slootweg, A. W. Ehlers, F. Hartl, B. de Bruin, M. Lutz, A. L. Spek, K. Lammertsma, *Angew. Chem.* **2009**, *121*, 3150–3153; *Angew. Chem. Int. Ed.* **2009**,

- 48, 3104–3107; c) R. Wolf, A. W. Ehlers, M. M. Khusniyarov, F. Hartl, B. de Bruin, G. J. Long, F. Grandjean, F. M. Schappacher, R. Pöttgen, J. C. Slootweg, M. Lutz, A. L. Spek, K. Lammertsma, *Chem. Eur. J.* **2010**, *16*, 14322–14334.
- 7 Electrochemical measurements and preparative studies have shown that **1a** is readily oxidized to neutral $[\text{Co}(\eta^4\text{-P}_2\text{C}_2\text{tBu}_2)_2]$. A half-wave potential of $E_{1/2} = -0.73$ V vs. Fc/Fc⁺ was determined for **1a** by cyclic voltammetry, see ref. 6c.
- 8 a) J. Malberg, T. Wiegand, H. Eckert, M. Bodensteiner, R. Wolf, *Chem. Eur. J.* **2013**, *19*, 2356–2369; b) J. Malberg, M. Bodensteiner, D. Paul, T. Wiegand, H. Eckert, R. Wolf, *Angew. Chem. Int. Ed.* **2014**, *53*, 2771–2775; c) J. Malberg, T. Wiegand, H. Eckert, M. Bodensteiner, R. Wolf, *Eur. J. Inorg. Chem.* **2014**, *2014*, 1638–1651; d) C. Rödl, R. Wolf, *Eur. J. Inorg. Chem.* **2016**, *2016*, 736–742.
- 9 P. Pyykkö, *J. Phys. Chem. A.* **2015**, *119*, 2326–2337.
- 10 Example for the insertion of tetrahydrofuran into a P–Si bond: H. G. Horn, H. J. Lindner, *Chemiker Zeitung* **1988**, *112*, 195–200.
- 11 E. V. Ivanova, H. M. Muchall, *J. Phys. Chem. A.* **2007**, *111*, 10824–10833.
- 12 G. W. Chantry, E. A. Nicol, D. J. Harrison, *Spectrochim. Acta A* **1974**, *80*, 1717–1722.
- 13 K. Itoh, M. Fukui, Y. Ishii, *J. Chem. Soc. C* **1969**, 2002–2004.
- 14 a) *SCALE3ABS*, *CrysAlis^{Pro}*, Agilent Technologies Inc., Oxford, GB, **2012**, b) G. M. Sheldrick, *SADABS*, Bruker AXS, Madison, USA, **2007**.
- 15 R. C. Clark, J. S. Reid, *Acta Cryst. Sect. A* **1995**, *51*, 887–897.
- 16 M. C. Burla, R. Caliandro, M. Camalli, B. Carrozzini, G. L. Casciarano, L. De Caro, C. Giacovazzo, G. Polidori, D. Siliqi, R. Spagna, *J. Appl. Cryst.* **2007**, *40*, 609–613.
- 17 G. M. Sheldrick, *Acta Cryst.* **2008**, *A64*, 112–122.
- 18 G. M. Sheldrick, *Acta Cryst.* **2015**, *A71*, 3–8.
- 19 G. M. Sheldrick, *Acta Cryst.* **2015**, *C71*, 3–8.

3 1,3-DIPHOSPHACYCLOBUTENE COBALT COMPLEXES^[a,b]

CHRISTIAN RÖDL, KAI SCHWEDTMANN, JAN J. WEIGAND, AND ROBERT WOLF



[a] Reproduced with permission from C. Rödl, K. Schwedtmann, J. J. Weigand, R. Wolf, *Chem. Eur. J.* **2019**, 25, 6180-6188. Copyright 2019 Wiley-VCH, License number: 4625760483313.

[b] C. Rödl synthesized and characterized all compounds reported in this chapter. K. Schwedtmann (TU Dresden, Germany) performed VT and 2D NMR studies on compounds **1-3**, and **5**, and he prepared Figure S15. C. Rödl prepared all remaining Figures and Schemes and wrote the manuscript with input from K. Schwedtmann, J. J. Weigand (TU Dresden), and R. Wolf.

3.1 Introduction

Over the past three decades, diphosphacyclobutadiene complexes have attracted considerable attention.¹⁻³ In 1986, Regitz, Binger and co-workers, as well as Nixon and co-workers independently reported the preparation of the first 1,3-diphosphacyclobutadiene complexes by reaction of (cyclopentadienyl)cobalt-ethene complexes with phosphalkynes.⁴ Subsequently, numerous 1,3-diphosphacyclobutadiene transition metal complexes, as well as a few 1,2-diphosphacyclobutadiene complexes, have been prepared by the metal-mediated cyclodimerization of phosphalkynes.^{5,6} Although the coordination properties^{1,2} and the isomerization between the 1,2- and 1,3-isomers^{6b} have been intensively investigated, the ambiphilicity of 1,3-diphosphacyclobutadiene has attracted less attention so far.

Zenneck and co-workers demonstrated that treatment of $[\text{Mo}(\eta^4\text{-1,3-P}_2\text{C}_2\text{tBu}_2)_2(\text{CO})_2]$ (**A**) with $n\text{BuLi}$ followed by hydrolysis, affords complexes **B** and **C** (Figure 1), which clearly result from nucleophilic attack of $n\text{BuLi}$ at a P atom.⁷ In case of **C**, the initial step is followed by subsequent reaction steps, which result in the partial degradation of the newly formed 1,3-diphosphacyclobutenyl ligand. Nixon and co-workers showed that the treatment of $[\text{Mo}(\eta^5\text{-C}_9\text{H}_7)(\text{CO})_2(\text{CH}_3\text{CN})_2][\text{BF}_4]$ with an excess of $t\text{Bu-C}\equiv\text{P}$ gives $[\text{Mo}(\eta^5\text{-C}_9\text{H}_7)(\text{CO})_2(\eta^4\text{-1,3-P}_2\text{C}_2\text{tBu}_2)][\text{BF}_4]$ (**D**, Figure 1).⁸ Green and co-workers synthesized mixed valence complexes $[\text{CpMoCl}(\text{CO})\{\eta^3\text{-PC}_2\text{tBu}_2\text{PH}(\text{OR})\}]$ (**E**, R = H, Me, Figure 1) via the facile oxidation of $[\text{CpMoCl}(\text{CO})(\eta^4\text{-1,3-P}_2\text{C}_2\text{tBu}_2)]$ with water and methanol.⁹

We previously reported the synthesis of $[\text{K}([\text{18}]\text{crown-6})(\text{thf})_2][\text{Co}(\text{P}_2\text{C}_2\text{tBu}_2)_2]$ (**F**) by reaction of the Co^- source $[\text{Co}(\eta^4\text{-anthracene})_2]^-$ with $t\text{Bu-C}\equiv\text{P}$ (Figure 2a).^{10,11} This complex is a rare homoleptic 1,3-diphosphacyclobutadiene complex in which all four P atoms can potentially bind to further metal cations. The $[\text{Co}(\text{P}_2\text{C}_2\text{tBu}_2)_2]^-$ anion of **F** and closely related derivatives $[\text{Co}(\text{P}_2\text{C}_2\text{R}_2)_2]^-$ (R = adamantyl or *tert*-pentyl) turned out to be highly versatile and flexidentate metalloligands towards a range of late transition metal cations, as shown by the isolation of structurally diverse and appealing oligonuclear complexes, coordination polymers and supramolecular aggregates.¹²⁻¹⁴

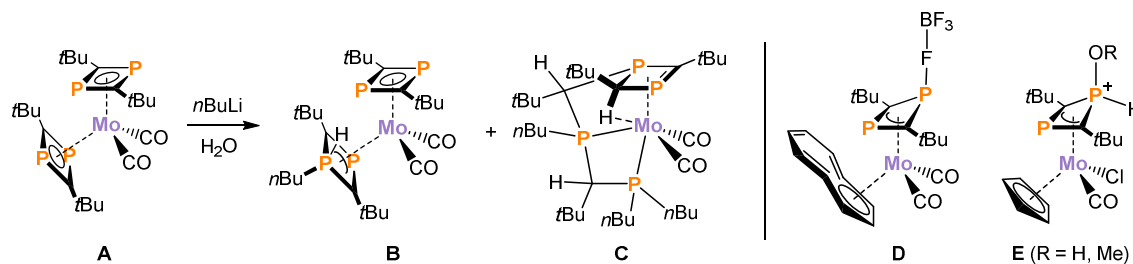


Figure 1. Previously reported derivatizations of 1,3-diphosphacyclobutadiene complexes through the attack of nucleophiles.⁷⁻⁹

Initially, we examined the reactivity of the potassium salt **F** toward electrophiles (Figure 2a) and showed that the reactions of **F** with $\text{HCl}\cdot\text{Et}_2\text{O}$, MeI , and Ph_2PCl afforded structurally distinct neutral species **G–I**.¹⁰ However, the redox activity and the high basicity of **F** seemed to limit the substrate scope.¹⁵ Therefore, in this report we present the reaction of hydride complex **G** with lithium organyls ($n\text{BuLi}$, $t\text{BuLi}$, and PhLi) which gave rise to unprecedented cobalt complexes $[\text{Li}(\text{solv})_x\{\text{Co}(\eta^3\text{-P}_2\text{C}_2\text{tBu}_2\text{HR})(\eta^4\text{-P}_2\text{C}_2\text{tBu}_2)\}]$ [**1**: $\text{R} = n\text{Bu}$, $(\text{solv})_x = (\text{Et}_2\text{O})_2$; **2**: $\text{R} = t\text{Bu}$, $(\text{solv})_x = (\text{thf})_2$; **3**: $\text{R} = \text{Ph}$, $(\text{solv})_x = (\text{THF}/\text{Et}_2\text{O})_x$] with 1,3-diphosphacyclobutene ligands. Moreover, the neutral derivative of **1**, $[\text{Co}(\eta^3\text{-P}_2\text{C}_2\text{tBu}_2\text{H}n\text{Bu})(\eta^4\text{-P}_2\text{C}_2\text{tBu}_2\text{SiMe}_3)$ (**5**), is formed from the reaction of **1** with Me_3SiCl , demonstrating that the salts **1–3** can be further functionalized with suitable electrophiles.

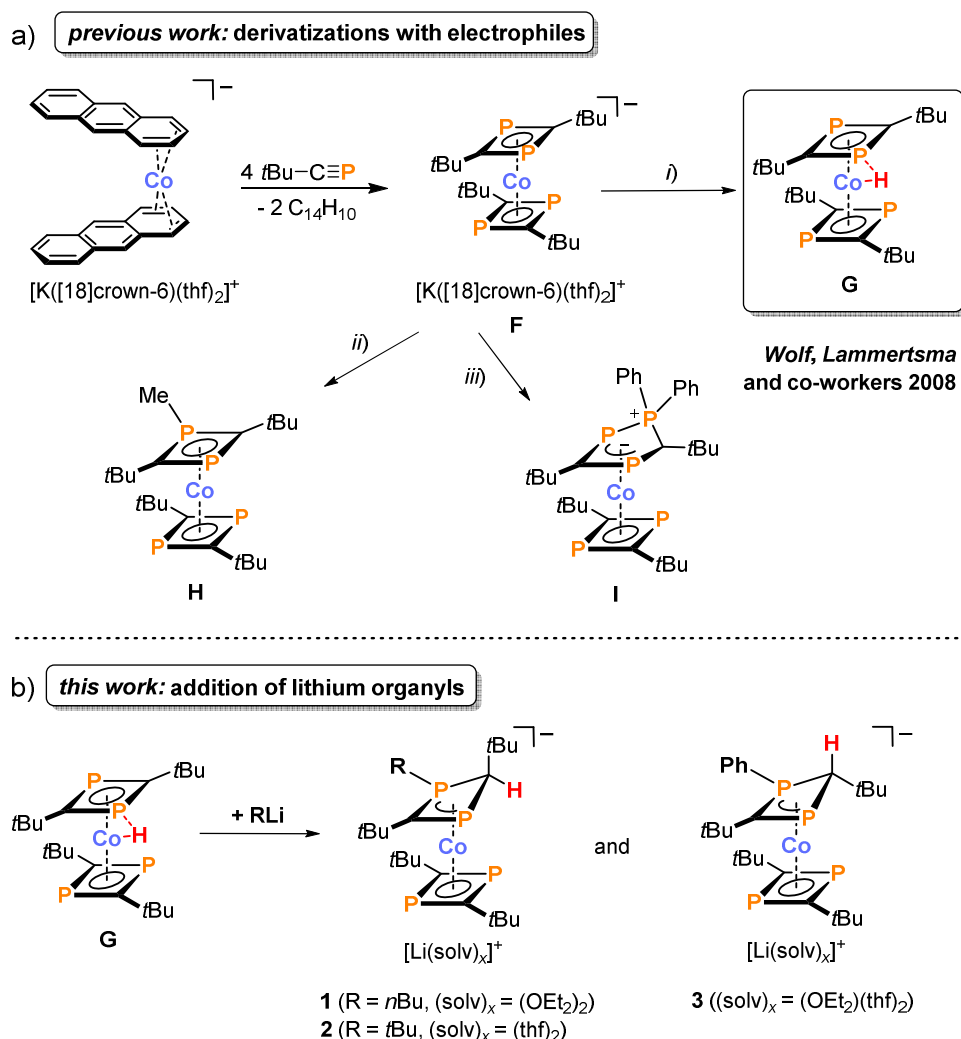


Figure 2. a) Functionalization of **F** by treatment with electrophiles (previous work): *i*) $+\text{HCl}\cdot\text{Et}_2\text{O}/\text{-KCl}$, $-\text{[18]crown-6}$; *ii*) $+\text{MeI}/\text{-KI}$, $-\text{[18]crown-6}$; *iii*) $+\text{Ph}_2\text{PCl}/\text{-KCl}$, $-\text{[18]crown-6}$; b) synthesis of anionic 1,3-diphosphacyclobutene complexes **1–3** by addition of lithium organyls to **G** (this work).

3.2 Results and Discussion

3.2.1 Reaction of [Co(P₂C₂tBu₂)H] with Lithium Organyls

The reaction of [Co(P₂C₂tBu₂)₂H] (**G**) with *n*BuLi (one equiv., Figure 2b) proceeds in a selective fashion at low temperature (> -80 °C) and afforded [Li(OEt)₂{Co(η³-P₂C₂tBu₂H*n*Bu)-(η⁴-P₂C₂-*t*Bu₂)}] (**1**). The ³¹P NMR spectrum of **1** shows resonances at δ(³¹P) = -82.1, -42.7, and -13.9 ppm, which integrate in a 1:1:2 ratio (**G**: δ(³¹P) = -181.3, 18.2 and 118.3 ppm).^{10a} Deep orange-colored, X-ray quality crystals of **1** are obtained in 75% yield from a diethyl ether solution stored at -35 °C. Although **1** is thermally stable in the solid state at ambient temperature, it decomposes in THF, diethyl ether, and benzene over the course of several hours giving an intractable mixture of several compounds (see Figure S3, Supporting Information).

The molecular structure of **1** (Figure 3) shows that an addition of one equivalent of *n*BuLi to **G** has occurred. The *n*-butyl group is now connected to one of the P atoms (P1–C21 1.855(6) Å) and the former hydride ligand is shifted to a carbon atom (C1) of the same P₂C₂ ring with a freely refined C1–H1 distance of 0.98001(4) Å. The reaction of **G** with *n*BuLi thus results in the formation of a 1,3-diphosphacyclobutene ligand. While free diphosphacyclobutenes are well known,¹⁶ metal complexes of them are rather scarce. Yoshifuji and co-workers described chromium and molybdenum pentacarbonyl complexes of several 1,3-diphosphacyclobutenes, which were obtained by treatment of Mes*–C≡P (Mes* = 2,4,6-tri-*tert*-butylphenyl) with nucleophiles.¹⁷ Stannylated 1,3-diphosphacyclobutenes were reported by Regitz and co-workers.¹⁸ An unusual 1,3-diphosphacyclobutene compound ClSb(P₂C₂tBu₂) with a side-on coordinated SbCl unit was obtained by Russel and co-workers by treatment of [Cp₂Zr(P₂C₂tBu₂)] with SbCl₃.¹⁹ The 1,3-diphosphacyclobutene ligand in **1** is clearly η³-coordinated (Co1–P1 2.180(2) Å, Co1–P2 2.300(2) Å, Co1–C1 3.051(1) Å, Co1–C2 2.010(5) Å) with a fold angle around the P1–P2 vector of 34.3°. The P–C distances of P1–C1 1.839(6) Å, P1–C2 1.767(6) Å, and P2–C2 1.822(6) Å suggest that these bonds have some multiple bonding character, whereas the P2–C1 bond length of 1.930(7) Å is indicative of a single bond. The lithium cation is coordinated by two P atoms (Li1–P2 3.5434(2), Li1–P3 2.5034(1) Å) and two diethyl ether molecules in a distorted tetrahedral fashion. The Co1–Li1 distance of 3.04(1) Å indicates that there is an interaction between the metal atoms in the solid state (sum of van-der-Waals radii of the respective atoms $\sum r_{\text{vdW}}(\text{Co}, \text{Li}) = 3.82 \text{ \AA}$).²⁰

A DFT optimization with the B3LYP-D3BJ/def2-TZVP level of theory reproduced the molecular structure of **1** accurately (see the Supporting Information). The Wiberg bond indices (WBIs) support partial multiple bond character for P1–C2 and P2–C2 (WBIs of 1.02 and 1.05, respectively), whereas the P1–C1 and P2–C1 (WBI 0.91 and 0.85, respectively) and the P1–C21 bonds (WBI 0.86) have lower WBIs. WBIs of 0.03 and 0.06 were calculated for Li1–P2 and Li1–P3, in line with the presumably ionic character of these bonds.

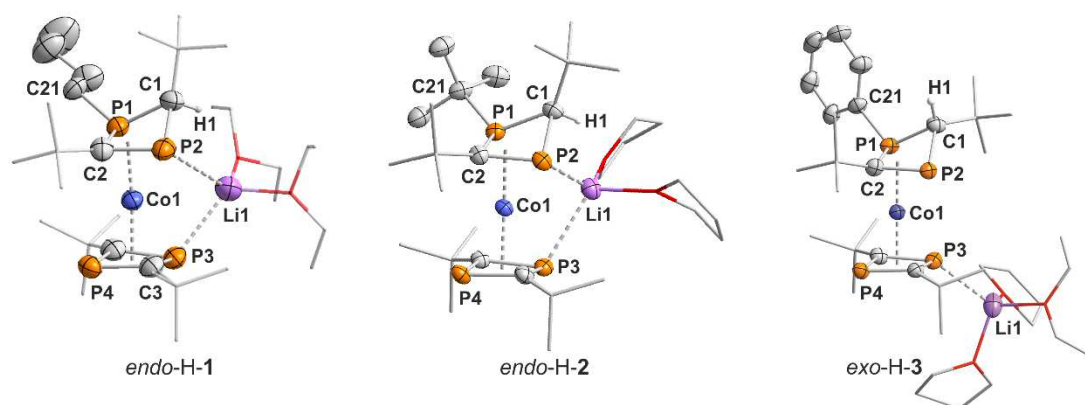
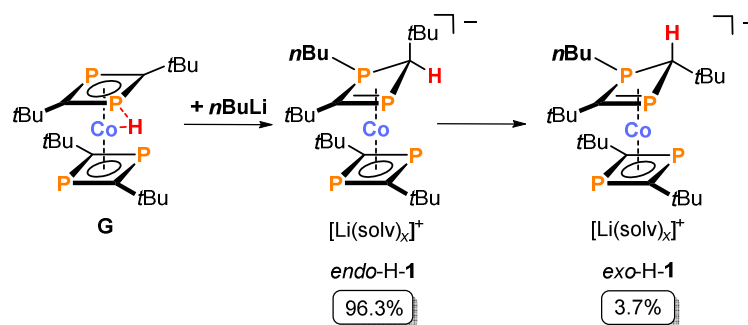


Figure 3. Solid-state molecular structures of **1-3**. The hydrogen atoms, except H1, are omitted for clarity. Thermal ellipsoids are drawn at the 50% probability level. Selected bond lengths [Å] and angles [°] for *endo-H-1*: P1–C1 1.839(6), P1–C2 1.767(6), P1–C21 1.855(6), P2–C1 1.930(7), P2–C2 1.822(6), C1–H1 0.98001(4), Co1–P1 2.180(2), Co1–P2 2.300(2), Co1–P3 2.298(2), Co1–P4 2.254(2), Co1–C1 3.051(1), Co1–C2 2.010(5), Co1–C3 2.052(5), Co1–C4 2.057(6), Co1–Li1 3.04(1), Li1–P2 3.5434(2), Li1–P3 2.5034(1), P1–C1–P2 82.8(2), C2–P1–C1 91.4(3), C1–P2–C2 86.9(3), P1–C2–P2/P2–C1–P1 34.3; *endo-H-2*: P1–C1 1.858(3), P1–C2 1.778(3), P1–C21 1.889(3), P2–C1 1.937(3), P2–C2 1.824(3), C1–H1 0.98000(2), Co1–P1 2.1903(8), Co1–P2 2.2853(7), Co1–P3 2.2390(8), Co1–P4 2.2653(8), Co1–C1 3.079(1), Co1–C2 2.021(3), Co1–C3 2.086(2), Co1–C4 2.072(3), Co1–Li1 2.726(5), Li1–P2 3.053(5), Li1–P3 2.578(5), P1–C1–P2 81.9(1), C2–P1–C1 91.4(1), C1–P2–C2 87.6(1), P1–C2–P2/P2–C1–P1 35.6; *exo-H-3*: P1–C1 1.840(3), P1–C2 1.784(3), P1–C21 1.845(3), P2–C1 1.932(3), P2–C2 1.805(3), C1–H1 0.94400(2), Co1–P1 2.2105(8), Co1–P2 2.2943(8), Co1–P3 2.2685(8), Co1–P4 2.2535(8), Co1–C1 3.079(1), Co1–C2 1.981(3), Co1–C3 2.051(3), Co1–C4 2.069(3), Li1–P3 2.667(6), P1–C1–P2 83.0(1), C2–P1–C1 89.3(1), C1–P2–C2 85.8(1), P1–C2–P2/P2–C1–P1 38.7.

The NMR data of **1** (recorded in $[D_8]THF$) supports the crystallographically determined structure in solution, however, it also suggests the presence of a second compound (*exo-H-1*) in trace amounts (3.7%). Presumably, the crystallographically characterized isomer, labeled *endo-H-1* from now on (Scheme 1), appears to be a kinetic product, whereas *exo-H-1* is the thermodynamic product ($\Delta\Delta G = -0.9 \text{ kcal mol}^{-1}$ according to DFT calculations, see below). Unfortunately, we could not observe the interconversion of *endo-H-1* into *exo-H-1* due to the gradual decomposition of the compound into an intractable product mixture (see above and Figure S3, SI).



Scheme 1. Formation of *endo-H-1* and *exo-H-1*, ratio determined by $^{31}P\{^1H\}$ NMR spectroscopy; $(\text{solv})_x = (\text{OEt}_2)_2$.

In the ^1H NMR spectrum of *endo*-H-1, three singlets in a 2:1:1 integral ratio at $\delta(^1\text{H}) = 0.92$, 1.06, and 1.39 ppm were assigned to the chemically different *tert*-butyl substituents, whereas a set of four additional signals in the aliphatic region arises from the *n*-butyl substituent. A doublet at $\delta(^1\text{H}) = 2.22$ ppm, with $^2J_{\text{H,P}} = 7.8$ Hz, was assigned to the hydrogen atom (H1) of the 1,3-diphosphacyclobutene ligand of *endo*-H-1. The ^{31}P NMR spectrum shows three major resonances for *endo*-H-1 of which the singlet at $\delta(^{31}\text{P}) = -14.8$ ppm was assigned to the P atoms of the $\text{P}_2\text{C}_2t\text{Bu}_2$ ligand (P3 and P4). This signal splits into two signals upon cooling and from the decoalescence temperature at 260 K (see Figure S9, Supporting Information, for the VT ^{31}P NMR spectra) a rotational barrier of $10.3 \text{ kcal mol}^{-1}$ was determined for the hindered rotation of the 1,3-diphosphacyclobutadiene ligand around the centroid(P_2C_2)–cobalt axis following the method reported by Gutowsky and Holm.²¹

The further observed, presumed AX spin system ($\delta(^{31}\text{P}_\text{A}) = -83.0$ ppm, $\delta(^{31}\text{P}_\text{X}) = -43.5$ ppm; $^2J_{\text{P,P}} = 54.6$ Hz), is assigned to the P atoms of the 1,3-diphosphacyclobutene moiety $\text{P}_2\text{C}_2t\text{Bu}_2\text{H}n\text{Bu}$ (P1 and P2). To fully assign the connectivity of the 1,3-diphosphacyclobutene moiety, 2D ^1H - ^{31}P correlation NMR experiments were performed (Figure 4). The ^1H - ^{31}P HMBC NMR spectrum reveals a strong correlation between the *n*-butyl resonances ($\delta(^1\text{H}) = 1.23$ – 1.36 and 1.47 – 1.66 ppm) and the ^{31}P resonance at $\delta(^{31}\text{P}) = -43.5$ ppm (marked in green in Figure 4),

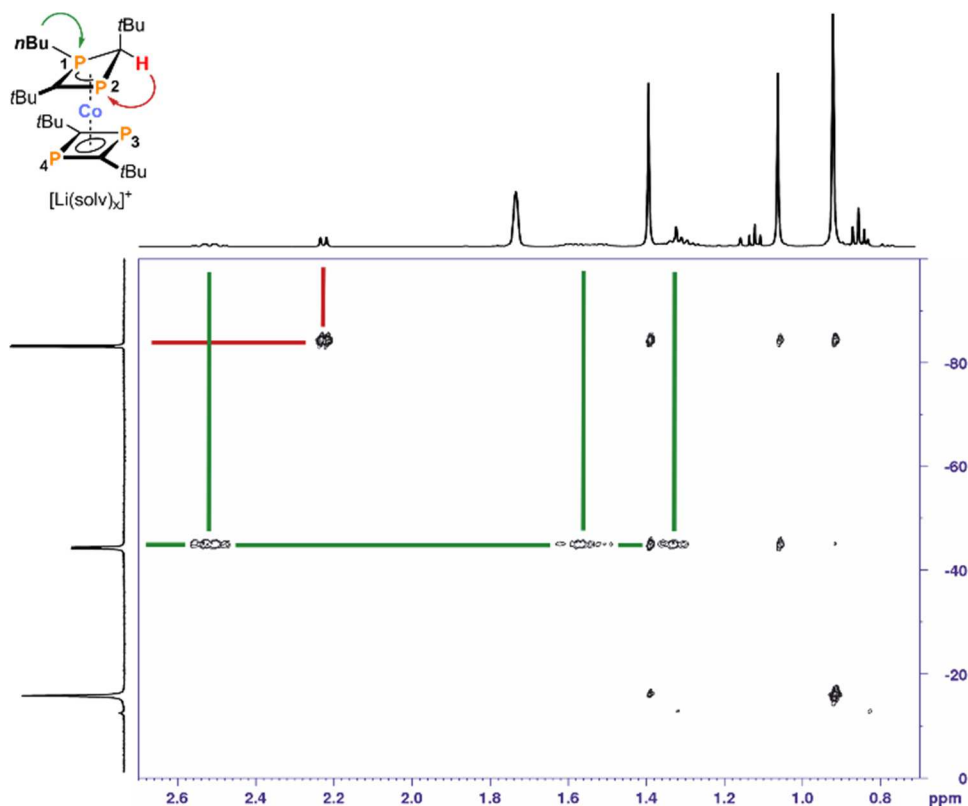


Figure 4. ^1H - ^{31}P HMBC NMR spectrum of *endo*-H-1; correlation of H1 and P2 is marked in red and correlation between the *n*-butyl protons and P1 is marked in green.

which confirms that this ^{31}P NMR resonance arises from the tricoordinate P1 atom. Interestingly, the H1 proton ($\delta(^1\text{H}) = 2.22$ ppm) shows only a correlation to the disubstituted P2 atom ($\delta(^{31}\text{P}) = -83.0$ ppm, marked in red), indicating the spatial proximity of H1 to P2 and thus, confirming the equatorial arrangement of H1 also in solution.

Furthermore, the second, minor species observed in the ^{31}P NMR spectrum with resonances at $\delta(^{31}\text{P}) = -132.9$, -57.0 , and -13.7 ppm in a 1:1:2 integral ratio is attributed to *exo*-H-**1** (Figure S9, Supporting Information). The assignment of the signals is analogous to *endo*-H-**1**. However, the resonance of P2 in *exo*-H-**1** ($\delta(^{31}\text{P}) = -132.9$ ppm) is strongly shifted to higher field compared with the P2 atom in *endo*-H-**1** ($\delta(^{31}\text{P}) = -83.0$ ppm). The ratio of *endo*-H-**1**:*exo*-H-**1** is 96.3:3.7 according to the signal ratio in the ^{31}P NMR spectrum (Scheme 1).

The cyclic voltammogram of **1** recorded in THF/[*n*Bu₄N]PF₆ shows a reversible oxidation wave at $E_{1/2} = -1.38$ V (vs. ferrocene/ferrocenium, Fc/Fc⁺, see Figure S16a in the Supporting Information), suggesting the formation of a putative neutral derivative [Co(η^3 -P₂C₂tBu₂H*n*Bu)(η^4 -P₂C₂tBu₂)]. It is proposed that this redox event is metal-centered, because the HOMO is mainly localized at the cobalt atom (Figure S17). Attempts to isolate this oxidized species on a preparative scale by oxidation **1** with [Cp₂Fe]PF₆ have failed so far.

Similar to the reaction with *n*BuLi, hydride complex **G** also reacts cleanly with *t*BuLi and PhLi to afford [Li(thf)₂{Co(η^3 -P₂C₂tBu₃H)(η^4 -P₂C₂tBu₂)}] (**2**) and [Li(Et₂O)₂(thf){Co(η^3 -P₂C₂tBu₂PhH)(η^4 -P₂C₂tBu₂)}] (**3**), respectively. Deep-red crystals of **2** were isolated from *n*-hexane (55% yield), whereas the deep-orange compound **3** was crystallized from diethyl ether (66% yield). Similar to **1**, both complexes are stable as solids for weeks at ambient temperature, however, they decompose slowly in solution to a mixture of products (see Figure S5 and S7, Supporting Information). Single-crystal X-ray structure analyses revealed that the structure of **2** (Figure 3) is essentially analogous to **1**, whereas **3** crystallized as a distinct diastereomer with respect to **1** and **2**. In the structure of **3**, the hydrogen atom on the tetracoordinate carbon atom C1 assumes an axial position, pointing away from the cobalt center, whereas the *tert*-butyl group on C1 assumes the equatorial position and points towards the cobalt atom. In contrast to **1** and **2**, the lithium cation in **3** is coordinated by just one P atom of the remaining 1,3-diphosphacyclobutadiene ligand (Li1–P3 2.667(6) Å). The distorted tetrahedral coordination sphere of Li1 is completed by one THF and two diethyl ether molecules.

The NMR spectra of **2** and **3** in [D₈]THF reflect the different structural arrangements observed in the solid state. Similar to **1**, the ^1H NMR and $^{31}\text{P}\{^1\text{H}\}$ NMR spectra of **2** show the signals of a single diastereomer (presumably *endo*-H-**2**), whereas a second diastereomer was not detected. The ^1H NMR spectrum shows that **2** gives rise to a doublet resonance at $\delta(^1\text{H}) = 2.45$ ppm ($^2J_{\text{H,P}} = 5.9$ Hz) for the H1 proton. The $^{31}\text{P}\{^1\text{H}\}$ NMR spectrum of **2** (Figure S4, Supporting Information) is comparable to that of **1** and shows a singlet at $\delta(^{31}\text{P}) = -14.8$ ppm, which is

attributed to the P atoms at the 1,3-diphosphacyclobutadiene moiety, P3 and P4. The AX spin system of the 1,3-diphosphacyclobutene ligand is detected at $\delta(^{31}\text{P}_A) = -102.0$ ppm and $\delta(^{31}\text{P}_X) = -2.4$ ppm ($^2J_{\text{P,P}} = 54.2$ Hz). The A part was, similar to complex **1**, assigned to the disubstituted P2 atom, and consequently the X part was assigned to the tricoordinate P1 atom. In analogy to complex **1**, the assignment was made by the ^1H - ^{31}P HMBC NMR experiment (see Figure S10).

In contrast, the ^{31}P NMR spectrum of **3** in $[\text{D}_8]\text{THF}$ (Figure S6, Supporting Information) shows two broad resonances for P3 and P4 at $\delta(^{31}\text{P}) = -11.0$ ppm and -6.6 ppm, with a coalescence temperature of 320 K (see Figure S11 for VT ^{31}P NMR spectra). The observation of two NMR signals for the 1,3-diphosphacyclobutadiene ligand is likely due to hindered rotation of this ring around the centroid (P_2C_2)-cobalt axis. Using the method reported by Gutowsky and Holm,²¹ a rotational barrier of 13.4 kcal mol⁻¹ was determined for this hindered rotation. The resonances for the AX spin system of the diphosphacyclobutene moiety (P1 and P2) were found at $\delta(^{31}\text{P}_A) = -109.1$ ppm and $\delta(^{31}\text{P}_X) = -89.3$ ppm ($^2J_{\text{P,P}} = 48.6$ Hz). The pronounced upfield-shifted resonance of the P1 atom ($\delta(^{31}\text{P}) = -89.3$ ppm) compared with those of **1** and **2** (-42.7 and -2.4 ppm, respectively) is indicative for a different diastereomer, that is, *exo*-H-**3** instead of *endo*-H-**1** and *endo*-H-**2**. Accordingly, the doublet for the H1 proton ($\delta(^1\text{H}) = 4.90$ ppm, $^2J_{\text{H,P}} = 14.3$ Hz) is substantially shifted to lower field compared with **1** and **2** (2.22 and 2.45 ppm, respectively). For comparison, the stacked ^1H NMR spectra of *endo*-H-**2** and *exo*-H-**3** are depicted in Figure 5.

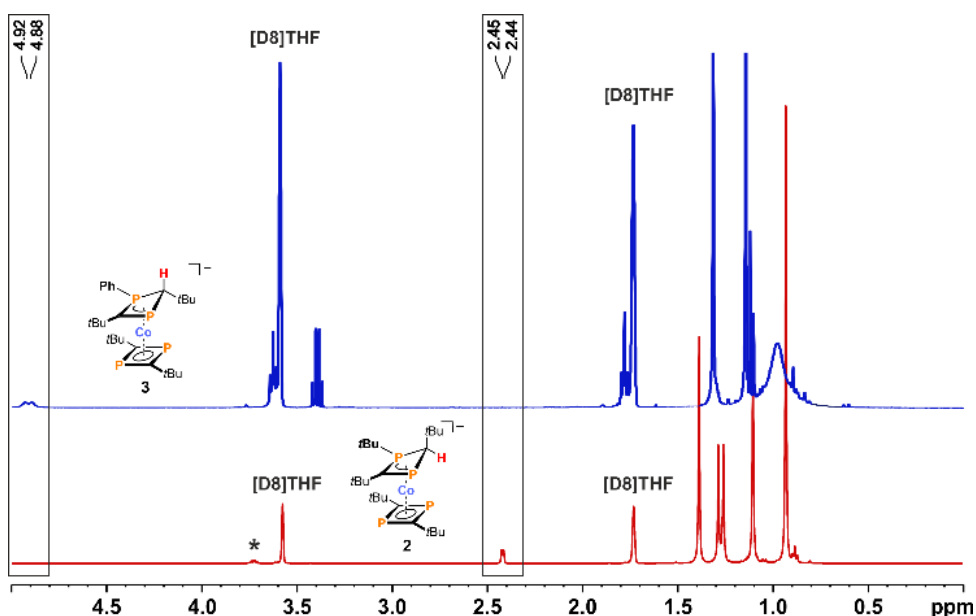


Figure 5. Comparison of ^1H NMR signals assigned to H1 of *endo*-H-**2** (bottom) and *exo*-H-**3** (top). The asterisk denotes an impurity.

The 2D ^1H - ^{31}P correlation NMR experiments further support the presence of the *exo*-H-diastereomer of **3** (Figure 6). The ^1H - ^{31}P -HMBC spectrum shows, in contrast to **1** and **2**, a correlation between the resonance of P1 ($\delta(^{31}\text{P}) = -89.3$ ppm) only to the *ortho* protons of the phenyl-substituent ($\delta(^1\text{H}) = 7.57$ – 7.66) and to H1 ($\delta(^1\text{H}) = 4.90$ ppm).

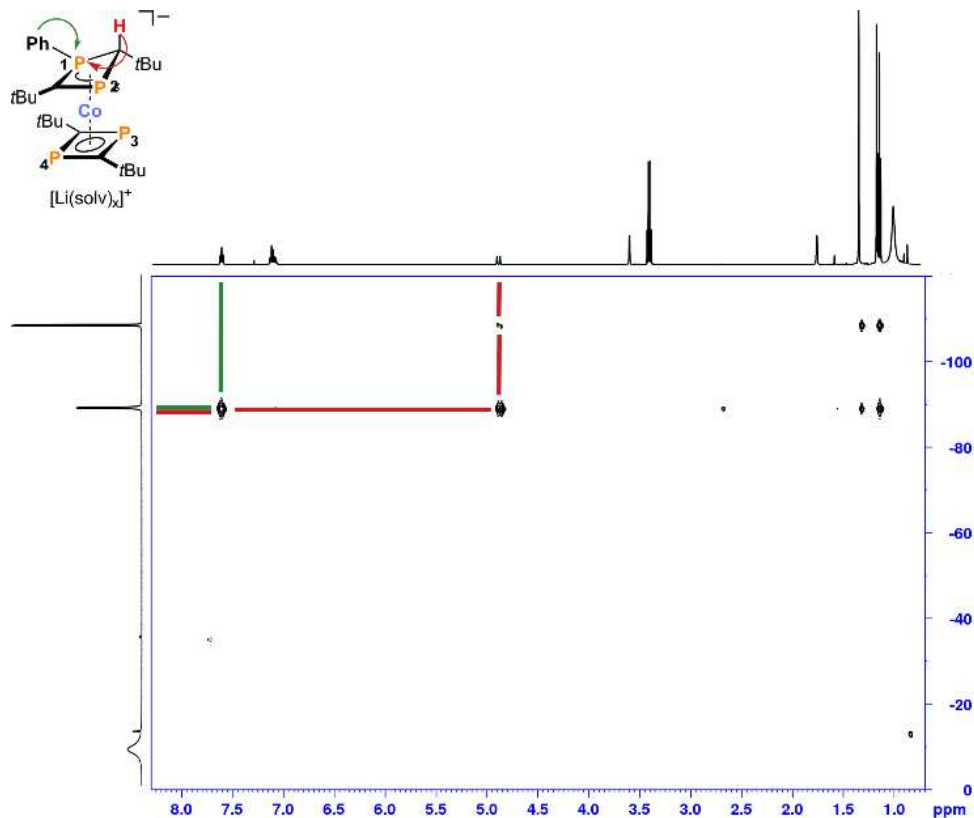
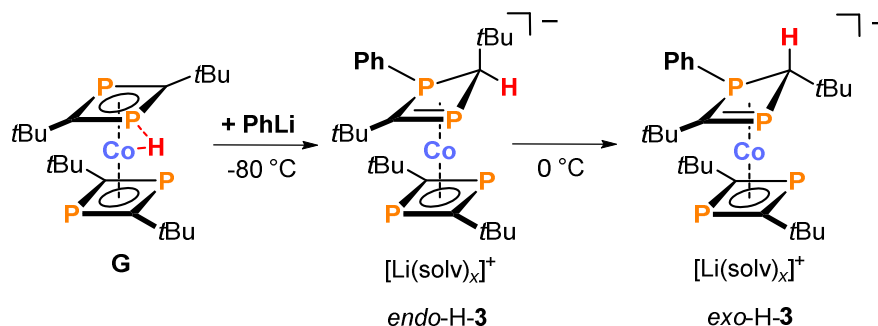


Figure 6. ^1H - ^{31}P HMBC NMR spectrum of *exo*-H-**3** at 320 K; correlation of H1 and P2 is marked in red and correlation between the phenyl protons and P1 is marked in green.

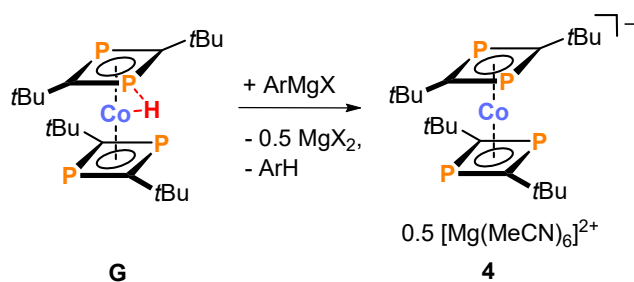
To elucidate the formation of *exo*-H-**3**, the reaction of **G** with one equivalent PhLi was monitored by ^{31}P NMR spectroscopy, which showed that the formation of *exo*-H-**3** proceeds via *endo*-H-**3** (Scheme 2 and Figure S12, see Supporting Information for further details). Compound *endo*-H-**3** already forms at 193 K and shows four resonances in the ^{31}P NMR spectrum. In accordance with the previous findings, the resonances at $\delta(^{31}\text{P}) = -22.1$ and -4.3 ppm were assigned to the 1,3-diphosphacyclobutadiene ligand, whereas the AX spin system at $\delta(^{31}\text{P}_\text{A}) = -92.0$ and $\delta(^{31}\text{P}_\text{X}) = -34.6$ ppm was assigned to P2 and P1, respectively. However, the reaction appears to be slow until 253 K, which was demonstrated by the presence of large amounts of **G** (ca. 86%). At 273 K, the formation of the *exo*-H isomer starts, although there is still some **G** left (ratio **G**/*endo*-H/*exo*-H = 31:68:1). Although **G** is fully consumed at 283 K, the ratio of *endo*-H/*exo*-H decreases (84:17).

Scheme 2. Formation of *exo*-H-3 via the *endo*-H isomer; (solv)_x = (OEt₂)(thf)₂.

The cyclic voltammograms of **2** and **3** recorded in THF/[*n*Bu₄N]PF₆ (Supporting Information, Figures S16b and S16c) each feature a reversible oxidation process at $E_{1/2} = -1.44$ V (**2**) and $E_{1/2} = -1.29$ V (**3**) (vs. Fc/Fc⁺), which is very similar to **1** ($E_{1/2} = -1.38$ V vs. Fc/Fc⁺).

3.2.2 Reaction of [Co(P₂C₂tBu₂)H] with Grignard Reagents

In contrast to the reaction of **G** with PhLi (which affords **3**), reaction of **G** with aryl Grignard reagents such as *p*-fluorophenyl magnesium bromide and *p*-tolyl magnesium chloride cleanly afford [Mg(MeCN)₆][Co(η⁴-P₂C₂tBu₂)₂]₂ (**4**, Scheme 3), which is formed by deprotonation of **G**. Single-crystal X-ray diffraction analysis on crystals obtained from acetonitrile/THF solution revealed an ion-separated molecular structure consisting of two [Co(P₂C₂tBu₂)₂]⁻ sandwich anions and a [Mg(MeCN)₆]²⁺ cation (see Supporting Information, Figure S1).²² The structural parameters and the redox properties of **4** are unremarkable;^{10,12} further details are discussed in the Supporting Information. The divergent reactivity of aryl Grignard and aryl lithium reagents may be rationalized by the different basicity and nucleophilicity of such reagents.²³

Scheme 3. Synthesis of magnesium salt **4**; Ar = C₆H₄-4-Me, X = Cl; Ar = C₆H₄-4-F, X = Br.

3.2.3 Computational Studies

DFT calculations were performed to investigate the isomers of **1–3** in more detail. Optimizations at the B3LYP-D3/def2-TZVP level of theory^{24–26} showed that the *endo*-H and the *exo*-H isomers of **1–3** are viable species. The calculated Gibbs energies (calculated at the B3LYP-D3/def2-TZVP level of theory on the optimized structures (see the Supporting Information for details), furthermore showed that the *exo*-H isomer is energetically favored for all three species, although

the energy differences are relatively small (Table 1). The same general trend was found for a range of other functionals and basis sets (see the Supporting Information).

Table 1. Gibbs energies ΔG [Hartree] and Gibbs-energy differences $\Delta\Delta G$ [kcal mol⁻¹] of both isomers (*endo*-H and *exo*-H) of compounds 1–3 calculated at the B3LYP-D3/def2-TZVP level of theory.

Isomer	1	2	3
<i>endo</i> -H [Hartree]	-3690.941896	-3690.934175	-3764.803146
<i>exo</i> -H [Hartree]	-3690.943280	-3690.940641	-3764.809042
$\Delta\Delta G$ [kcal mol ⁻¹]	-0.9	-4.1	-3.7

In addition, the calculations revealed a potential pathway for the transformation of *endo*-H-3 into *exo*-H-3 (Figure 7). For computational efficiency, these calculations were performed at the B3LYP-D3/def2-TZVP level of theory on the truncated model 3', in which the *t*Bu substituents were replaced by methyl groups and the lithium cation as well as the solvent molecules were omitted. The isomerization of *endo*-H-3' to *exo*-H-3' is initiated by an insertion of cobalt into a P–C bond of the diphosphacyclobutene ligand, resulting in the formation of intermediate Int-3', which contains a five-membered CoP₂C₂ ring. No transition state was found for this process.

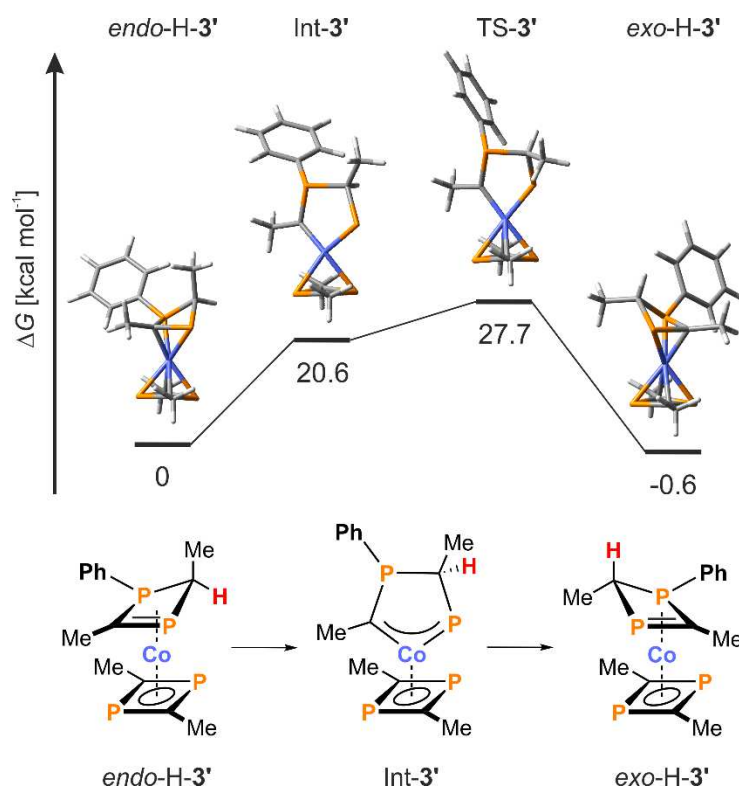
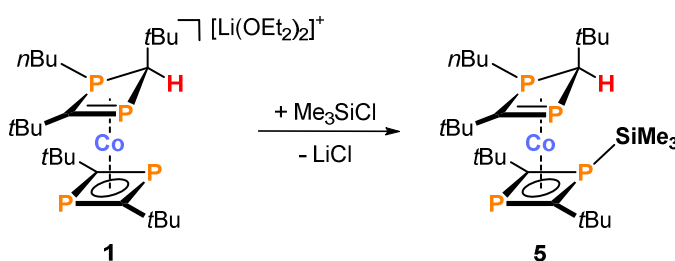


Figure 7. Postulated mechanism for the formation of the *exo*-H isomer from the *endo*-H isomer through oxidative addition of the 1,3-diphosphacyclobutene ligand to cobalt. Gibbs energies [kcal mol⁻¹] are given.

The subsequent conversion of Int-**3'** to *exo*-H-**3'** represents a ring flip, which leads to an inversion of the configuration of the phenyl-substituted P atom. It is important to note that the energy of the transition state TS-**3'** associated with this transformation (+27.7 kcal mol⁻¹) inevitably entails a large degree of uncertainty due to the use of a simplified model complex. Nevertheless, the energy of TS-**3'** is too high for the transformation to occur below room temperature. Thus, alternative pathways cannot be excluded definitively at present.

3.2.4 Synthesis of **5** by Trimethylsilylation of **1**

As an initial test regarding the reactivity of **1**, we investigated the reaction with trimethylchlorosilane (Scheme 4). Addition of Me₃SiCl (one equivalent) to a toluene solution of **1** at -60 °C resulted in the quantitative formation of [Co(η³-P₂C₂tBu₂H*n*Bu)(η⁴-P₂C₂tBu₂SiMe₃)] (5). Deep-red crystals of **5** was isolated from *n*-hexane in 52% yield.



Scheme 4. Synthesis of **5**.

The molecular structure of **5** (Figure 8) shows that the overall structural arrangement observed for **1** is retained in **5**. The Me₃Si group (P3–Si1 2.3238(6) Å) is bound to a phosphorus atom of the previously unsubstituted P₂C₂ ring. As a result, this formerly planar ligand is tilted (P3-C3-P4/P4-C4-P3 planes 27.9°; the same dihedral angle amounts to 12.5° in *endo*-H-**1** and 7.5° in **G**), and the Co1–P3 distance (2.4066(5) Å) is significantly elongated compared with Co1–P4 (2.2584(5) Å). In contrast to related trimethylsilylated bis(1,3-diphosphacyclobutadiene) complexes [Co(P₂C₂R₂)₂(SiMe₃)],¹⁵ the Me₃Si moiety assumes an *endo*-configuration pointing towards cobalt. This unexpected arrangement might be explained by a template effect of the lithium cation, which assumes a bridging position in the molecular structure of *endo*-H-**1**. The folding of the P1-C1-P1-C2 ring along the P1-P2 axis (P1-C2-P2/P2-C1-P1 33.1°) is very similar to that of *endo*-H-**1** (33.4°).

The NMR data of **5** in C₆D₆ is in line with the crystallographically determined molecular structure. The ¹H NMR spectrum displays four signals at δ(¹H) = 1.21, 1.31, 1.34, and 1.36 ppm which correspond to the *t*Bu moieties and four signals for the *n*-butyl substituent (δ(¹H) = 0.76, 1.12-1.19, 1.44-1.76, and 2.43-2.57 ppm). The SiMe₃ group gives rise to a doublet resonance at δ(¹H) = 0.55 ppm with a ³J_{H,P} = 5.3 Hz. The characteristic resonance of H1 attached to the 1,3-diphosphacyclobutene ligand appears as a doublet resonance at δ(¹H) = 2.77 ppm (2.22 ppm in *endo*-H-**1**). The ³¹P{¹H} NMR spectrum (Figure S8, Supporting Information) gives rise to two

AX spin systems. The AX spin system at $\delta(^{31}\text{P}_\text{A}) = -195.8$ ppm and $\delta(^{31}\text{P}_\text{X}) = 60.3$ ppm ($^2J_{\text{P,P}} = 41.9$ Hz) is attributed to the silyl-substituted ligand. This assignment is supported by 2D ^1H - ^{31}P correlation NMR experiments which reveal the A-part ($\delta(^{31}\text{P}_\text{A}) = -195.8$ ppm) arises from the P3 atom, which carries the silyl substituent. The second AX spin system at $\delta(^{31}\text{P}_\text{A}) = -71.7$ ppm and $\delta(^{31}\text{P}_\text{X}) = -30.6$ ppm ($^2J_{\text{P,P}} = 51$ Hz) is, therefore, attributed to the *n*-butyl substituted P₂C₂ ligand. Similar to *endo*-H-1 and *endo*-H-2, the A-part can be assigned to the disubstituted P2 atom and the X-part to the tricoordinate P1 atom. The assignment was confirmed by an ^1H - ^{31}P HMBC NMR experiment (Supporting Information, Figure S13).

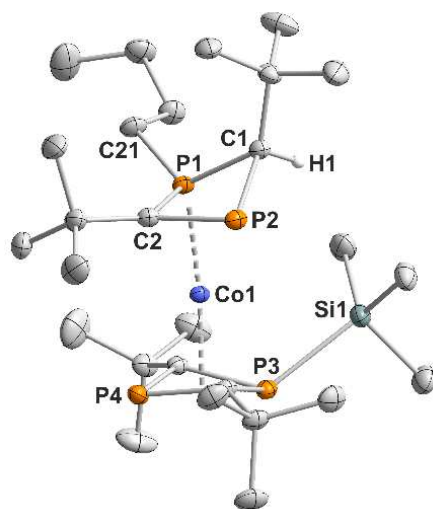


Figure 8. Solid-state molecular structure of **5**. The hydrogen atoms, except H1, are omitted for clarity. Thermal ellipsoids are drawn at the 50% probability level. Selected bond lengths [Å] and angles [°]: P1–C1 1.834(2), P1–C2 1.772(2), P1–C21 1.837(2), P2–C1 1.934(2), P2–C2 1.812(2), C1–H1 0.90573(4), P3–C3 1.830(2), P3–C4 1.183(2), P3–Si1 2.3238(6), P4–C3 1.794(2), P4–C4 1.790(2), Co1–P1 2.1827(5), Co1–P2 2.2986(5), Co1–P3 2.4066(5), Co1–P4 2.2584(5), Co1–C1 3.020(1), Co1–C2 2.027(2), Co1–C3 2.011(2), Co1–C4 2.000(2), P1–C1–P2 83.26(7), C2–P1–C1 91.27(8), P1–C2–P2/P2–C1–P1 33.1, P3–C3–P4/P4–C4–P3 27.9.

During the course of the NMR measurements we found that complex **5** slowly decomposed in THF. The ^{31}P NMR spectrum shows an AX spin system similar to that of complex **5** with $\delta(^{31}\text{P}_\text{A}) = -80.3$ ppm and $\delta(^{31}\text{P}_\text{X}) = -34.0$ ppm ($^2J_{\text{P,P}} = 58$ Hz). These signals were assigned to P2 and P1, respectively. However, the resonances of the second AX spin system at $\delta(^{31}\text{P}_\text{A}) = -159.8$ ppm and $\delta(^{31}\text{P}_\text{X}) = 89.9$ ppm ($^2J_{\text{P,P}} = 61$ Hz) are significantly shifted downfield (Figure S14, Supporting Information). Additionally, the silyl fragment seems to be rearranged, because there is no coupling to phosphorus observed in the ^1H NMR spectrum as well as in the 2D ^1H - ^{31}P correlation NMR experiments. The silyl fragment gives rise to a singlet resonance at $\delta(^1\text{H}) = 0.08$ ppm in the ^1H NMR spectrum (see Figure S15). Attempts to determine the structure of this complex in more detail by NMR spectroscopy, X-ray analysis and DFT calculations have so far been unsuccessful.

3.3 Conclusion

Although reactions of the bis(1,3-diphosphacyclobutadiene) cobalt hydride [Co(P₂C₂tBu₂)₂H] (**G**) with aryl Grignard reagents selectively deprotonate **G** to afford the first magnesium salt of the [Co(η⁴-P₂C₂tBu₂)₂]⁻ anion, reactions with organyl lithium reagents (*n*BuLi, *t*BuLi, and PhLi) resulted in the formation of unprecedented 1,3-diphosphacyclobutene cobalt complexes **1–3**. The reactions proceed by nucleophilic attack at a P atom and hydride transfer from cobalt to a carbon atom, forming η³-coordinated 1,3-diphosphacyclobutene ligands. Due to the presence of a chiral carbon center and planar chirality, **1–3** may form diastereomers. Compounds **1** and **2** showed the *endo*-H-diastereomer (*endo*-H-**1** and *endo*-H-**2**), whereas the structure of **3** shows another diastereomeric form (*exo*-H-**3**). Salt metathesis of complex **1** with Me₃SiCl affords trimethylsilyl-substituted complex **5**, showing that anions such as **1–3** can in principle be further functionalized. The stereochemistry is conserved in this reaction. Considering the high reactivity of closely related silylated 1,3-diphosphacyclobutadiene complexes,¹⁵ a plethora of functionalized sandwich complexes should be accessible by insertion reactions in the phosphorus-silicon bond of such complexes.

3.4 Supporting Information

3.4.1 General Procedures

All experiments were performed under an atmosphere of dry argon using standard Schlenk techniques or a MBraun UniLab glovebox. Solvents were dried and degassed with a MBraun SPS800 solvent purification system. Acetonitrile, tetrahydrofuran, toluene, and diethyl ether were stored over molecular sieves (3 Å). *n*-Hexane was stored over a potassium mirror. NMR spectra were recorded on either Bruker Avance 300/400 spectrometers at 300 K or on a Bruker Avance III HD Nanobay 400 MHz Ultrashield and on a Bruker Avance III HDX 500 Mhz Ascend. The spectra are referenced to residual solvent resonances as internal standard. Melting points were measured on samples in sealed capillaries on a Stuart SMP10 melting point apparatus. UV/Vis spectra were recorded on an Ocean Optics Flame Spectrometer. Elemental analyses were determined by the analytical department of Regensburg University. Compound [Co(P₂C₂tBu₂)₂H] (**G**) was synthesized according to a literature procedure.^{10a} The reagents *n*BuLi, *t*BuLi, PhLi, (C₆H₄-4-Me)MgCl, and (C₆H₄-4-F)MgBr were purchased from Sigma Aldrich and used as received.

3.4.2 Synthesis and Characterization

3.4.2.1 Synthesis of [Li(OEt)₂{Co(η³-P₂C₂tBu₂*n*Bu)(η⁴-P₂C₂tBu₂)}] (*endo*-H-1)

A solution of [Co(P₂C₂tBu₂)₂H] (**G**, 0.11 mg, 0.24 mmol, 1.0 eq) in diethyl ether (7 mL) was cooled to -80 °C. A solution of *n*BuLi (2.5 M in *n*-hexane, 100 μL, 0.25 mmol, 1.05 eq) was added to the pre-cooled, red solution of [Co(P₂C₂tBu₂)₂H] via a syringe. The reaction mixture was allowed to warm to ambient temperature while stirring. The color changed to deep-orange. Subsequently, the solvent was removed *in vacuo*, and the residue was extracted with Et₂O (3 mL). The deep-orange solution was concentrated to ca. 2 mL and stored at -35 °C. Deep-orange crystals formed upon storing the solution for three days. Yield 97 mg (75%); m.p. >300 °C; ¹H NMR (400.13 MHz, [D₈]THF, 300 K) δ /ppm = 0.85 (t, ³J_{H,H} = 7.4 Hz, 3H, (CH₂)₃CH₃), 0.92 (s, 18H, C(CH₃)₃), 1.06 (s, 9H, C(CH₃)₃), 1.23–1.36 (m, 3H, -CHHCH₂CH₂CH₃), 1.39 (s, 9H, C(CH₃)₃), 1.47–1.66 (m, 2H, -CH₂CH₂CH₂CH₃), 2.22 (d, ²J_{H,P} = 7.8 Hz, 1H, P₂C₂H), 2.52 (m, 1H, -CHHCH₂CH₂CH₃); ¹³C{¹H} NMR (100.61 MHz, [D₈]THF, 300 K) δ /ppm = 13.9 (s, -(CH₂)₃CH₃), 25.5 (overlapping with solvent signal, -CH₂CH₂CH₃), 28.0 (d, ²J_{C,P} = 7.1 Hz, -CH₂CH₂CH₃), 30.8 (dd, ³J_{C,P} = 6.9 Hz, ³J_{C,P} = 4.8 Hz, C(CH₃)₃), 33.1 (s, C(CH₃)₃), 35.3 (br, C(CH₃)₃ and C(CH₃)₃), 36.4 (d, ³J_{C,P} = 10.3 Hz, C(CH₃)₃), 37.0 (s, C(CH₃)₃), 80.0 (s, C₂P₂), the resonances for the remaining three quaternary carbon atoms of the C₂P₂ ligands were not detected; ³¹P{¹H} (161.98 MHz, [D₈]THF, 300 K) δ /ppm = -82.1 (d, ²J_{P,P} = 54.6 Hz, 1P; P₂), -42.7 (d, ²J_{P,P} = 54.6 Hz, 1P; P₁), -13.9 (s, 2P; P₃ and P₄); UV/Vis (Et₂O, λ_{max} /nm, (ε_{max} /L·mol⁻¹·cm⁻¹):

307 (35000); elemental analysis calcd. for $C_{24}H_{46}P_4CoLi \cdot (C_4H_6O)_{0.25}$ ($M = 541.92$): C 55.41, H 8.84, found: C 55.59, H 8.20.

3.4.2.2 Synthesis of $[Li(thf)_2\{Co(\eta^3-P_2C_2tBu_3)(\eta^4-P_2C_2tBu_2)\}]$ (*endo*-H-2)

A solution of $[Co(P_2C_2tBu_2)_2H]$ (**G**, 92 mg, 0.20 mmol, 1.0 eq) in THF (5 mL) was cooled to $-80\text{ }^\circ\text{C}$. A solution of *t*BuLi (1.7 M in *n*-hexane, 120 μL , 0.20 mmol, 1.0 eq) was added to the pre-cooled, red solution of $[Co(P_2C_2tBu_2)_2H]$ via a syringe. The color changed over forest-green to dark-red while stirring the reaction mixture at $-80\text{ }^\circ\text{C}$ for one hour. The reaction mixture was subsequently allowed to warm to ambient temperature, the solvent was removed *in vacuo*, and the residue was extracted with *n*-hexane (4 mL). The dark-red solution was concentrated to ca. 2 mL and stored at $-35\text{ }^\circ\text{C}$. Deep-red crystals formed upon storing the solution overnight. Yield 68 mg (51%); m.p. $>300\text{ }^\circ\text{C}$; ^1H NMR (400.13 MHz, $[D_8]$ THF, 300 K) δ /ppm = 0.97 (s, 18H, $C(CH_3)_3$), 1.14 (s, 9H, $C(CH_3)_3$), 1.31 (d, $^3J_{H,P} = 13.4$ Hz, 9H, $C(CH_3)_3$), 1.42 (s, 9H, $C(CH_3)_3$), 2.45 (d, $^2J_{H,P} = 5.8$ Hz, 1H, P_2C_2H); $^{13}\text{C}\{^1\text{H}\}$ NMR (100.61 MHz, $[D_8]$ THF, 300 K) δ /ppm = 28.9 (d, $^2J_{C,P} = 9.9$ Hz, $C(CH_3)_3$), 30.3 (t, $^3J_{C,P} = 6.8$ Hz, $C(CH_3)_3$), 32.3 (s, $C(CH_3)_3$), 34.3 (d, $^2J_{C,P} = 5.2$ Hz, $C(CH_3)_3$), 34.6 (t, $^1J_{C,P} = 8.0$ Hz, $C(CH_3)_3$), 34.9 (m, $C(CH_3)_3$), 35.1 (s, $C(CH_3)_3$), 35.6 (dd, $^2J_{C,P} = 11.9$ Hz, 2.7 Hz, $C(CH_3)_3$), 72.3 (s, C_2P_2), 83.4 (dd, $^1J_{C,P} = 32.5$ Hz, 15.0 Hz, C_2P_2), 94.3 (s, C_2P_2); ^{31}P (161.98 MHz, $[D_8]$ THF, 300 K) δ /ppm = -101.1 (d, $^2J_{P,P} = 54.2$ Hz, 1P; P2), -13.8 (s, 2P; P3 and P4), -1.5 (br, 1P; P1); $^{31}\text{P}\{^1\text{H}\}$ (161.98 MHz, $[D_8]$ THF, 300 K) δ /ppm = -102.0 (d, $^2J_{P,P} = 54.8$ Hz, 1P; P2), -14.8 (s, 2P; P3 and P4), -2.4 (d, $^2J_{P,P} = 54.8$ Hz, 1P; P1); UV/Vis (*n*-hexane, λ_{max} /nm, (ϵ_{max} /L·mol $^{-1}$ ·cm $^{-1}$)): 279 (32900), 307 (36800); elemental analysis calcd. for $C_{24}H_{46}P_4CoLi \cdot (C_4H_8O)_2$ ($M = 668.61$): C 57.48, H 9.35, found: C 57.49, H 9.22.

3.4.2.3 Synthesis of $[Li(OEt_2)(thf)_2\{Co(\eta^3-P_2C_2tBu_2Ph)(\eta^4-P_2C_2tBu_2)\}]$ (*exo*-H-3)

A solution of $[Co(P_2C_2tBu_2)_2H]$ (**G**, 40 mg, 0.09 mmol, 1.0 eq) in diethyl ether (3 mL) was cooled to $-80\text{ }^\circ\text{C}$. A solution of PhLi (1.9 M in dibutyl ether, 45 μL , 0.09 mmol, 1.0 eq) was added to the pre-cooled, red solution of **G** via syringe. The reaction mixture was allowed to warm to room temperature while stirring. The color slowly changed to deep orange while the solution was warmed up. The solvent was removed *in vacuo*, and the residue was extracted with Et $_2$ O (3 mL). The deep-orange solution was concentrated to ca. 1 mL and stored at $-35\text{ }^\circ\text{C}$. Deep-orange crystals formed upon storage of the solution for four days. Yield 34 mg (66%); m.p. $>300\text{ }^\circ\text{C}$; ^1H NMR (400.13 MHz, $[D_8]$ THF, 300 K) δ /ppm = 0.97 (br, $v_{\text{FWHM}} = 36$ Hz, 18H, $C(CH_3)_3$), 1.14 (s, 9H, $C(CH_3)_3$), 1.31 (s, 9H, $C(CH_3)_3$), 4.90 (d, $^2J_{H,P} = 14.3$ Hz, 1H, P_2C_2H), 7.05–7.17 (m, 3H, m-/p- H_{Ar}), 7.57–7.66 (m, 2H, o- H_{Ar}); $^{13}\text{C}\{^1\text{H}\}$ NMR (100.61 MHz, $[D_8]$ THF, 300 K) δ /ppm = 32.4 (m, $C(CH_3)_3$), 34.1 (s, $C(CH_3)_3$), 35.6 (d, $^2J_{C,P} = 3.7$ Hz, $C(CH_3)_3$), 37.4 (d, $^2J_{C,P} = 4.9$ Hz, $C(CH_3)_3$), 36.6 (br, $C(CH_3)_3$), 37.4 (br, $C(CH_3)_3$), 127.4 (d, $^3J_{C,P} = 6.1$ Hz, m-/p- C_{Ar}), 127.4 (d, $^2J_{C,P} = 12.5$ Hz, o- C_{Ar}), the resonances for the quaternary carbon atoms of the C_2P_2 ligand and the *ipso*- C_{Ar} could not be detected; $^{31}\text{P}\{^1\text{H}\}$ (161.98 MHz, $[D_8]$ THF, 300 K) δ /ppm = -109.1 (d,

$^2J_{P,P} = 48.3$ Hz, 1P; P2), -89.3 (d, $^2J_{P,P} = 48.3$ Hz, 1P; P1), -11.0 (br, 1P; P3 or P4), -6.6 (br, 1P; P4 or P3); UV/Vis (THF, λ_{\max} /nm, (ϵ_{\max} /L·mol $^{-1}$ ·cm $^{-1}$)): 310 (66500), 640sh (5200); elemental analysis calcd. for C₂₆H₄₁P₄CoLi·(C₄H₁₀O)_{0.4} (M = 573.03): C 57.85, H 7.92, found: C 56.94, H 7.95.

3.4.2.4 Synthesis of [Mg(MeCN)₆][Co(η^4 -P₂C₂tBu₂)₂] (4)

A solution of [Co(P₂C₂tBu₂)₂H] (**G**, 71 mg, 0.15 mmol, 1.0 eq) in THF (7 mL) was cooled to -80 °C. A solution of *p*-tolyl magnesium chloride (1.0 M in THF, 150 μ L, 0.15 mmol, 1.0 eq) was added to the pre-cooled, red solution of **G** via syringe. The reaction mixture was allowed to warm to room temperature while the color changed to dark red and a precipitate formed. The precipitate was separated by filtration and redissolved in acetonitrile (4 mL). The dark-red solution was concentrated to ca. 2 mL. Dark-red crystals were obtained by diffusion of THF into the acetonitrile solution. Yield 51 mg (65%); m.p. >144 °C (decomp. to a dark reddish-black solid); ^1H NMR (400.13 MHz, CD₃CN, 300 K) δ /ppm = 1.01 (s, 36H, C(CH₃)₃), 1.96 (sept, 14H, CH₃CN); $^{13}\text{C}\{^1\text{H}\}$ NMR (100.61 MHz, CD₃CN, 300 K) δ /ppm = 33.6 (d, $^3J_{C,P} = 4.1$ Hz, C(CH₃)₃), 35.9 (t, $^2J_{C,P} = 7.3$ Hz, C(CH₃)₃), 103.8 (t, $^1J_{C,P} = 49.5$ Hz, C₂P₂); $^{31}\text{P}\{^1\text{H}\}$ NMR (161.98 MHz, CD₃CN, 300 K) δ /ppm = 5.0 (s); UV/Vis (CH₃CN, λ_{\max} /nm, (ϵ_{\max} /L·mol $^{-1}$ ·cm $^{-1}$)): 330 (20900); elemental analysis calcd. for C₄₀H₇₂P₈Co₂Mg·(C₂H₃N)₄·(C₄H₈O)_{1.5} (M = 1215.35): C 53.37, H 7.96, found: C 52.85, H 7.42.

3.4.2.5 Synthesis of [Co(η^3 -P₂C₂tBu₂*n*Bu)(η^4 -P₂C₂tBu₂SiMe₃)] (5)

A solution of [Co(P₂C₂tBu₂)₂H] (**G**, 95 mg, 0.21 mmol, 1.0 eq) in toluene (4 mL) was cooled to -80 °C. A solution of *n*BuLi (2.5 M in *n*-hexane, 85 μ L, 0.21 mmol, 1.0 eq) was added to the pre-cooled, red solution of **G** via syringe. The reaction mixture was allowed to warm to room temperature while stirring; the color slowly changed to deep orange. The solution again was cooled to -60 °C. After addition of Me₃SiCl (0.15 M in toluene, 1.35 mL, 0.21 mmol, 1.0 eq) via syringe, the reaction mixture was stirred at ambient temperature while the color changed to bright orange-red. The solvent was removed *in vacuo*, and the residue was extracted with *n*-hexane (3 mL). The deep-orange solution was concentrated to ca. 2 mL and stored at -35 °C. Deep-orange crystals formed upon storing the solution overnight. Yield 64 mg (52%); m.p. >121 °C (decomp. to a black oil); ^1H NMR (400.13 MHz, C₆D₆, 300 K) δ /ppm = 0.55 (d, $^3J_{H,P} = 5.3$ Hz, 9H, SiMe₃), 0.76 (t, $^3J_{H,H} = 7.3$ Hz, 3H, (CH₂)₃CH₃), 1.12–1.19 (m, 2H, -(CH₂)₂CH₂CH₃), 1.21 (s, 9H, C(CH₃)₃), 1.31 (s, 9H, C(CH₃)₃), 1.34 (s, 9H, C(CH₃)₃), 1.36 (s, 9H, C(CH₃)₃), 1.44–1.76 (m, 3H, -CHHCH₂CH₂CH₃), 2.43–2.57 (m, 1H, -CHH(CH₂)₂CH₃), 2.77 (d, $^2J_{H,P} = 7.6$ Hz, 1H, P₂C₂tBu₂H); $^{13}\text{C}\{^1\text{H}\}$ NMR (100.61 MHz, C₆D₆, 300 K) δ /ppm = 8.5 (d, $^3J_{C,P} = 14.2$ Hz, SiMe₃), 13.1 (s, -(CH₂)₃CH₃), 24.2 (d, $^2J_{C,P} = 14.4$ Hz, -CH₂CH₂CH₂CH₃), 26.5 (d, $^3J_{C,P} = 3.8$ Hz, -(CH₂)₂CH₂CH₃), 30.1 (dd, $^3J_{C,P} = 7.1$ Hz, $^3J_{C,P} = 5.1$ Hz, C(CH₃)₃), 31.3 (dd, $^1J_{C,P} = 34.7$ Hz, $^3J_{C,P} = 5.1$ Hz, -CH₂(CH₂)₂CH₃), 32.2 (br, C(CH₃)₃), 34.5 (t, $^3J_{C,P} = 4.7$ Hz, C(CH₃)₃), 35.6 (t,

$^2J_{C,P} = 6.1$ Hz, $C(CH_3)_3$, 36.4 (dd, $^2J_{C,P} = 9.4$ Hz, $^2J_{C,P} = 2.5$ Hz, $C(CH_3)_3$), 36.8 (t, $^2J_{C,P} = 6.1$ Hz, $C(CH_3)_3$), 36.9 (dd, $^2J_{C,P} = 5.0$ Hz, $^2J_{C,P} = 0.9$ Hz, $C(CH_3)_3$), 70.7 (d, $^1J_{C,P} = 31.1$ Hz, C1), 95.0 (s, dd, $^1J_{C,P} = 72.1$ Hz, $^1J_{C,P} = 15.1$ Hz, C2), the resonances for C3 and C4 were not detected; $^{31}P\{^1H\}$ (161.98 MHz, C_6D_6 , 300 K) δ /ppm = -195.8 (br, $\nu_{FWHM} = 172$ Hz, 1P; P3), -71.7 (d, $^2J_{P,P} = 48.9$ Hz, 1P; P2), -30.6 (br, 1P; P1), 64.3 (d, $^2J_{P,P} = 37.4$ Hz, 1P; P4); ^{29}Si DEPT NMR (79.49 MHz, C_6D_6 , 300 K) δ /ppm = -0.8 (d, $^1J_{Si,P} = 90.0$ Hz); UV/Vis (*n*-hexane, λ_{max} /nm, (ϵ_{max} /L·mol $^{-1}$ ·cm $^{-1}$)): 294 (38600), 343sh (12500), 422sh (3500); elemental analysis calcd. for $C_{27}H_{55}P_4CoSi$ (M = 590.65): C 54.91, H 9.39, found: C 55.36, H 9.38.

3.4.3 Reaction of $[Co(P_2C_2tBu_2)_2H]$ with Grignard Reagents

We investigated the reactivity of $[Co(P_2C_2tBu_2)_2H]$ (**G**) toward the aryl Grignard reagents *p*-fluorophenyl magnesium bromide and *p*-tolyl magnesium chloride (Scheme 3 in the manuscript). The reaction was performed in an analogous fashion to **1-3**. The $^{31}P\{^1H\}$ NMR spectra of the reaction mixtures are identical, showing only one singlet at 3.1 ppm that can be unequivocally assigned to the $[Co(P_2C_2tBu_2)_2]^-$ anion since the potassium salts $[K([18]crown-6)(thf)_2][Co(P_2C_2tBu_2)_2]$ (**F**, 2.4 ppm) and $[K(thf)_2][Co(P_2C_2tBu_2)_2]$ (5.1 ppm) show very similar ^{31}P NMR shifts in $[D_8]THF$.^{10,12} Diffusion of THF into an acetonitrile solution of the reaction product afforded crystals of $[Mg(MeCN)_6][Co(\eta^4-P_2C_2tBu_2)_2]_2$ (**4**). Single-crystal X-ray diffraction revealed that the compound crystallizes in the space group *I4/m*. An ion-separated molecular structure is observed consisting of two $[Co(P_2C_2tBu_2)_2]^-$ sandwich anions and a $[Mg(MeCN)_6]^{2+}$ cation (Figure S1).²² The molecular structure and the redox properties (Figure S16d) of the $[Co(P_2C_2tBu_2)_2]^-$ anion is identical to those of the previously reported potassium salts.^{10,27}

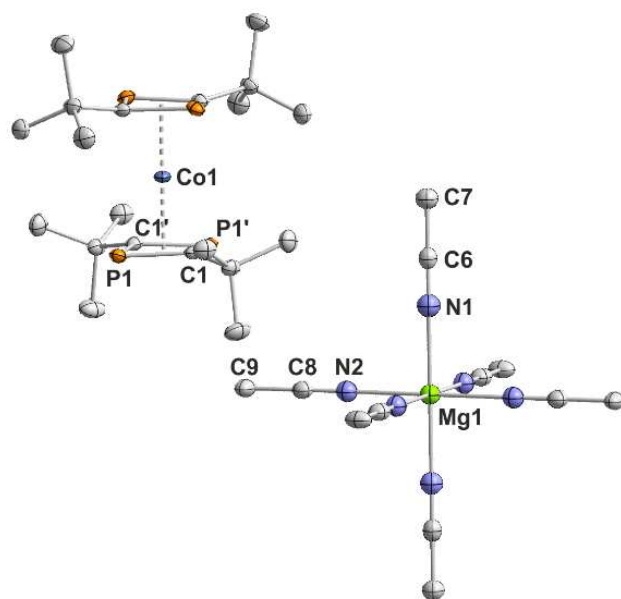


Figure S1. Solid-state molecular structure of **4**. The hydrogen atoms and the second $[\text{Co}(\text{P}_2\text{C}_2\text{tBu}_2)]^-$ anion are omitted for clarity. Thermal ellipsoids are drawn at the 50% probability level. Selected bond lengths [Å] and angles [°]: P1–C1 1.799(2), P1–C1' 1.797(2), Co1–P1 2.2534(4), Co1–C1 2.082(2), Mg1–N1 2.147(3), Mg1–N2 2.157(2), N1–C6 1.139(5), N2–C8 1.135(3), C1–P1–C1' 80.68(7), P1'–C1–P1 99.18(7).

3.4.4 $^{31}\text{P}\{^1\text{H}\}$ NMR Spectra of 1-3, and 5

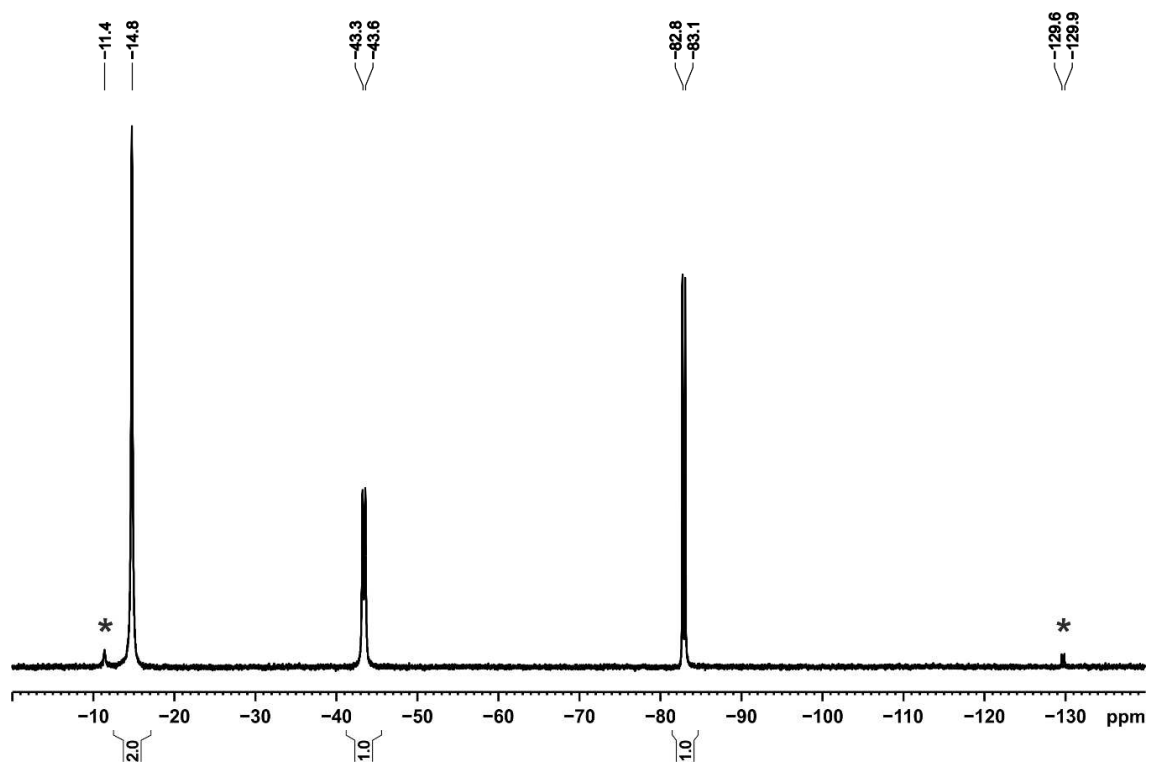


Figure S2. $^{31}\text{P}\{^1\text{H}\}$ NMR spectrum (161.49 MHz, $[\text{D}_8]\text{THF}$, 300 K) of *endo*-H-**1**. The signals marked with an asterisk are assigned to the *exo*-H isomer of **1**.

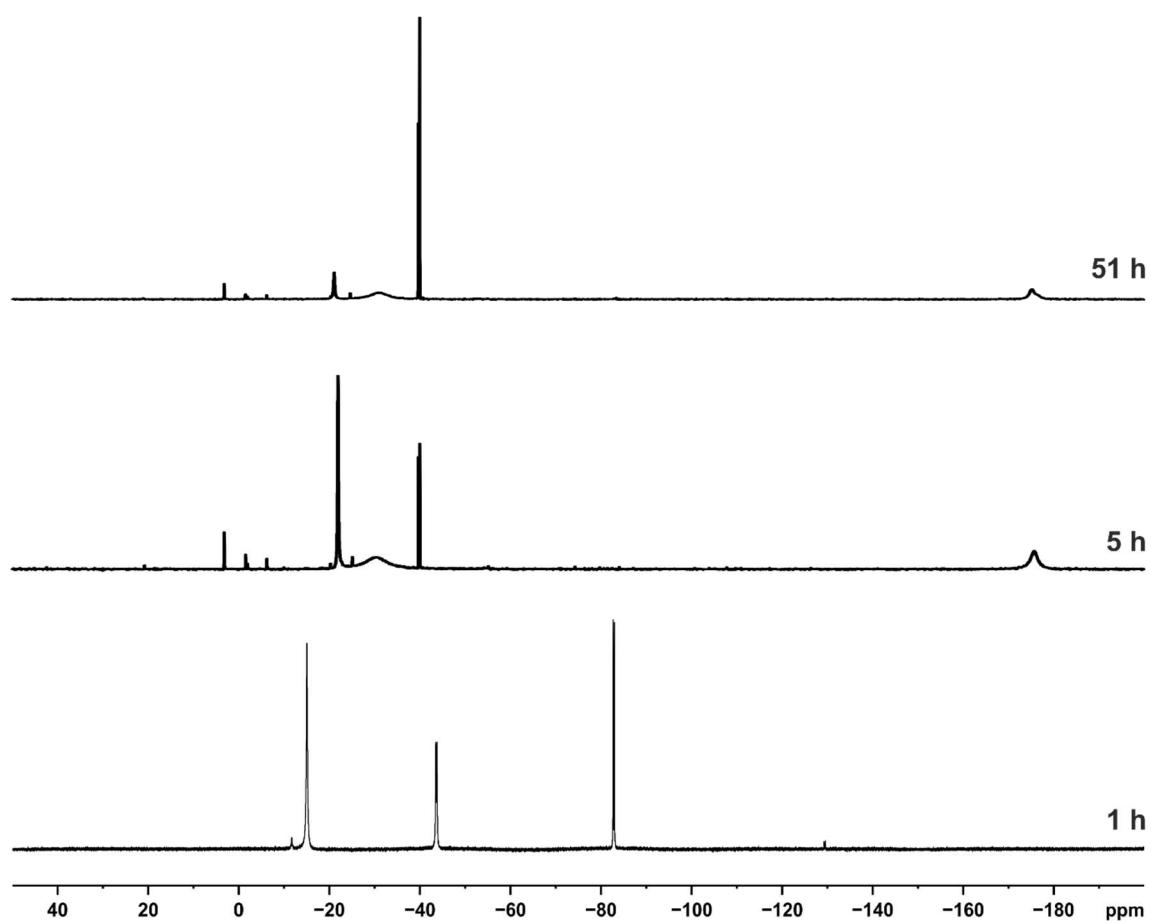


Figure S3. $^{31}\text{P}\{^1\text{H}\}$ NMR monitoring (161.49 MHz, C_6D_6 capillary, 300 K) of a reaction mixture of **G** with *n*BuLi in THF; spectra were recorded after 1, 5 and 51 hours, respectively.

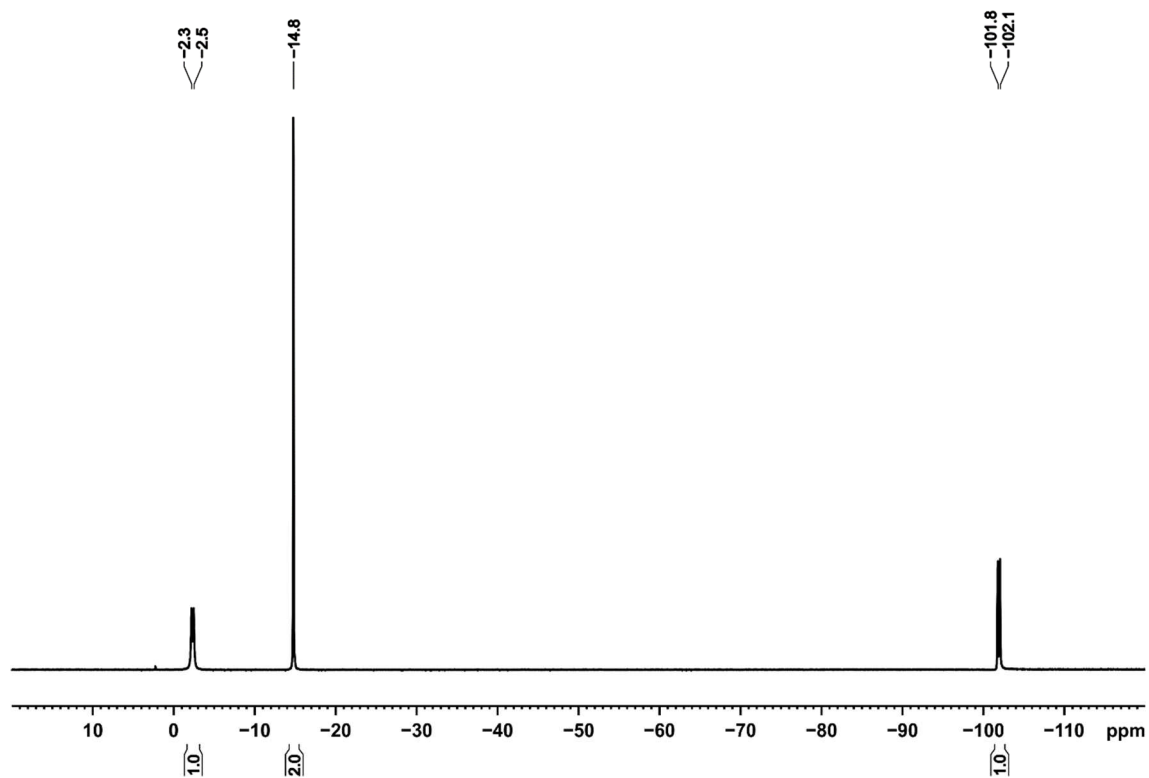


Figure S4. $^{31}\text{P}\{^1\text{H}\}$ NMR spectrum (161.49 MHz, $[\text{D}_8]\text{THF}$, 300 K) of *endo*-H-2.

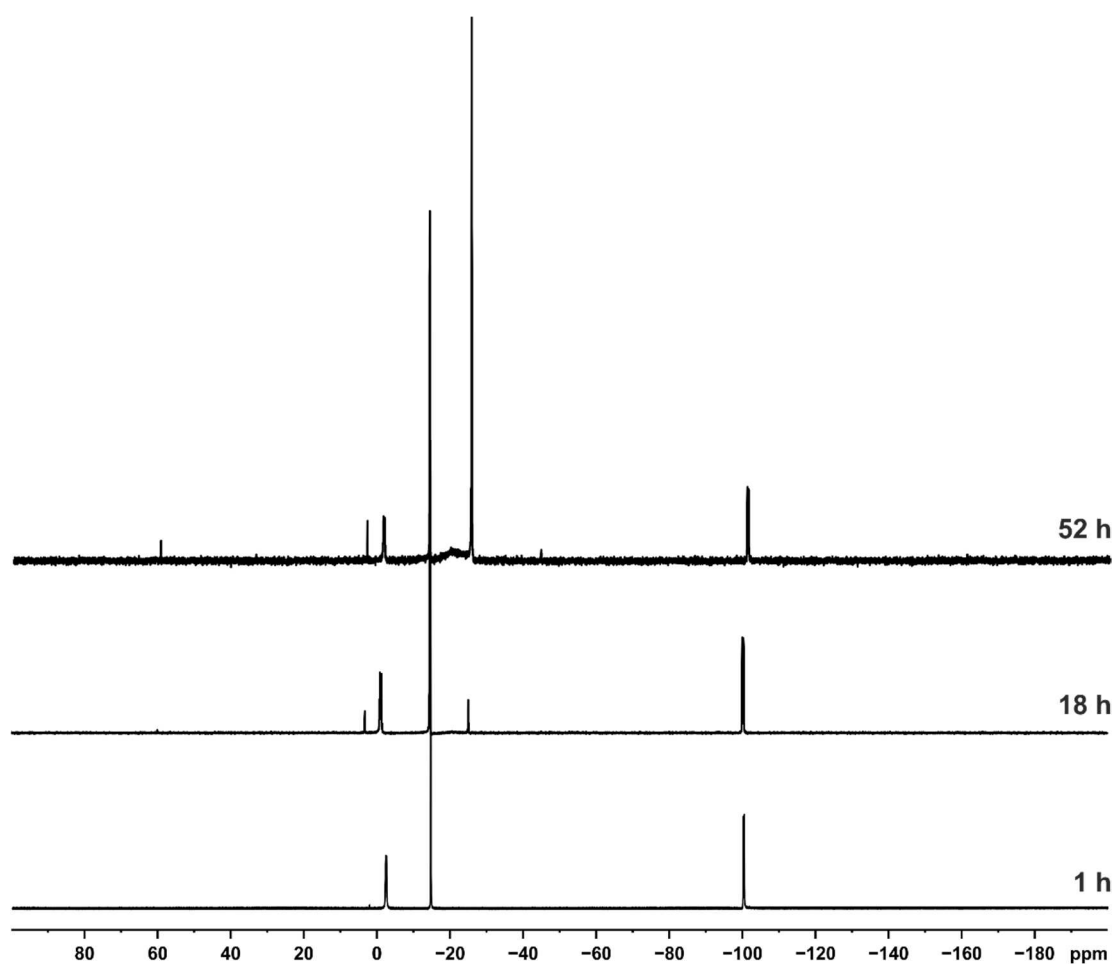


Figure S5. $^{31}\text{P}\{^1\text{H}\}$ NMR monitoring (161.49 MHz, C_6D_6 capillary, 300 K) of a reaction mixture of **G** with *t*BuLi in THF; spectra were recorded after 1, 18 and 52 hours, respectively.

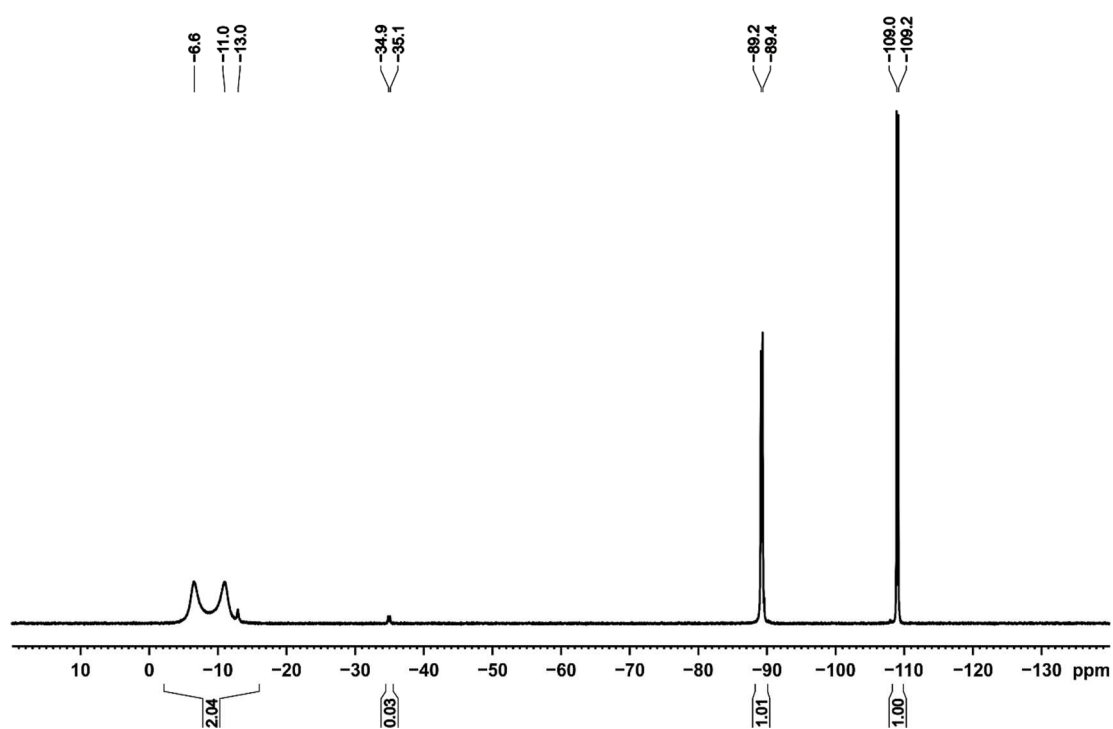


Figure S6. $^{31}\text{P}\{^1\text{H}\}$ NMR spectrum (161.49 MHz, $[\text{D}_8]\text{THF}$, 300 K) of *exo*-H-**3**. The signals at $\delta = -35.0$ and -13.0 ppm are assigned to the *endo*-H isomer of **3** (cf. Figure S12).

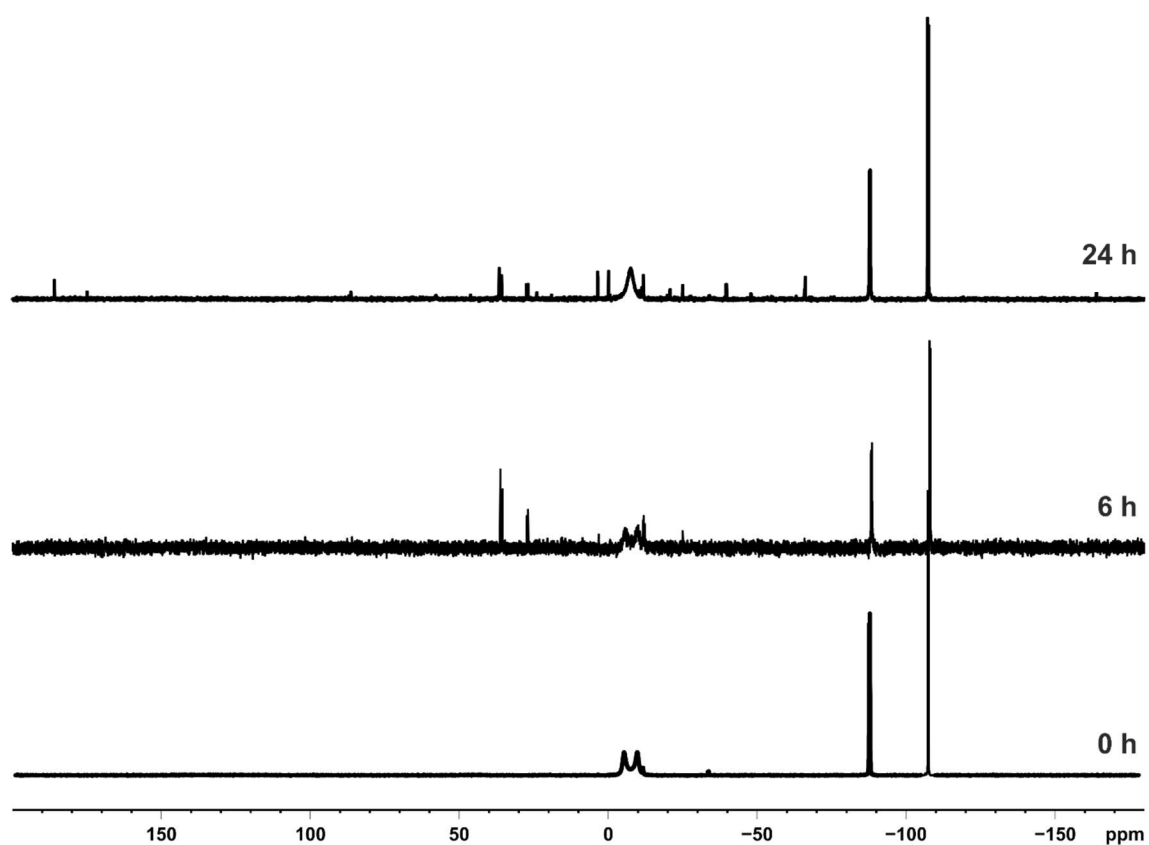


Figure S7. $^{31}\text{P}\{^1\text{H}\}$ NMR monitoring (161.49 MHz, C_6D_6 capillary, 300 K) of the decomposition of freshly isolated crystals of *exo*-H-3 in $[\text{D}_8]\text{THF}$ solutions; spectra were recorded immediately after preparing the sample and after 6 and 24 hours, respectively.

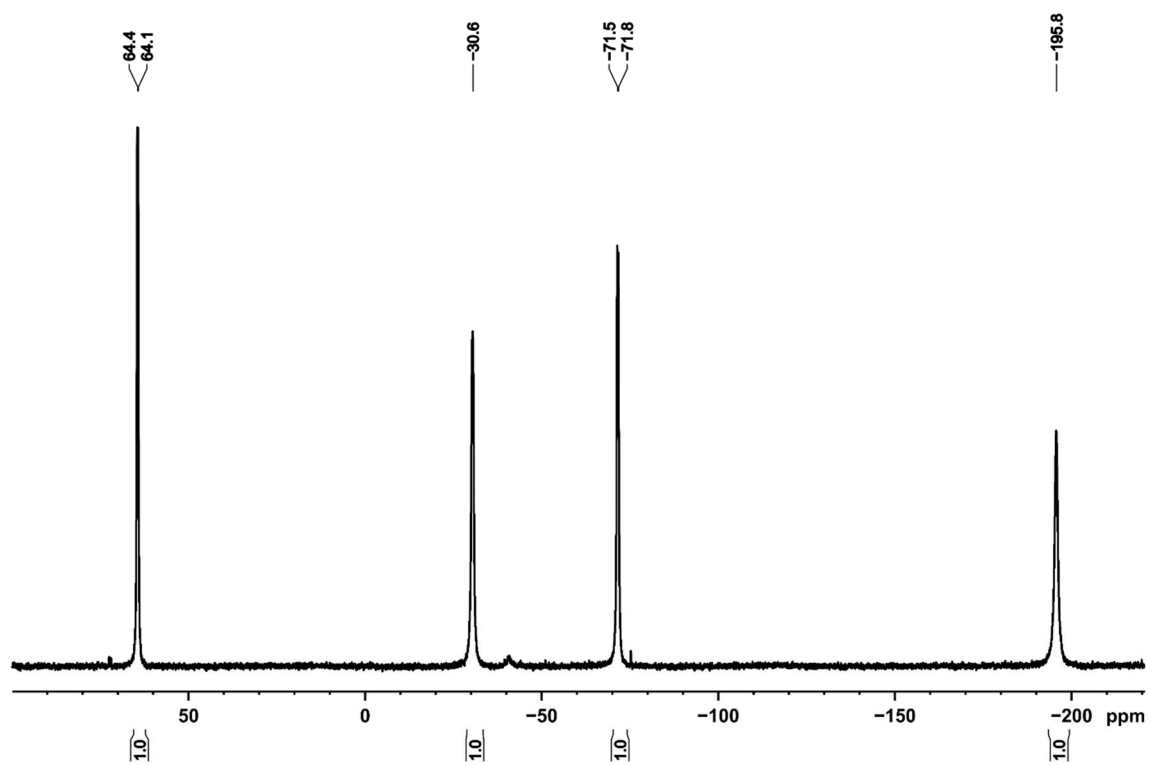


Figure S8. $^{31}\text{P}\{^1\text{H}\}$ NMR spectrum (161.49 MHz, $[\text{D}_8]\text{THF}$, 300 K) of 5.

3.4.5 Variable Temperature and 2D Correlation NMR Spectroscopy

Variable Temperature (VT) and 2D Correlation NMR spectra were recorded on a Bruker Avance III HD Nanobay 400 MHz Ultrashield and on a Bruker Avance III HDX 500 MHz Ascend internally referenced to residual solvent resonances.

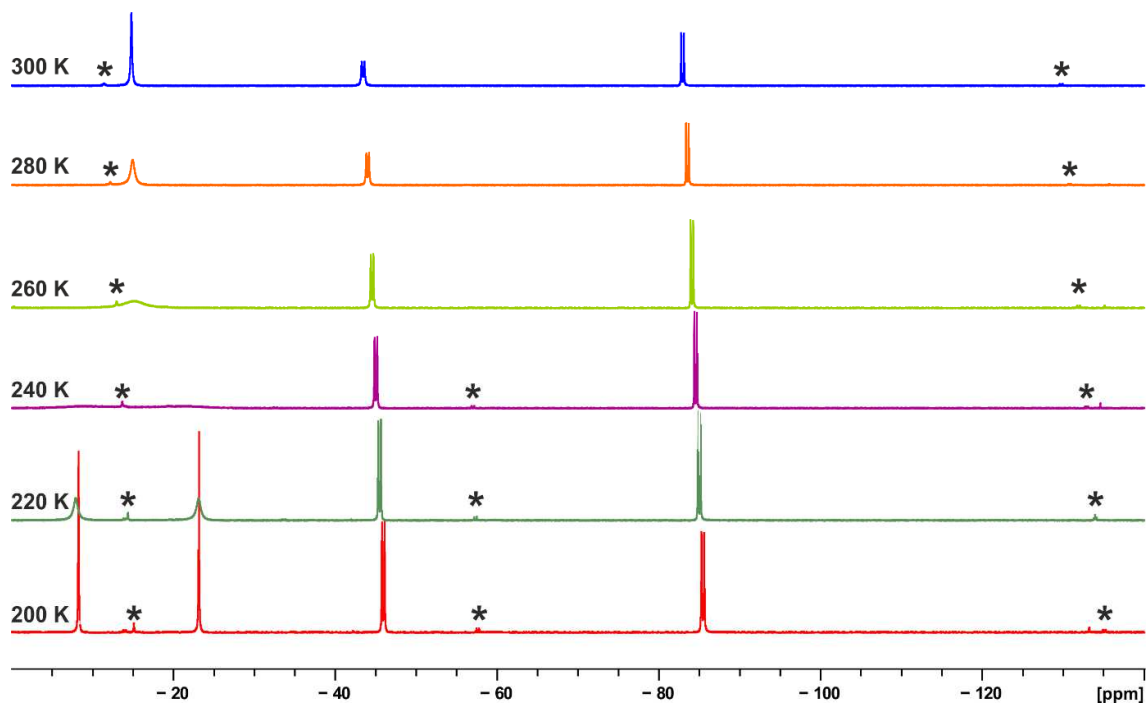
3.4.4.1 Variable Temperature $^{31}\text{P}\{^1\text{H}\}$ NMR Spectra of **1**

Figure S9. $^{31}\text{P}\{^1\text{H}\}$ NMR spectra (161.49 MHz, $[\text{D}_8]\text{THF}$) of *endo*-H-**1** at different temperatures. The signals marked with an asterisk are assigned to the *exo*-H isomer of **1**.

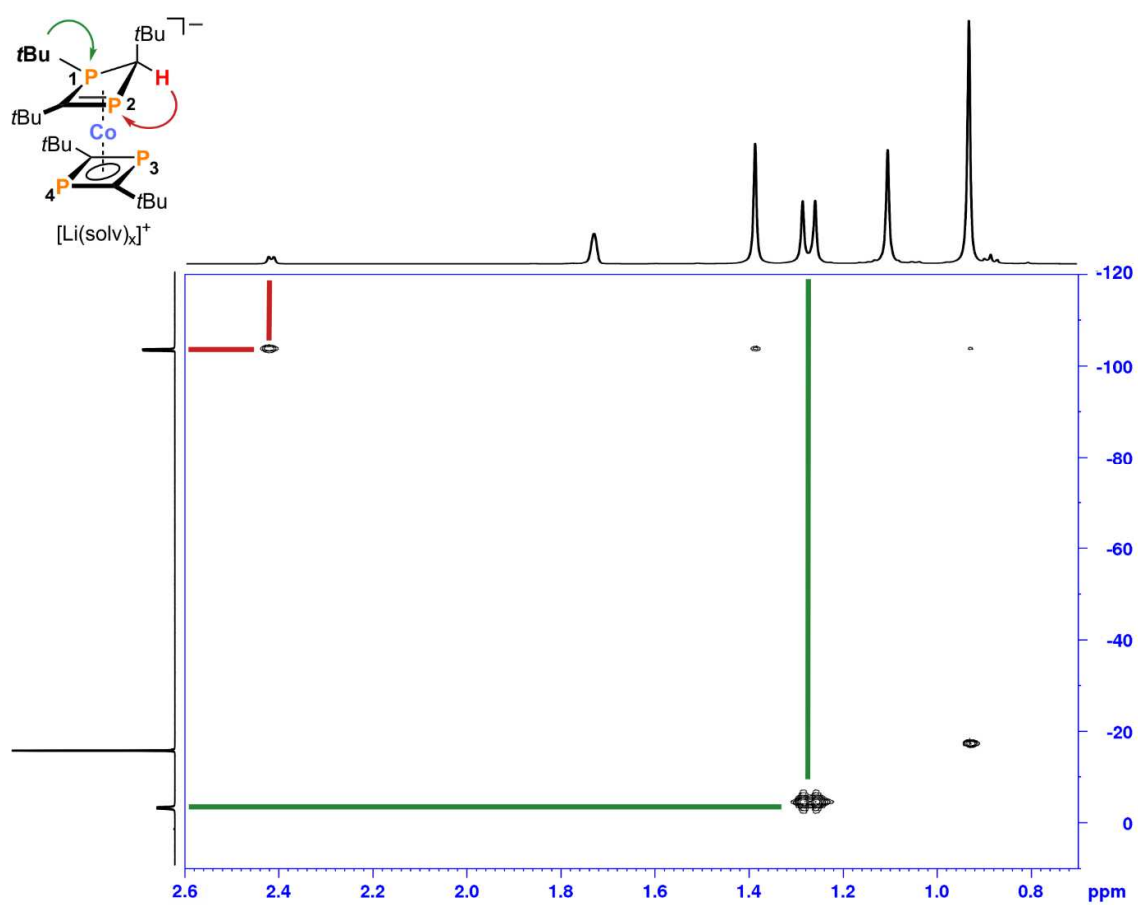
3.4.4.2 2D ^1H - ^{31}P Correlation NMR Spectrum of 2

Figure S10. ^1H - ^{31}P HMBC NMR spectrum of *endo*-H-2; correlation of H1 and P2 is marked in red and correlation between the *tert*-butyl protons and P1 is marked in green.

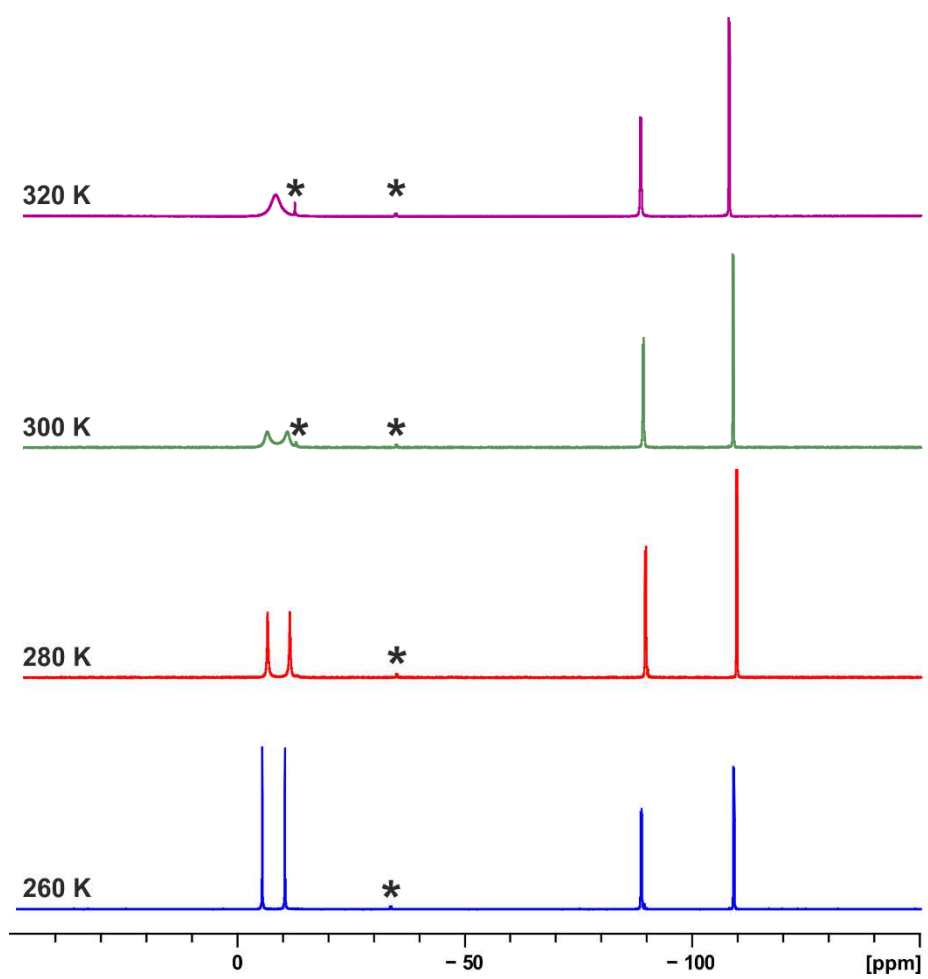
3.4.4.3 Variable Temperature $^{31}\text{P}\{^1\text{H}\}$ NMR Spectra of **3**

Figure S11. $^{31}\text{P}\{^1\text{H}\}$ NMR spectra (161.49 MHz, $[\text{D}_8]\text{THF}$) of *exo*-H-**3** at different temperatures. The signals marked with an asterisk are assigned to the *endo*-H isomer of **3**.

3.4.4.4 Monitoring of the reaction of **G** with PhLi by $^{31}\text{P}\{^1\text{H}\}$ NMR spectroscopy

$[\text{Co}(\text{P}_2\text{C}_2\text{tBu}_2)_2\text{H}]$ (**G**, 14 mg, 0.03 mmol) was dissolved in $[\text{D}_8]\text{THF}$ (0.4 mL), transferred to a screw cap NMR tube and cooled to 183 K. PhLi (1.9 M in di-*n*-butylether, 16 μL , 0.03 mmol) was added. The NMR tube was sealed with the screw cap and transferred to a pre-cooled (193 K) Bruker Avance400 NMR device. The reaction was monitored by $^{31}\text{P}\{^1\text{H}\}$ NMR spectroscopy starting at 193 K, followed by subsequent heating in steps of 20 K up to 273 K. Above 273 K the steps were reduced to 10 K. Selected $^{31}\text{P}\{^1\text{H}\}$ NMR spectra are shown in Figure S5.

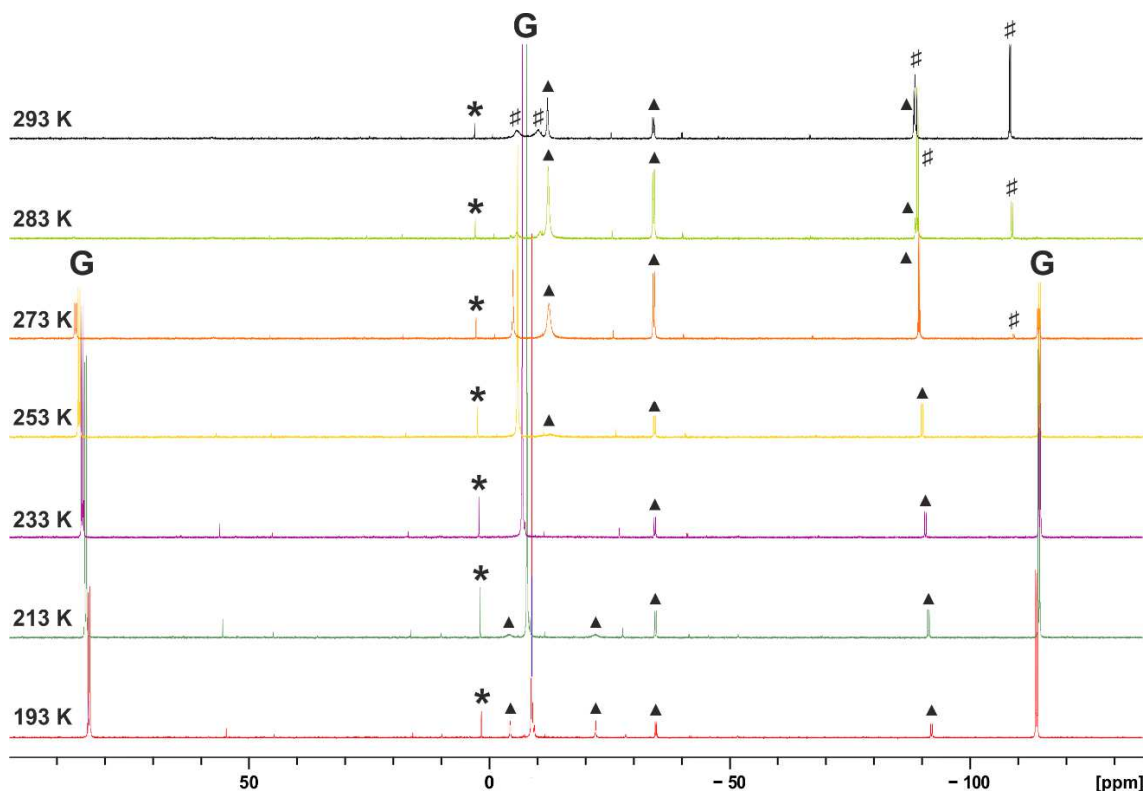


Figure S12. $^{31}\text{P}\{^1\text{H}\}$ NMR monitoring (161.49 MHz, $[\text{D}_8]\text{THF}$) of the reaction of **G** with PhLi starting from 193 K. The signals marked with ▲ are assigned to the *endo*-H isomer of **3**, while # marks the signals of the *exo*-H isomer. The signals marked with an asterisk are assigned to an unidentified species.

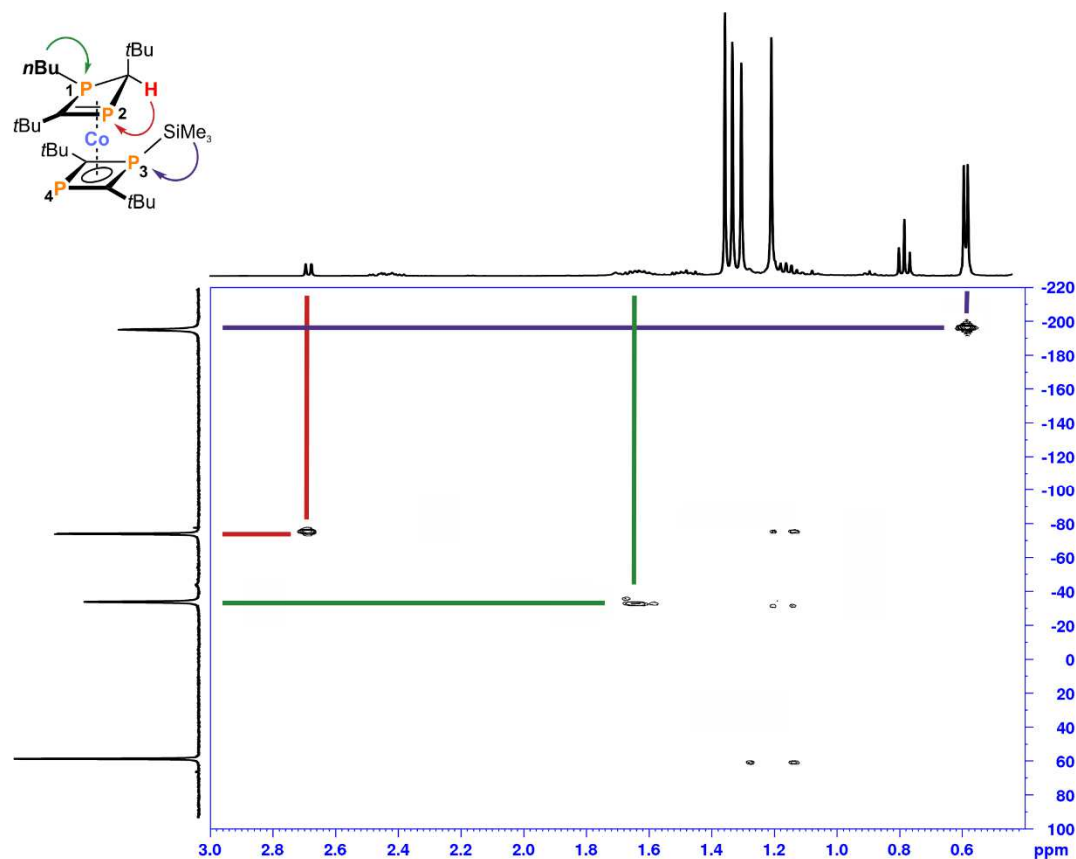
3.4.4.5 2D ^1H - ^{31}P Correlation NMR Spectrum of **5**, ^{31}P NMR Spectrum of **5** in THF, and Comparison of ^1H and $^1\text{H}\{^{31}\text{P}\}$ NMR Spectra

Figure S13. ^1H - ^{31}P HMBC NMR spectrum of **5**; correlation of H1 and P2 is marked in red, correlation between the *n*-butyl protons and P1 is marked in green and correlation between the SiMe₃ group and P3 is marked in blue.

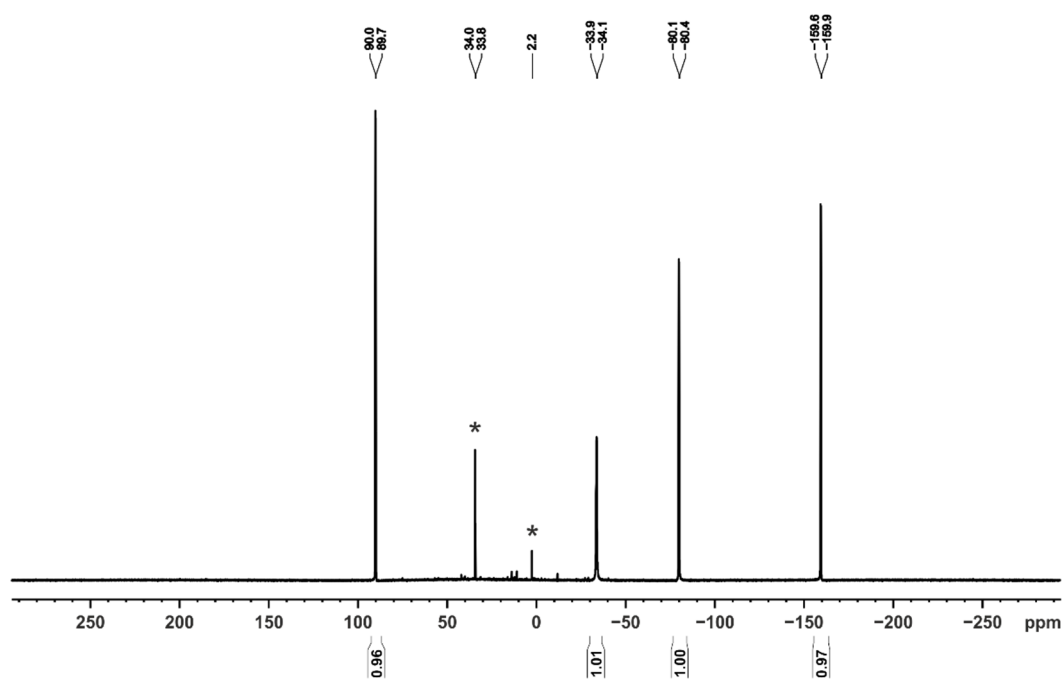


Figure S14. $^{31}\text{P}\{^1\text{H}\}$ NMR spectrum (161.49 MHz, C_6D_6 , 300 K) of the unknown product obtained from **5** in THF. The signals marked with an asterisk are assigned to unidentified species.

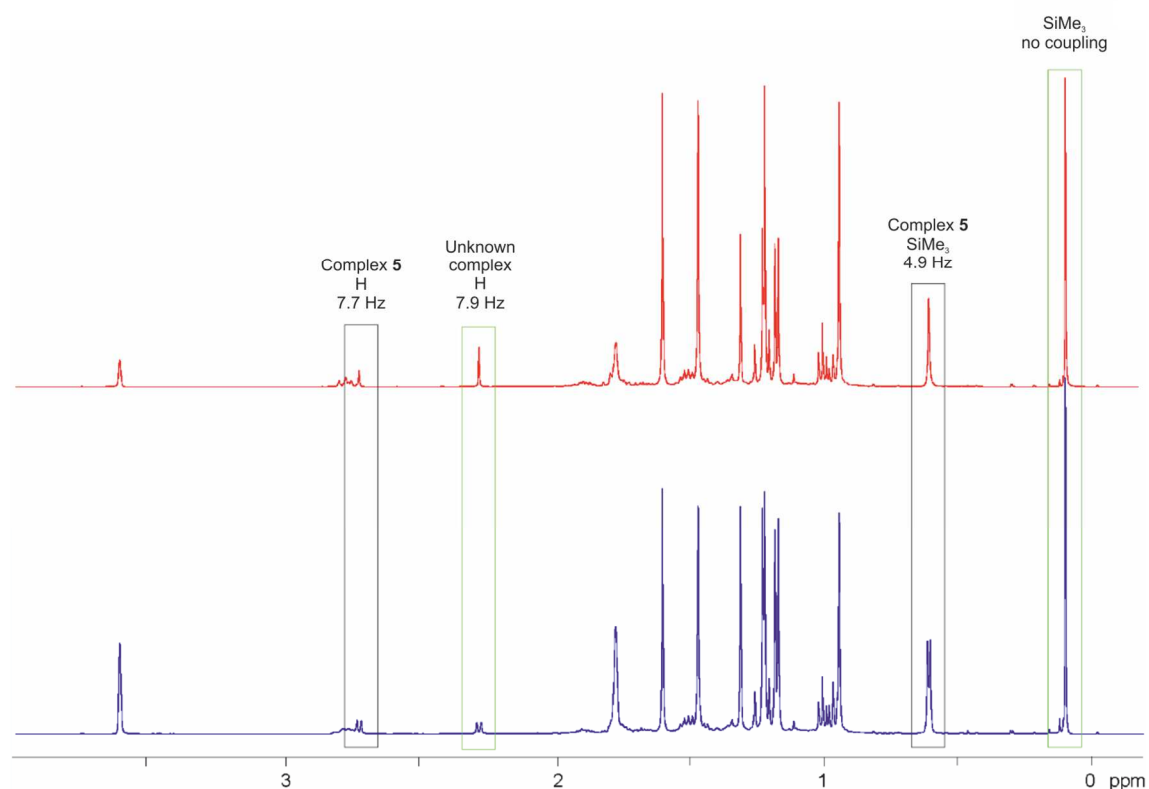


Figure S15. ^1H NMR spectrum (bottom) and $^1\text{H}\{^{31}\text{P}\}$ NMR spectrum (top) (400.13 MHz, $[\text{D}_8]\text{THF}$, 300 K) of **5** and the unknown complex.

3.4.6 Cyclic Voltammetry

Cyclic voltammetry experiments were performed in a single-compartment cell inside a nitrogen-filled glovebox using a CH Instruments CHI600E potentiostat. The cell was equipped with a platinum disc working electrode (2 mm diameter) polished with 0.05 μm alumina paste, a platinum wire counter electrode and a silver/silver nitrate reference electrode. The supporting electrolyte, tetra-*n*butylammonium hexafluorophosphate, was dried in vacuo at 110 $^{\circ}\text{C}$ for three days. All redox potentials are reported versus the ferrocene/ferrocenium (Fc/Fc^+) couple. The scan rate is $\nu = 100 \text{ mV s}^{-1}$.

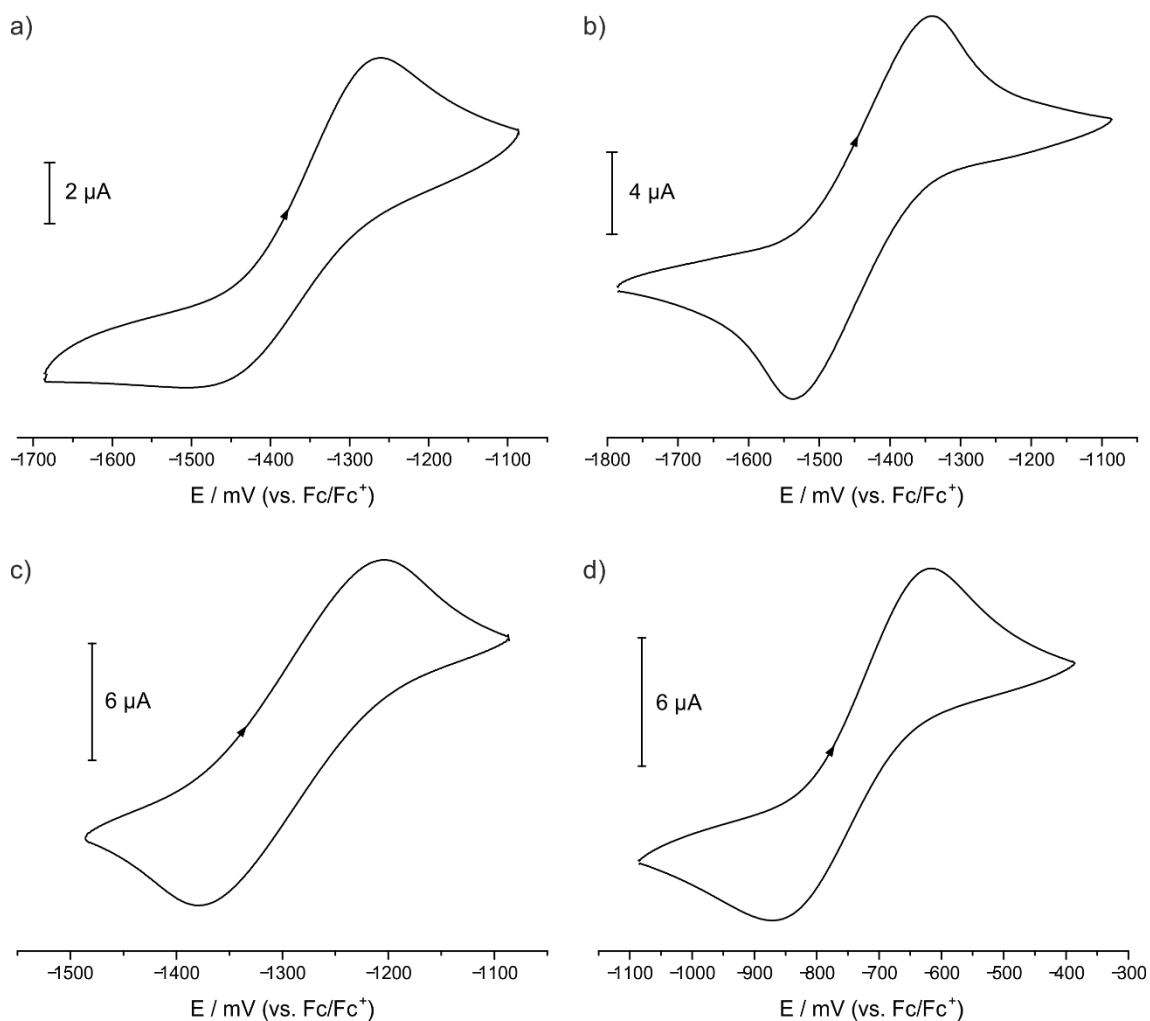


Figure S16. Cyclic voltammograms of *endo*-H-1 (a), *endo*-H-2 (b), *exo*-H-3 (c), and **4** (d) recorded in THF/TBAH.

3.4.7 X-ray Crystallography

The crystals were measured with an Agilent Technologies SuperNova device. Multi-scan absorption correction²⁸ was applied to the data. The structure was solved by SHELXS²⁹ and least-square refinements on F^2 were carried out with SHELXL.³⁰ Crystallographic data is given in Table S1.

CCDC 1888854-1888858 contain the supplementary crystallographic data for this paper. These data can be obtained free of charge from The Cambridge Crystallographic Data Centre via www.ccdc.cam.ac.uk/data_request/cif.

Table S1. Crystallographic data and structure refinement of 1–5.

Compound	<i>endo</i> -H-1	<i>endo</i> -H-2	<i>exo</i> -H-3
Empirical formula	C ₃₂ H ₆₆ CoLiO ₂ P ₄	C ₃₈ H ₇₁ CoLiO ₃ P ₄	C ₃₂ H ₆₂ CoLiO ₂ P ₄
Formula weight	672.59	765.69	668.56
Temperature [K]	123.0(2)	123.0(1)	123.0(1)
Crystal system	monoclinic	orthorhombic	monoclinic
Space group	<i>P</i> 2 ₁ / <i>c</i>	<i>Pbca</i>	<i>P</i> 2 ₁ / <i>c</i>
a [Å]	20.245(2)	20.4752(5)	16.1137(3)
b [Å]	10.4733(5)	19.7415(6)	10.4937(2)
c [Å]	19.440(1)	21.1433(8)	21.8089(5)
α [°]	90	90	90
β [°]	109.476(8)	90	94.730(2)
γ [°]	90	90	90
Volume [Å ³]	3886.2(5)	8546.4(5)	3675.2(1)
Z	4	8	4
ρ _{calc} [g/cm ³]	1.150	1.190	1.208
μ [mm ⁻¹]	5.193	4.802	5.491
F(000)	1456.0	3304.0	1440.0
Crystal size [mm ³]	0.172 × 0.145 × 0.125	0.209 × 0.138 × 0.087	0.27 × 0.22 × 0.103
Radiation	CuK _α (λ = 1.54184)	CuK _α (λ = 1.54184)	CuK _α (λ = 1.54184)
2θ range for data collection [°]	9.208 to 148.79	7.496 to 147.504	8.136 to 148.476
Index ranges	-24 ≤ h ≤ 24, -13 ≤ k ≤ 12, -23 ≤ l ≤ 24	-25 ≤ h ≤ 25, -21 ≤ k ≤ 24, -22 ≤ l ≤ 25	-16 ≤ h ≤ 19, -12 ≤ k ≤ 12, -27 ≤ l ≤ 26
Reflections collected	36433	38284	33530
Independent reflections	7708 [R _{int} = 0.1621, R _{sigma} = 0.0984]	8532 [R _{int} = 0.0594, R _{sigma} = 0.0453]	7350 [R _{int} = 0.0642, R _{sigma} = 0.0419]
Data / restraints / parameters	7708 / 4 / 380	8532 / 98 / 517	7350/2/380
Goodness-of-fit on F ²	1.161	1.022	1.019
Final R indexes [I >= 2σ (I)]	R ₁ = 0.0934, wR ₂ = 0.2520	R ₁ = 0.0510, wR ₂ = 0.1226	R ₁ = 0.0468, wR ₂ = 0.1149
Final R indexes [all data]	R ₁ = 0.1253, wR ₂ = 0.3026	R ₁ = 0.0687, wR ₂ = 0.1339	R ₁ = 0.0530, wR ₂ = 0.1191
Largest diff. peak/hole [e Å ⁻³]	1.02/-1.40	0.73/-0.51	0.88/-0.52
CCDC	1888854	1888855	1888857

Compound	4	5
Empirical formula	C ₅₂ H ₉₀ C ₀₂ MgN ₆ P ₈	C ₂₇ H ₅₅ CoP ₄ Si
Formula weight	1271.33	590.61
Temperature [K]	123.0(1)	123.0(1)
Crystal system	tetragonal	triclinic
Space group	<i>I4/m</i>	<i>P</i> -1
a [Å]	12.6865(2)	9.8833(4)
b [Å]	12.6865(2)	11.1780(5)
c [Å]	21.3540(6)	15.3846(7)
α [°]	90	80.948(4)
β [°]	90	87.496(3)
γ [°]	90	78.863(3)
Volume [Å ³]	3436.9(2)	1646.7(1)
Z	2	2
ρ _{calc} [g/cm ³]	1.229	1.191
μ [mm ⁻¹]	5.932	6.359
F(000)	1348.0	636.0
Crystal size [mm ³]	0.222 × 0.14 × 0.11	0.219 × 0.198 × 0.128
Radiation	CuK _α (λ = 1.54184)	CuK _α (λ = 1.54184)
2θ range for data collection [°]	8.106 to 148.62	8.156 to 148.572
Index ranges	-15 ≤ h ≤ 11, -15 ≤ k ≤ 14, -26 ≤ l ≤ 25	-11 ≤ h ≤ 12, -13 ≤ k ≤ 13, -18 ≤ l ≤ 19
Reflections collected	5625	10814
Independent reflections	1753 [R _{int} = 0.0309, R _{sigma} = 0.0267]	6342 [R _{int} = 0.0313, R _{sigma} = 0.0420]
Data / restraints / parameters	1753 / 0 / 90	6342 / 0 / 318
Goodness-of-fit on F ²	1.073	1.028
Final R indexes [I >= 2σ (I)]	R ₁ = 0.0295, wR ₂ = 0.0751	R ₁ = 0.0328, wR ₂ = 0.0820
Final R indexes [all data]	R ₁ = 0.0335, wR ₂ = 0.0773	R ₁ = 0.0346, wR ₂ = 0.0835
Largest diff. peak/hole [e Å ⁻³]	0.26/-0.26	0.55/-0.35
CCDC	1888856	1888858

3.4.8 Theoretical Investigations

3.4.7.1 Computational Methods

Geometry optimizations of **1–3** were performed with the Gaussian09 program package (Revision E.01)³¹ using the xyz coordinates obtained from X-ray crystallography as starting point. The B3LYP density functional²⁴ and the Ahlrichs def2-TZVP basis set²⁶ were employed for all atoms. Atom-pairwise dispersion correction to the DFT energy with Becke–Johnson damping (D3BJ) was applied.²⁵ The nature of the stationary points was verified by numerical frequency analyses. Molecular orbitals were visualized with the program GaussView5.³² The isosurface value is set to 0.05 for all figures.

3.4.7.2 Comparison of Functionals

In order to determine suitable functionals for the quantum mechanical investigations of compounds **1–3**, geometry optimizations of the singlet state in the gas phase were performed using pure GGA functionals (BP86 and OPBE),^{33,34} meta-GGA functionals (TPSS)³⁵ and hybrid-functionals (B3LYP)²⁴ with the Ahlrichs def2-TZVP basis set.²⁶ The B3LYP functional reproduced the solid-state molecular structures very well (cf. Tables S2–4). For the sake of computational cost the geometry optimizations were performed without the $[\text{Li}(\text{solv})_x]^+$ cation.

Table S2. Comparison of some characteristic bond lengths [Å] and angles [°] of *endo*-H-1 with the calculated ones.

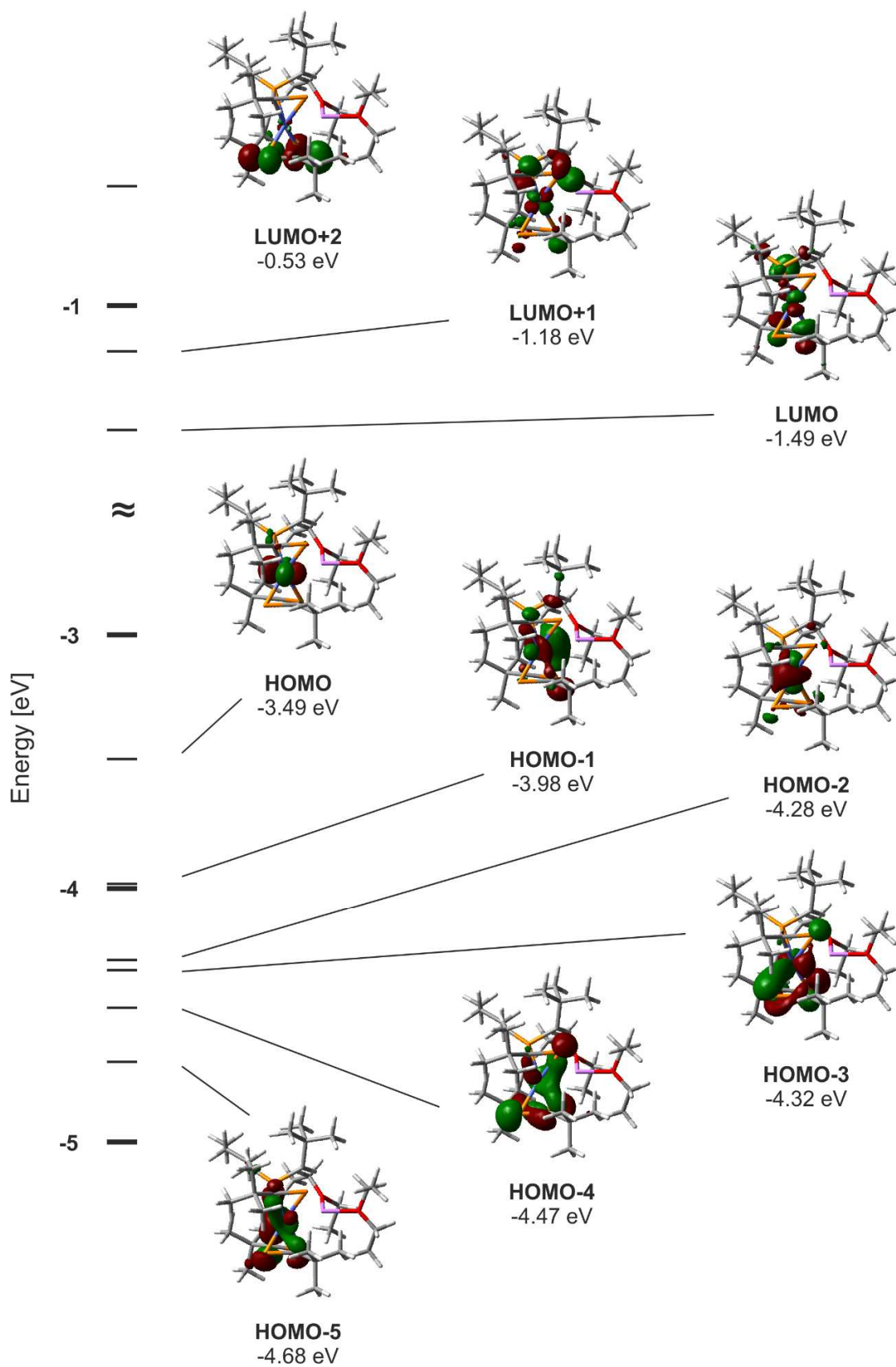
<i>endo</i> -H-1	Exp	BP86	OPBE	TPSS	B3LYP
P1–C1	1.839(6)	1.846	1.845	1.842	1.836
P1–C2	1.767(6)	1.777	1.777	1.774	1.771
P1–C21	1.855(6)	1.863	1.865	1.864	1.854
P2–C1	1.930(7)	1.957	1.954	1.952	1.946
P2–C2	1.822(6)	1.831	1.831	1.828	1.821
Co1–C1	3.051(1)	3.033	3.042	3.028	3.042
P1–C1–P2	82.8(2)	82.0	81.7	81.7	82.3
C2–P1–C1	91.4(3)	92.5	92.9	92.8	92.7
C1–P2–C2	86.9(3)	87.4	87.8	87.6	87.6
E [Hartree]	-	-3691.504690	-3688.909126	-3691.432164	-3691.221077

Table S3. Comparison of some characteristic bond lengths [\AA] and angles [$^\circ$] of *endo*-H-2 with the calculated ones.

<i>endo</i> -H-2	Exp	BP86	OPBE	TPSS	B3LYP
P1–C1	1.858(3)	1.867	1.867	1.863	1.855
P1–C2	1.778(3)	1.785	1.785	1.782	1.779
P1–C21	1.889(3)	1.916	1.919	1.912	1.903
P2–C1	1.937(3)	1.943	1.941	1.940	1.935
P2–C2	1.824(3)	1.830	1.830	1.827	1.820
Co1–C1	3.079(1)	3.032	3.040	3.027	3.038
P1–C1–P2	81.9(1)	81.8	81.4	81.4	81.9
C2–P1–C1	91.4(1)	92.3	92.6	92.5	92.3
C1–P2–C2	87.6(1)	88.5	88.8	88.7	88.6
E [Hartree]	-	-3691.499950	-3688.902243	-3691.424820	-3691.212656

Table S4. Comparison of some characteristic bond lengths [\AA] and angles [$^\circ$] of *exo*-H-3 with the calculated ones.

<i>exo</i> -H-3	Exp	BP86	OPBE	TPSS	B3LYP
P1–C1	1.840(3)	1.836	1.836	1.833	1.826
P1–C2	1.784(3)	1.808	1.807	1.801	1.796
P1–C21	1.845(3)	1.831	1.835	1.834	1.834
P2–C1	1.932(3)	1.951	1.950	1.949	1.940
P2–C2	1.805(3)	1.830	1.829	1.827	1.820
Co1–C1	3.079(1)	3.150	3.161	3.146	3.156
P1–C1–P2	83.0(1)	83.0	82.6	82.4	83.2
C2–P1–C1	89.3(1)	89.9	90.2	90.3	90.0
C1–P2–C2	85.8(1)	85.8	86.1	86.0	85.8
E [Hartree]	-	-3765.341761	-3762.668016	-3765.280132	-3765.051441

Figure S17. Kohn-Sham frontier orbitals of *endo*-H-1 calculated at the B3LYP/def2TZVP level of theory.

3.5 References

- 1 K. B. Dillon, F. Mathey, J. F. Nixon, *Phosphorus: The Carbon Copy*, Wiley, Chichester, **1998**.
- 2 Reviews on Diphosphacyclobutadiene Complexes: a) A. Chirila, R. Wolf, J. C. Sloatweg, K. Lammertsma, *Coord. Chem. Rev.* **2014**, 270-271, 57–74; b) F. Mathey, *Angew. Chem. Int. Ed.* **2003**, 42, 1578; c) M. Regitz, *Chem. Rev.* **1990**, 90, 191–213; d) M. Regitz, P. Binger, *Angew. Chem. Int. Ed. Engl.* **1988**, 27, 1484–1508; e) J. F. Nixon, *Chem. Rev.* **1988**, 88, 1327–1362.
- 3 a) M. T. Nguyen, L. Landuyt, L. G. Vanquickenborne, *J. Org. Chem.* **1993**, 58, 2817–2821; b) S. Creve, M. T. Nguyen, L. G. Vanquickenborne, *Eur. J. Inorg. Chem.* **1999**, 1999, 1281–1289; c) T. Höltzl, D. Szieberth, M. T. Nguyen, T. Veszprémi, *Chem. Eur. J.* **2006**, 12, 8044–8055.
- 4 a) P. Binger, R. Milczarek, R. Mynott, M. Regitz, W. Rösch, *Angew. Chem.* **1986**, 98, 645–646; *Angew. Chem. Int. Ed. Engl.* **1986**, 25, 644–645; b) P. B. Hitchcock, M. J. Maah, J. F. Nixon, *J. Chem. Soc., Chem. Commun.* **1986**, 737–738; c) P. Binger, R. Milczarek, R. Mynott, C. Krüger, Y. H. Tsay, E. Raabe, M. Regitz, *Chem. Ber.* **1988**, 121, 637–645; d) P. Binger, B. Biedenbach, R. Schneider, M. Regitz, *Synthesis* **1989**, 960–961; e) D. W. N. Wilson, A. Hinz, J. Goicoechea, *Angew. Chem.* **2018**, 130, 2210–2215; *Angew. Chem. Int. Ed.* **2018**, 57, 2188–2193.
- 5 Selected examples for 1,3-diphosphacyclobutadiene complexes: a) P. Binger, B. Biedenbach, R. Mynott, C. Krüger, P. Betz, M. Regitz, *Angew. Chem.* **1988**, 100, 1219–1221; *Angew. Chem. Int. Ed. Engl.* **1988**, 27, 1157–1158; b) P. Binger, B. Biedenbach, R. Mynott, R. Benn, A. Ruffinska, P. Betz, C. Krüger, *J. Chem. Soc., Dalton Trans.* **1990**, 1771–1777; c) P. B. Hitchcock, M. J. Maah, J. F. Nixon, *Heteroatom. Chem.* **1991**, 2, 253–264; d) A. G. Avent, F. G. N. Cloke, K. R. Flower, P. B. Hitchcock, J. F. Nixon, D. M. Vickers, *Angew. Chem.* **1994**, 106, 2406–2408; *Angew. Chem. Int. Ed. Engl.* **1994**, 33, 2330–2332; e) D. Böhm, F. Knoch, S. Kummer, U. Schmidt, U. Zenneck, *Angew. Chem.* **1995**, 107, 251–254; *Angew. Chem. Int. Ed. Engl.* **1995**, 34, 198–201; f) P. A. Arnold, F. G. N. Cloke, P. B. Hitchcock, J. F. Nixon, *J. Am. Chem. Soc.* **1996**, 118, 7630; g) M. Scheer, J. Krug, *Z. Anorg. Allg. Chem.* **1998**, 624, 399–405; h) F. G. N. Cloke, P. B. Hitchcock, J. F. Nixon, D. M. Vickers, *J. Organomet. Chem.* **2001**, 635, 212–221; i) A. D. Burrows, A. Dransfeld, M. Green, J. C. Jeffery, C. Jones, J. M. Lyman, M. T. Nguyen, *Angew. Chem.* **2001**, 113, 3321–3324; *Angew. Chem. Int. Ed.* **2001**, 40, 3221–3224; j) D. Himmel, M. Seitz, M. Scheer, *Z. Anorg. Allg. Chem.* **2004**, 630, 1220–1228; k) E.-M. Rummel, M. Eckhardt, M. Bodensteiner, E.V. Peresyphkina, W. Kremer, C. Gröger, M. Scheer, *Eur. J. Inorg. Chem.* **2014**, 1625–1637.
- 6 1,2-Diphosphacyclobutadiene complexes: a) P. Binger, G. Glaser, S. Albus, C. Krüger, *Chem. Ber.* **1995**, 128, 1261–1265; b) F. W. Heinemann, S. Kummer, U. Seiss-Brandl, U. Zenneck, *Organometallics* **1999**, 18, 2021–2029; c) P. Kramkowski, M. Scheer, *Eur. J. Inorg. Chem.* **2000**, 1869–1876; d) C. Jones, C. Schulten, A. Stasch, *Dalton Trans.* **2006**,

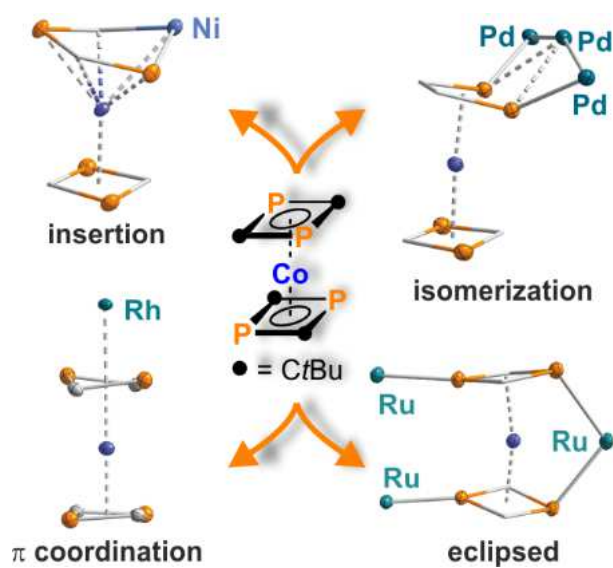
- 3733–3735; e) E.-M. Rummel, G. Balazs, V. Heinl, M. Scheer, *Angew. Chem.* **2017**, *129*, 9720–9725; *Angew. Chem. Int. Ed.* **2017**, *56*, 9592–9596.
- 7 C. Topf, T. Clark, F. W. Heinemann, M. Hennemann, S. Kummer, H. Pritzkow, U. Zenneck, *Angew. Chem.* **2002**, *114*, 4221–4226; *Angew. Chem. Int. Ed.* **2002**, *41*, 4047–4052.
- 8 P. B. Hitchcock, M. J. Maah, J. F. Nixon, *J. Organomet. Chem.* **1994**, *466*, 153–158.
- 9 A. S. Weller, C. D. Andrews, A. D. Burrows, M. Green, J. M. Lynam, M. F. Mahon, C. Jones, *Chem. Commun.* **1999**, 2147–2148.
- 10 a) R. Wolf, A. W. Ehlers, J. C. Slootweg, M. Lutz, D. Gudat, M. Hunger, A. L. Spek, K. Lammertsma, *Angew. Chem.* **2008**, *120*, 4660–4663; *Angew. Chem. Int. Ed.* **2008**, *47*, 4584–4587; b) R. Wolf, J. C. Slootweg, A. W. Ehlers, F. Hartl, B. de Bruin, M. Lutz, A. L. Spek, K. Lammertsma, *Angew. Chem. Int. Ed.* **2009**, *48*, 3104–3107; *Angew. Chem.*, **2009**, *121*, 3150–3152; c) R. Wolf, A. W. Ehlers, M. M. Khusniyarov, F. Hartl, B. de Bruin, G. J. Long, F. Grandjean, F. M. Schappacher, R. Pöttgen, J. C. Slootweg, M. Lutz, A. L. Spek, K. Lammertsma, *Chem. Eur. J.* **2010**, *16*, 14322–14334.
- 11 Highlight article: C. A. Russell, *Angew. Chem.* **2009**, *121*, 4992–4894; *Angew. Chem. Int. Ed.* **2009**, *48*, 4895–4897.
- 12 Cu^I, Ag^I, and Au^I complexes: a) J. Malberg, T. Wiegand, H. Eckert, M. Bodensteiner, R. Wolf, *Chem. Eur. J.* **2013**, *19*, 2356–2369; b) T. Wiegand, H. Eckert, S. Grimme, J. Malberg, R. Wolf, *Solid State Nucl. Magn. Reson.* **2013**, *53*, 13–19; c) J. Malberg, T. Wiegand, H. Eckert, M. Bodensteiner, R. Wolf, *Eur. J. Inorg. Chem.* **2014**, 1638–1651; d) J. Malberg, M. Bodensteiner, D. Paul, T. Wiegand, H. Eckert, R. Wolf, *Angew. Chem.* **2014**, *126*, 2812–2816; *Angew. Chem. Int. Ed.* **2014**, *53*, 2771–2775.
- 13 Ni^{II} and Co^I complexes: C. Rödl, R. Wolf, *Eur. J. Inorg. Chem.* **2016**, *2016*, 736–742.
- 14 Various further oligonuclear complexes were prepared with Ru^{II}, Rh^I, Ni^{II}, and Pd^{II}, which are described in chapter 4 of this thesis and in C. Rödl, R. Wolf, *Chem. Eur. J.* **2019**, *25*, 6180–6188.
- 15 For trimethylsilylated derivatives of **F** and their use in subsequent functionalization reactions, see chapter two of this thesis and: C. Rödl, J. Bissmeyer née Malberg, R. Wolf, *Z. Naturforsch. B* **2018**, *73*, 895–909.
- 16 a) R. Appel, V. Barth, F. Knoch, *Chem. Ber.* **1983**, *116*, 938–950; b) M. Soleilhavoup, A. Baceiredo, F. Dahan, G. Bertrand, *J. Chem. Soc., Chem. Commun.* **1994**, 337–338.
- 17 a) S. Ito, H. Sugiyama, M. Yoshifuji, *Chem. Commun.* **2002**, 1744–1745; b) S. Ito, H. Sugiyama, M. Yoshifuji, *Phosphorus, Sulfur, and Silicon* **2004**, *179*, 785–788; c) S. Ito, H. Miyake, H. Sugiyama, M. Yoshifuji, *Heteroatom Chem.* **2005**, *16*, 357–360.
- 18 M. Schmitz, R. Göller, U. Bergsträßer, S. Leininger, M. Regitz, *Eur. J. Inorg. Chem.* **1998**, *1998*, 227–235.

- 19 C. Fish, M. Green, J. C. Jeffery, R. J. Kilby, J. M. Lynam, J. E. McGrady, D. A. Pantazis, C. A. Russell, C. E. Williams, *Angew. Chem.* **2006**, *118*, 6837–6841; *Angew. Chem. Int. Ed.* **2006**, *45*, 6685–6689.
- 20 *CRC Handbook of Chemistry and Physics, Internet Version 2005*, (Ed.: D. R. Lide), CRC Press, Boca Raton, **2005**.
- 21 H. S. Gutowsky, C. H. Holm, *J. Chem. Phys.* **1956**, *25*, 1228–1234.
- 22 The $[\text{Mg}(\text{MeCN})_6]^{2+}$ cation has previously been characterized by X-ray crystallography. The most recent publications are listed: a) G. Vveryasov, K. Matsumoto, R. Hagiwara, *Dalton Trans.* **2016**, *45*, 2810–2813; b) W. Levason, D. Pugh, J. M. Purkis, G. Reid, *Dalton Trans.* **2016**, *45*, 7900–7911; c) E. N. Keyzer, H. F. J. Glass, Z. Liu, P. M. Bayley, S. E. Dutton, C. P. Grey, D. S. Wright, *J. Am. Chem. Soc.* **2016**, *138*, 8682–8685.
- 23 a) G. S. Zweifel, M. H. Nantz, *Modern Organic Synthesis: An Introduction*, W. H. Freeman and Company, New York, **2007**; b) A. F. Holleman, E. Wiberg, N. Wiberg, *Lehrbuch der Anorganischen Chemie*, 102. Auflage, de Gruyter, Berlin, **2007**.
- 24 a) C. Lee, W. Yang, R. G. Parr, *Phys. Rev. B* **1988**, *37*, 785–789; b) P. J. Stephens, F. J. Devlin, C. F. Chabalowski, M. J. Frisch, *J. Phys. Chem.* **1994**, *98*, 11623–11627.
- 25 a) S. Grimme, S. Ehrlich, L. Goerigk, *J. Comput. Chem.* **2011**, *32*, 1456–1465; b) S. Grimme, J. Antony, S. Ehrlich, H. Krieg, *J. Chem. Phys.* **2010**, *132*, 154104–154119.
- 26 a) A. Schäfer, C. Huber, R. Ahlrichs, *J. Chem. Phys.* **1994**, *100*, 5829–5835; b) F. Weigend, *Phys. Chem. Chem. Phys.* **2006**, *8*, 1057–1065.
- 27 The cyclic voltammogram of **4** recorded in THF/ $[\text{nBu}_4\text{N}]\text{PF}_6$ (Figure S9d) features a reversible oxidation wave at $E_{1/2} = -0.74$ V vs. Fc/Fc⁺ which is identical to that observed for **F**.^{10a}
- 28 a) SCALE3ABS, CrysAlisPro, Agilent Technologies Inc., Oxford, GB, **2015**; b) G. M. Sheldrick, SADABS, Bruker AXS, Madison, USA, **2007**.
- 29 G. M. Sheldrick, *Acta Cryst.* **2015**, *A71*, 3–8.
- 30 G. M. Sheldrick, *Acta Cryst.* **2015**, *C71*, 3–8.
- 31 Gaussian 09, Revision E.01, M. J. Frisch, G. W. Trucks, H. B. Schlegel, G. E. Scuseria, M. A. Robb, J. R. Cheeseman, G. Scalmani, V. Barone, G. A. Petersson, H. Nakatsuji, X. Li, M. Caricato, A. Marenich, J. Bloino, B. G. Janesko, R. Gomperts, B. Mennucci, H. P. Hratchian, J. V. Ortiz, A. F. Izmaylov, J. L. Sonnenberg, D. Williams-Young, F. Ding, F. Lipparini, F. Egidi, J. Goings, B. Peng, A. Petrone, T. Henderson, D. Ranasinghe, V. G. Zakrzewski, J. Gao, N. Rega, G. Zheng, W. Liang, M. Hada, M. Ehara, K. Toyota, R. Fukuda, J. Hasegawa, M. Ishida, T. Nakajima, Y. Honda, O. Kitao, H. Nakai, T. Vreven, K. Throssell, J. A. Montgomery, Jr., J. E. Peralta, F. Ogliaro, M. Bearpark, J. J. Heyd, E. Brothers, K. N. Kudin, V. N. Staroverov, T. Keith, R. Kobayashi, J. Normand, K. Raghavachari, A. Rendell, J. C. Burant, S. S. Iyengar, J. Tomasi, M. Cossi, J. M. Millam, M. Klene, C. Adamo, R. Cammi, J. W. Ochterski, R. L. Martin, K. Morokuma, O. Farkas, J. B. Foresman, and D. J. Fox, Gaussian, Inc., Wallingford CT, **2016**.

- 32 GaussView 5.0.9: R. Dennington, T. A. Keith, J. M. Millam, Semichem Inc., Shawnee Mission, KS, **2016**.
- 33 a) A. D. Becke, *Phys. Rev. A* **1988**, *38*, 3098–3100; b) J. P. Perdew, *Phys. Rev. B* **1986**, *33*, 8822–8824.
- 34 a) J. P. Perdew, K. Burke, M. Ernzerhof, *Phys. Rev. Lett.* **1996**, *77*, 3865–3868; b) J. P. Perdew, K. Burke, M. Ernzerhof, *Phys. Rev. Lett.* **1997**, *78*, 1396.
- 35 J. Tao, J. P. Perdew, V. N. Staroverov, G. E. Scuseria, *Phys. Rev. Lett.* **2003**, *91*, 146401–146404.

4 FLEXIDENTATE COORDINATION BEHAVIOR AND CHEMICAL NON-INNOCENCE OF A BIS(1,3-DIPHOSPHACYCLOBUTADIENE) SANDWICH ANION^[a]

CHRISTIAN RÖDL, AND ROBERT WOLF



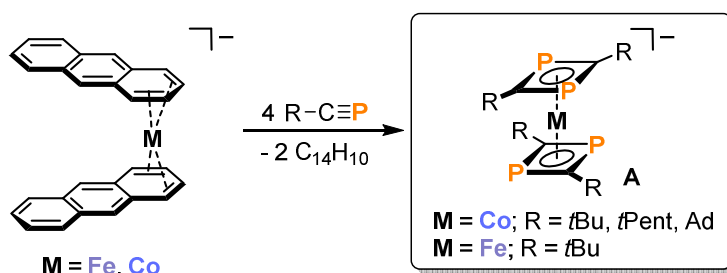
[a] C. Rödl performed all experiments and theoretical calculations and wrote the manuscript. R. Wolf supervised the project. Part of this work was published in C. Rödl, R. Wolf, *Chem. Eur. J.* **2019**, *25*, 8332-8343. Copyright 2019 Wiley-VCH, License number: 4625760311655.

4.1 Introduction

Diphosphacyclobutadienes are labile molecules, but can be stabilized via the formation of π -complexes with transition metals, which are prepared by the metal-mediated cyclodimerization of phosphalkynes, $R-C\equiv P$.^{1,2} Both the 1,2- and 1,3-diphosphacyclobutadiene isomers are accessible. While the 1,2-isomer is more stable with small organic substituents, bulky groups such as $R = tBu$ favor the formation of the 1,3-isomer.³

The first 1,3-diphosphacyclobutadiene complexes were reported independently by Regitz, Binger and co-workers as well as Nixon and co-workers in 1986.⁴ Since then, numerous 1,3-diphosphacyclobutadiene complexes as well as some 1,2-diphosphacyclobutadiene complexes have been described.^{5,6} Our group developed anionic bis(1,3-diphosphacyclobutadiene) sandwich complexes $[M(P_2C_2R_2)_2]^-$ ($M = Fe, Co$; type **A**, Scheme 1)⁷ which can be obtained from the reaction of bis(anthracene) metalates $[M(\eta^4-C_{14}H_{10})_2]^-$ ($M = Fe, Co$; $C_{14}H_{10}$ = anthracene)⁸ with phosphalkynes such as $tBu-C\equiv P$, $tPent-C\equiv P$, and $Ad-C\equiv P$ (tBu = *tert*-butyl, $tPent$ = *tert*-pentyl, Ad = adamantyl). Four P atoms are present in these molecules, which may potentially enable a rich coordination chemistry.

Previously, we reported the preparation of various complexes with copper(I), silver(I), and gold(I) of type **A** anions (Figure 1).⁹ In the molecular structure of these products, one or two phosphorus atoms of the sandwich molecule are involved in metal coordination (Figure 1, **B** and **C**). A striking result was the synthesis of the octanuclear molecular square $[Au\{Co(P_2C_2tBu_2)_2\}_4]$ (**D**) composed of four $[Co(P_2C_2tBu_2)_2]^-$ molecules and four gold atoms.⁹



Wolf, Lammertsma and co-workers 2008-2010

Scheme 1. Synthesis of complexes of type **A**.

In order to gain more comprehensive insight into the coordination chemistry of type **A** anions, we next decided to investigate the synthesis of metal complexes with cations of groups 8-10, and 12. In a previous preliminary communication, we reported the synthesis of nickel(II) and cobalt(I) complexes (see Figure 1, structure **B**) with σ -coordinated $CpNi(PPh_3)$ and $(C_4Me_4)Co(CO)_2$ fragments.¹⁰ Here, we give a full account of our studies, which have revealed several new and intriguing features of the coordination chemistry of type **A** anions. In particular the chemical non-innocence of these seemingly robust sandwich complexes, which are unexpectedly

Previous work: σ -complexes of $[\text{Co}(\text{P}_2\text{C}_2\text{tBu}_2)_2]^-$ (type **A**) anions with (coinage) metal cations

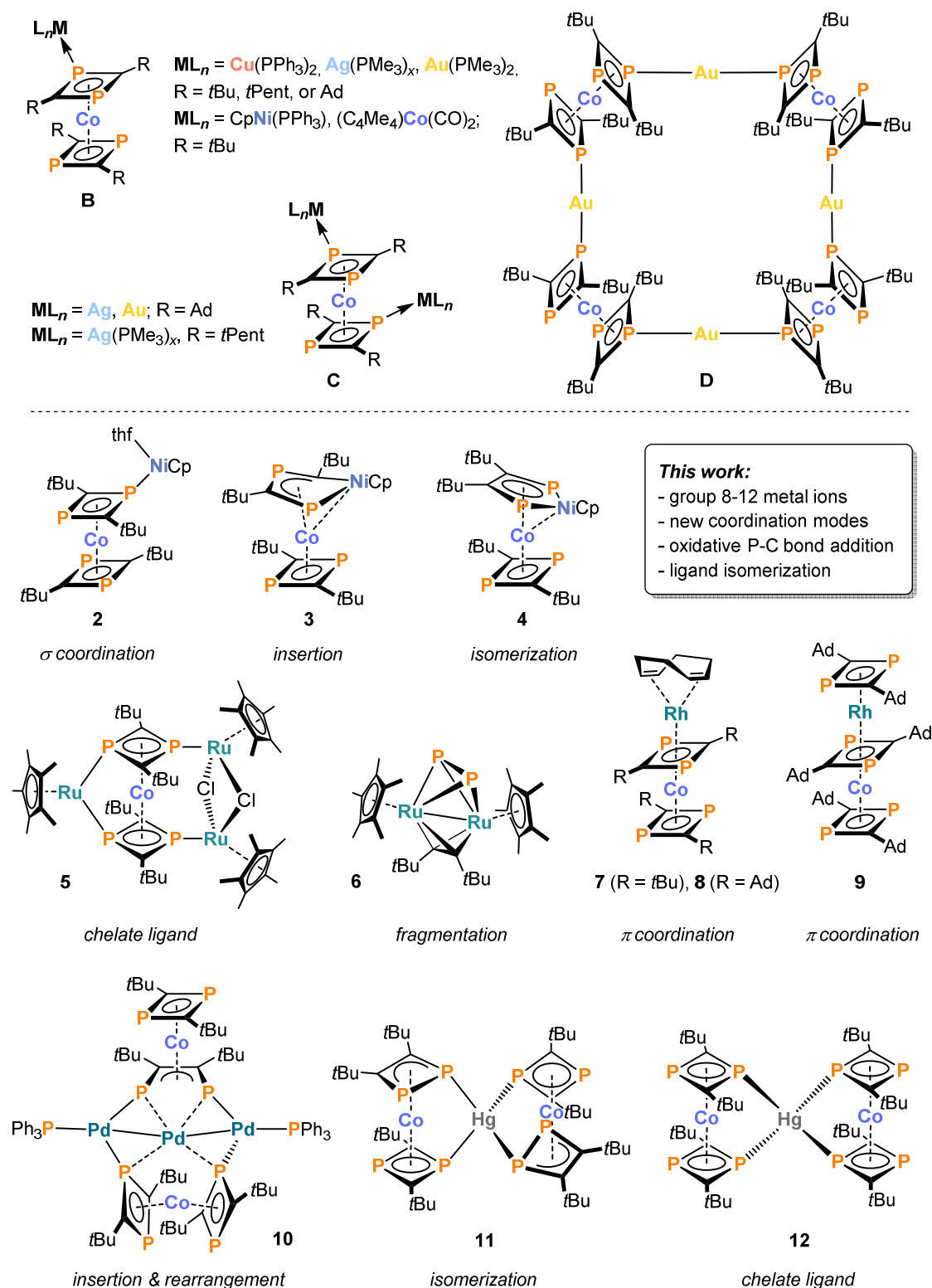


Figure 1. Previously reported transition metal complexes of type **A** anions (top); new coordination complexes **2–12**.

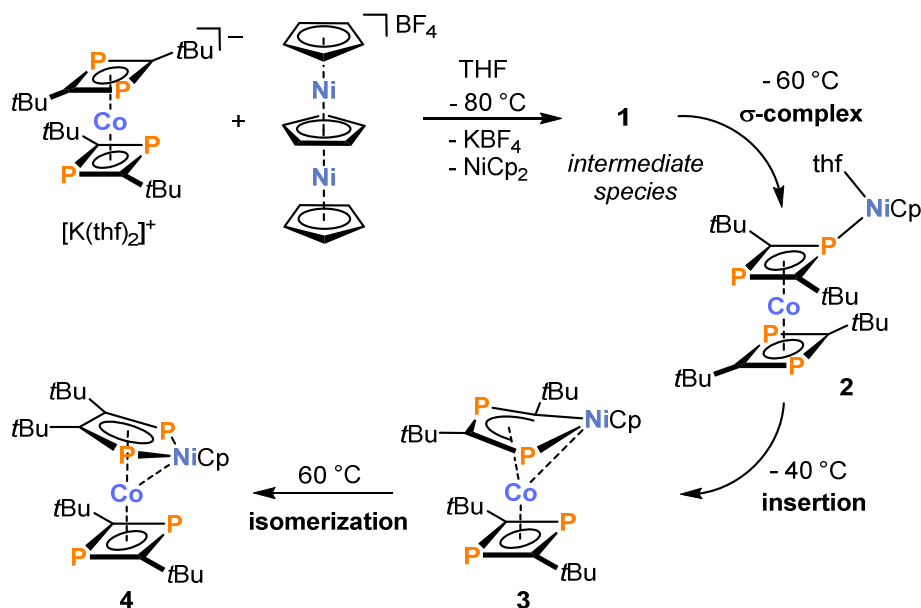
prone to rearrangements and the insertion of unsaturated metal complex fragments into the ligand framework, is noteworthy. Also, they show flexidentate coordination behavior demonstrated by the ability to act as a chelate ligand and to form π -complexes. These remarkable properties have

led to the synthesis of several new oligonuclear complexes **2–12** with unprecedented molecular structures. In addition to the thorough structural and spectroscopic characterization of these new compounds, we also describe electrochemical properties (ascertained by cyclic voltammetry) and use DFT calculations to analyze the electronic structures for selected examples.

4.2 Results and Discussion

4.2.1 Reaction of $[\text{K}(\text{thf})_2\{\text{Co}(\text{P}_2\text{C}_2\text{tBu}_2)_2\}]$ with $[\text{Ni}_2\text{Cp}_3]\text{BF}_4$

Aiming at the synthesis of the hypothetical tripledecker complex $[\text{CpNi}(\mu\text{-P}_2\text{C}_2\text{tBu}_2)\text{-Co}(\text{P}_2\text{C}_2\text{tBu}_2)]$, we began with the reaction of $[\text{K}(\text{thf})_2\{\text{Co}(\text{P}_2\text{C}_2\text{tBu}_2)_2\}]^7$ with Werner's classic complex $[\text{Ni}_2\text{Cp}_3]\text{BF}_4^{11}$ (one equivalent) in THF. This reaction produces five complexes in total, the ratio of which changes depending on reaction times and temperatures, according to $^{31}\text{P}\{^1\text{H}\}$ NMR monitoring (Scheme 2).



Scheme 2. Reaction between $[\text{K}(\text{thf})_2\{\text{Co}(\text{P}_2\text{C}_2\text{tBu}_2)_2\}]$ and $[\text{Ni}_2\text{Cp}_3]\text{BF}_4$.

When the reactants are mixed in an NMR tube in THF at 193 K, the first main product **1** (*intermediate species*, >92% according to $^{31}\text{P}\{^1\text{H}\}$ NMR) with $^{31}\text{P}\{^1\text{H}\}$ NMR signals at $\delta = -6.5$, -1.0 , 9.2 , and 10.3 ppm can be observed. This product is stable up to 213 K. The resonances of **1** are no longer observed when the temperature is raised to 233 K, whereupon a second species **2** forms which shows three $^{31}\text{P}\{^1\text{H}\}$ NMR signals at $\delta = -4.1$, 15.6 , and 31.5 ppm with an integral ratio of 1:2:1. Above 253 K, the formation of a third species **3** is observed, which is stable in solution at room temperature for at least one day (*vide infra*). When the temperature is increased to 333 K for >30 min, another species **4** forms, which gives rise to one $^{31}\text{P}\{^1\text{H}\}$ NMR signal at $\delta = 459.4$ ppm (*vide infra*) at this temperature. Finally, a fifth distinct species with a singlet resonance at 40.0 ppm is formed when the solution is kept at 333 K for three days.

While **1** could not be isolated due to its low stability, $[\text{CpNi}\{\text{Co}(\eta^4\text{-1,3-P}_2\text{C}_2\text{tBu}_2)_2\}(\text{thf})]$ (**2**) was synthesized on a preparative scale and characterized by single-crystal X-ray crystallography. The molecular structure (Figure 2) is similar to $[\text{CpNi}\{\text{Co}(\text{P}_2\text{C}_2\text{tBu}_2)_2\}(\text{PPh}_3)]$ (**E**, see Figure 1,

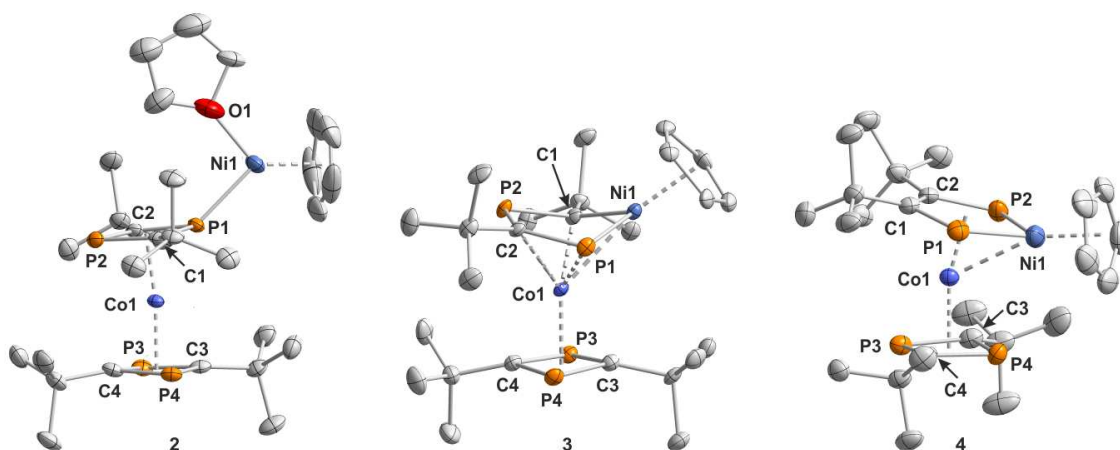


Figure 2. Solid-state molecular structures of **2** (left), **3** (middle), and **4** (right). The hydrogen atoms are omitted for clarity. Thermal ellipsoids are drawn at the 50% probability level. Selected bond lengths [Å] and angles [°] for **2**: Ni1–P1 2.1807(8), P1–C1 1.784(3), P1–C2 1.785(3), P2–C1 1.800(3), P2–C2 1.799(3), P1–C1–P2–C2/P3–C3–P4–C4 6.1; **3**: Ni1–Co1 2.536(1), Ni1–P1 2.179(2), Ni1–C1 1.902(7), P1–C2 1.770(7), C2–P2 1.754(7), P2–C1 1.783(6), P1–Ni1–C1 94.6(2), Ni1–C1–P2 116.3(3), P1–C1–P2–C2/P3–C3–P4–C4 12.5; **4**: Ni1–Co1 2.5447(7), Ni1–P1 2.144(1), Ni1–P2 2.1568(9), P1–C1 1.798(3), P2–C2 1.795(3), C1–C2 1.447(4), P2–Ni1–P1 88.54(3), Ni1–P1–C1 110.0(1), C2–P2–Ni1 110.0(1), Ni–P1–C1–P2–C2/P3–C3–P4–C4 13.7.

type **B**), previously prepared via a similar route and described by us in a preliminary communication.¹⁰ The nickel atom is coordinated by one phosphorus atom of a $[\text{Co}(\text{P}_2\text{C}_2t\text{Bu}_2)_2]^-$ anion, a cyclopentadienyl ligand, and a THF molecule, resulting in a two-legged piano-stool environment for Ni1. The Ni1–P1 distance is somewhat shorter than in **E** [2.1807(8) in **2** vs. 2.2022(5) Å in **E**].¹⁰ Similar to **E**, the coordinated P_2C_2 ligands are slightly tilted as a result of metal coordination; the dihedral angle between the P1–C1–P2–C2/P3–C3–P4–C4 planes in **2** is 6.09° vs. 11.35° in $[\text{CpNi}\{\text{Co}(\text{P}_2\text{C}_2t\text{Bu}_2)_2\}(\text{PPh}_3)]$.

The $^{31}\text{P}\{^1\text{H}\}$ NMR spectrum of crystalline **2** (recorded in $[\text{D}_8]\text{THF}$ at 233 K) is similar to that of $[\text{CpNi}\{\text{Co}(\text{P}_2\text{C}_2t\text{Bu}_2)_2\}(\text{PPh}_3)]$.¹⁰ Two doublets at $\delta = -4.1$ ppm [$^2J(^{31}\text{P},^{31}\text{P}) = 21.3$ Hz] and $\delta = 31.5$ ppm [$^2J(^{31}\text{P},^{31}\text{P}) = 21.3$ Hz] are assigned to the P atoms of the nickel-coordinated diphosphacyclobutadiene, while the second diphosphacyclobutadiene ligand of **2** gives rise to a singlet at $\delta = 15.6$ ppm. $[\text{CpNi}\{\text{Co}(\text{P}_2\text{C}_2t\text{Bu}_2)_2\}(\text{PPh}_3)]$ is stable in solution at ambient temperature, whereas **2** slowly transforms into **3** below 233 K, which prevented it from being isolated as a pure compound. $^{31}\text{P}\{^1\text{H}\}$ NMR spectra of samples isolated by crystallization at low temperature show an additional set of signals at $\delta = -10.6$, 14.5, and 33.6 ppm with the same pattern, indicating the presence of a second isomer of compound **2** (ratio 10:1). A third set of signals is assigned to compound **3** (*vide infra*).

Complex **3** was isolated by reacting $[\text{K}(\text{thf})_2\{\text{Co}(\text{P}_2\text{C}_2t\text{Bu}_2)_2\}]$ with $[\text{Ni}_2\text{Cp}_3]\text{BF}_4$ at 253 K for 2 h in THF, followed by extraction of the crude product with cold *n*-hexane. Crystals suitable for X-ray crystallography were obtained from a concentrated *n*-hexane solution stored at -35°C . As

shown by the molecular structure of **3** (Figure 2), an unprecedented insertion of the $[\text{CpNi}]^+$ fragment into a P–C bond of the $[\text{Co}(\text{P}_2\text{C}_2\text{tBu}_2)]^-$ anion results in a 1,4-diphospha-2-nickelacyclopentadiene unit, which forms a π -complex with the cobalt center. The Ni1–C1 [1.902(7) Å] and Ni1–P1 [2.179(2) Å] bond lengths of **3** are in the range of single bonds, whereas the P1–C2 [1.770(7) Å], C2–P2 [1.754(7) Å], and P2–C1 [1.783(6) Å] distances suggest a delocalized bonding situation similar to that in the cyclic 1,3-diphosphacyclobutadiene ligands present in the starting material.^{2,4,7} The Ni(P₂C₂tBu₂) framework is comparable to the 1,4-diphospha-2-rhodacyclopentadiene **F** (Figure 3, P1–C2 1.685 Å, C2–P2 1.801 Å, P2–C1 1.710 Å) synthesized by Binger and co-workers by reaction of *t*BuCP with $[\text{RhCl}(\eta^2\text{-C}_2\text{H}_4)_2]_2$ in presence of PMe_3 .^{5a} In addition, a relatively short Ni1–Co1 distance of 2.536(1) Å might indicate a metal-metal bond. However, our DFT calculations indicate that the Ni-Co bonding is weak (*vide infra*).

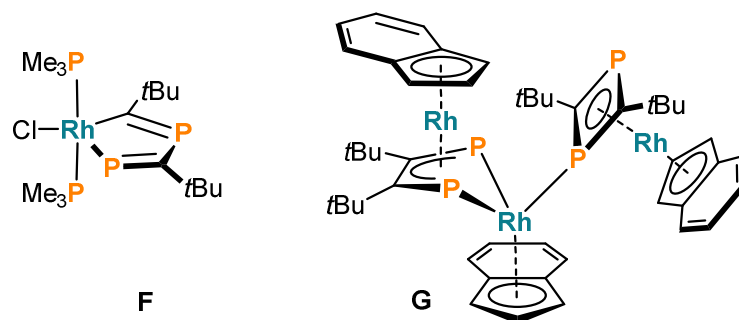


Figure 3. Known diphosphetallacyclopentadienes reported by Binger and co-workers.^{5a,b}

The NMR data of **3** is in agreement with the crystallographically determined structure. The ^1H NMR spectrum recorded in $[\text{D}_8]\text{THF}$ displays four signals for the chemically inequivalent *tert*-butyl substituents at $\delta = 0.83, 1.08, 1.46,$ and 1.79 ppm, and a singlet at $\delta = 5.31$ ppm for the Cp ligand. Similar to **F** reported by Binger and co-workers,^{5a} the $^{13}\text{C}\{^1\text{H}\}$ NMR spectrum of **3** in $[\text{D}_8]\text{THF}$ features two downfield shifted signals at $\delta = 172.4$ and 252.0 ppm for the carbon atoms in the 1,4-diphospha-2-nickelacyclopentadiene ring. The $^{31}\text{P}\{^1\text{H}\}$ NMR spectrum of **3** shows four signals at $\delta = 36.0, 71.4, 191.4,$ and 492.2 ppm. We assign the latter two downfield shifted signals to the two P atoms of the 1,4-diphospha-2-nickelacyclopentadiene unit (c.f. the similar values reported for rhodium compound **F**).⁵ The signal at $\delta = 492.2$ ppm likely arises from the P atom coordinated to nickel due to the strong downfield shift typical for terminal phosphinidene and metallated phosphalkene complexes.¹²⁻¹⁴ The deep orange color of **3** is similar to that of the starting material $[\text{K}(\text{thf})_2\{\text{Co}(\text{P}_2\text{C}_2\text{tBu}_2)\}]$. The UV/Vis spectrum in THF (SI, Figure S8) features an intense maximum at 333 nm and broad bands at 401, 476, 570, and 652 nm.

DFT optimization with the BP86-D3BJ and B3LYP-D3BJ functionals reproduced the molecular structure of **3** accurately (the def2-TZVP basis set was used, see the SI for details). The Wiberg bond indices (WBIs) suggest that the C–P bonds (WBIs of 1.18, 1.19 and 1.22) of the

diphosphametallacycle may possess partial double bond character. By contrast, the WBIs for the Ni1–P1 bond (WBI 0.53) as well as the Ni1–C1 bond (WBI 0.50) indicate single bond character. A low WBI of 0.12 was calculated for the cobalt-nickel bond, suggesting that this interaction is relatively weak. In line with this, no metal-metal bonding is apparent in the canonical Kohn-Sham orbitals (SI, Figure S17). The highest occupied molecular orbitals (HOMO) are mainly located at the CpNi(P₂C₂tBu₂) unit, while the lowest unoccupied orbitals (LUMO) are centered at the Co(P₂C₂tBu₂) fragment and individual Ni1, P1, and C1 atoms.

Remarkably, complex **3** is thermally stable at room temperature in the solid state, although in solution it slowly isomerizes to **4** at ambient temperature. Full conversion to **4** is achieved after heating a THF solution of **3** for 9 h at 60 °C. X-ray quality crystals were grown from a concentrated *n*-hexane solution. Single-crystal X-ray diffraction revealed a planar 1,3-diphospha-2-nickelacyclopentadienyl ligand, which is η⁵-coordinated to cobalt with a C–C bond length of 1.447(4) Å and C–P bond lengths of 1.795(3) and 1.798(3) Å. This ligand is similar to the structure of the rhodium complex **G** (Figure 3, C–C 1.415 Å, C–P 1.827 Å and 1.843 Å), which was obtained from [Rh(η⁵-indenyl)(alkene)₂] ((alkene)₂ = (C₂H₄)₂ or η⁴-1,5-cyclooctadiene) and *t*BuCP.⁵ The Ni–P [2.144(1) and 2.1568(9) Å] bond is significantly shorter than in **3**. The relatively short cobalt-nickel distance of 2.5447(7) Å is also noteworthy. This feature is presumably responsible for the tilted structure of the sandwich molecule: The dihedral angle between the planes Ni1P1C1C2P2 / P3C3P4C4 amounts to 13.7° (cf. P1C1C2P2 / P3C3P4C4 12.1° in **3**). The nickel atom is in an almost planar two-legged piano-stool environment [sum of angles around Ni1: 355.003(3)°].

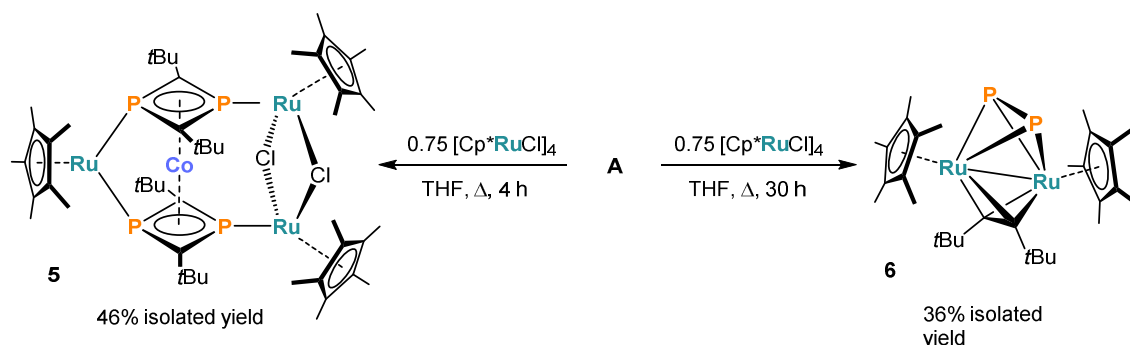
The NMR data of **4** (recorded in [D₈]THF) is in line with the crystal structure. The ¹H NMR spectrum shows two singlets at δ = 1.08 and 1.62 ppm for the *t*Bu groups and a singlet at δ = 5.26 ppm for the Cp ligand. The ³¹P{¹H} NMR spectrum shows a singlet at δ = 458.7 ppm at room temperature, which can be assigned to the P atoms of the 1,3-diphospha-2-nickelacyclopentadienyl ligand. Resonances for the 1,3-diphosphacyclobutadiene unit were not observed at room temperature, but the expected signals appear upon cooling of the NMR sample. Sharp resonances were observed at δ = –25.9, 76.6, and 457.0 ppm at 193 K in agreement with the crystallographically determined structure. This fluxional behavior is very likely caused by the rotation of the 1,3-diphosphacyclobutadiene ligand, which is fast on the NMR timescale above room temperature. At 343 K a broad signal appeared at δ = 29.3 ppm, which sharpened upon heating to 373 K (SI, Figure S2). The ³¹P{¹H} NMR spectrum of **4** at 193 K was qualitatively reproduced by DFT calculations at the B3LYP/def2-TZVP level of theory, which gave calculated chemical shift values of –11.9, 84.9, and 577.4 ppm (referenced vs. [Co(P₂C₂tBu₂)₂][–], see the SI).

Wiberg bond indices (WBIs) calculated by DFT indicate that the bonding situation of **4** is similar to **3**. For the diphosphametallacycle, high WBIs (1.34 for C1–C2, 1.16 for P1–C1, and 1.17 for P2–C2) indicate partial double bond character for the C–C and C–P bonds, while the WBIs of the

Ni–P bonds (0.56 for Ni1-P1 and Ni1-P2) indicate single bond character. Similar to **3**, the interaction between nickel and cobalt appears to be rather weak (WBI 0.10 for Ni1-Co1) despite the shorter metal-metal distance.

4.2.2 Reaction of $[\text{K}(\text{thf})_2\{\text{Co}(\text{P}_2\text{C}_2\text{tBu}_2)_2\}]$ with $[\text{Cp}^*\text{RuCl}]_4$

In the hopes of isolating the hypothetical tripledecker complex $[\text{Cp}^*\text{Ru}(\mu\text{-P}_2\text{C}_2\text{tBu}_2)\text{-Co}(\text{P}_2\text{C}_2\text{tBu}_2)]$, we investigated the reaction of $[\text{K}(\text{thf})_2\{\text{Co}(\text{P}_2\text{C}_2\text{tBu}_2)_2\}]$ with $[\text{Cp}^*\text{RuCl}]_4$ (0.25 equivalents, Scheme 3). Unexpectedly, this reaction led to the identification of $[(\text{Cp}^*\text{Ru})_3(\mu\text{-Cl})_2\{\text{Co}(\text{P}_2\text{C}_2\text{tBu}_2)_2\}]$ (**5**) and $[(\text{Cp}^*\text{Ru})_2(\mu,\eta^2\text{-P}_2)(\mu,\eta^2\text{-C}_2\text{tBu}_2)]$ (**6**) as products among other unidentified species. Monitoring of the reaction by $^{31}\text{P}\{^1\text{H}\}$ NMR spectroscopy (see SI, Figure S4) revealed that $[\text{K}(\text{thf})_2\{\text{Co}(\text{P}_2\text{C}_2\text{tBu}_2)_2\}]$ was already consumed after two hours while compound **5** formed. Compound **6** formed after 28 hours, whereas the signals assigned to compound **5** were no longer observed after 48 hours. After optimizing the stoichiometry and the reaction conditions, complexes **5** and **6** were both isolated as pure compounds. Reaction of $[\text{K}(\text{thf})_2\{\text{Co}(\text{P}_2\text{C}_2\text{tBu}_2)_2\}]$ (one equivalent) with $[\text{Cp}^*\text{RuCl}]_4$ (0.75 equivalents) in refluxing THF for four hours affords **5** in 46% isolated yield. Compound **6** can be isolated in 36% yield when an identical reaction mixture is refluxed for 30 hours.



Scheme 3. Synthesis of **5** and **6**.

Single-crystal X-ray structure determinations revealed the molecular structures of **5** and **6**. The molecular structure of **5** (Figure 4, left) shows the $[\text{Co}(\text{P}_2\text{C}_2\text{tBu}_2)_2]^-$ sandwich compound in an eclipsed conformation coordinated to a Cp^*Ru and a dimeric $(\text{Cp}^*\text{RuCl})_2$ fragment. This leads to a dihedral angle (between P1-P2-Co1 and Co1-P3-P4 planes) of only $\alpha = 2.6^\circ$. We are not aware of similar structures with eclipsed diphosphacyclobutadienes in the literature. The diphosphacyclobutadiene ligands are slightly tilted as a result of the metal coordination (dihedral angle between P1-C1-P2-C2/P3-C3-P4-C4 planes 11.6°). The ruthenium atom Ru1 shows a two-legged piano-stool environment composed of an $\eta^5\text{-Cp}^*$ ligand, and two phosphorus atoms of the $\text{Co}(\text{P}_2\text{C}_2\text{tBu}_2)_2$ unit. The Ru1–Co1 distance of 2.6449(1) Å is substantially larger than the sum of the covalent radii (2.36 Å).¹⁵ The remaining ruthenium atoms (Ru2 and Ru3) show a three-legged piano-stool environment formed by a Cp^* ligand, two chlorine atoms, and one phosphorus atom.

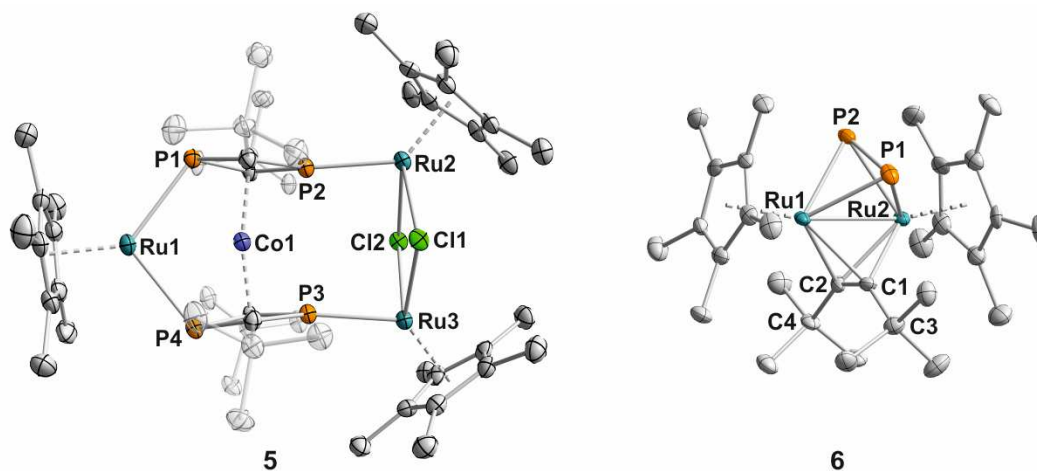


Figure 4. Solid-state molecular structures of **5** (left) and **6** (right). The hydrogen atoms are omitted for clarity. Thermal ellipsoids are drawn at the 50% probability level. Selected bond lengths [Å] and angles [°] for **5**: Ru1–P1 2.5233(8), Ru1–P4 2.4825(8), Ru1–Co1 2.6448(5), Ru2–P2 2.2920(7), Ru3–P3 2.2796(7), P4–Ru1–P1 105.22(2); **6**: Ru1–Ru2 2.6985(8), Ru1–P1 2.381(2), Ru1–P2 2.339(2), Ru1–C1 2.150(8), Ru1–C2 2.125(8), Ru2–C1 2.158(8), Ru2–C2 2.125(8), P1–P2 2.089(3), C1–C2 1.34(1).

The Ru1–P1 and Ru1–P4 bond lengths (2.5233(8) Å and 2.4825(8) Å) are significantly longer than the sum of covalent radii (2.36 Å) presumably because the diphosphacyclobutadiene ligands are tilted toward Ru2 and Ru3. Ru2–P2 (2.2920(7) Å) and Ru3–P3 (2.2796(7) Å) are much shorter and in the range of dative Ru–P bonds observed in phosphane complexes.¹⁶

The ¹H and ¹³C{¹H} NMR spectra of **5** (recorded in [D₈]THF) are in line with the solid-state structure, displaying one *tert*-butyl environment and two distinct Cp* signals. The ³¹P{¹H} NMR spectrum of **5** shows two singlets at $\delta = -13.5$ and 44.3 ppm in a 1:1 ratio. Based on DFT calculations (B3LYP/def2-TZVP level, see the SI for details), we assign the signal at $\delta = -13.5$ ppm to the chelating P atoms P1 and P4, whereas the signal at $\delta = 44.3$ ppm is assigned to P2 and P3, which coordinate to separate Ru atoms.

The molecular structure of **6** shows that the 1,3-diphosphocyclobutadiene ligands of the starting material were completely cleaved. The structure consists of a diphosphorus moiety and an alkyne (2,2,5,5-tetramethylhex-3-yne) bridging a Cp*RuRuCp* unit. To the best of our knowledge, the diphosphorus/alkyne bonding motif has not been observed before. The P₂ unit is oriented perpendicularly with respect to the intermetallic vector, resulting in a tetrahedral μ, η^2 geometry. The P1–P2 distance of 2.089(3) Å is similar to that of known diphosphorus-bridged complexes.¹⁷ The C1–C2 distance of the bent alkyne ligand is 1.34(1) Å; the *tert*-butyl substituents enclose C–C–C angles of 141.1(8)° and 144.8(8)°, respectively. Similar structural parameters are found in other alkyne-bridged diruthenium complexes.¹⁷ The Ru1–Ru2 distance of 2.6985(8) Å is 0.2 Å longer than the sum of covalent radii.¹⁵

DFT optimization (in this case, the BP86-D3BJ/def2-TZVP level was used, see the SI for details) reproduced the molecular of **6** very well, while attempted optimizations of the isomeric

bis(phosphaalkyne) complex $[(\text{Cp}^*\text{Ru})_2(\mu, \eta^2\text{-PCtBu})_2]$ (**6'**) also converged at **6**. This seems to indicate that **6'** is not a minimum on the potential energy hypersurface. Based on the Ru–Ru distance and the calculated Wiberg bond indices (WBI 0.26 for Ru1–Ru2, cf. WBI 0.48 for Ru1–C1, WBI 0.61 for Ru1–P1), Ru–Ru bonding is likely weak. WBIs of 1.22 for P1–P2 and 1.50 for C1–C2 indicate that there is significant multiple bonding in these units.

In accord with the solid-state molecular structure, just two ^1H NMR singlets are observed at $\delta = 1.41$ and 1.86 ppm for **6** in C_6D_6 , while the $^{13}\text{C}\{^1\text{H}\}$ NMR spectrum shows signals at $\delta = 12.6$ ppm and 96.0 ppm for the Cp^* ligands, and signals at $\delta = 34.3$ ppm and 35.7 ppm for the *tert*-butyl substituents. (We could not detect the signals of the alkyne carbon atoms.) The bridging P_2 unit gives rise to one extremely broad singlet ($\nu_{\text{FWHM}} = 360$ Hz) at $\delta = 128.9$ ppm in the $^{31}\text{P}\{^1\text{H}\}$ NMR spectrum. A similar chemical shift was reported by Dahl and co-workers for $[\text{Fe}_2\text{Cp}^*_2(\mu, \eta^2\text{-P}_2)_2]$ (126.6 ppm).^{17g} The $^{31}\text{P}\{^1\text{H}\}$ NMR signal broadens even further upon cooling the NMR sample to 253 K, presumably due to decoalescence. Heating leads to signal sharpening ($\nu_{\text{FWHM}} = 140$ Hz at 333 K). These $^{31}\text{P}\{^1\text{H}\}$ NMR observations may indicate that the P_2 fragment takes part in an unknown dynamic process; further investigations are needed to clarify the cause of this dynamic process.

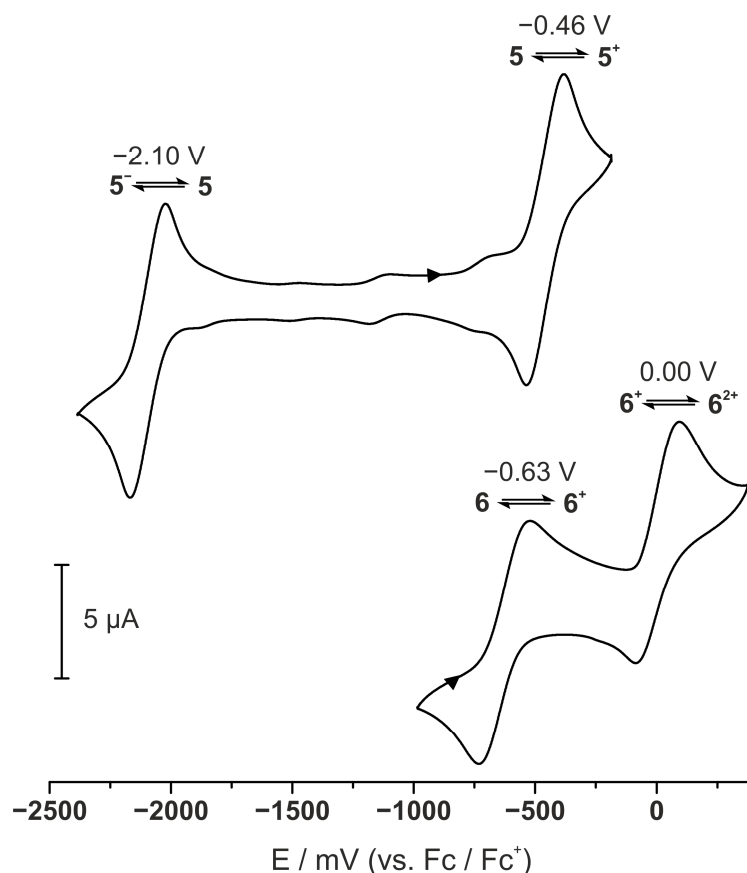
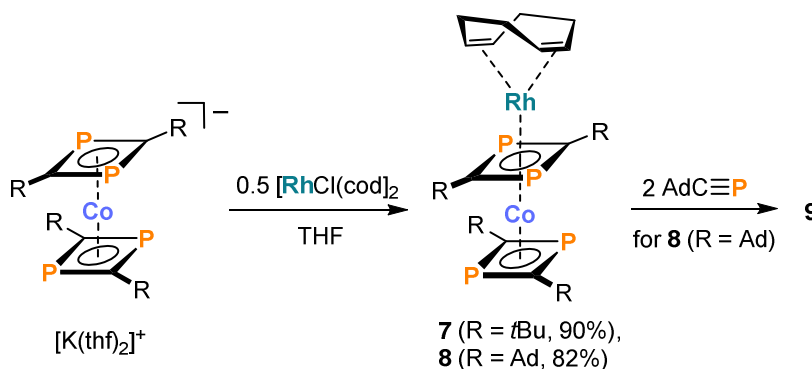


Figure 5. Cyclic voltammograms of **5** (top) and **6** (bottom) recorded in $\text{THF}/[n\text{Bu}_4\text{N}]\text{PF}_6$ with a platinum disc working electrode, a platinum wire as counter electrode, and silver/silver nitrate as reference electrode. $\nu = 100$ mV/s; potentials are referenced to the Fc/Fc^+ couple.

The cyclic voltammogram of **5** (THF/[*n*Bu₄N]PF₆, Figure 5) features two reversible redox events at $E_{1/2} = -0.46$ V vs. Fc/Fc⁺ and $E_{1/2} = -2.10$ V vs. Fc/Fc⁺, which may tentatively be assigned to the reversible oxidation and reduction of the complex. The cyclic voltammogram of **6** (THF/[*n*Bu₄N]PF₆, Figure 5) shows two successive reversible oxidation waves at $E_{1/2} = -0.63$ V vs. Fc/Fc⁺ and $E_{1/2} = 0.00$ V vs. Fc/Fc⁺. It is noteworthy that anions of type **A** show only one reversible oxidation event (observed at -0.73 V vs. Fc/Fc⁺ for [K([18]crown-6)(thf)₂{Co(P₂C₂*t*Bu₂)₂}]).⁷

4.2.3 Reaction of [K(thf)₂{Co(P₂C₂*t*Bu₂)₂}] with [RhCl(cod)]₂

We continued our investigation by reacting [K(thf)₂{Co(P₂C₂R₂)₂}] (R = *t*Bu, Ad) with [RhCl(cod)]₂ (0.5 equivalents). The reactions were performed in THF at room temperature and the crude product extracted with *n*-hexane (**7**) or toluene (**8**). Concentration of said solutions afforded deep yellow, crystalline π -complexes [Rh(cod){Co(P₂C₂R₂)₂}] (**7**, R = *t*Bu; **8**, R = Ad) in high yields of 90% for **7** and 82% for **8**.



Scheme 4. Synthesis of **7** and **8**, and reaction of **8** with adamantylphosphaalkyne.

Single-crystal X-ray diffraction (XRD) studies revealed the presence of a bridging 1,3-diphosphacyclobutadiene ligand that is π -coordinated to the Rh(cod)⁺ and Co(P₂C₂*t*Bu₂)⁻ units (Figure 6a). The main structural features of **7** and **8** are identical. The bridging P₂C₂ ring (average P–C 1.861(4) Å for **7** and 1.860(4) for **8** see also Figure 6) shows elongated P–C bonds compared to the terminal ligand (av. P–C 1.798(4) Å for **7** and 1.81(1) Å for **8**). The P–Co bond lengths of the bridging P₂C₂ ligand (for **7**: 2.3335(8) and 2.3411(8) Å, for **8**: 2x 2.337(1) Å) are also significantly elongated with respect to the terminal ligand (for **7**: 2.2683(8) and 2.2761(8) Å; for **8**: 2x 2.282(1) Å). The terminal ligand is puckered along the C1–C2 vector by 18.8°. Notably, μ - η^4 : η^4 -coordination of diphosphacyclobutadiene ligands has very rarely been observed.^{19–21} Thus, only three other complexes with an “inverted sandwich” structure similar to that observed for **7** and **8** have been described (Figure 6b), i.e. [Ni(Im^{*i*}Pr)₂]₂(μ : η^4 : η^4 -P₂C₂*t*Bu₂) (Im^{*i*}Pr = 1,3-di(*iso*-propyl)imidazolin-2-ylidene),¹⁹ [U(Ts^{Tol})₂(μ : η^4 : η^4 -P₂C₂*t*Bu₂)] (Ts^{Tol} = tris(*N*-tolylamidodimethylsilyl)methane),²⁰ and [Cp^{'''}Co]₂(μ : η^4 : η^4 -P₂C₂Me₂) (Cp^{'''} = 1,2,4-(*t*Bu)₃-C₅H₂).²¹

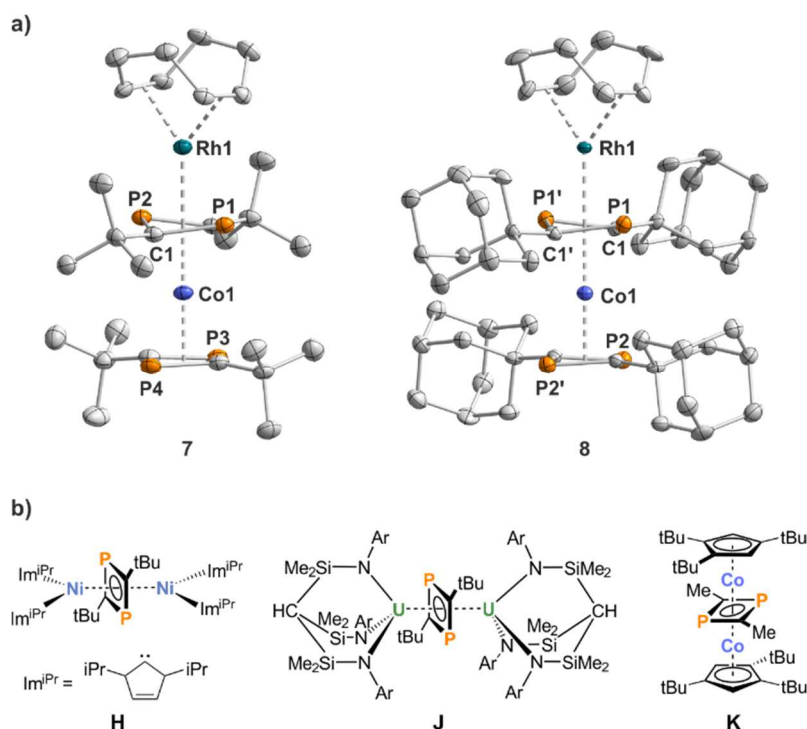


Figure 6. a) Solid-state molecular structures of **7** and **8**. The hydrogen atoms and the toluene solvate molecule of **8** are omitted for clarity. Thermal ellipsoids are drawn at the 50% probability level. Selected bond lengths [Å] and angles [°] for **7**: Rh1–P1 2.3889(7), Rh1–P2 2.4031(7), Co1–P1 2.3335(8), Co1–P2 2.3411(8), Co1–P3 2.2761(8), Co1–P4 2.2683(8), P1–C1 1.857(3), P1–C2 1.863(3), P2–C1 1.863(3), P2–C2 1.861(3), C1–P1–C2 / C2–P2–C1 18.8; for **8**: Rh1–P1 2.409(1), Rh1–P2 2.409(1), Co1–P1 2.337(1), Co1–P1' 2.337(1), Co1–P2 2.282(1), Co1–P2' 2.282(1), P1–C1 1.861(4), P1–C1' 1.858(4), P1'–C1 1.858(4), P1'–C1' 1.861(4), C1–P1–C1' / C1'–P1'–C1 18.5; b) Known complexes featuring the 1,3-diphosphacyclobutadiene ligand in bridging position.

In agreement with the solid-state structure, the ^1H NMR spectrum of **7** in C_6D_6 displays two *tert*-butyl signals and three signals for 1,5-cod molecule due to the presence of diastereotopic CH_2 groups. The $^{13}\text{C}\{^1\text{H}\}$ NMR spectrum features two sets of signals for the *tert*-butyl groups and a set of two signals for the 1,5-cod ligand. Moreover, a doublet of triplets at $\delta = 150.2$ ppm [$^1J_{\text{C,P}} = 75.7$ Hz, $^1J_{\text{C,Rh}} = 5.4$ Hz] can be assigned to the quaternary carbon atoms of the bridging P_2C_2 moiety. Notably, this resonance is shifted downfield by 47.1 ppm with respect to the starting material **A**. A triplet at $\delta = 118.0$ ppm [$^1J_{\text{C,P}} = 55.0$ Hz] can be assigned to the quaternary carbon atoms of the terminal P_2C_2 ligand. As expected, the $^{31}\text{P}\{^1\text{H}\}$ NMR spectrum of **7** shows a singlet and a doublet at $\delta = 29.4$ and 72.2 ppm in a 1:1 ratio. We assign the singlet at $\delta = 29.4$ ppm to the terminal ligand, whereas the doublet at $\delta = 72.2$ ppm with a coupling constant $^1J(^{31}\text{P},^{103}\text{Rh}) = 17$ Hz can be assigned to the bridging ligand. The same $^{31}\text{P}\{^1\text{H}\}$ NMR signal pattern (singlet at $\delta = 23.2$ ppm and doublet at $\delta = 72.3$ ppm with $^1J(^{31}\text{P},^{103}\text{Rh}) = 17$ Hz) was observed for **8**. The ^1H and ^{13}C NMR data of **8** are also similar to **7**, but a detailed assignment of the ^1H NMR signals was not possible due to overlap of the adamantyl signals.

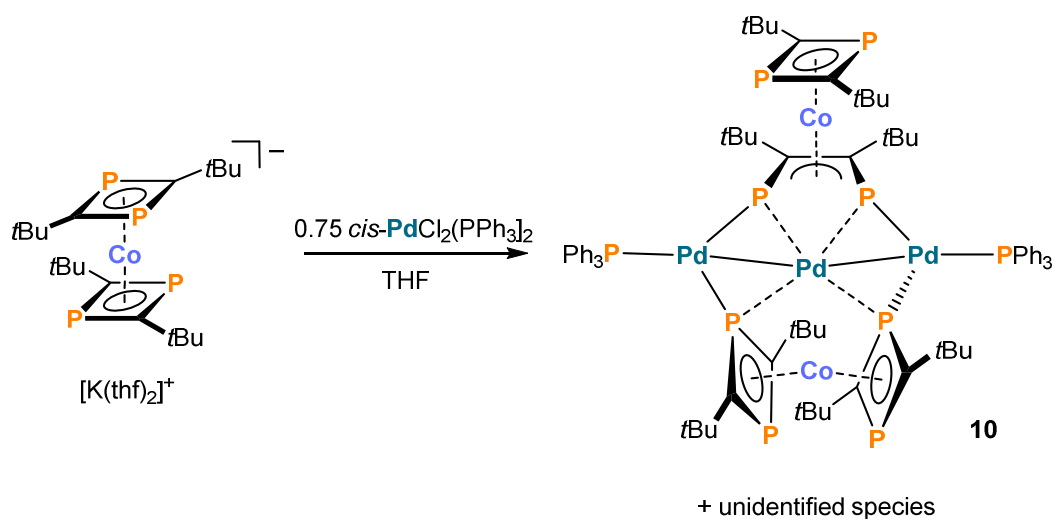
The cyclic voltammogram of **7** (THF/[*n*Bu₄N]PF₆, Figure S15) features an irreversible reduction process at $E_{pc} = -2.02$ V vs. Fc/Fc⁺ followed by a reversible oxidation wave at $E_{1/2} = -0.73$ V vs. Fc/Fc⁺. The latter process is assigned to the oxidation of the [Co(P₂C₂*t*Bu₂)₂]⁻ sandwich anion,^{7d} indicating that a fragmentation of **7** occurs.

Aiming at the synthesis of a genuine tripledecker complex by replacing the labile 1,5-cyclooctadiene ligand with another 1,3-diphosphacyclobutadiene unit, we investigated reactions of RC≡P (two equivalents, R = *t*Bu, Ad) with [Rh(cod){Co(P₂C₂R₂)₂}] (**7**: R = *t*Bu, **8**: R = Ad, Scheme 4). ³¹P{¹H} NMR studies revealed that the phosphalkyne was consumed, but the reactions were unselective in most cases. By contrast, the reaction of [Rh(cod){Co(P₂C₂Ad₂)₂}] (**8**) with AdC≡P (two equivalents) gave one major species **9**, which may well be the desired product [Rh(P₂C₂Ad₂){Co(P₂C₂Ad₂)₂}] according to multinuclear NMR data. The ¹H NMR spectrum of **9** (recorded in [D₈]THF at 270 K, see the SI, Figure S5) shows signals of three different adamantyl substituents in the region from 1.40 to 2.60 ppm.²² The ³¹P{¹H} NMR spectrum of **9** (SI, Figure S7) shows three resonances in a 1:1:1 ratio, i.e. a singlet at $\delta = 37.6$ and two doublets at $\delta = 91.9$ [$^1J(^{31}\text{P},^{103}\text{Rh}) = 33.5$ Hz] and 95.2 ppm [$^1J(^{31}\text{P},^{103}\text{Rh}) = 14.7$ Hz]. It is noteworthy that similar ³¹P–¹⁰³Rh couplings were observed for the terminal 1,3-diphosphacyclobutadiene complexes [(η^5 -Cp)Rh(η^4 -P₂C₂*t*Bu₂)] [$^1J(^{31}\text{P},^{103}\text{Rh}) = 31.7$ Hz], [(η^5 -C₅Me₅)Rh(η^4 -P₂C₂*t*Bu₂)] [$^1J(^{31}\text{P},^{103}\text{Rh}) = 29.3$ Hz], and [(η^5 -C₉H₇)Rh(η^4 -P₂C₂*t*Bu₂)] [$^1J(^{31}\text{P},^{103}\text{Rh}) = 31.3$ Hz, C₉H₇ = indenyl].^{4b,5b} Comparing with the ³¹P{¹H} NMR spectrum of **8**, it is tempting to assign the resonance at $\delta = 91.9$ ppm to a terminal 1,3-diphosphacyclobutadiene ligand and the resonance at $\delta = 95.2$ ppm to a bridging 1,3-diphosphacyclobutadiene unit (as observed for **8**). Accordingly, the singlet at $\delta = 37.6$ ppm might be assigned to the terminal ligand coordinated to cobalt (cf. similar values reported for [(η^5 -Cp)M(η^4 -P₂C₂*t*Bu₂)] (M = Co: $\delta = 37.1$ ppm; M = Rh: $\delta = 47.0$ ppm) and [(η^5 -C₅Me₅)M(η^4 -P₂C₂*t*Bu₂)] (M = Co: $\delta = 25.1$ ppm; M = Rh: $\delta = 36.7$ ppm).^{4b} Moreover, theoretical calculations confirmed the assignment of the signals giving ³¹P{¹H} NMR shifts of 32.7, 96.2, and 107.6 ppm (see SI for further details). While compound **9** appears to be relatively stable as a solid (at least over the course of days), it unfortunately decomposes to an intractable mixture in polar and apolar solvents when stored at ambient temperature for >1 hour. For this reason, attempts to grow crystals suitable for single-crystal XRD have been unsuccessful, and the proposed tripledecker structure thus awaits confirmation.

4.2.5 Reaction of [K(thf)₂{Co(P₂C₂*t*Bu₂)₂}] with *cis*-PdCl₂(PPh₃)₂

In order to examine the coordination properties of our [Co(P₂C₂*t*Bu₂)₂]⁻ anion further, we decided to explore the reaction of [K(thf)₂{Co(P₂C₂*t*Bu₂)₂}] with *cis*-PdCl₂(PPh₃)₂. This reaction affords crystals of the structurally unique compound [Pd₃(PPh₃)₂{Co(P₂C₂*t*Bu₂)₂}] (**10**). This pentanuclear species is formed in a fairly selective fashion (³¹P{¹H} NMR monitoring) when the

ratio of cobaltate anion per palladium complex is 2:1.5 (Scheme 5). Hydride complex $[\text{Co}(\text{P}_2\text{C}_2\text{tBu}_2)_2\text{H}]^{7a}$ and an unknown compound with $^{31}\text{P}\{^1\text{H}\}$ NMR signals at $\delta = 0.5, 3.2, 4.9, 105.7,$ and 107.5 ppm were identified as the main by-products. Dark orange **10** is stable in *n*-hexane but decomposes to an intractable mixture in diethyl ether. Crystalline **10** can be isolated as a pure compound in 23% yield after chromatographic work-up.

Scheme 5. Synthesis of **10**.

The molecular structure of **10** (Figure 7) shows a Pd_3 chain coordinated by two $\text{Co}(\text{P}_2\text{C}_2\text{tBu}_2)_2$ moieties and two PPh_3 ligands. The terminal palladium atoms (Pd1 and Pd3) show a trigonal planar environment by three phosphorus atoms with Pd-P distances ranging from 2.2408(9) to 2.3031(9) Å. The Pd-P bonds of the P_2C_2 units (Pd1-P1 2.2752(9) Å; Pd1-P6 2.2408(9) Å; Pd3-P2 2.2569(9) Å; Pd3-P5 2.244(1) Å) are much shorter than the bonds to the triphenylphosphane molecules (Pd1-P9 2.2986(9) Å; Pd3-P10 2.3031(9) Å). The Pd_3 chain is bent (Pd3-Pd2-Pd1 159.15(1)°). The central palladium atom Pd2 is coordinated by four P atoms with Pd-P distances ranging from 2.4550(9) to 2.6427(9) Å. These values are significantly longer than the Pd-P bonds of the terminal Pd atoms Pd1 and Pd3 .

Similarly arranged palladium atoms were previously observed in $[\text{Pd}_3(\text{InCp}^*)_4(\mu\text{-InCp}^*)_4]$, $[\text{Pd}_3(\mu\text{-SO}_2)_2(\mu\text{-PPh}_2\text{py})_2(\text{PBz}_3)_2]$ ($\text{R} = t\text{Bu}, 2,6\text{-dimethylphenyl}$ and cyclohexyl , $\text{Bz} = \text{benzyl}$), $[\{\text{Pd}_3(\mu\text{-GePh}_2)_2(\mu\text{-H})(\mu_3\text{-GePh}_2(\text{SC}_6\text{H}_4\text{tBu-4}))\}_2(\mu\text{-dmpe})]$, and $[\text{Pd}\{\text{PdL}(\mu\text{-OAc})_2\}_2]$ ($\text{L} = \text{metalated di(pentan-3-yl) amine}$).²³ The Pd-Pd distances (2.6786(4) and 2.6633(4) Å) are >0.1 Å shorter than in $[\text{Pd}_3(\text{InCp}^*)_4(\mu\text{-InCp}^*)_4]$ and $[\{\text{Pd}_3(\mu\text{-GePh}_2)_2(\mu\text{-H})(\mu_3\text{-GePh}_2(\text{SC}_6\text{H}_4\text{tBu-4}))\}_2(\mu\text{-dmpe})]$. The most remarkable feature of the molecular structure of **10** is the presence of a 1,4-diphospha-2-butene ligand, which is unusual in phosphoorganometallic chemistry. Its formation may be explained by an isomerization of a 1,3-diphospha-cyclobutadiene unit to the 1,2-isomer (as observed for the rearrangement of **3** to **4**), followed by an oxidative addition of the

resulting P–P bond on palladium. The P1–P2 distance of 2.401(1) Å, i.e. approximately 0.2 Å longer than in known 1,2-diphosphacyclobutadiene complexes,⁶ indicates that the P–P bond is partially broken. A similar structural motif was reported by the group of Binger (**G**, see Figure 3).^{5b} The structure of **10** thus may be viewed as a product of an arrested P–P bond addition onto palladium.

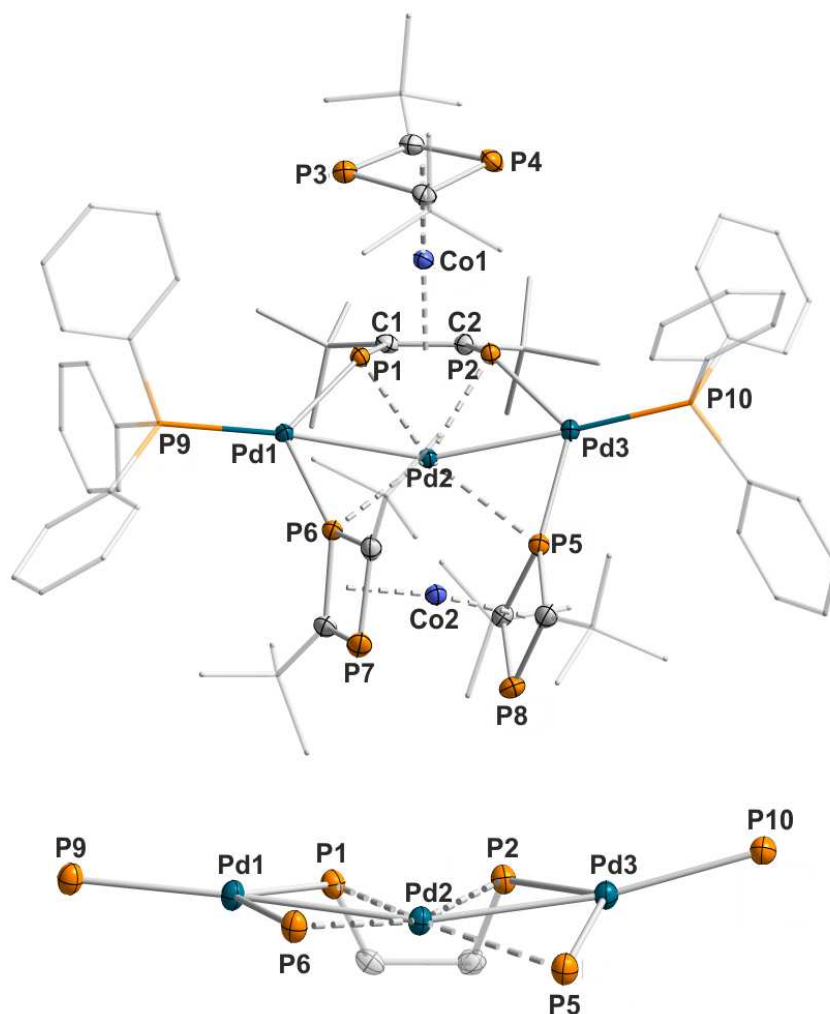


Figure 7. Solid-state molecular structure of **10** (top) and a section of the structure showing the palladium atoms and their donor environment (bottom). The hydrogen atoms are omitted for clarity. Thermal ellipsoids are drawn at the 50% probability level. Selected bond lengths [Å] and angles [°] for **10**: Pd1–Pd2 2.6786(4), Pd2–Pd3 2.6633(4), Pd1–P1 2.2752(9), Pd1–P6 2.2408(9), Pd1–P9 2.2986(9), Pd2–P1 2.4577(9), Pd2–P2 2.4550(9), Pd2–P5 2.6427(9), Pd2–P6 2.4805(9), Pd3–P2 2.2569(9), Pd3–P5 2.244(1), Pd3–P10 2.3031(9), Pd3–Pd2–Pd1 159.15(1), P6–Pd1–P1 118.59(3), P2–Pd3–P5 121.73(3).

A WBI analysis on the DFT-optimized structure of **10** gave relatively low WBIs (0.11 and 0.10) for the palladium-palladium bonds, while a WBI of 0.50 was calculated for the partially broken P1–P2 bond of the 1,4-diphospha-2-butene ligand, indicating that there is still a substantial covalent interaction between these P atoms.

Multinuclear NMR spectra indicate that the structure of **10** is retained in C₆D₆ solution. The ¹H and ¹³C{¹H} NMR spectra each show four signals for the *t*Bu environments and one set of phenyl resonances. The ³¹P{¹H} NMR spectrum recorded in C₆D₆ shows two singlets at $\delta = -43.0$ and 38.7 ppm that can be assigned to the non-coordinated P atoms of the 1,3-diphosphacyclobutadiene ligands. The triphenylphosphane ligands give rise to two overlapping triplets at $\delta = 30.3$ and 30.5 ppm. The presence of two signals suggests that the structure of **10** is rather rigid in solution. By contrast, the downfield shifted broad doublets at $\delta = 201.7$ and 214.8 ppm can be assigned to the coordinating P atoms of the intact Co(P₂C₂*t*Bu₂)₂ fragment and the P atoms of the 1,4-diphospha-2-butene ligand, respectively. These signals show a remarkably large P–P coupling of ${}^2J({}^{31}\text{P}, {}^{31}\text{P}) = 218$ Hz, which presumably arises from intramolecular through bond or through space coupling mediated by the coordination of this ligand to palladium. The latter may explain the broadening of the signals (nuclear spin (¹⁰⁵Pd) = 5/2) which leads to unresolved coupling constants of the coupling between the triphenylphosphane ligands and the coordinated P atoms, and between the P atoms of the 1,4-diphospha-2-butene ligand.²⁴ A similar ligand, 1-rhoda-2,5-diphosphacyclopentenediyl in complex **G** (Figure 3, *vide supra*), has been described by the group of Binger and co-workers.^{5b}

A cyclic voltammogram of **10** (Figure 8) recorded in THF/[*n*Bu₄N]PF₆ shows a reversible oxidation wave at $E_{1/2} = 0.06$ V vs. Fc/Fc⁺ and a reversible reduction wave at $E_{1/2} = -1.73$ V vs. Fc/Fc⁺, respectively. Most likely, these redox processes are centered at the Co(P₂C₂*t*Bu₂)₂ moiety (oxidation) and the Pd₃ chain (reduction), respectively, as DFT calculations (BP86/def2-TZVP level) on the truncated model compound **10'** (where the *t*Bu groups were replaced by Me groups) show that the HOMO is mainly located at the cobaltate fragment, while the LUMO is situated at the palladium atoms with minor contributions from the cobalt and the phosphorus atoms coordinated to palladium.

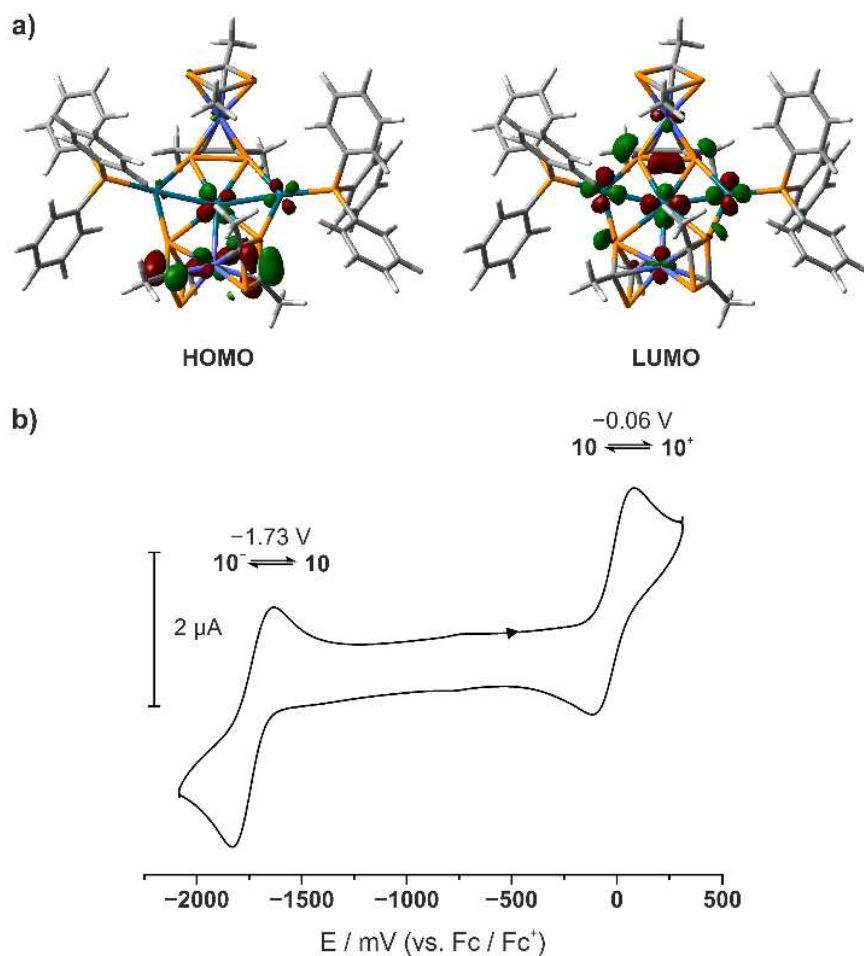


Figure 8. a) DFT-calculated (BP86/def2-TZVP) Kohn-Sham frontier orbitals for the truncated model compound **10'** (where the *t*Bu groups were replaced by Me groups); b) Cyclic voltammogram of **10** recorded in THF/[nBu₄N]PF₆ with a platinum disc working electrode, a platinum wire as counter electrode, and silver/silver nitrate as reference electrode. $\nu = 100$ mV/s; potentials are referenced to the Fc/Fc⁺ couple.

4.2.6 Reaction of [K(thf)₂{Co(P₂C₂tBu₂)₂}] with HgCl₂

We were also interested in exploring the coordination behavior of our homoleptic [Co(P₂C₂tBu₂)₂]⁻ sandwich anion toward Hg(II). The initially targeted tetradecker compound [Hg(μ-P₂C₂tBu₂)₂{Co(P₂C₂tBu₂)₂}₂] was not detected during the reaction which was performed in THF solutions (2:1 stoichiometry). The reaction proceeds rather unselective giving the neutral [Co(P₂C₂tBu₂)₂] sandwich compound as main product (Scheme 6) according to ³¹P{¹H} NMR studies (ca. 50%). A second species with a broad signal in the ³¹P{¹H} NMR spectrum at $\delta = 22.5$ ppm was also identified together with traces of the known tetra-*tert*-butyltetraphosphacubane²⁷ and some unidentified species (Figure 9). Extractions with *n*-hexane and toluene followed by concentration of the bright red solutions and storage at -35 °C afforded X-ray quality crystals.

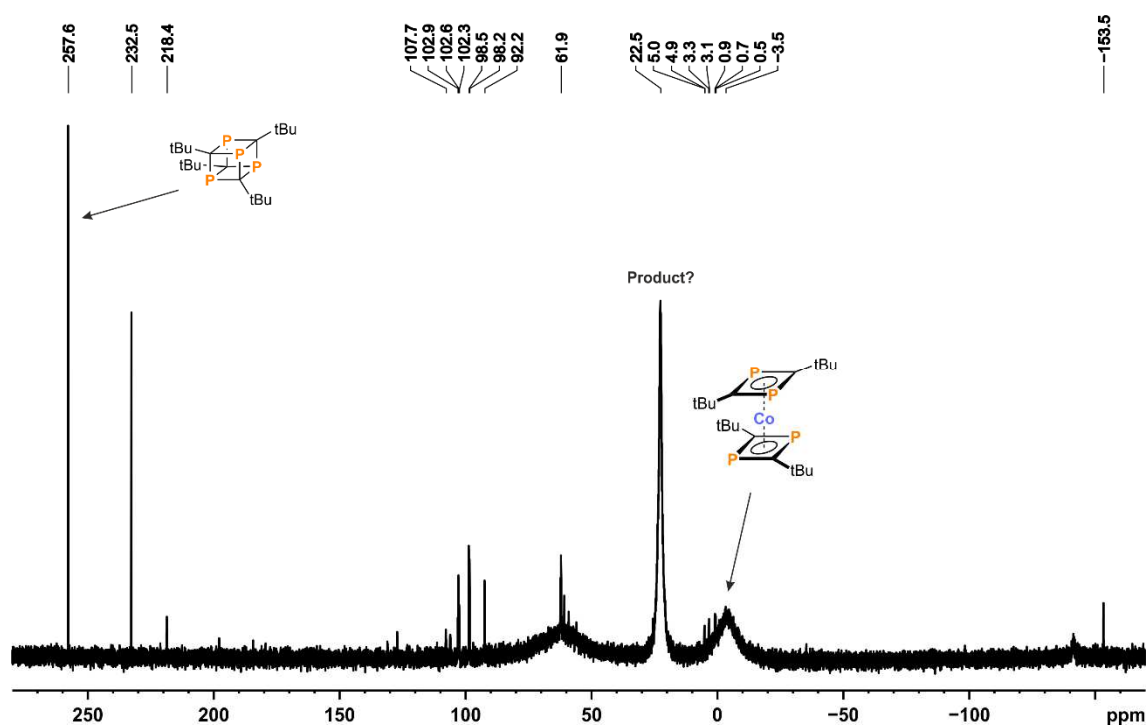
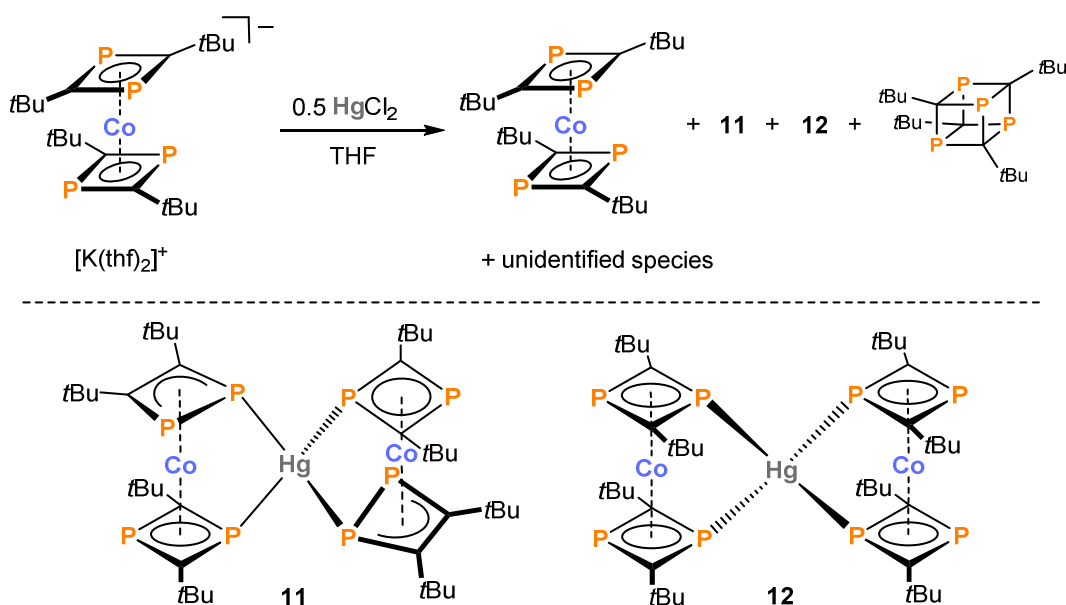


Figure 9. $^{31}\text{P}\{^1\text{H}\}$ NMR spectrum ($[\text{D}_8]\text{THF}$) of the reaction of $[\text{K}(\text{thf})_2\{\text{Co}(\text{P}_2\text{C}_2\text{tBu}_2)_2\}]$ with HgCl_2 .



Scheme 6. Reaction of $[\text{K}(\text{thf})_2\{\text{Co}(\text{P}_2\text{C}_2\text{tBu}_2)_2\}]$ with HgCl_2 (0.5 equivalents).

Single-crystal X-ray diffraction (XRD) experiments revealed the molecular structures of **11** and **12** in the solid state which are constitutional isomers of $[\text{Hg}\{\text{Co}(\text{P}_2\text{C}_2\text{tBu}_2)_2\}_2]$. The molecular structure of **11** (Figure 10, top) shows a trinuclear dicobalt mercury compound in which the mercury atom is coordinated by four phosphorus atoms of the ligand framework of the two $\text{Co}(\text{P}_2\text{C}_2\text{tBu}_2)_2$ moieties. One of the P_2C_2 ligand of each sandwich molecule shows an isomerization to 1,2-diphosphacyclobutadiene which we also observed for the palladium

compound **10**. By contrast, the P–P bond lengths (P1–P2 2.165(2) Å, P5–P6 2.165(2) Å) are in the range of 1,2-diphosphacyclobutadiene complexes.⁶

The Hg–P distances are in the range of 2.591(1) – 2.625(1) Å, which are significantly longer than the sum of covalent radii (2.44 Å)¹⁵ indicating a weak covalent interaction. Moreover, a weak electrostatic interaction is assumed for cobalt and mercury demonstrated by their distances of 2.9013(6) Å (Hg1–Co1) and 2.8916(6) Å (Hg1–Co2), respectively (sum of covalent radii 2.44 Å).¹⁵ The sandwich molecules are slightly tilted by their centroid(P₂C₂)–Co–centroid(P₂C₂) angle (168°) which is close to 180° in the starting material. This may be explained by the coordination to mercury. Furthermore, the 1,3-diphosphacyclobutadiene ligands are tilted by 13.7° (between C4–P3–C3 / C3–P4–C4 planes).

The molecular structure of **12** (Figure 10, bottom) shows a constitutional isomer of the trinuclear dicobalt mercury compound. The mercury atom is surrounded by two Co(P₂C₂tBu₂)₂ moieties. As a consequence, the Co(P₂C₂tBu₂)₂ sandwich molecules adopt dihedral angles (between P1–P2–Co1 and Co1–P3–P4 planes, and between P5–P6–Co2 and Co2–P7–P8 planes) of 31.3° and 41.7°, respectively, which is in between the staggered and the eclipsed conformation. As a result of coordination, the sandwich molecules are tilted by their centroid(P₂C₂)–Co–centroid(P₂C₂) angle of 162.4° and 161.7°, respectively. The Hg–P distances are longer by 0.2 Å (2.7156(8) – 2.8432(8) Å) compared to **11**. In contrast, the Hg–Co distances are shortened by 0.2 Å (2.7339(5) Å for Hg1–Co1 and 2.7340(5) Å for Hg1–Co2) compared to **11**.

Compounds **11** and **12** have been isolated as bright red solids in low yields of 13% and 17%, respectively. However, NMR characterizations proved to be challenging. Both compounds seem to decompose in solution, which is suggested by their very similar ³¹P{¹H} NMR spectra showing each the characteristic, broad signal at $\delta = -4.6$ ppm assigned to [Co(P₂C₂tBu₂)₂], as main component. Moreover, broad signals at $\delta = 22.5$ ppm and $\delta = 62.9$ ppm were observed, which presumably may be assigned to compounds **11** and **12**. The assignment is only speculative as recrystallization or sublimation rather led to even more complex spectra which was indicative for decomposition. This was confirmed by the obvious formation of Hg(0) which precipitated as a metallic mirror on the surface of the reaction vessel after storing solutions of the reaction mixture for one day. Due to the obvious decomposition in solution **11** and **12** could not be isolated as pure compounds. Hence, further characterization of these complexes remains unsuccessful.

In order to gain further insight into the bonding situation of these complexes we performed a WBI analysis on the DFT-optimized structures of **11** and **12**. WBIs of 0.19–0.25 were calculated for the Hg–P bonds which are similar to the WBIs of the Co–P bonds (0.29–0.35) confirming weak covalent interactions as suggested by the solid-state molecular structures. A WBI of 0.04 (for **11**) and a WBI of 0.07 (for **12**) for the Hg–Co bonds suggest that covalent bonding between these

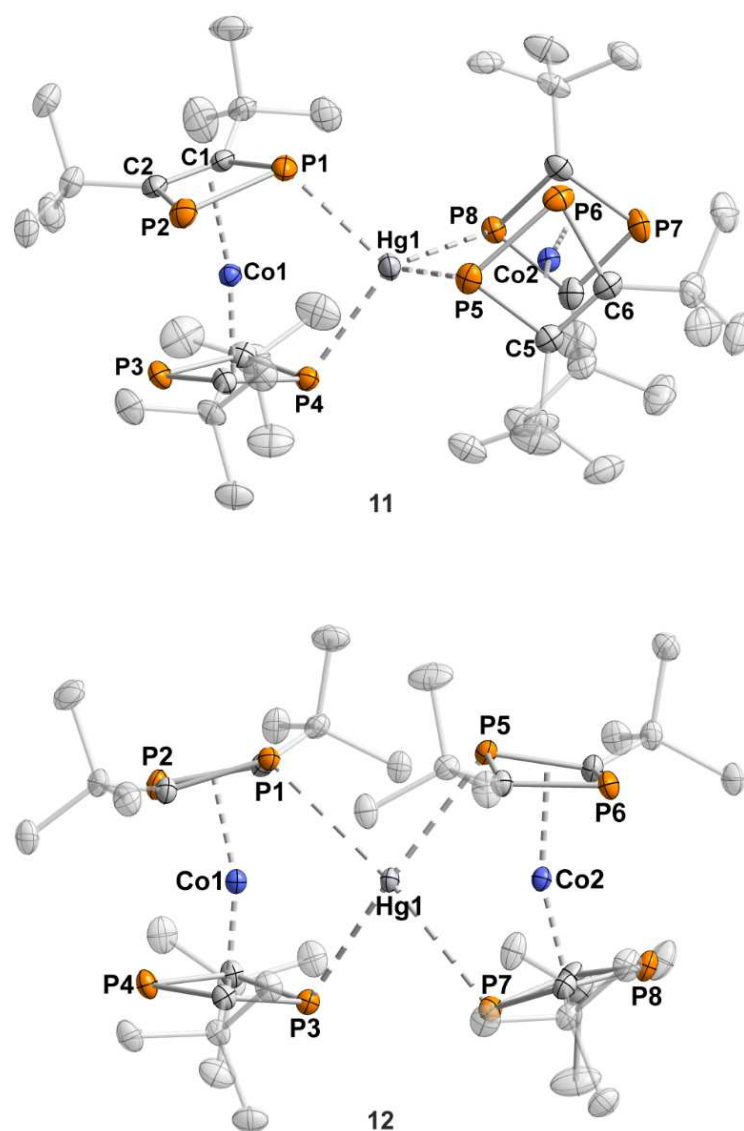


Figure 10. Solid-state molecular structures of $[\text{Hg}\{\text{Co}(1,2\text{-P}_2\text{C}_2\text{tBu}_2)(1,3\text{-P}_2\text{C}_2\text{tBu}_2)\}_2]$ (**11**, top) and $[\text{Hg}\{\text{Co}(1,3\text{-P}_2\text{C}_2\text{tBu}_2)\}_2]$ (**12**, bottom). The hydrogen atoms are omitted for clarity. Thermal ellipsoids are drawn at the 50% probability level. Selected bond lengths [Å] and angles [°] for **11**: Hg1–P1 2.625(1), Hg1–P4 2.591(1), Hg1–P5 2.625(1), Hg1–P8 2.601(1), Hg1–Co1 2.9013(6), Hg1–Co2 2.8916(6), Co1–P1 2.347(1), Co1–P2 2.255(1), Co1–P3 2.265(1), Co1–P4 2.328(1), P1–P2 2.165(2), C1–C2 1.437(6), P1–Hg1–P4 99.29(3), C4–P3–C3/C3–P4–C4 13.7; for **12**: Hg1–P1 2.8432(8), Hg1–P3 2.7156(8), Hg1–P5 2.7267(8), Hg1–P7 2.8367(8), Hg1–Co1 2.7339(5), Hg1–Co2 2.7340(5), Co1–P1 2.324(1), Co1–P2 2.269(1), Co1–P3 2.338(1), Co1–P4 2.273(1), P1–Hg1–P3 99.99(2), C4–P3–C3/C3–P4–C4 12.2; P1–P2–Co1/Co1–P3–P4 31.3.

metal atoms is negligible. Complexes **11** and **12** can be seen as ionic compounds consisting of Hg^{2+} which is coordinated by two $[\text{Co}(\text{P}_2\text{C}_2\text{tBu}_2)_2]^-$ moieties which appear as heteroleptic $[\text{Co}(1,2\text{-P}_2\text{C}_2\text{tBu}_2)(1,3\text{-P}_2\text{C}_2\text{tBu}_2)]^-$ anions in **11** and as homoleptic $[\text{Co}(1,3\text{-P}_2\text{C}_2\text{tBu}_2)_2]^-$ anions in **12**.

4.3 Conclusion

While earlier work had demonstrated the formation of molecular complexes, coordination polymers and metallocsupramolecular structures based on σ -coordination of the $[\text{Co}(\text{P}_2\text{C}_2\text{tBu}_2)_2]^-$ sandwich to coinage metal cations, this study has revealed several novel and intriguing aspects of this remarkable anion. Transmetalation reactions of $[\text{K}(\text{thf})_2\{\text{Co}(\text{P}_2\text{C}_2\text{tBu}_2)_2\}]$ with $[\text{Ni}_2\text{Cp}_3]\text{BF}_4$, $[\text{Cp}^*\text{RuCl}]_4$, $[\text{RhCl}(\text{cod})]_2$, *cis*- $\text{PdCl}_2(\text{PPh}_3)_2$, and HgCl_2 afforded new oligonuclear complexes **2-12**. The molecular structures of these compounds illustrate a highly versatile coordination behavior of the $[\text{Co}(\text{P}_2\text{C}_2\text{tBu}_2)_2]^-$ complex. Moreover, the results show that this robust sandwich molecule is chemically “non-innocent” as it is prone to rearrangements, insertions and fragmentations. An insertion of a transition metal fragment into an intact 1,3-diphosphacyclobutadiene ligand was observed for nickel complex **3** for the first time. This reaction occurs at remarkably low temperatures and is followed by an isomerization of **3** to the thermodynamically more stable complex **4**. An analogous process occurred during the formation of palladium complex **10**. Furthermore, with Ru(II) and Hg(II) we have observed for the first time that the $[\text{Co}(\text{P}_2\text{C}_2\text{tBu}_2)_2]^-$ anion is capable of acting as a chelate ligand simply by adopting an eclipsed conformation (complex **5**) or a conformation in between the staggered and the eclipsed one (complex **12**). Similar to **10**, complex **11** shows an isomerization of the 1,3-diphosphacyclobutadiene ligand to its 1,2-derivative. By contrast, the P–P bond in **10** is partially broken, while in **11** it behaves as a 1,2-diphosphacyclobutadiene ligand. Additionally, complexes **7** and **8** are the first examples showing that the π -coordination mode is also accessible for the $[\text{Co}(\text{P}_2\text{C}_2\text{R}_2)_2]^-$ anion. Compound **9** indicates that the synthesis of unique tripeldecker compounds based on 1,3-diphosphacyclobutadiene ligands might be feasible, and the synthesis of related complexes is currently underway in our laboratory.

In summary, the results of this study have revealed a remarkable, flexidentate coordination behaviour for the $[\text{Co}(\text{P}_2\text{C}_2\text{tBu}_2)_2]^-$ anion, which enables the synthesis of a rich class of oligonuclear coordination compounds. Further studies will focus on further investigations of this rich reactivity as well as applications of the resulting complexes, e.g. in homogeneous catalysis.

4.4 Supporting Information

4.4.1 General Procedures

All experiments were performed under an atmosphere of dry argon using standard Schlenk techniques or a MBraun UniLab glovebox. Solvents were dried and degassed with a MBraun SPS800 solvent purification system. Tetrahydrofuran, toluene, and diethyl ether were stored over molecular sieves (3 Å). *n*-Hexane was stored over a potassium mirror. NMR spectra were recorded on Bruker Avance 300 and Avance 400 spectrometers at 300 K and internally referenced to residual solvent resonances. Melting points were measured on samples in sealed capillaries on a Stuart SMP10 melting point apparatus. UV/Vis spectra were recorded on an Ocean Optics Flame Spectrometer. Elemental analyses were determined by the analytical department of Regensburg University. $[\text{Ni}_2\text{Cp}_3]\text{BF}_4$, $[\text{Cp}^*\text{RuCl}]_4$, and $t\text{BuC}\equiv\text{P}$ were prepared according to literature procedures.¹¹ *cis*- $\text{PdCl}_2(\text{PPh}_3)_2$ and HgCl_2 were purchased from abcr GmbH and Merck, respectively, and used as received.

4.4.2 Optimized Synthesis of $[\text{K}(\text{thf})_{1.75}\{\text{Co}(\text{P}_2\text{C}_2t\text{Bu}_2)_2\}]$ (A)

We report an improved procedure for the synthesis of $[\text{K}(\text{thf})_{1.75}\{\text{Co}(\text{P}_2\text{C}_2t\text{Bu}_2)_2\}]^{\text{9c,d,10}}$ using $[\text{K}(\text{thf})_{0.2}][\text{Co}(1,5\text{-cod})_2]$ (cod = cyclooctadiene) instead of $[\text{K}(\text{dme})_2][\text{Co}(\text{C}_{14}\text{H}_{10})_2]$ used previously. This procedure obviates the use of anthracene, which can be difficult to remove from the product. $[\text{K}(\text{thf})_{0.2}][\text{Co}(1,5\text{-cod})_2]$ (4.39 g, 13.4 mmol, 1.0 eq) in THF (120 mL) was cooled to -80°C . A solution of $t\text{BuC}\equiv\text{P}$ (2.56 M in $(\text{Me}_3\text{Si})_2\text{O}$, 21.5 mL, 55 mmol, 4.1 eq) was added slowly via syringe while stirring. The reaction mixture was allowed to warm to room temperature. Subsequently, the volatiles were removed *in vacuo*. The orange powder was washed with *n*-hexane (10 mL) and dried *in vacuo*. The dried solid contains a variable number of THF molecules. The number of THF molecules present per formula unit was determined by ^1H NMR spectroscopy individually on each sample. Yield 7.84 g (94%, $x = 1.75$).

4.4.3 Synthesis of $[\text{CpNi}\{\text{Co}(\text{P}_2\text{C}_2t\text{Bu}_2)_2\}(\text{thf})]$ (2)

A solution of $[\text{K}(\text{thf})_{1.75}\{\text{Co}(\text{P}_2\text{C}_2t\text{Bu}_2)_2\}]$ (46 mg, 0.08 mmol, 1.0 eq) in THF (2 mL) was cooled to -80°C and added to a cooled solution (-80°C) of $[\text{Ni}_2\text{Cp}_3]\text{BF}_4$ (30 mg, 0.08 mmol, 1.0 eq) in THF (2 mL) via cannula. Upon stirring the reaction mixture at -60°C for 30 min the color changed to dark violet. The solvent was removed *in vacuo*. Subsequently, the residue was extracted with cold Et_2O (-60°C , 10 mL). The dark violet solution was concentrated to ca. 5 mL and stored at -60°C . Dark violet crystals formed upon storing the solution for three days. The isolated sample was contaminated with ca. 50% of **3** according to the $^{31}\text{P}\{^1\text{H}\}$ NMR spectrum. ^1H NMR (400.13 MHz, $[\text{D}_8]\text{THF}$, 233 K) δ /ppm = 1.02 (s, 9H, $\text{C}(\text{CH}_3)_3$), 1.07 (s, 18H, $\text{C}(\text{CH}_3)_3$), 1.28 (s, 9H, $\text{C}(\text{CH}_3)_3$), 5.59 (s, 5H, C_5H_5); $^{13}\text{C}\{^1\text{H}\}$ NMR (100.61 MHz, $[\text{D}_8]\text{THF}$, 233 K) δ /ppm = 32.6 (s, $\text{C}(\text{CH}_3)_3$), 33.1 (s, $\text{C}(\text{CH}_3)_3$), 33.3 (s, $\text{C}(\text{CH}_3)_3$), 36.0 (br, $\text{C}(\text{CH}_3)_3$), 36.6 (br, $\text{C}(\text{CH}_3)_3$),

37.4 (br, C(CH₃)₃); The resonances for the quaternary carbon atoms of the C₂P₂ ligand were not detected; ³¹P{¹H} NMR (161.98 MHz, [D₈]THF, 233 K) δ /ppm = -4.1 (d, ²J_{P,P} = 20.5 Hz, 1P; P2), 15.6 (s, 2P; P3 and P4), 31.5 (d, ²J_{P,P} = 20.5 Hz, 1P; P1).

4.4.4 Synthesis of [Co(η⁴-CpNi{1,3-P₂C₂tBu₂-κP,κC})(η⁴-1,3-P₂C₂tBu₂)] (3)

A solution of [K(thf)_{1.75}{Co(P₂C₂tBu₂)₂}] (86 mg, 0.15 mmol, 1.0 eq) in THF (4 mL) was added to a solution of [Ni₂Cp₃]BF₄ (60 mg, 0.15 mmol, 1.0 eq) in THF (2 mL) at room temperature. After stirring the reaction mixture for two hours, the solvent was removed *in vacuo* and the residue was extracted with *n*-hexane (10 mL). The filtrate was concentrated to 3 mL and stored at -35 °C. Dark orange crystals of **3** formed upon storing for two days. Yield 63 mg (72%); m.p. >139 °C (decomp. to a black oil); ¹H NMR (400.13 MHz, [D₈]THF, 253 K) δ /ppm = 0.83 (s, 9H, C(CH₃)₃), 1.08 (s, 9H, C(CH₃)₃), 1.46 (s, 9H, C(CH₃)₃), 1.79 (br, 9H, C(CH₃)₃), 5.31 (s, 5H, C₅H₅); ¹³C{¹H} NMR (100.61 MHz, [D₈]THF, 253 K) δ /ppm = 32.2 (s, C(CH₃)₃), 32.4 (s, C(CH₃)₃), 35.3 (t, ²J_{C,P} = 7.2 Hz, C(CH₃)₃), 35.8 (br, C(CH₃)₃), 37.1 (br, C(CH₃)₃), 40.3 (dd, ²J_{C,P} = 10.6 Hz, ²J_{C,P} = 17.2 Hz, C(CH₃)₃), 50.9 (d, ²J_{C,P} = 16.5 Hz, C(CH₃)₃), 94.2 (s, C₅H₅), 114.1 (s, C₂P₂), 121.0 (t, ¹J_{C,P} = 57.5 Hz, C₂P₂), 172.4 (dd, ¹J_{C,P} = 76.0 Hz, ¹J(C,P) = 98.5 Hz, C₂P₂Ni), 252.0 (d, ¹J_{C,P} = 69.4 Hz, C₂P₂Ni); ³¹P{¹H} NMR (161.98 MHz, [D₈]THF, 253 K) δ /ppm = 36.0 (d, ²J_{P,P} = 40.4 Hz, 1P; P3), 71.4 (s, 1P; P4), 191.4 (d, ²J_{P,P} = 18.4 Hz, 1P; P2), 492.2 (dd, ²J_{P,P} = 18.4 Hz, ²J_{P,P} = 40.4 Hz, 1P; P1); UV/Vis (THF, λ_{max} /nm, (ε_{max} /L·mol⁻¹·cm⁻¹)): 333 (52000), 401sh (14600), 476 (6600), 570 (4500), 652 (3000); elemental analysis calcd. for C₂₅H₄₁P₄CoNi (M = 583.10): C 51.49, H 7.09, found: C 51.75, H 6.70.

4.4.5 Synthesis of [Co(η⁴-CpNi{1,4-P₂C₂tBu₂-κ²P,P})(η⁴-1,3-P₂C₂tBu₂)] (4)

A solution of [K(thf)_{1.75}{Co(P₂C₂tBu₂)₂}] (84 mg, 0.13 mmol, 1.0 eq) in THF (3 mL) was added to a solution of [Ni₂Cp₃]BF₄ (51 mg, 0.13 mmol, 1.0 eq) in THF (2 mL). Subsequently, the reaction mixture was heated to 60 °C for nine hours. The solvent was removed *in vacuo*, and the residue was extracted with *n*-hexane (3 mL). The filtrate was concentrated to 2 mL and stored at -35 °C. Yellow crystals of **4** formed upon storage for one day. Crystals suitable for X-ray diffraction were obtained by slow evaporation of *n*-hexane at room temperature. Yield 34 mg (46%); m.p. >152 °C (decomp. to a black oil); ¹H NMR (400.13 MHz, C₆D₆, 300 K) δ /ppm = 1.20 (s, 18H, C(CH₃)₃), 1.70 (s, 18H, C(CH₃)₃), 5.09 (s, 5H, C₅H₅); ¹³C{¹H} NMR (100.61 MHz, C₆D₆, 300 K) δ /ppm = 32.9 (s, C(CH₃)₃), 35.5 (t, ³J_{C,P} = 6.8 Hz, C(CH₃)₃), 35.9 (t, ²J(C,P) = 7.4 Hz, C(CH₃)₃), 41.2 (t, ²J_{C,P} = 7.4 Hz, C(CH₃)₃), 94.9 (s, C₅H₅), 108.0 (t, ¹J_{C,P} = 54.5 Hz, C₂P₂), 161.9 (d, ¹J_{C,P} = 94.3 Hz, C₂P₂Ni); ³¹P{¹H} (161.98 MHz, C₆D₆, 300 K) δ /ppm = 458.7 (s, 2P; P1 and P2); The resonances for P3 and P4 were not observed at room temperature; ³¹P{¹H} NMR (161.98 MHz, [D₈]THF, 193 K) δ /ppm = -25.9 (s, 1P), 76.6 (s, 1P), 457.0 (s, 2P); UV/Vis (THF, λ_{max} /nm, (ε_{max} /L·mol⁻¹·cm⁻¹)): 299 (18500), 402 (4700), 657 (600); elemental analysis calcd. for C₂₅H₄₁P₄CoNi (M = 583.10): C 51.49, H 7.09, found: C 51.79, H 6.84.

4.4.6 Synthesis of $[(Cp^*Ru)_3(\mu-Cl)_2\{Co(P_2C_2tBu_2)_2\}]$ (5)

A solution of $[K(thf)_{1.75}\{Co(P_2C_2tBu_2)_2\}]$ (0.16 g, 0.25 mmol, 1.0 eq) in THF (4 mL) was added to a solution of $[Cp^*RuCl]_4$ (0.20 g, 0.19 mmol, 0.75 eq) in THF (3 mL). Subsequently, the reaction mixture was refluxed for four hours. The solvent was removed *in vacuo* and the residue was washed with *n*-hexane (3 mL) followed by extraction with toluene (3 mL). The filtrate was concentrated to 2 mL and stored at $-35\text{ }^\circ\text{C}$. Dark orange crystals of **5** formed upon storage for two days. Crystals suitable for X-ray diffraction were obtained by diffusion of *n*-hexane into a concentrated toluene solution. Yield 0.14 g (46%); m.p. $>226\text{ }^\circ\text{C}$ (decomp. to a black oil); ^1H NMR (400.13 MHz, $[D_8]$ THF, 300 K) δ /ppm = 1.25 (s, 36H, $C(CH_3)_3$), 1.63 (s, 30H, $C_5(CH_3)_5$), 1.84 (s, 15H, $C_5(CH_3)_5$); $^{13}\text{C}\{^1\text{H}\}$ NMR (100.61 MHz, $[D_8]$ THF, 300 K) δ /ppm = 11.2 (s, $C_5(CH_3)_5$), 12.0 (s, $C_5(CH_3)_5$), 35.7 (s, $C(CH_3)_3$), 36.6 (s, $C(CH_3)_3$), 77.2 (s, $C_5(CH_3)_5$), 82.5 (s, $C_5(CH_3)_5$), 110.3 (br, C_2P_2); $^{31}\text{P}\{^1\text{H}\}$ NMR (161.98 MHz, $[D_8]$ THF, 300 K) δ /ppm = -13.5 (s, 2P), 44.3 (s, 2P); UV/Vis (THF, λ_{max} /nm, (ϵ_{max} /L·mol $^{-1}$ ·cm $^{-1}$)): 381 (7100), 540 (2100), 745 (1000); elemental analysis calcd. for $C_{50}H_{81}P_4Cl_2CoRu_3$ (M = 1239.14): C 48.47, H 6.59, found: C 48.76, H 6.48.

4.4.7 Synthesis of $[(Cp^*Ru)_2(\mu,\eta^2-P_2)(\mu,\eta^2-C_2tBu_2)]$ (6)

A solution of $[K(thf)_{1.75}\{Co(P_2C_2tBu_2)_2\}]$ (0.12 g, 0.19 mmol, 1.0 eq) in THF (2 mL) was added to a solution of $[Cp^*RuCl]_4$ (0.15 g, 0.14 mmol, 0.75 eq) in THF (2 mL). Subsequently, the reaction mixture was refluxed for 30 hours. The solvent was removed *in vacuo* and the residue was extracted with *n*-hexane (3 mL). The filtrate was concentrated to 2 mL and stored at $-35\text{ }^\circ\text{C}$. Dark orange crystals of **6** formed upon storing for two days. Crystals suitable for X-ray diffraction were obtained by slow evaporation of a *n*-hexane solution. Yield 47 mg (36%); m.p. $>300\text{ }^\circ\text{C}$ (decomp. to a black oil); ^1H NMR (400.13 MHz, C_6D_6 , 300 K) δ /ppm = 1.41 (s, 18H, $C(CH_3)_3$), 1.86 (s, 30H, $C_5(CH_3)_5$); $^{13}\text{C}\{^1\text{H}\}$ NMR (100.61 MHz, $[D_8]$ THF, 300 K) δ /ppm = 12.6 (s, $C_5(CH_3)_5$), 34.3 (s, $C(CH_3)_3$), 35.7 (s, $C(CH_3)_3$), 93.9 (br, C_2tBu_2), 96.0 (s, $C_5(CH_3)_5$); $^{31}\text{P}\{^1\text{H}\}$ NMR (161.98 MHz, C_6D_6 , 300 K) δ /ppm = 128.9 (br, 2P); UV/Vis (THF, λ_{max} /nm, (ϵ_{max} /L·mol $^{-1}$ ·cm $^{-1}$)): 373 (12000), 426 (5700); elemental analysis calcd. for $C_{30}H_{48}P_2Ru_2$ (M = 672.80): C 53.56, H 7.19, found: C 54.13, H 7.38.

4.4.8 Synthesis of $[Rh(cod)\{Co(P_2C_2tBu_2)_2\}]$ (7)

A solution of $[K(thf)_{1.75}\{Co(P_2C_2tBu_2)_2\}]$ (0.77 g, 1.23 mmol, 1.0 eq) in THF (10 mL) was added to a solution of $[RhCl(cod)]_2$ (0.30 g, 0.62 mmol, 0.5 eq) in THF (3 mL). The reaction mixture was stirred overnight whereupon the color changed red to yellow. The solvent was removed *in vacuo* and the residue was extracted with small portions of *n*-hexane (5x3 mL). The filtrate was concentrated to approximately 4 mL and stored at $-35\text{ }^\circ\text{C}$. Dark yellow crystals of **7** formed upon storage for three days. Crystals suitable for X-ray diffraction were obtained by slow evaporation

of *n*-hexane at room temperature. Yield 0.75 g (90%); m.p. >300 °C; ^1H NMR (400.13 MHz, C_6D_6 , 300 K) δ /ppm = 1.18 (s, 18H, $\text{C}(\text{CH}_3)_3$), 1.64 (s, 18H, $\text{C}(\text{CH}_3)_3$), 1.81 (m, 4H, cod- CH_{axial}), 2.11 (m, 4H, cod- $\text{CH}_{\text{equatorial}}$), 5.28 (s, 4H, cod- CH); $^{13}\text{C}\{^1\text{H}\}$ NMR (100.61 MHz, C_6D_6 , 300 K) δ /ppm = 30.7 (s, $\text{C}(\text{CH}_3)_3$), 31.2 (s, cod- CH_2), 37.0 (m, $\text{C}(\text{CH}_3)_3$ and $\text{C}(\text{CH}_3)_3$), 38.8 (t, $^2J_{\text{C,P}} = 4.7$ Hz, $\text{C}(\text{CH}_3)_3$), 77.5 (dt, $^1J_{\text{C,Rh}} = 12.7$ Hz, $^2J_{\text{C,P}} = 2.2$ Hz, cod- CH), 118.0 (t, $^1J_{\text{C,P}} = 55.0$ Hz, C_2P_2), 150.2 (dt, $^1J_{\text{C,P}} = 75.7$ Hz, $^1J_{\text{C,Rh}} = 5.4$ Hz, C_2P_2); $^{31}\text{P}\{^1\text{H}\}$ NMR (161.98 MHz, $[\text{D}_8]\text{THF}$, 300 K) δ /ppm = 29.4 (s, 2P), 73.2 (d, $^1J_{\text{P,Rh}} = 17$ Hz, 2P); UV/Vis (THF, λ_{max} /nm, (ϵ_{max} / $\text{L}\cdot\text{mol}^{-1}\cdot\text{cm}^{-1}$): 375 (37800); elemental analysis calcd. for $\text{C}_{28}\text{H}_{48}\text{P}_4\text{CoRh}$ ($M = 670.43$): C 50.16, H 7.22, found: C 50.37, H 7.31.

4.4.9 Synthesis of $[\text{Rh}(\text{cod})\{\text{Co}(\text{P}_2\text{C}_2\text{Ad}_2)_2\}]$ (**8**)

A solution of $[\text{K}(\text{thf})_2\{\text{Co}(\text{P}_2\text{C}_2\text{Ad}_2)_2\}]$ (0.12 g, 0.12 mmol, 1.0 eq) in THF (3 mL) was added to a solution of $[\text{RhCl}(\text{cod})]_2$ (30 mg, 0.06 mmol, 0.5 eq) in THF (1 mL). The reaction mixture was stirred overnight whereupon the color changed from dark red to yellow. The solvent was removed *in vacuo* and the residue was washed with *n*-hexane (5 mL) and extracted with toluene (10 mL). The filtrate was concentrated to 5 mL and stored at -35 °C. Dark yellow crystals of **8** formed upon storage for four days. Crystals suitable for X-ray diffraction were obtained by diffusion of *n*-hexane into a toluene solution. Yield 0.12 g (82%); m.p. >300 °C; ^1H NMR (400.13 MHz, C_6D_6 , 300 K) δ /ppm = 1.45–2.07 (m, 60H, overlapping with solvent signal, Ad), 2.15 (m, 4H, cod- CH_{axial}), 2.38 (m, 4H, cod- $\text{CH}_{\text{equatorial}}$), 5.38 (s, 4H, cod- CH), 7.04–7.23 (m, 5H, toluene); $^{13}\text{C}\{^1\text{H}\}$ NMR (100.61 MHz, C_6D_6 , 300 K) δ /ppm = 21.3 (s, toluene), 29.5 (s, C3 and C7 of Ad), 30.9 (s, C5 of Ad), 31.7 (s, cod- CH_2), 37.1 (s, C9 and C10 of Ad), 37.2 (s, C2, C4, C6, and C8 of Ad), 78.2 (d, $^1J_{\text{C,Rh}} = 12.2$ Hz, cod- CH); $^{31}\text{P}\{^1\text{H}\}$ NMR (161.98 MHz, C_6D_6 , 300 K) δ /ppm = 23.2 (s, 2P), 72.3 (d, $^1J_{\text{P,Rh}} = 17$ Hz, 2P); UV/Vis (THF, λ_{max} /nm, (ϵ_{max} / $\text{L}\cdot\text{mol}^{-1}\cdot\text{cm}^{-1}$): 378 (48800); elemental analysis calcd. for $\text{C}_{52}\text{H}_{72}\text{P}_4\text{CoRh} \cdot \text{C}_7\text{H}_8$ ($M = 1075.02$): C 65.92, H 7.50, found: C 66.63, H 7.25.

4.4.10 Synthesis of **9** by Reaction of **8** with Adamantyl-Phosphaalkyne (AdCP)

A solution of $[\text{Rh}(\text{cod})\{\text{Co}(\text{P}_2\text{C}_2\text{Ad}_2)_2\}]$ (93 mg, 0.08 mmol, 1.0 eq) in THF (7 mL) was cooled to -40 °C. A solution of AdCP (30 mg, 0.17 mmol, 2.1 eq) in THF (4 mL) was slowly added via syringe. The reaction mixture was stirred at 10 °C for 24 h whereupon the color changed from dark yellow to dark orange. The solvent was removed *in vacuo* and the residue was extracted with cold *n*-pentane (10 mL). The filtrate was concentrated to 3 mL and stored at -80 °C. Trace amounts of dark orange powder precipitated after storage for five days. This substance was submitted for characterization by multinuclear NMR spectroscopy. Crystals suitable for X-ray measurements could not have been obtained even after recrystallization from *n*-pentane at -80 °C. ^1H NMR (400.13 MHz, $[\text{D}_8]\text{THF}$, 270 K) δ /ppm = 1.40–2.50 (m, 90H, overlapping with solvent signal, Ad); $^{13}\text{C}\{^1\text{H}\}$ NMR (100.61 MHz, $[\text{D}_8]\text{THF}$, 270 K) δ /ppm = 28.8–31.2 (m, Ad),

35.7–38.7 (m, Ad), 41.5–48.8 (very br, Ad); $^{31}\text{P}\{^1\text{H}\}$ NMR (161.98 MHz, $[\text{D}_8]\text{THF}$, 270 K) δ /ppm = 37.6 (s, 2P), 91.9 (d, $^1J_{\text{P,Rh}} = 33.5$ Hz, 2P), 95.2 (d, $^1J_{\text{P,Rh}} = 14.7$ Hz, 2P).

4.4.11 Synthesis of $[\text{Pd}_3(\text{PPh}_3)_2\{\text{Co}(\text{P}_2\text{C}_2\text{tBu}_2)_2\}_2]$ (10)

A solution of $[\text{K}(\text{thf})_{1.75}\{\text{Co}(\text{P}_2\text{C}_2\text{tBu}_2)_2\}]$ (0.13 g, 0.21 mmol, 1.5 eq) in THF (4 mL) was added to a suspension of $[\text{PdCl}_2(\text{PPh}_3)_2]$ (0.10 g, 0.14 mmol, 1 eq) in THF (3 mL). The reaction mixture was stirred for 3 h at room temperature followed by removal of the solvent *in vacuo*. Subsequently, the residue was purified by column chromatography (stationary phase: neutral aluminum oxide activity grade super I, 13.5 x 1 cm, eluent: *n*-hexane/toluene gradient 10/0 to 1/1). The by-product $[\text{Co}(\text{P}_2\text{C}_2\text{tBu}_2)_2\text{H}]$ eluted first as a bright orange band (R_f (*n*-hexane/toluene, 10/1 = 0.6), followed by a colorless band of PPh_3 (R_f (*n*-hexane/toluene, 10/1 = 0.3). **9** eluted as the last band (R_f (*n*-hexane/toluene, 10/1 = 0.2). Recrystallization from *n*-hexane at -35 °C gave dark orange crystals of **9**·*n*-hexane. Crystals suitable for X-ray diffraction were obtained by slow evaporation of an *n*-hexane solution. Yield 0.02 g (23%, based on Pd); m.p. >300 °C (decomp. to a black oil); ^1H NMR (400.13 MHz, C_6D_6 , 300 K) δ /ppm = 0.77 (s, 18H, $\text{C}(\text{CH}_3)_3$), 0.88 (t, $^3J_{\text{H,H}} = 7.0$ Hz, 8H, *n*-hexane), 1.04 (s, 18H, $\text{C}(\text{CH}_3)_3$), 1.23 (m, 12H, *n*-hexane) 1.26 (s, 18H, $\text{C}(\text{CH}_3)_3$), 1.34 (s, 18H, $\text{C}(\text{CH}_3)_3$), 7.08 (t, $^3J_{\text{H,H}} = 7.4$ Hz, 6H, *p*- H_{Aryl}), 7.24 (t, $^3J_{\text{H,H}} = 7.4$ Hz, 12H, *o*- H_{Aryl}), 7.91 (m, 12H, *m*- H_{Aryl}); $^{13}\text{C}\{^1\text{H}\}$ NMR (100.61 MHz, C_6D_6 , 300 K) δ /ppm = 14.3 (s, *n*-hexane), 23.0 (s, *n*-hexane), 31.9 (s, *n*-hexane), 33.8 (br, $\text{C}(\text{CH}_3)_3$), 34.0 (d, $^2J_{\text{C,P}} = 2.3$ Hz, $\text{C}(\text{CH}_3)_3$), 34.1 (d, $^2J_{\text{C,P}} = 2.3$ Hz, $\text{C}(\text{CH}_3)_3$), 34.3 (br, $\text{C}(\text{CH}_3)_3$), 34.4 (br, $\text{C}(\text{CH}_3)_3$), 34.9 (s, $\text{C}(\text{CH}_3)_3$), 36.2 (m, $\text{C}(\text{CH}_3)_3$), 36.6 (m, $\text{C}(\text{CH}_3)_3$), 129.0 (m, *o*- C_{Aryl}), 130.3 (s, *p*- C_{Aryl}), 134.9 (m, *m*- C_{Aryl}); The signals for the quaternary carbon atoms of the P_2C_2 units as well as the ipso- C_{Aryl} were not detected. $^{31}\text{P}\{^1\text{H}\}$ NMR (121.49 MHz, C_6D_6 , 300 K) δ /ppm = -43.6 (s, 2P; P7 and P8), 30.4 (dd, $^1J_{\text{P,Pd}}=27.5$ Hz, 2P; P9 and P10), 38.5 (s, 2P; P3 and P4), 201.7 (d, $^1J_{\text{P,Pd}}=218.5$ Hz, 2P; P5 and P6), 214.8 (d, $^1J_{\text{P,Pd}}=218.5$ Hz, 2P; P1 and P2); UV/Vis (THF, λ_{max} /nm, (ϵ_{max} / $\text{L}\cdot\text{mol}^{-1}\cdot\text{cm}^{-1}$): 292 (95500), 407 (37600), 469 (25900), 650 (8000); elemental analysis calcd. for $\text{C}_{76}\text{H}_{102}\text{P}_{10}\text{Co}_2\text{Pd}_3\cdot(\text{C}_6\text{H}_{14})_{1.5}$ ($M = 1891.78$): C 53.97, H 6.55, found.: C 54.44, H 6.68.

4.4.12 Synthesis of $[\text{Hg}\{\text{Co}(\text{P}_2\text{C}_2\text{tBu}_2)_2\}_2]$ (11,12)

A solution of $[\text{K}(\text{thf})_{1.75}\{\text{Co}(\text{P}_2\text{C}_2\text{tBu}_2)_2\}]$ (0.24 g, 0.38 mmol, 1.0 eq) in THF (6 mL) was cooled to -80 °C and added dropwise via cannula to a cooled (-80 °C) suspension of HgCl_2 (0.05 g, 0.19 mmol, 0.5 eq) in THF (3 mL). Subsequently, the reaction mixture was stirred for four hours while allowed to come to ambient. The solvent was removed *in vacuo* and the residue was extracted with *n*-hexane (10 mL). The bright red filtrate was concentrated to 3 mL and stored at -35 °C. Bright red crystals of **11** formed upon storing for one day. The insoluble residue was further extracted with toluene (5 mL). The bright red solution was concentrated to 2 mL and stored at -35 °C. Bright red crystals of **12** formed upon storing for one day. **11**: Yield 23 mg (11%); **12**: Yield 27 mg (13%). Unfortunately, further characterization of compounds **11** and **12**

could not be performed due to unresolved problems with purification of these compounds. NMR samples of crystalline **11** or **12** could not be evaluated due to the presence of signals which could not be assigned to the structures obtained by X-ray crystallography. Hence, spectroscopic characterization of these compounds remains outstanding.

4.4.13 X-ray Crystallography

The single crystal X-ray diffraction data were recorded on an Agilent Technologies SuperNova diffractometer with Cu K α radiation ($\lambda = 1.54184 \text{ \AA}$, for **2-8**, **11**, **12**) or Mo K α radiation ($\lambda = 0.71073 \text{ \AA}$, for **10**). Semi-empirical multi-scan absorption corrections²⁸ were applied to the data. The structures were solved with SHELXT²⁹ and least-square refinements on F^2 were carried out with SHELXL.³⁰ Crystallographic data is given in Tables S1-S4.

CCDC 1890505-1890512 contain the supplementary crystallographic data for this paper (compounds **2-10**). This data can be obtained free of charge from The Cambridge Crystallographic Data Centre via www.ccdc.cam.ac.uk/data_request/cif.

Table S1. Crystal and structure refinement data of **2**, **3**, and **4**.

Compound	2	3	4
Empirical formula	C ₂₉ H ₄₅ CoNiOP ₄	C ₂₅ H ₄₁ CoNiP ₄	C ₂₅ H ₄₁ CoNiP ₄
Formula weight	651.17	583.10	583.10
Temperature [K]	123(1)	123(1)	123(1)
Crystal system	monoclinic	monoclinic	monoclinic
Space group	<i>P2₁/c</i>	<i>P2₁</i>	<i>P2₁/c</i>
a [Å]	10.8145(2)	14.9620(3)	14.8671(4)
b [Å]	15.9967(3)	12.1695(2)	18.4294(4)
c [Å]	18.7559(3)	15.4893(3)	10.1684(3)
α [°]	90	90	90
β [°]	104.098(2)	98.529(2)	99.199(3)
γ [°]	90	90	90
Volume [Å ³]	3147.0(1)	2789.10(9)	2750.2(1)
Z	4	2	4
ρ _{calc} [g/cm ³]	1.374	0.694	1.408
μ [mm ⁻¹]	6.943	3.869	7.847
F(000)	1368.0	612.0	1224.0
Crystal size [mm ³]	0.165 × 0.135 × 0.081	0.155 × 0.082 × 0.055	0.18 × 0.091 × 0.087
Radiation	CuK _α (λ = 1.54184)	CuK _α (λ = 1.54184)	CuK _α (λ = 1.54184)
2θ range for data collection [°]	7.36 to 147.392	7.666 to 147.378	7.7 to 148.128
Index ranges	-11 ≤ h ≤ 13, -19 ≤ k ≤ 16, -23 ≤ l ≤ 22	-18 ≤ h ≤ 17, -15 ≤ k ≤ 15, -19 ≤ l ≤ 19	-18 ≤ h ≤ 18, -22 ≤ k ≤ 18, -12 ≤ l ≤ 12
Reflections collected	19906	30891	29990
Independent reflections	6248 [R _{int} = 0.0432, R _{sigma} = 0.0379]	10844 [R _{int} = 0.0746, R _{sigma} = 0.0731]	5524 [R _{int} = 0.0546, R _{sigma} = 0.0349]
Data / restraints / parameters	6248 / 18 / 337	10844 / 1 / 583	5524/0/292
Goodness-of-fit on F ²	1.044	1.020	1.062
Final R indexes [I >= 2σ (I)]	R ₁ = 0.0447, wR ₂ = 0.1198	R ₁ = 0.0552, wR ₂ = 0.1367	R ₁ = 0.0421, wR ₂ = 0.1061
Final R indexes [all data]	R ₁ = 0.0530, wR ₂ = 0.1267	R ₁ = 0.0600, wR ₂ = 0.1419	R ₁ = 0.0491, wR ₂ = 0.1105
Largest diff. peak/hole [e Å ⁻³]	0.81/-0.66	1.10/-0.57	0.91/-0.71
Flack parameter	–	-0.028(4)	–
CCDC	1890505	1890506	1890511

Table S2. Crystal and structure refinement data of **5**, **6**, and **7**.

Compound	5	6	7
Empirical formula	C ₅₀ H ₈₁ Cl ₂ CoP ₄ Ru ₃	C ₃₀ H ₄₈ P ₂ Ru ₂	C ₂₈ H ₄₈ P ₄ CoRh
Formula weight	1239.06	672.76	670.38
Temperature [K]	123(1)	123(1)	123(1)
Crystal system	triclinic	monoclinic	triclinic
Space group	<i>P</i> -1	<i>P</i> 2 ₁ / <i>n</i>	<i>P</i> -1
a [Å]	11.8663(3)	8.8709(2)	10.1095(4)
b [Å]	12.0079(4)	15.9186(2)	11.3810(5)
c [Å]	19.9954(4)	20.5809(3)	13.7071(7)
α [°]	88.483(2)	90	79.721(4)
β [°]	75.724(2)	90.570(2)	78.688(4)
γ [°]	71.236(2)	90	87.516(4)
Volume [Å ³]	2610.1(1)	2906.13(9)	1521.6(1)
Z	2	4	2
ρ _{calc} [g/cm ³]	1.577	1.538	1.463
μ [mm ⁻¹]	11.682	9.564	10.748
F(000)	1268.0	1384.0	696.0
Crystal size [mm ³]	0.216 × 0.181 × 0.153	0.1707 × 0.0731 × 0.024	0.198 × 0.181 × 0.134
Radiation	CuK _α (λ = 1.54184)	CuK _α (λ = 1.54184)	CuK _α (λ = 1.54184)
2θ range for data collection [°]	7.788 to 147.212	7.02 to 146.698	6.678 to 147.264
Index ranges	-14 ≤ h ≤ 14, -14 ≤ k ≤ 14, -24 ≤ l ≤ 24	-10 ≤ h ≤ 10, -19 ≤ k ≤ 19, -25 ≤ l ≤ 25	-12 ≤ h ≤ 12, -13 ≤ k ≤ 14, -16 ≤ l ≤ 13
Reflections collected	25395	42772	13802
Independent reflections	10141 [R _{int} = 0.0343, R _{sigma} = 0.0358]	5798 [R _{int} = 0.0506, R _{sigma} = 0.0240]	5881 [R _{int} = 0.0244, R _{sigma} = 0.0269]
Data / restraints / parameters	10141 / 0 / 568	5798 / 0 / 324	5881 / 0 / 319
Goodness-of-fit on F ²	1.039	1.199	1.048
Final R indexes [I >= 2σ (I)]	R ₁ = 0.0366, wR ₂ = 0.0975	R ₁ = 0.0653, wR ₂ = 0.1879	R ₁ = 0.0339, wR ₂ = 0.0924
Final R indexes [all data]	R ₁ = 0.0393, wR ₂ = 0.1005	R ₁ = 0.0685, wR ₂ = 0.1942	R ₁ = 0.0367, wR ₂ = 0.0982
Largest diff. peak/hole [e Å ⁻³]	1.67/-1.62	3.28/-2.13	0.69/-1.14
CCDC	1890509	1890508	1890510

Table S3. Crystal and structure refinement data of **8**, **10**, and **11**.

Compound	8	10	11
Empirical formula	C ₆₆ H ₈₆ P ₄ CoRh	C ₈₂ H ₁₁₆ Co ₂ P ₁₀ Pd ₃	C ₄₀ H ₇₂ P ₈ Co ₂ Hg
Formula weight	1165.06	1848.50	1119.18
Temperature [K]	123.0(1)	123(1)	123(1)
Crystal system	monoclinic	monoclinic	monoclinic
Space group	<i>I</i> 2/a	<i>P</i> 2 ₁ / <i>n</i>	<i>P</i> 2 ₁ / <i>n</i>
a [Å]	18.4785(6)	14.2770(2)	15.6449(5)
b [Å]	12.2198(4)	22.0290(3)	12.1393(5)
c [Å]	24.928(1)	27.6151(5)	25.4591(9)
α [°]	90	90	90
β [°]	97.942(4)	96.876(2)	90.713(3)
γ [°]	90	90	90
Volume [Å ³]	5574.8(4)	8622.7(2)	4834.8(3)
Z	4	4	4
ρ _{calc} [g/cm ³]	1.388	1.424	1.538
μ [mm ⁻¹]	6.114	1.216	13.592
F(000)	2456.0	3800.0	2264.0
Crystal size [mm ³]	0.081 × 0.063 × 0.035	0.258 × 0.22 × 0.155	0.169 × 0.149 × 0.103
Radiation	CuK _α (λ = 1.54184)	MoK _α (λ = 0.71073)	CuK _α (λ = 1.54184)
2θ range for data collection [°]	7.162 to 147.096	5.728 to 58.184	6.668 to 148.466
Index ranges	-22 ≤ h ≤ 20, -10 ≤ k ≤ 14, -26 ≤ l ≤ 30	-17 ≤ h ≤ 19, -30 ≤ k ≤ 27, -36 ≤ l ≤ 35	-19 ≤ h ≤ 19, -13 ≤ k ≤ 14, -29 ≤ l ≤ 31
Reflections collected	9824	120461	21579
Independent reflections	5370 [R _{int} = 0.0625, R _{sigma} = 0.0926]	21202 [R _{int} = 0.0817, R _{sigma} = 0.0718]	9531 [R _{int} = 0.0475, R _{sigma} = 0.0485]
Data / restraints / parameters	5370 / 0 / 328	21202/14/910	9531 / 0 / 484
Goodness-of-fit on F ²	1.022	1.061	1.028
Final R indexes [I > 2σ (I)]	R ₁ = 0.0557, wR ₂ = 0.1283	R ₁ = 0.0451, wR ₂ = 0.0823	R ₁ = 0.0369, wR ₂ = 0.0933
Final R indexes [all data]	R ₁ = 0.0815, wR ₂ = 0.1406	R ₁ = 0.0739, wR ₂ = 0.0934	R ₁ = 0.0408, wR ₂ = 0.0963
Largest diff. peak/hole [e Å ⁻³]	0.89/-1.35	0.89/-0.62	1.35/-2.15
CCDC	1890507	1890512	–

Table S4. Crystal and structure refinement data of **12**.

Compound	12
Empirical formula	C ₄₀ H ₇₂ P ₈ Co ₂ Hg
Formula weight	1119.18
Temperature [K]	123(1)
Crystal system	triclinic
Space group	<i>P</i> -1
a [Å]	9.7886(2)
b [Å]	10.6248(2)
c [Å]	24.5776(6)
α [°]	79.512(2)
β [°]	82.859(2)
γ [°]	72.081(2)
Volume [Å ³]	2385.5(1)
Z	2
ρ _{calc} [g/cm ³]	1.558
μ [mm ⁻¹]	13.773
F(000)	1132.0
Crystal size [mm ³]	0.1458 × 0.0888 × 0.0323
Radiation	CuK _α (λ = 1.54184)
2θ range for data collection [°]	7.334 to 149.172
Index ranges	-11 ≤ h ≤ 12, -13 ≤ k ≤ 13, -30 ≤ l ≤ 30
Reflections collected	39608
Independent reflections	9648 [R _{int} = 0.0377, R _{sigma} = 0.0247]
Data / restraints / parameters	9648 / 0 / 484
Goodness-of-fit on F ²	1.170
Final R indexes [I ≥ 2σ (I)]	R ₁ = 0.0267, wR ₂ = 0.0676
Final R indexes [all data]	R ₁ = 0.0274, wR ₂ = 0.0680
Largest diff. peak/hole [e Å ⁻³]	0.88/-1.08
CCDC	-

4.4.14 Variable Temperature NMR Monitoring

[Ni₂Cp₃]BF₄ (12 mg, 0.03 mmol) was transferred to a screw cap NMR tube. **A** (17.2 mg, 0.03 mmol) was dissolved in [D₈]THF and cooled to -90 °C. This solution was transferred to the pre-cooled (-90 °C) NMR tube via syringe. The NMR tube was sealed with the screw cap and transferred to a pre-cooled (-80 °C) Bruker Avance400 NMR device. The reaction was monitored by ³¹P{¹H} NMR spectroscopy starting at 193 K, and subsequent heating in steps of 20 K. This procedure was continued up to 333 K. Selected ³¹P{¹H} NMR spectra are shown in Figure S1.

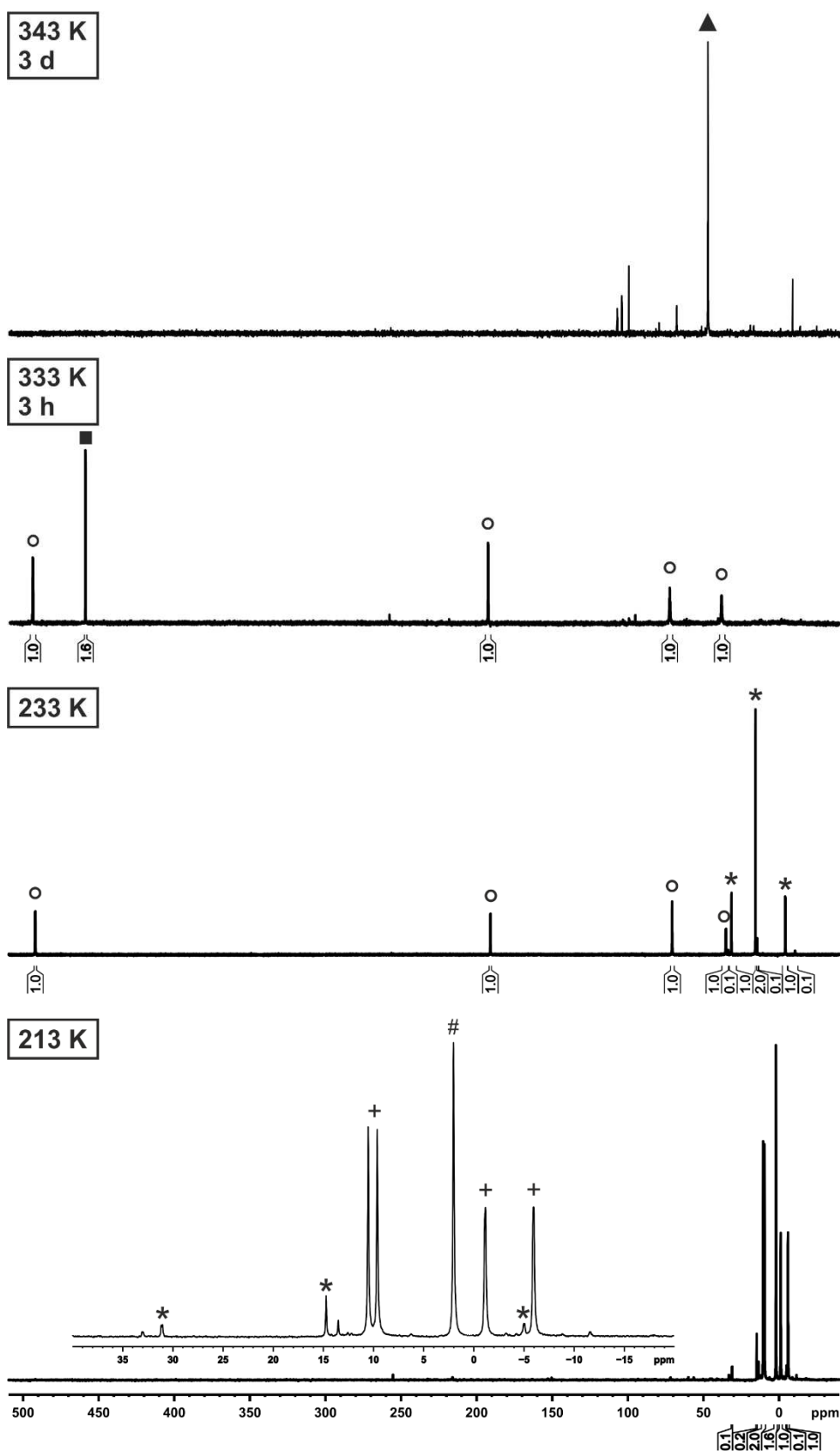


Figure S1. Variable temperature $^{31}\text{P}\{^1\text{H}\}$ NMR monitoring of the reaction of $[\text{K}(\text{thf})_2\{\text{Co}(\text{P}_2\text{C}_2\text{tBu}_2)_2\}]$ (**A**) with $[\text{Ni}_2\text{Cp}_3]\text{BF}_4$ in $[\text{D}_8]\text{THF}$. **213 K**: # marks **A**, + intermediate species **1**, * complex **2**; **233 K**: * complex **2**, \circ complex **3**; **333 K/3h**: \circ complex **3**, \blacksquare complex **4**; **343 K/3d**: \blacktriangle marks an unidentified decomposition product.

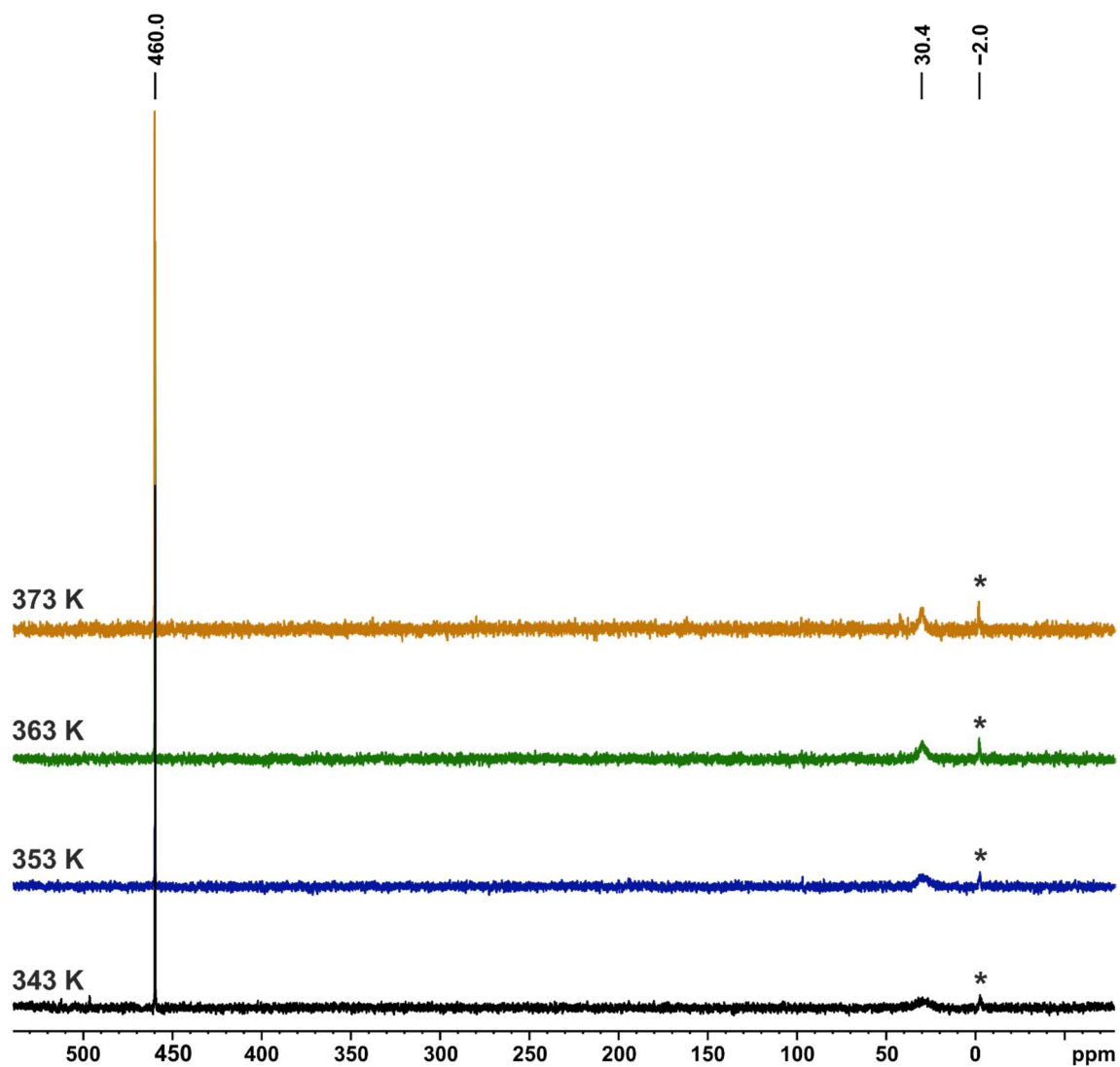


Figure S2. Variable temperature $^{31}\text{P}\{^1\text{H}\}$ NMR monitoring of **4** in $[\text{D}_8]\text{toluene}$. The signal at $\delta = 30.4$ ppm sharpens upon heating from 343 to 373 K. The asterisk marks an unidentified species.

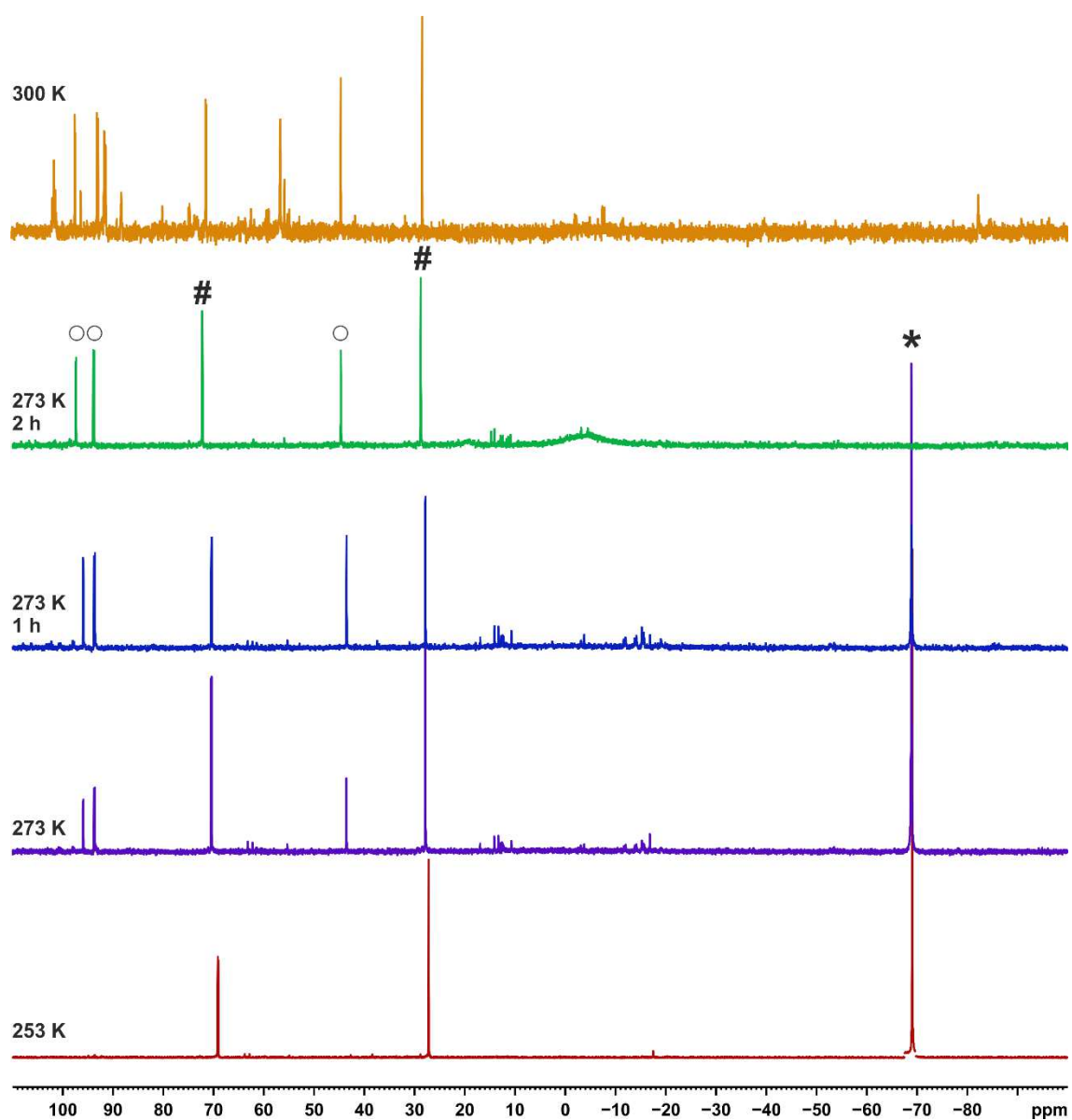


Figure S3. Variable temperature $^{31}\text{P}\{^1\text{H}\}$ NMR monitoring of the reaction of $[\text{Rh}(\text{cod})\{\text{Co}(\text{P}_2\text{C}_2\text{tBu}_2)_2\}]$ (**7**) with $\text{AdC}\equiv\text{P}$ in $[\text{D}_8]\text{THF}$. * marks $\text{AdC}\equiv\text{P}$, # marks **7**, o is assigned to the presumed tripledecker complex $[(\text{P}_2\text{C}_2\text{tBu}_2)\text{Rh}\{\text{Co}(\text{P}_2\text{C}_2\text{tBu}_2)_2\}]$.

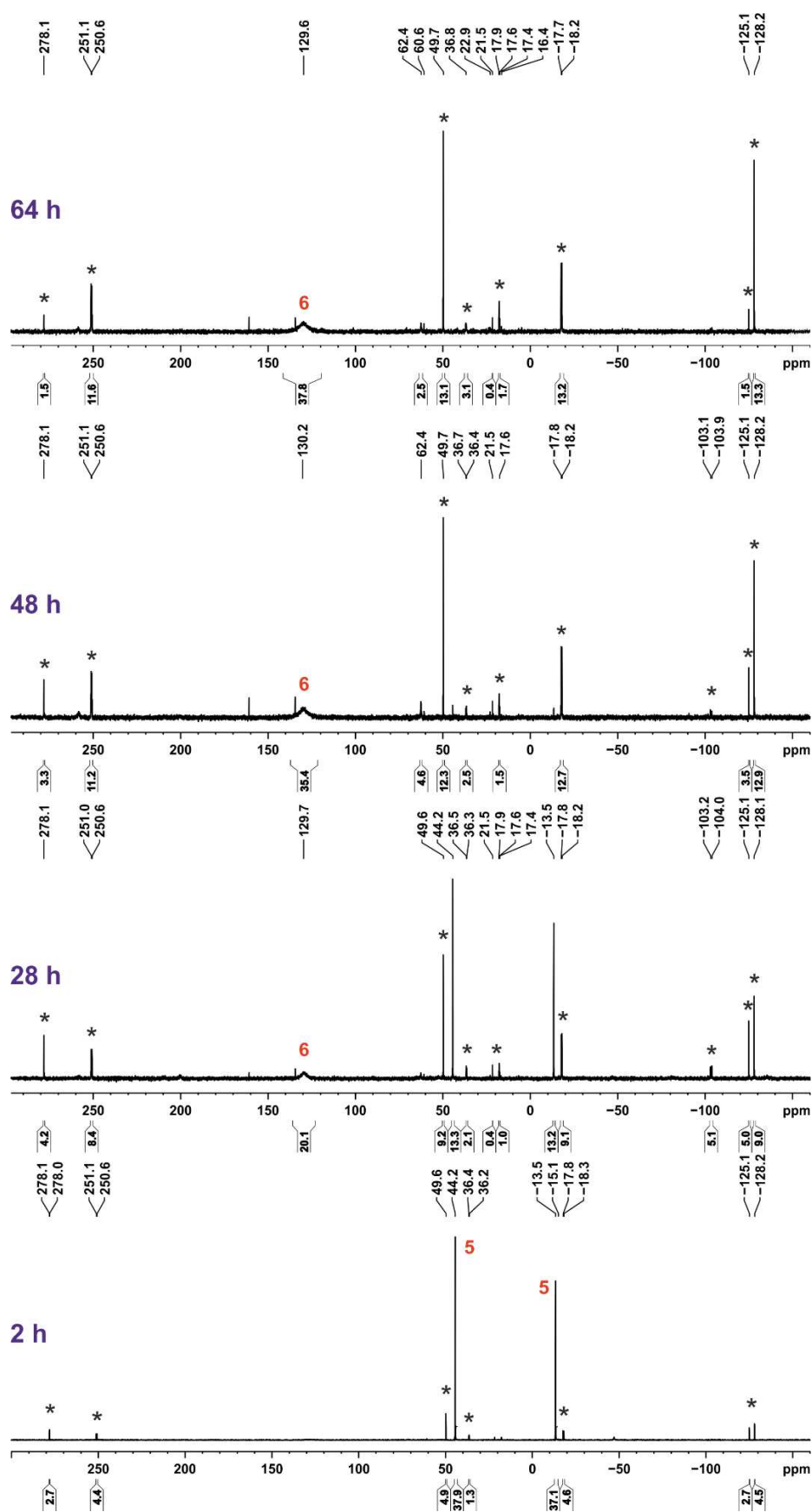
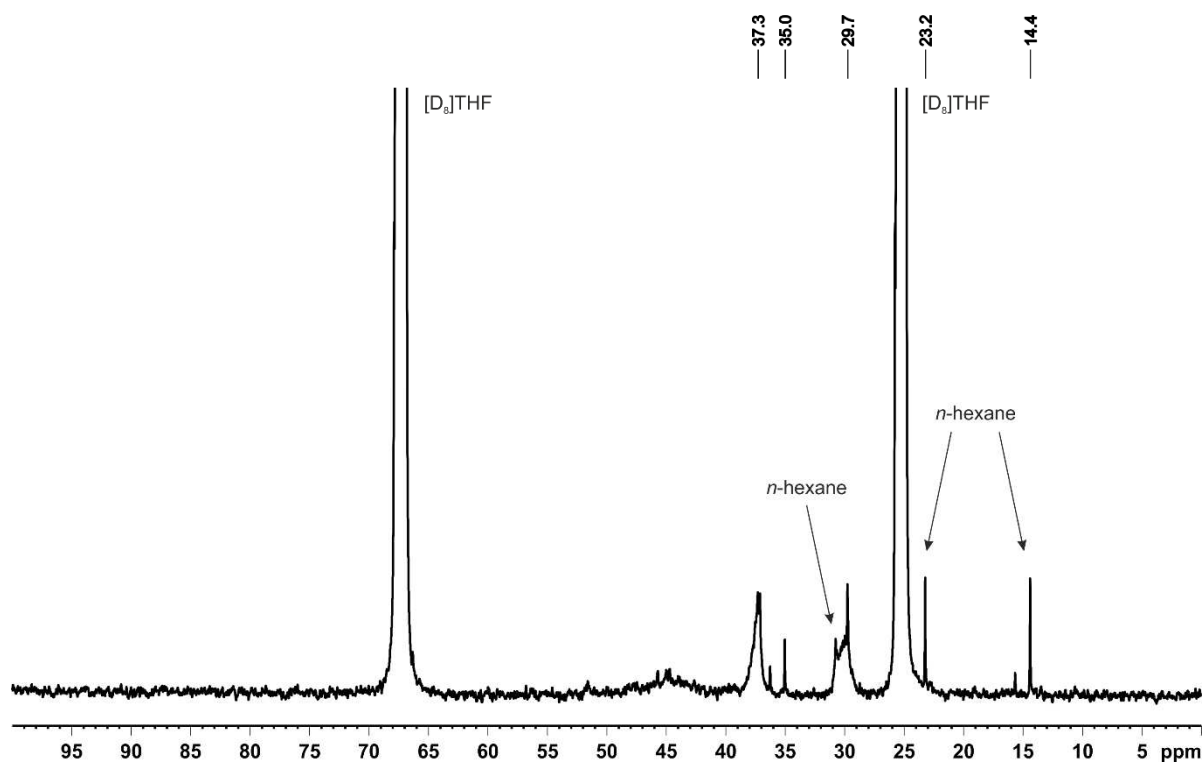
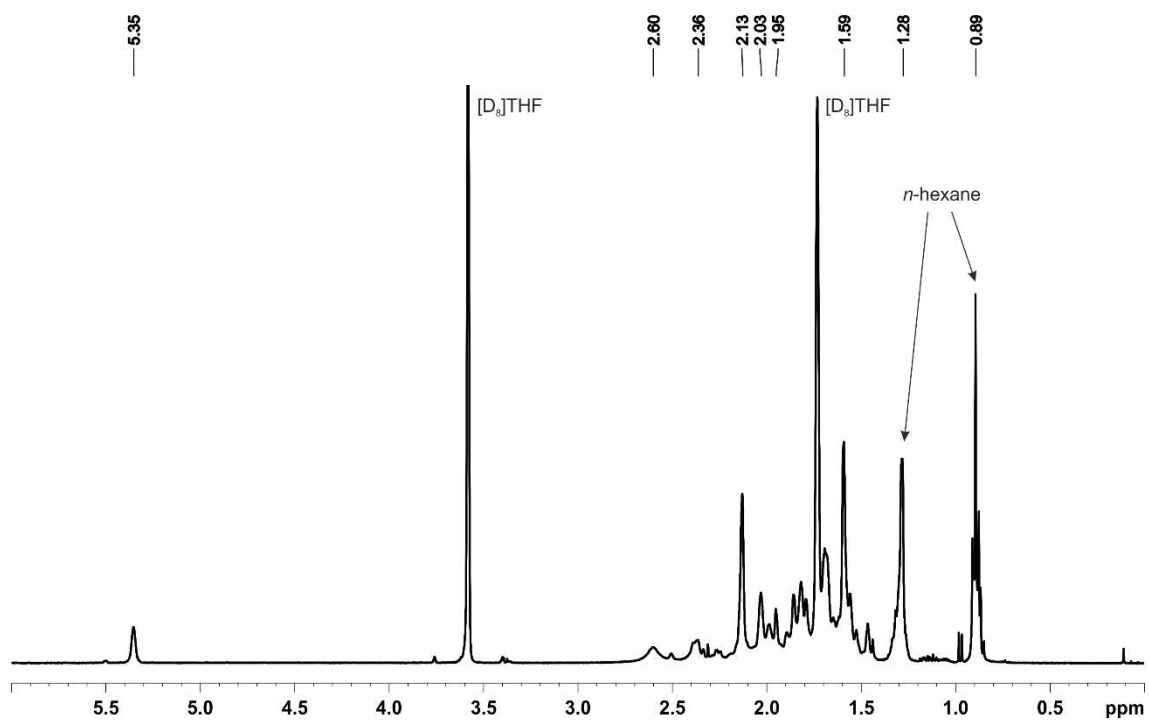


Figure S4. $^{31}\text{P}\{^1\text{H}\}$ NMR monitoring (161.98 MHz, 300 K, $[\text{D}_8]$ THF) of the reaction of $[\text{K}(\text{thf})_2\{\text{Co}(\text{P}_2\text{C}_2\text{tBu})_2\}]$ with $[\text{Cp}^*\text{RuCl}]$ (0.75 equivalents) at 60°C . The signals marked with an asterisk are assigned to unidentified species, while 5 and 6 mark signals assigned to complexes 5 and 6.



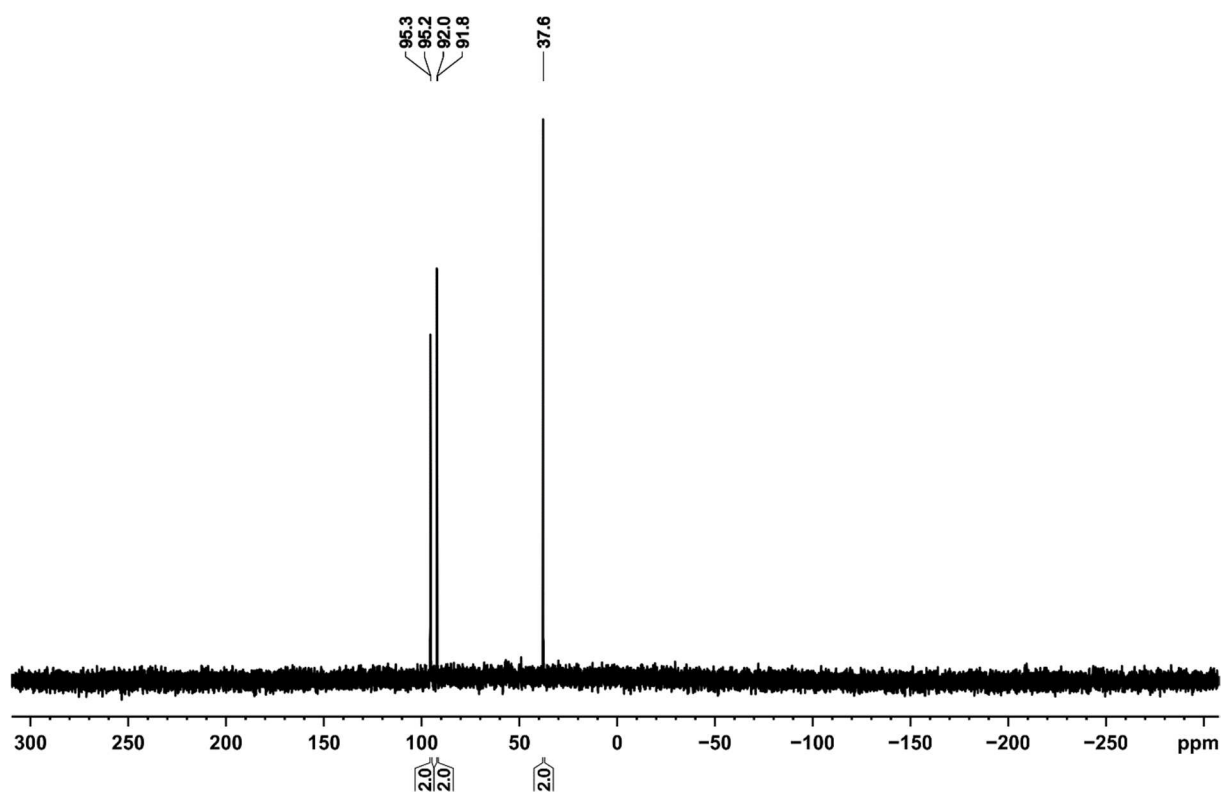


Figure S7. $^{31}\text{P}\{^1\text{H}\}$ NMR spectrum (161.98 MHz, 270 K, $[\text{D}_8]\text{THF}$) of $[\text{Rh}(\text{P}_2\text{C}_2\text{Ad}_2)\{\text{Co}(\eta^4\text{-P}_2\text{C}_2\text{Ad}_2)_2\}]$ (**9**).

4.4.15 UV/Vis Spectra

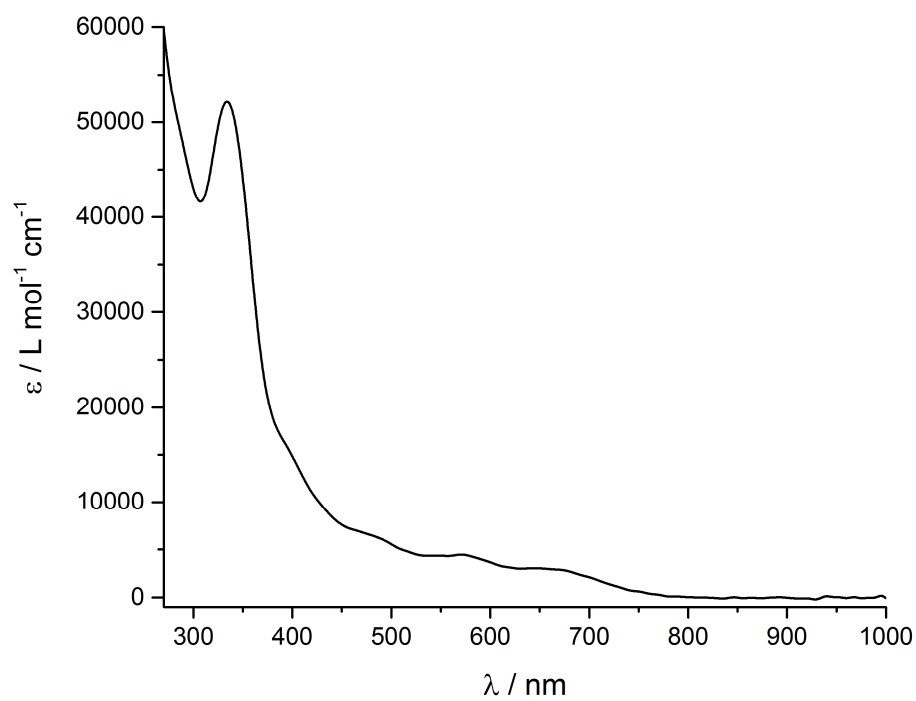
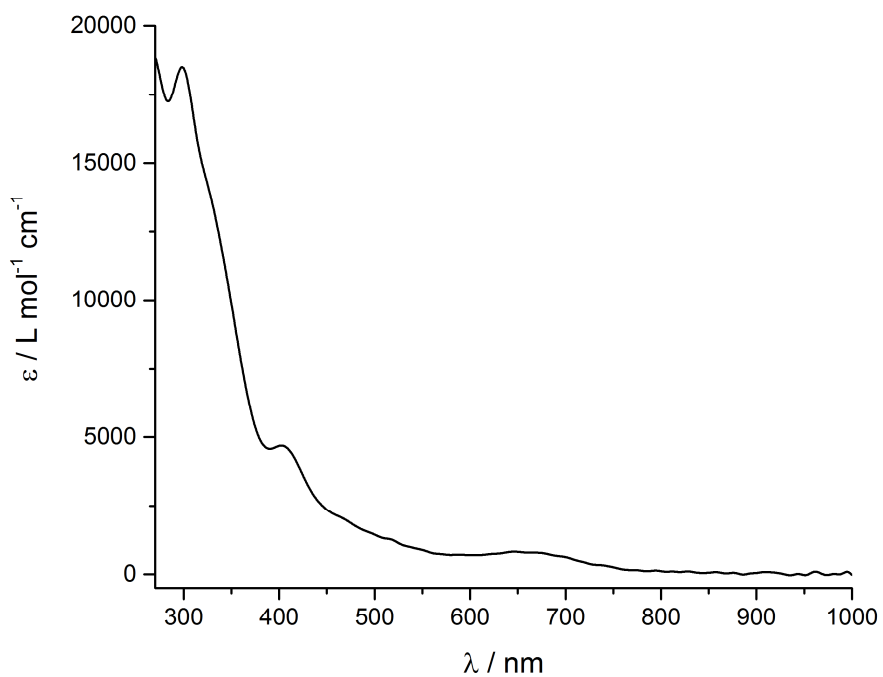
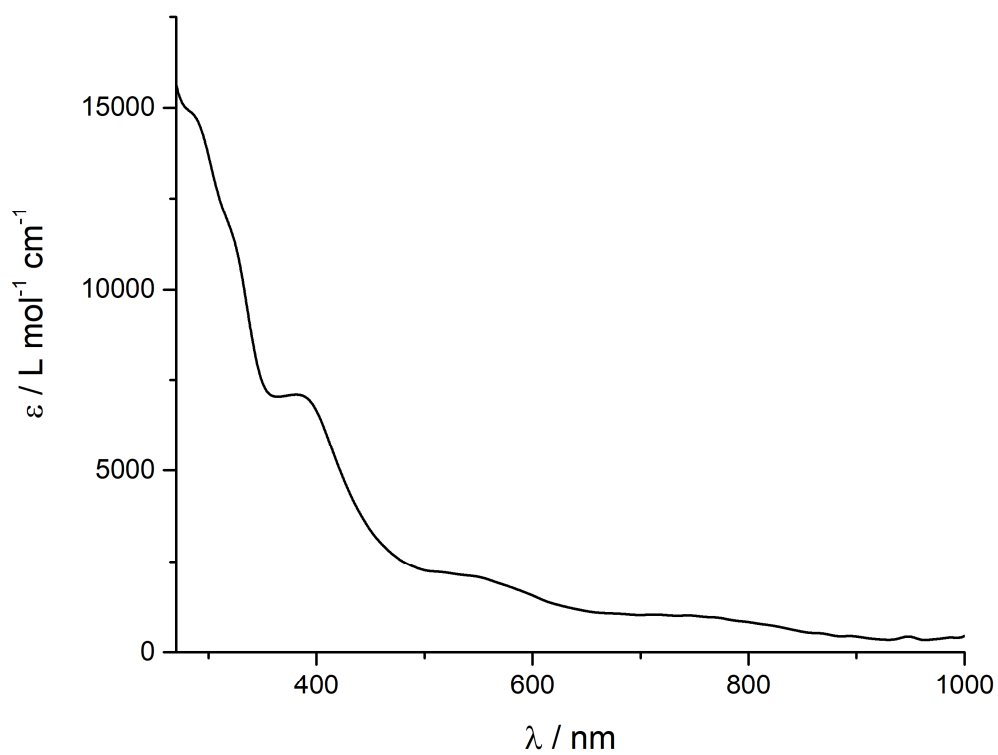
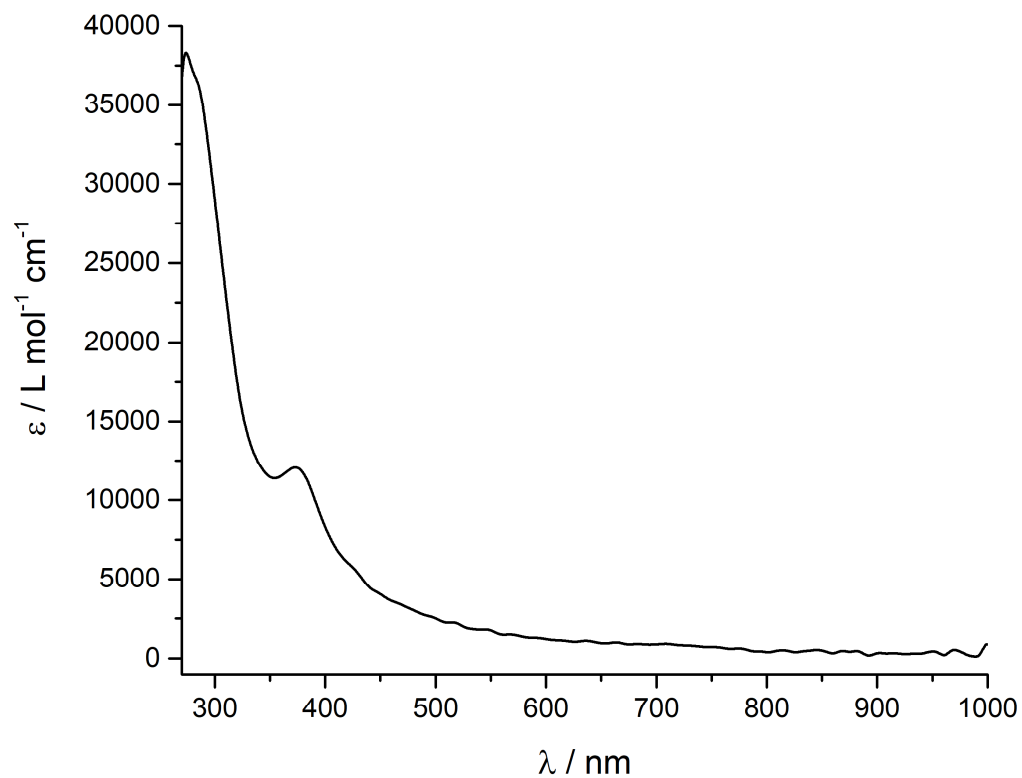
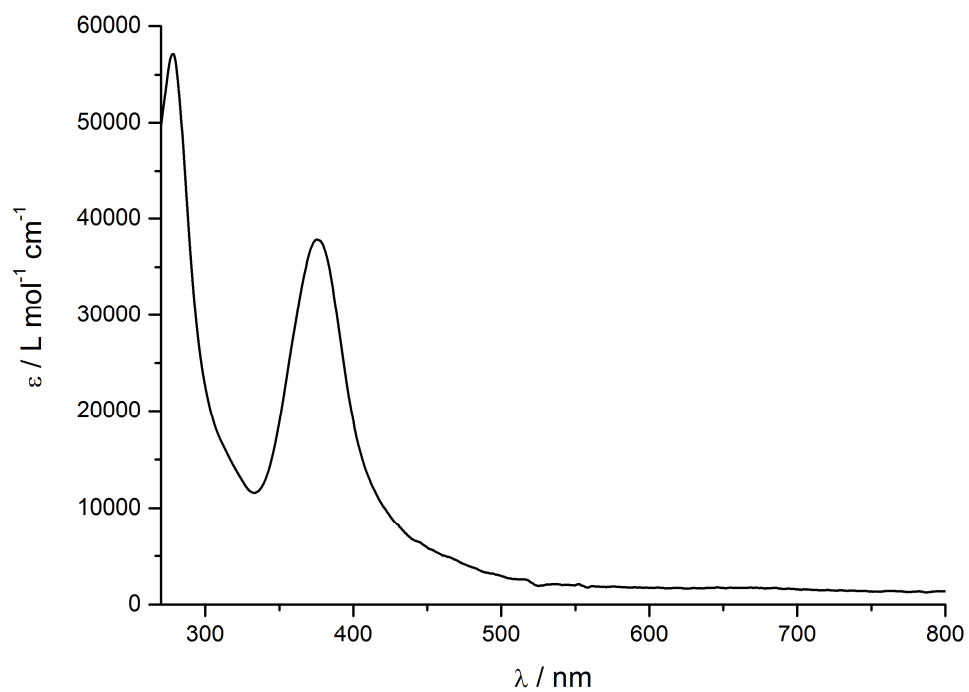
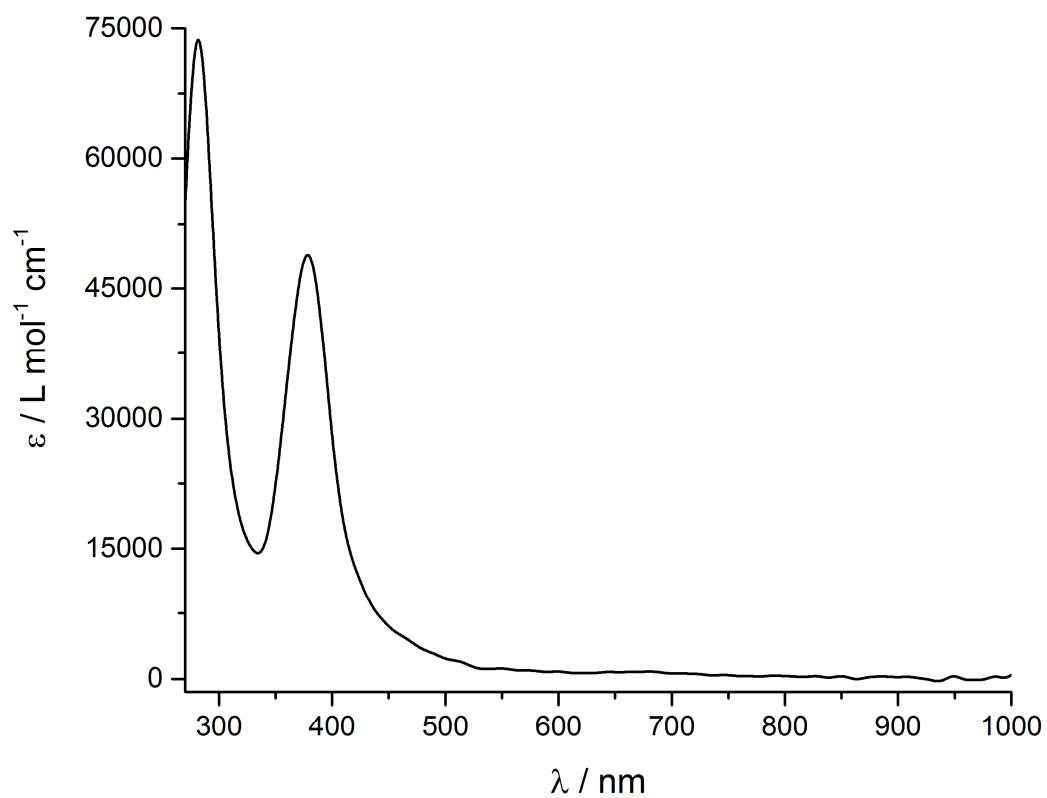
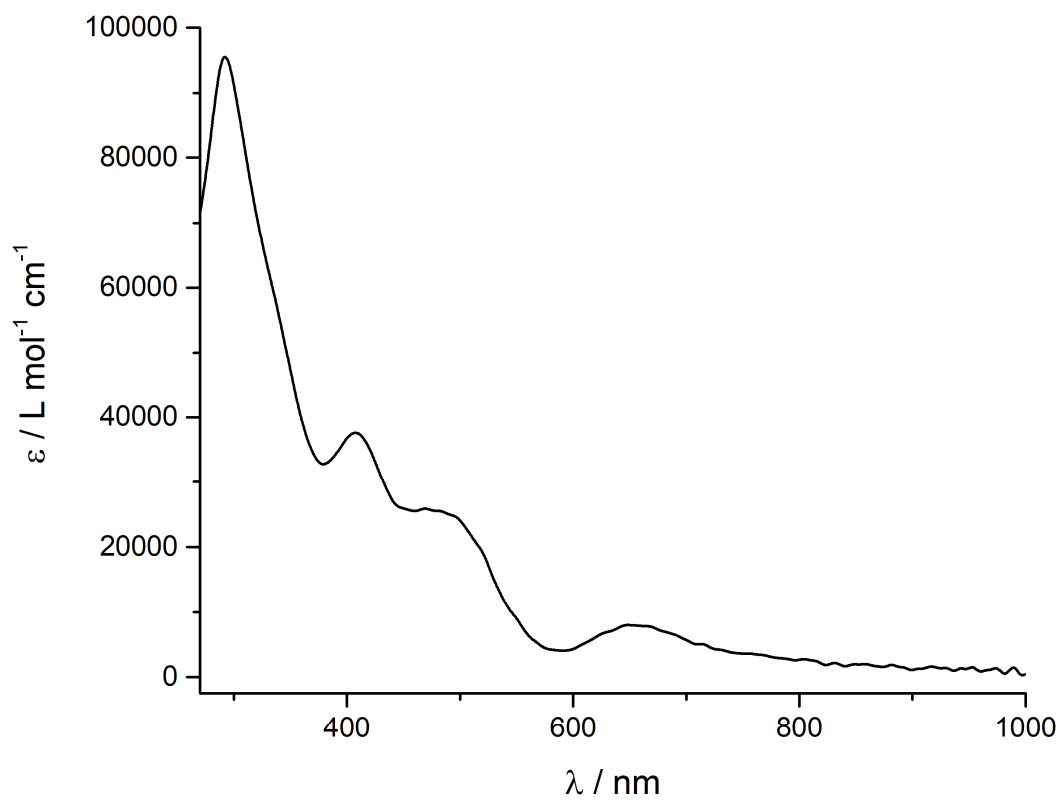


Figure S8. UV/Vis spectrum of **3** in THF.

Figure S9. UV/Vis spectrum of **4** in THF.Figure S10. UV/Vis spectrum of **5** in THF.

Figure S11. UV/Vis spectrum of **6** in THF.Figure S12. UV/Vis spectrum of **7** in THF.

Figure S13. UV/Vis spectrum of **8** in THF.Figure S14. UV/Vis spectrum of **10** in THF.

4.4.16 Cyclic Voltammetry

Cyclic voltammetry experiments were performed in a single-compartment cell inside a nitrogen-filled glovebox using a CH Instruments CHI600E potentiostat. The cell was equipped with a platinum disc working electrode (2 mm diameter) polished with 0.05 μm alumina paste, a platinum wire counter electrode and a silver/silver nitrate reference electrode. The supporting electrolyte, tetra-*n*-butylammonium hexafluorophosphate, was dried in vacuo at 110 $^{\circ}\text{C}$ for three days. All redox potentials are reported versus the ferrocene/ferrocenium (Fc/Fc^+) couple. The scan rate is $\nu = 100 \text{ mV s}^{-1}$.

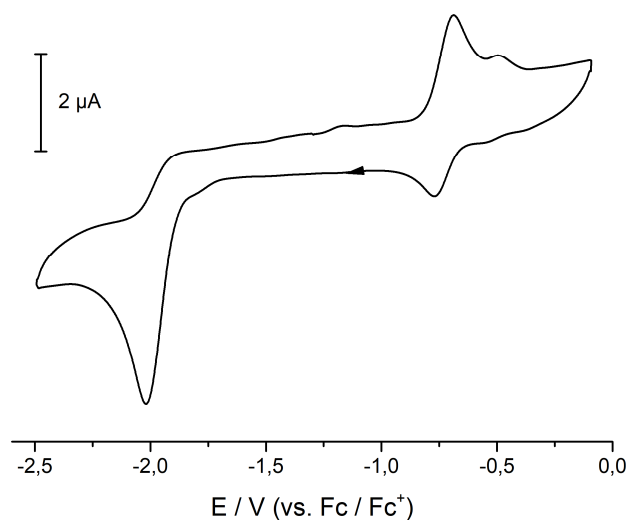


Figure S15. Cyclic voltammogram of **7** recorded in THF/ $[\text{nBu}_4\text{N}]\text{PF}_6$ with a platinum disc working electrode, a platinum wire as counter electrode, and silver/silver nitrate as reference electrode. $\nu = 100 \text{ mV/s}$; potentials are referenced to the Fc/Fc^+ couple.

4.4.17 Theoretical Calculations

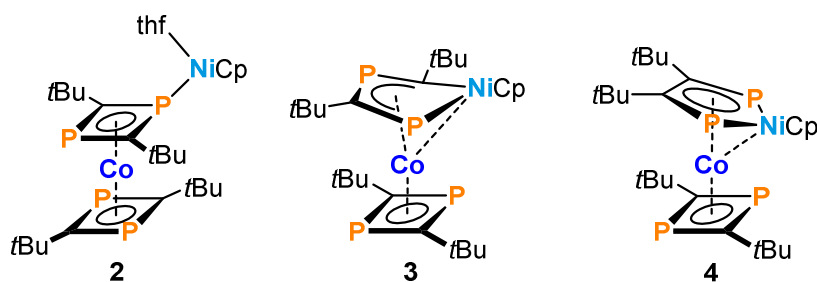
4.4.17.1 Computational Methods

Geometry optimizations of **2–7**, **9'** (*t*Bu instead of adamantyl) and **10'** (Me instead of *t*Bu) were performed with the Gaussian09 program package (Revision E.01).³¹ The BP86 density functional³² and the Ahlrichs def2-TZVP basis set³³ were employed for all atoms. Atom-pairwise dispersion correction to the DFT energy with Becke–Johnson damping (D3BJ) was applied.³⁴ The nature of the stationary points was verified by numerical frequency analyses. Scalar relativistic effects were taken into account for the second-row transition metal elements (Ru, Pd) by means of Stuttgart effective core potential.³⁵ The calculation of the molecular orbitals and the UV/Vis spectra was performed with the B3LYP hybrid functional,³⁶ and the def2-TZVP basis set for all atoms. Magnetic shieldings were calculated using the SCF GIAO method as implemented in Gaussian09, and the B3LYP/def2-TZVP level of theory. The chemical shifts (ppm) were determined using the [Co(P₂C₂tBu₂)₂][−] (magnetic shielding (³¹P) = 273.3 ppm) as reference ($\delta(^{31}\text{P}) = 3.2$ ppm). Molecular orbitals were visualized with the program GaussView5.³⁷ The isosurface value is set to 0.05 for all figures.

Magnetic shieldings (³¹P/ppm) for **3**: 253.5 (P3), 193.0 (P4), 58.5 (P2), −329.1 (P1); for **4**: 322.7 (P4), 192.5 (P3), −298.9 (P1 and P2); for **5**: 298.0 (P2 and P3), 190.3 (P1 and P4); for **9'**: 243.8 (P3 and P4), 180.3 (P1 and P2), 168.9 (P5 and P6); for **10'**: 312.3 (P7 and P8), 227.7 (P9), 224.3 (P10), 213.4 (P3 and P4), 26.5 (P5 and P6), 3.5 (P1 and P2).

4.4.17.2 Wiberg Bond Indices

Wiberg bond indices (WBIs) were calculated with the NBO6 program package implemented in Gaussian09.³⁸ The coordinates of the optimized geometries were used, and the B3LYP hybrid functional and the def2-TZVP basis set were employed for all atoms.

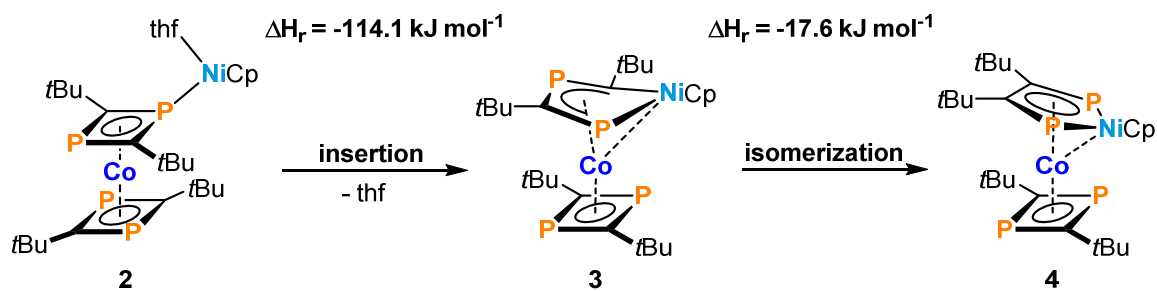
Figure S16. Molecular structures of **2–4**.Table S5. Selected bond lengths (Å) and angles (°) of **2–4**, derived from X-ray and DFT (BP86-D3BJ/def2-TZVP). The atom labeling refers to the X-ray structures.

	2		3		4	
	Exp	Calc	Exp	Calc	Exp	Calc
Ni1–P1	2.1807(8)	2.140	2.1792	2.1795	2.144(1)	2.145
Ni1–P2	–	–	–	–	2.1568(9)	2.148
Ni1–C1	–	–	1.9017	1.9043	–	–
Ni1–Co1	–	–	2.5358	2.539	2.5447(7)	2.589
Ni1–O1	1.891(3)	1.981	–	–	–	–
P1–C1	1.784(3)	1.789	–	–	1.798(3)	1.791
P2–C2	1.799(3)	1.801	1.7542	1.7717	1.795(3)	1.793
C1–C2	–	–	–	–	1.447(4)	1.436
P1–Ni1–C1	–	–	94.56	94.11	–	–
P2–Ni1–P1	–	–	–	–	88.54	88.83

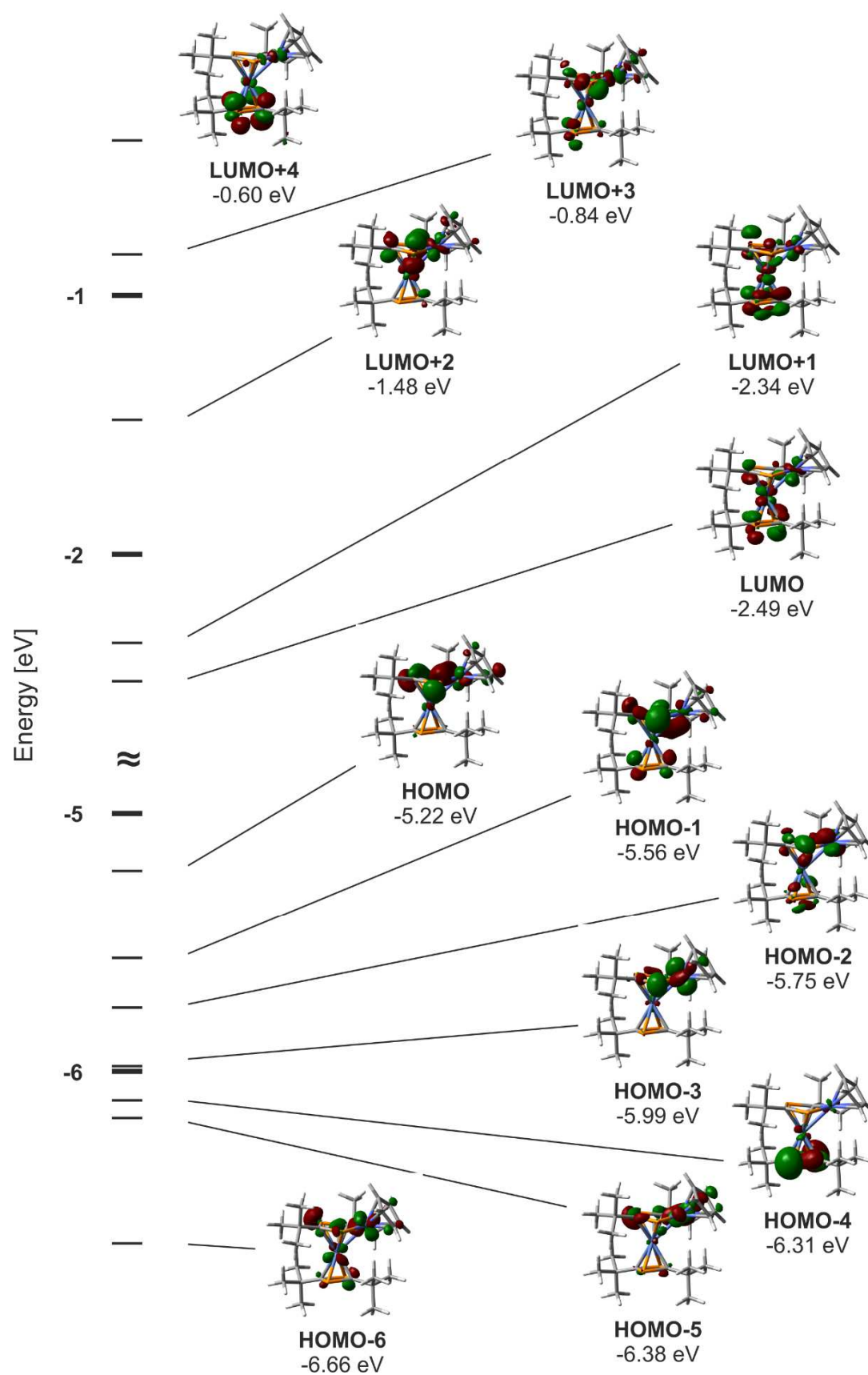
4.4.17.3 Thermochemistry of **2–4**

In order to determine the enthalpies of the reaction from **2** to **4** we performed single-point energy calculations (1 atm, 273.15 K) at the B3LYP/def2-TZVP level of theory for each molecule using the coordinates of the optimized geometries.

The experimentally observed reaction process has shown that complex **2** could not be isolated as a pure compound due to the insertion reaction to **3** which proceeds even at low temperature. Furthermore, we observed that compound **3** is stable in the solid state at room temperature, but not in solution. When a THF solution of **3** was stored at room temperature for a few days compound **4** partly formed. This behavior is in accord with the calculated enthalpies of the reaction displayed in Scheme S1.



Scheme S1. Thermal enthalpies (ΔH_r) of the reaction of **2** to **4** via **3** calculated at the B3LYP/def2-TZVP level of theory.

Figure S17. Kohn-Sham frontier orbitals of **3** calculated at BP86/def2-TZVP level of theory.

4.4.17.4 Cartesian Coordinates of 2–10

Cartesian Coordinates of 2:

Thermal enthalpy H / a.u. -5467.045768

Co	-1.45754600	-0.05711500	-0.00302700	C	-0.92224400	-2.41124400	-2.87495200
Ni	2.76475000	0.83797400	0.03916900	H	-1.09150900	-3.31082900	-2.28000100
P	0.72200200	0.06860400	0.10346700	H	-0.73129000	-2.72045100	-3.90520900
P	-2.95322000	0.47472000	-1.61371300	H	-1.82969000	-1.81221000	-2.85321900
P	-0.70266600	-2.13942100	0.47385400	C	-4.29943000	-2.11043900	1.47858000
P	-3.16015300	0.99789600	1.05170700	H	-3.30632000	-2.52584700	1.64015400
O	3.67478600	-0.90899800	-0.03507900	H	-5.03390000	-2.90658600	1.62075800
C	-0.08715700	-0.76607300	1.44660700	H	-4.48004500	-1.34889800	2.23996200
C	0.05387500	-1.24695100	-0.88411500	C	-1.26051800	-1.18509200	3.61164600
C	-2.45725900	1.71960300	-0.42679100	H	-2.18575500	-0.73853300	3.25281300
C	-1.89552400	3.09754600	-0.64945200	H	-1.20684900	-1.05319500	4.69466300
C	-0.05077000	-0.53109500	2.93366600	H	-1.29495900	-2.25673600	3.40468400
C	4.83820500	-1.14971000	-0.86358900	C	1.23868200	-1.15814200	3.49856900
H	4.51295500	-1.18104100	-1.90512200	H	1.28532800	-2.22402300	3.26909700
H	5.52430800	-0.31670800	-0.72820600	H	1.27972800	-1.03858200	4.58381200
C	0.26395300	-1.60703400	-2.33139200	H	2.11718800	-0.67312900	3.06980000
C	-3.51746700	-0.32639500	-0.10751300	C	-0.03793000	0.96964400	3.25302400
C	-4.42016600	-1.52093100	0.06828200	H	0.79220700	1.46889900	2.74847600
C	0.45926100	-0.34209000	-3.17741900	H	0.08063000	1.12728700	4.32755800
H	-0.43853000	0.27245000	-3.15891900	H	-0.96673600	1.43684300	2.93266200
H	0.68057600	-0.60688300	-4.21392200	C	-0.81728300	3.08327000	-1.73991300
H	1.29124000	0.25611500	-2.79729700	H	0.00837300	2.43717800	-1.44959300
C	-1.32210400	3.65659300	0.65824700	H	-0.43756200	4.09222900	-1.92029100
H	-2.10598800	3.76793000	1.40947900	H	-1.22098100	2.70303800	-2.68012500
H	-0.86983700	4.63791700	0.49634500	C	-4.12519700	-2.60863000	-0.97042200
H	-0.57245200	2.98329200	1.06920800	H	-4.19034600	-2.21105900	-1.98513600
C	-3.05227300	4.00860400	-1.10831200	H	-4.84853300	-3.42257500	-0.88231400
H	-3.47560400	3.64960000	-2.04725700	H	-3.12695900	-3.01810600	-0.82717300
H	-2.69843600	5.03211400	-1.25682700	C	1.53339500	-2.47188700	-2.44126800
H	-3.84828500	4.02336700	-0.36256100	H	2.40194900	-1.91370000	-2.09527300

H	1.70807800	-2.77159600	-3.47736200	C	3.34493700	2.56504400	1.26690100
H	1.43755600	-3.37434300	-1.83485600	H	3.22367600	2.59255700	2.33623700
C	-5.86726200	-1.02332900	-0.13631200	C	4.14206400	-3.21595600	0.10466100
H	-6.11556100	-0.24981400	0.59191600	H	4.36719300	-3.99861500	0.82736700
H	-6.57454800	-1.84815300	-0.01935300	H	3.60766800	-3.66518800	-0.73191000
H	-5.99178600	-0.60072800	-1.13441800	C	2.91634700	2.74068100	-1.02228600
C	4.21984800	2.29173000	-0.85968600	H	2.40374000	2.93168500	-1.94956600
H	4.92129100	2.06753500	-1.64697600	C	2.32963900	2.82615100	0.29477100
C	4.47759500	2.15785000	0.56050500	H	1.33251900	3.16762500	0.50394200
H	5.40363700	1.81319200	0.99388400	C	5.39455100	-2.48252300	-0.38692300
C	3.31742200	-2.10100300	0.72281100	H	5.91584600	-3.01324500	-1.18212800
H	2.24364600	-2.23777500	0.63882300	H	6.09403200	-2.32700300	0.43633400
H	3.57897700	-1.92064400	1.76539000				

Cartesian Coordinates of THF:

Thermal enthalpy H / a.u. **-232.421103**

O	-0.00011187	1.24676358	0.00022069	C	0.73287441	-0.99547008	0.22386335
C	-1.16715569	0.42657301	0.12879647	H	1.33740873	-1.75534431	-0.27177203
H	-1.53644743	0.48394848	1.15987011	H	0.80045670	-1.15851748	1.30208242
H	-1.94250799	0.81648160	-0.53396723	C	-0.73257383	-0.99574023	-0.22371807
C	1.16697174	0.42682381	-0.12917172	H	-1.33691114	-1.75560387	0.27217032
H	1.94270599	0.81704518	0.53294796	H	-0.80008062	-1.15922579	-1.30187448
H	1.53551782	0.48403710	-1.16053679				

Cartesian Coordinates of 3:

Thermal enthalpy H / a.u. **-5234.023688**

Co	-0.45900800	0.16150000	-0.05470600	P	-1.16730100	2.06136500	0.96682400
Ni	2.02353500	-0.37242300	-0.14627200	P	-0.36232100	-1.88497200	1.14339700
P	0.57587000	-0.99435200	-1.64838900	C	1.58843000	3.37299000	-0.30285200
P	-1.86477800	1.22749700	-1.50952300	H	1.18649700	3.84854000	0.59379800

H	2.09957800	2.46223200	-0.00170700	C	1.18235600	-0.16163600	2.73942200
H	2.31988200	4.05399000	-0.74341500	C	0.81812000	-0.57975900	1.30665500
C	-1.37114400	-3.02808400	-1.27426000	C	-0.45845100	-4.14565300	-1.82374400
C	-0.54871800	2.13717500	-0.70794300	H	0.21644900	-3.75720800	-2.58692500
C	0.47532700	3.06183500	-1.30735400	H	0.14406400	-4.58282200	-1.02582600
C	-3.70823200	0.55132800	0.75352700	H	-1.06552000	-4.93713300	-2.26856100
C	-0.43096500	-2.00464300	-0.61339100	C	2.16614000	-1.19353000	3.32799100
C	3.68226500	-0.08858300	-1.62476400	H	2.38548000	-0.94222600	4.36768700
H	3.52218900	0.24416400	-2.63691300	H	1.73651600	-2.19638500	3.30381400
C	-0.26374000	4.37439200	-1.64850600	H	3.10441900	-1.21513400	2.78148200
H	-0.71993200	4.80580100	-0.75636800	C	-3.53029900	-0.111100800	2.12465900
H	0.43614400	5.10264000	-2.06427500	H	-2.92140800	-1.01091200	2.05162700
H	-1.05200300	4.19753400	-2.38176000	H	-3.04283400	0.56703800	2.82666300
C	-0.05633500	-0.14459300	3.65948100	H	-4.50302500	-0.37970200	2.54226200
H	-0.78713100	0.58269700	3.31437400	C	-2.35023800	-3.67537900	-0.28548700
H	-0.53972300	-1.11960500	3.71671500	H	-1.82265900	-4.25164200	0.47552500
H	0.25159500	0.13605800	4.66871100	H	-2.96703300	-2.94249000	0.23029600
C	3.82346300	-1.44932100	0.21938000	H	-3.01278700	-4.35732100	-0.82202300
H	3.81830700	-2.31433400	0.85998700	C	-4.42421300	-0.40638200	-0.20214400
C	4.16382900	-0.11444700	0.60001300	H	-4.56262600	0.04924300	-1.18470000
H	4.45037400	0.19821500	1.58923500	H	-3.86579000	-1.32799100	-0.33224400
C	-2.39344800	1.02860200	0.18669200	H	-5.41029100	-0.66408700	0.18913000
C	1.06759800	2.48426200	-2.59683700	C	1.81058900	1.23615000	2.80135900
H	1.71647400	3.21892100	-3.07844000	H	1.08954500	1.99348300	2.49992100
H	1.65256700	1.59325800	-2.38608700	H	2.12393100	1.45731200	3.82442800
H	0.28199300	2.21371600	-3.30512200	H	2.67738100	1.32085900	2.15275500
C	-2.14565300	-2.41310800	-2.44837800	C	3.54247100	-1.43832400	-1.16768800
H	-2.79057700	-1.60179400	-2.12098600	H	3.29872800	-2.29134700	-1.77775900
H	-1.46691600	-2.00958300	-3.20034000	C	-4.59286400	1.80652500	0.92335600
H	-2.76488100	-3.17598400	-2.92476900	H	-4.14012400	2.51062400	1.62253800
C	4.11081700	0.70735000	-0.54362900	H	-4.72888700	2.31660300	-0.03169400
H	4.29798600	1.76747200	-0.57256800	H	-5.57640800	1.52461300	1.30625400

Cartesian Coordinates of **4**:Thermal enthalpy H / a.u. -5234.028481

Co	-0.03124700	0.30950900	0.13751800	C	-1.71016900	3.74071800	-1.08087600
Ni	1.18873600	-1.53396300	-1.11306300	C	0.61225900	4.61220300	-1.27777400
P	-0.16983000	2.21188500	1.37649600	C	-0.12050400	2.77998100	-2.80031000
P	-0.63860200	-0.65700000	-1.79305100	C	2.99796200	2.09408700	2.97948800
P	0.29608000	-1.80360400	0.81285600	C	1.39514500	0.33886700	3.73899800
P	1.82723600	1.52423000	-0.31207700	C	3.22962400	-0.24315500	2.13306800
C	-1.41234000	-1.28871500	0.75817100	H	-4.28027200	-1.65142100	1.42175000
C	-1.85619500	-0.74488900	-0.49203900	H	-3.90861800	-2.50851500	2.90020400
C	0.26324900	2.38179100	-0.34242800	H	-3.37580800	-3.16377500	1.35487800
C	1.34216000	1.24901500	1.39198200	H	-1.43117300	0.18835000	3.23225200
C	2.03632300	-3.35315000	-1.73116900	H	-3.03045500	-0.36121200	3.73315800
H	1.56342600	-4.30130000	-1.53845500	H	-2.82661800	0.59473000	2.26267200
C	3.00896300	-2.71549300	-0.90791900	H	-1.24715800	-3.42399600	2.62704200
H	3.36762400	-3.07720700	0.04103600	H	-1.95891200	-2.53824700	3.98062300
C	2.65758500	-1.38725300	-2.75078500	H	-0.41147300	-2.03890200	3.32042700
H	2.70670400	-0.55810700	-3.43636000	H	-3.59758700	-2.12522300	-2.09670600
C	3.37692500	-1.50299400	-1.52994200	H	-5.08774200	-1.32197400	-1.59369500
H	4.05781600	-0.76978300	-1.13250600	H	-4.15912500	-2.27826300	-0.44128000
C	1.83578400	-2.53067100	-2.88346800	H	-4.30823000	0.10547900	0.95605000
H	1.16428300	-2.74043900	-3.69893300	H	-4.93048300	0.97381000	-0.43046400
C	-2.18012200	-1.50486900	2.10458200	H	-3.39960000	1.45679800	0.30111800
C	-3.27712500	-0.31195200	-0.95147900	H	-2.68493400	1.39125800	-2.22034000
C	-0.26099900	3.34014100	-1.38030600	H	-4.27794900	0.72626700	-2.54686500
C	2.21831800	0.83251800	2.54719000	H	-2.84159900	-0.12202000	-3.10336900
C	-3.51925400	-2.23970100	1.91666300	H	-2.36525700	2.87588400	-1.02984800
C	-2.38517000	-0.18608500	2.86862000	H	-2.09028200	4.41141100	-1.85390500
C	-1.38918400	-2.43128200	3.05558800	H	-1.77550100	4.26116700	-0.12340600
C	-4.07854000	-1.59283200	-1.27460600	H	0.57382100	5.02767300	-0.26985700
C	-4.01829900	0.59904200	0.03755100	H	0.25551300	5.37148600	-1.97766000
C	-3.25049200	0.46744000	-2.28518300	H	1.65343500	4.38863000	-1.51446200

H	0.91307700	2.48794100	-2.99829300	H	0.64623600	1.07657700	4.03346600
H	-0.40263000	3.53561400	-3.53675000	H	2.04151800	0.15595700	4.59986200
H	-0.74134100	1.89963100	-2.94789600	H	0.88547300	-0.58919800	3.49422400
H	3.59731900	2.48061000	2.15371500	H	2.72717000	-1.17431000	1.87760600
H	3.66705200	1.85926600	3.81044400	H	3.92585300	-0.44099100	2.95087000
H	2.31405700	2.88159500	3.29894700	H	3.81272600	0.07974700	1.26840200

Cartesian Coordinates of 5:

Thermal enthalpy $H / \text{a.u.}$ -3891.327289

Ru	-2.50872600	-1.85557900	-0.07358200	C	-4.40550300	-2.74553300	0.66439800
Ru	-2.48086300	1.86493100	-0.07326500	C	-0.11629900	-1.84808100	3.50292900
Ru	3.80769100	0.00543700	-0.09522300	H	0.05048700	-0.80248800	3.77298000
Co	1.25700100	-0.00795400	0.17412600	H	-0.20521000	-2.43290800	4.43190600
Cl	-2.48604300	0.01074300	-1.67583300	H	-1.06842000	-1.90214800	2.95650800
P	-0.26856900	-1.72541400	0.01181900	C	1.17173800	-2.08705400	-2.60920100
Cl	-2.73100200	-0.00529400	1.51688300	C	0.92253500	1.62515100	1.52190900
P	-0.25298400	1.71998400	0.17534100	C	-3.06090400	3.62721500	-1.21106900
P	2.40176200	-1.98593000	0.07805200	C	5.62702600	1.20836000	-0.31319300
P	2.40716800	1.95107000	0.52184500	C	-3.56740500	3.34771100	1.06185400
C	1.02561200	-1.82110900	1.24329900	C	0.77714500	2.02333200	2.97587600
C	1.09550600	-1.69641900	-1.14629600	C	-2.68100900	4.00976000	0.13540500
C	5.55918500	-0.88916500	0.73229200	C	-3.27142200	-3.59764000	0.97721200
C	1.03533500	-2.38156500	2.64373300	C	5.60174100	0.19102400	-1.33641200
C	-0.63720000	1.76056200	3.50517900	C	-4.54351800	2.59644300	0.27788000
H	-1.36728100	2.31943100	2.90660000	C	-4.23063800	2.77350000	-1.09848800
H	-0.71971500	2.08105000	4.55584800	C	0.27359300	1.89995300	-3.15726500
H	-0.92065800	0.70778500	3.42715300	H	0.39298500	0.82212200	-3.30231900
C	-4.48755500	-2.58435900	-0.74645200	H	0.31627800	2.39550600	-4.13982500
C	5.57864100	-1.10409900	-0.69992900	H	-0.72056400	2.06137200	-2.71673800
C	-3.40243300	-3.34997200	-1.35256000	C	1.36594900	2.43819100	-2.22782800
C	1.21338600	1.87943400	-0.83558600	C	-2.67950200	-3.99938300	-0.28398800
C	5.57079300	0.53850000	0.96988800	C	0.85789700	-3.91291100	2.49593400

H	-0.11330600	-4.13916500	2.03834600	C	2.40501000	-2.14081900	3.30360100
H	0.90195400	-4.40356100	3.48150700	H	3.16221800	-2.78625200	2.83579500
H	1.64600800	-4.33381100	1.85404800	H	2.37090100	-2.38038300	4.37772000
C	-0.16072700	-1.86741400	-3.33267300	H	2.73491800	-1.10327600	3.17465400
H	-0.96131100	-2.40854500	-2.81467000	C	-5.32540100	-2.15570400	1.68181900
H	-0.09776200	-2.23038100	-4.37049800	H	-4.77872000	-1.83649700	2.57907700
H	-0.45723900	-0.81373700	-3.34367400	H	-6.07763900	-2.90158600	1.98910700
C	-1.60717400	-5.02765900	-0.45584900	H	-5.85532800	-1.27957900	1.28847900
H	-1.14251700	-4.95478300	-1.44744600	C	5.80520400	2.67857200	-0.51870200
H	-2.02924900	-6.04214500	-0.35812100	H	5.46610100	2.99141600	-1.51457000
H	-0.81111800	-4.92091700	0.29238300	H	6.87011800	2.95419100	-0.42986700
C	-5.48580400	-1.76945100	-1.50232300	H	5.24166900	3.25919300	0.22365600
H	-5.98977400	-1.05388600	-0.83961700	C	1.21210100	3.97309000	-2.10642700
H	-6.25694000	-2.40926500	-1.96329600	H	0.22118900	4.22790200	-1.71181600
H	-4.99681900	-1.19141100	-2.29939300	H	1.32744100	4.45326200	-3.09128600
C	2.31426100	-1.37436800	-3.34529500	H	1.96890000	4.38328500	-1.42141600
H	2.04945300	-0.33759400	-3.57654300	C	1.84425200	1.37493200	3.86686900
H	2.54461200	-1.88772600	-4.29236700	H	1.84499000	1.84193700	4.86435500
H	3.22144500	-1.35654600	-2.72114700	H	2.84556300	1.50357200	3.42721800
C	5.66354000	-1.94796900	1.77933000	H	1.66560100	0.30368100	3.99223000
H	5.20930900	-1.62346900	2.72354900	C	1.47454400	-3.60812900	-2.61886400
H	6.72417200	-2.18187400	1.97666600	H	2.46265800	-3.80941600	-2.17901200
H	5.16542400	-2.87490300	1.46649100	H	1.45856300	-3.99576500	-3.64985300
C	5.74369200	0.41839600	-2.80702300	H	0.72751500	-4.15380700	-2.02589600
H	5.16989600	-0.31558300	-3.38818900	C	-3.26390800	-3.58538600	-2.82187700
H	6.80298300	0.32228300	-3.10220400	H	-3.32921100	-2.64398700	-3.38554500
H	5.40420800	1.41890400	-3.09896800	H	-4.06813100	-4.24998000	-3.18257000
C	2.76702900	2.16239500	-2.78371300	H	-2.30553500	-4.05775100	-3.07082400
H	3.51284300	2.73415500	-2.21398200	C	-2.98840800	-4.15969700	2.33302200
H	2.83909900	2.46151500	-3.84160300	H	-1.98421100	-4.59507800	2.39106200
H	3.02462700	1.10150500	-2.69075300	H	-3.71094500	-4.95615900	2.58538800
C	5.68523400	-2.42481600	-1.39428500	H	-3.06018100	-3.38740900	3.11138200
H	5.22877700	-3.22640800	-0.79962300	C	5.62485800	1.20045100	2.30825500
H	6.74277600	-2.68929900	-1.56757600	H	5.16150400	2.19488100	2.27551000
H	5.18251100	-2.40852100	-2.37120900	H	6.66961900	1.32100800	2.64390400

H	5.09388900	0.60745300	3.06501700	C	-5.65599600	1.78938100	0.86153600
C	1.00810400	3.55800500	3.01760300	H	-6.12812000	1.15381200	0.10059200
H	0.32644500	4.06990800	2.32499800	H	-6.43618500	2.44131400	1.28857700
H	2.03839200	3.80636800	2.72263200	H	-5.28117400	1.13418000	1.66217400
H	0.82777600	3.93844100	4.03575900	C	-2.57384400	4.22263700	-2.49313500
C	-1.66177100	5.04327300	0.49474000	H	-2.51477600	3.47006300	-3.29152400
H	-1.39149400	4.98125700	1.55653100	H	-1.57875900	4.66908700	-2.38319600
H	-2.06158300	6.05479500	0.31055900	H	-3.25888500	5.01843700	-2.83621100
H	-0.73886600	4.93635700	-0.08963400	C	-3.65855700	3.55178700	2.53975600
C	-4.96235200	2.19451600	-2.26455600	H	-4.50489700	4.21649900	2.78607400
H	-4.26299400	1.83747900	-3.03278800	H	-2.74736100	4.01031100	2.94388300
H	-5.61333900	2.95774400	-2.72312800	H	-3.81709100	2.59937500	3.06545100
H	-5.58838600	1.34375600	-1.96890500				

Cartesian Coordinates of **6**:

Thermal enthalpy $H / \text{a.u.}$ **-2043.789141**

Ru	1.34044400	-0.27194000	-0.08153400	H	-2.17989700	2.21114900	2.03313000
Ru	-1.34301500	-0.27414200	-0.08646200	C	3.48213400	0.57236800	0.07567700
P	-0.00022200	-2.17776600	0.10545000	C	-2.99148300	-2.94087700	-1.21648500
P	0.00198200	-1.24876500	-1.79878500	H	-2.52020900	-2.81031200	-2.21067400
C	3.04504500	-1.65281500	-0.44140400	H	-4.01619100	-3.34470300	-1.37160000
C	3.01786000	-1.51208700	1.00759200	H	-2.40260000	-3.70840300	-0.67722900
C	3.30181500	-0.15043000	1.32359200	C	4.07943100	1.94652300	-0.03400500
C	-0.00588000	1.18376100	0.65262500	H	4.07044000	2.31536800	-1.07615500
C	-3.34086600	-0.34849300	-1.02660200	H	5.14215500	1.91636200	0.29495700
C	-3.04903200	-1.64859200	-0.45391200	H	3.56490500	2.70001800	0.59128300
C	1.19467000	2.95659500	1.97034100	C	-3.30224900	-0.15811900	1.32255600
H	2.13711800	2.40513400	1.82427500	C	3.33837800	-0.35803500	-1.02417800
H	1.24235700	3.48441200	2.94617300	C	-0.00052700	1.25429400	-0.72163900
H	1.11756100	3.72093200	1.17159300	C	-3.48211000	0.57449900	0.08096300
C	-1.28217400	2.84750600	2.05152400	C	-0.04144300	1.57682500	-3.22905500
H	-1.35276000	3.57320500	1.21710400	H	0.83863000	0.91909300	-3.37048000
H	-1.27764200	3.41905400	3.00350800	H	-0.05000500	2.33405500	-4.04170400

H	-0.94760600	0.94701000	-3.32299000	H	4.72056100	0.20699400	2.89874200
C	0.07028100	1.01574200	3.12629900	H	3.07807500	-0.18150400	3.48434300
H	-0.77322400	0.29927000	3.08242200	C	0.00408900	2.26573800	-1.85313700
H	0.04198300	1.55438800	4.09697200	C	-2.86141900	-2.63487000	1.98073400
H	0.99977200	0.41958400	3.06881200	H	-2.22219300	-3.44591100	1.57839100
C	-0.00636700	1.99239300	1.93623700	H	-3.84946800	-3.07884800	2.23740900
C	-1.22801400	3.18261000	-1.72484200	H	-2.39528800	-2.28230400	2.92162700
H	-2.15506100	2.58549200	-1.80050800	C	-3.64232500	-0.07657800	-2.47146800
H	-1.23609300	3.94439400	-2.53264000	H	-3.40438800	0.96928300	-2.74916000
H	-1.24093800	3.71072500	-0.75106600	H	-4.71767100	-0.24952900	-2.70262600
C	2.98777700	-2.94983500	-1.19613900	H	-3.04236300	-0.73351600	-3.13123400
H	2.39572700	-3.71365700	-0.65518200	C	-4.06568900	1.95488000	-0.02342800
H	4.01262500	-3.35591600	-1.34473700	H	-3.55383200	2.69459700	0.61968900
H	2.52138300	-2.82421300	-2.19322700	H	-5.13520500	1.93130700	0.28306300
C	-3.62787500	0.32630200	2.70700700	H	-4.03413300	2.33376900	-1.06159600
H	-2.80838300	0.14187300	3.43017100	C	-3.01562200	-1.51618400	0.99533400
H	-4.52686700	-0.20439300	3.09125200	C	3.63889700	-0.10139300	-2.47200700
H	-3.85452400	1.40864300	2.72735600	H	3.00908100	-0.73605400	-3.12577100
C	1.28496500	3.12011600	-1.77892600	H	4.70522300	-0.31529600	-2.71035100
H	1.36531100	3.65317100	-0.81165300	H	3.43925400	0.95203600	-2.75074700
H	1.29841800	3.87555400	-2.59267900	C	2.86275000	-2.63372200	1.98984000
H	2.17649600	2.47599400	-1.88735400	H	2.42813600	-2.28013200	2.94538700
C	3.63625200	0.35829500	2.69448500	H	3.84540600	-3.10398200	2.21736300
H	3.43137600	1.43796200	2.81585300	H	2.19366700	-3.42509400	1.59685200

Cartesian Coordinates of $\mathbf{9}'$:

Thermal enthalpy H / a.u. -4716.102360

Rh	-1.81762000	0.00000000	0.00002500	C	0.23675900	-0.52404200	-2.67611100
P	0.15554400	-1.39217900	0.27332400	C	0.23694600	0.52405500	2.67611900
P	0.15551900	1.39220300	-0.27331300	P	3.75940100	-0.27548700	-1.32497500
C	0.20474600	-0.23014100	-1.16943400	P	3.75942200	0.27549200	1.32490400
C	0.20480000	0.23016600	1.16944200	C	3.67187500	-1.14140800	0.23631300
Co	1.93880500	0.00000900	-0.00002000	C	3.67187300	1.14141600	-0.23638300

C	3.86162300	-2.61211100	0.53491400	H	-1.08916600	-0.83750700	-4.36749100
C	3.86162600	2.61212100	-0.53497600	C	0.92302200	-1.87819700	-2.92537300
P	-3.77330900	0.01840900	-1.35033400	H	0.90106400	-2.12285600	-3.99843700
C	-3.69263100	1.17118400	0.01450200	H	1.96834600	-1.86193300	-2.59816200
C	-3.69260100	-1.17120900	-0.01444000	H	0.40465700	-2.68823100	-2.38731500
P	-3.77329900	-0.01843700	1.35039900	C	0.98901600	0.59591400	-3.41563400
C	-3.79578900	-2.67741600	-0.00019400	H	0.52283300	1.57527800	-3.22239800
C	-3.79588300	2.67739000	0.00023300	H	2.03860700	0.64793200	-3.10809700
C	-3.20329300	3.23978200	-1.30325900	H	0.95641800	0.41928700	-4.50185100
H	-3.31610600	4.33466000	-1.33713500	C	-1.16832300	0.59742500	3.29548900
H	-2.13322500	2.99862800	-1.38052600	H	-1.77684000	1.37330800	2.81742500
H	-3.71372400	2.82257500	-2.18600900	H	-1.69687900	-0.35870300	3.19705200
C	-5.29815400	3.03191200	0.07378400	H	-1.08873400	0.83710500	4.36776300
H	-5.74789400	2.64581000	1.00164600	C	0.98987000	-0.59559300	3.41542700
H	-5.43748100	4.12475500	0.05132500	H	0.52405900	-1.57515500	3.22228800
H	-5.84635300	2.59698400	-0.77618900	H	2.03940500	-0.64715200	3.10761100
C	-3.06997400	3.29430700	1.20639100	H	0.95747900	-0.41900300	4.50165600
H	-3.45710200	2.89108600	2.15539100	C	0.92268200	1.87849400	2.92528400
H	-1.99089100	3.08897600	1.15942900	H	0.90083500	2.12311200	3.99836000
H	-3.21249400	4.38617900	1.22304100	H	1.96794700	1.86268700	2.59786200
C	-3.06984900	-3.29425300	-1.20637600	H	0.40386400	2.68832200	2.38735400
H	-1.99078200	-3.08883100	-1.15943100	C	5.38822300	-2.85675700	0.58538400
H	-3.21228000	-4.38613600	-1.22304700	H	5.60016100	-3.91611300	0.80322300
H	-3.45702500	-2.89104300	-2.15536200	H	5.85911300	-2.59994700	-0.37585300
C	-3.20315600	-3.23980300	1.30328100	H	5.85859800	-2.24195300	1.36797000
H	-3.31589200	-4.33469000	1.33712800	C	3.25124600	-2.99636900	1.89145500
H	-2.13310400	-2.99857500	1.38055100	H	3.65659200	-2.37360300	2.70409300
H	-3.71361200	-2.82265600	2.18604500	H	2.15979100	-2.87678200	1.87897700
C	-5.29804300	-3.03201100	-0.07374400	H	3.47922600	-4.04742700	2.12924000
H	-5.74780700	-2.64591100	-1.00159500	C	3.25263100	-3.49297900	-0.56738200
H	-5.43731600	-4.12486200	-0.05130800	H	2.16032300	-3.38333900	-0.59994600
H	-5.84625900	-2.59712900	0.77624100	H	3.65496300	-3.23043900	-1.55831200
C	-1.16862100	-0.59804100	-3.29516000	H	3.48584700	-4.55330100	-0.38161300
H	-1.77661600	-1.37432200	-2.81707200	C	3.25267100	3.49297900	0.56734900
H	-1.69766300	0.35779200	-3.19643500	H	2.16036300	3.38334900	0.59994000

H	3.65502600	3.23042200	1.55826500	H	3.47920000	4.04746600	-2.12926800
H	3.48589200	4.55330200	0.38158800	C	5.38822700	2.85675300	-0.58547900
C	3.25122000	2.99640600	-1.89149600	H	5.60017000	3.91610900	-0.80331000
H	3.65654000	2.37365200	-2.70415600	H	5.85913800	2.59992500	0.37574300
H	2.15976400	2.87682600	-1.87899100	H	5.85857800	2.24195500	-1.36808400

Cartesian Coordinates of 10:

Thermal enthalpy H / a.u. -9519.002017

Pd	-0.03531300	-0.63930900	-0.32166300	C	5.28675400	0.86698600	1.89041400
Pd	-2.63399100	-0.07415600	-0.18352700	C	5.68038800	-1.83926200	0.93530200
Pd	2.63986200	-0.34503400	0.12760900	C	0.41274800	-2.75451100	2.90731400
Co	-0.26459000	-3.39215700	-0.29333600	C	2.63360300	-4.47955800	-1.65823200
P	1.31293600	1.43667500	-0.31949000	C	-1.06972200	-2.33289000	-3.40969700
P	-2.11999600	-2.22826600	-0.60145400	C	-3.23639600	-4.60732600	0.89757600
P	1.66072100	-2.37347800	0.23047000	P	1.54042700	4.31619100	1.39530500
P	-1.09795200	1.55469200	-0.45761300	P	-1.15122200	4.71968900	1.06163700
P	-4.78995500	0.32404000	0.35743600	C	-0.02691900	3.58888700	1.92883400
P	4.85332800	-0.26646500	0.53096400	C	0.42160300	5.33163400	0.41447900
P	-1.60400400	-4.66971600	-1.58332800	C	2.12727000	2.71873100	-2.75202800
P	0.99174000	-4.89987000	0.82072600	C	-1.46719100	2.90524400	-3.01478100
C	0.79498700	-3.25668400	1.52657600	C	-4.73862000	3.08142400	0.28280600
C	1.73726200	-3.96965100	-0.54857000	C	-6.55115500	2.09655800	-1.02268400
C	-1.34507500	-2.95412500	-2.05064900	C	-4.14475000	-0.32391500	2.99101100
C	-2.30539100	-3.92346200	-0.08619800	C	-6.17708500	0.99936200	2.73335700
Co	0.16790400	3.25699400	-0.06298000	C	-5.68354500	-1.38035800	-1.62972100
C	0.94877900	2.39613200	-1.81947500	C	-6.97394500	-1.51341000	0.43517000
C	-0.48893100	2.44146000	-1.91936600	C	6.60682400	1.49180500	-0.85145600
C	0.00871400	-1.23458000	-3.36678000	C	5.47465800	-0.21745300	-2.17387800
C	-0.63220000	-1.62798700	2.81258900	C	4.53640000	2.05795000	2.01419600
C	-5.44593200	1.94138700	-0.16441800	C	6.33424200	0.60201600	2.79715300
C	-5.06955500	0.33811400	2.15893800	C	6.89356100	-2.24554800	0.34330100
C	-5.93244600	-0.92929400	-0.31337000	C	5.02898700	-2.69522100	1.85053500
C	5.74596300	0.37845700	-0.92134200	C	-0.12779700	-3.91220900	3.76903700

C	1.68951500	-2.18663600	3.57515300	C	-6.24555800	4.51627700	-0.97532400
C	4.00322400	-4.81271100	-1.01094900	C	-5.44561100	0.29881200	4.94930400
C	2.86572200	-3.39857900	-2.72897700	C	-7.52095100	-2.96393700	-1.44656200
C	2.03605500	-5.75193100	-2.29046800	C	6.91988800	1.40626200	-3.26713600
C	-0.65583700	-3.43473900	-4.40679800	C	5.88596800	2.71443000	3.92906100
C	-2.39975200	-1.69283800	-3.88429000	C	6.79607100	-4.34429100	1.58057300
C	-3.62869500	-3.68348900	2.06257000	H	-0.29256900	-0.40297900	-2.69465700
C	-2.61165500	-5.91909100	1.41184300	H	-0.26683700	-0.80896400	2.15977200
C	-4.53343500	-4.93441700	0.10817200	H	0.17816900	-0.81226300	-4.37941700
C	-0.26210800	2.63451300	3.08184000	H	0.96684400	-1.62413900	-2.98510400
C	0.75557900	6.67205800	-0.22156300	H	-0.86608700	-1.20552600	3.81213400
C	3.37059200	3.05431800	-1.89489100	H	-1.55905100	-2.00495200	2.34721900
C	1.90753800	3.89519700	-3.71990800	H	-2.76622000	-3.44257500	2.71016300
C	2.42379200	1.42599100	-3.55462800	H	-4.40636000	-4.15870100	2.69534700
C	-1.16843700	2.16323800	-4.33689300	H	-4.04677300	-2.73326300	1.67358000
C	-2.91082500	2.53925200	-2.60844100	H	-2.35683300	-6.59205800	0.56662900
C	-1.43767100	4.43207700	-3.20266200	H	-3.31499800	-6.45781000	2.08139500
C	-5.14319200	4.36226900	-0.11218800	H	-1.67155700	-5.72301400	1.96308600
C	-6.94415000	3.38495000	-1.42994700	H	-4.99279900	-4.00732000	-0.29057100
C	-4.33561100	-0.34957200	4.38089000	H	-5.27635600	-5.43691400	0.76368900
C	-6.36284800	0.97656200	4.12460800	H	-4.31595100	-5.60240800	-0.75051900
C	-6.48191400	-2.38279200	-2.19753500	H	-0.42510800	-2.99973700	-5.40151500
C	-7.76064100	-2.53172200	-0.13143700	H	-1.46562200	-4.18241000	-4.53402200
C	7.18751800	2.00462200	-2.02435300	H	0.24394300	-3.97509300	-4.05182400
C	6.06630300	0.28884900	-3.33892100	H	-2.69924000	-0.87883800	-3.18940300
C	4.84279200	2.98174200	3.02328300	H	-3.21562700	-2.44460100	-3.90346500
C	6.62689800	1.52437000	3.81657400	H	-2.29481200	-1.25906400	-4.90104900
C	7.44292100	-3.50019500	0.66192100	H	-3.84542700	2.96154000	0.91743300
C	5.59019000	-3.93578700	2.18040100	H	-4.57340700	5.23742300	0.23710900
C	-1.61702100	1.91407100	2.96149500	H	-6.55519400	5.52205800	-1.29991600
C	0.88693600	1.61038200	3.17487400	H	-7.80462400	3.50297300	-2.10737900
C	-0.26999200	3.49349900	4.37460500	H	-7.10130100	1.21046600	-1.37502800
C	0.76585100	7.70595900	0.93802100	H	-3.26270100	-0.79943100	2.53888500
C	-0.29454400	7.11264900	-1.25696900	H	-3.60498100	-0.86812600	5.02089300
C	2.15474900	6.64365900	-0.86564500	H	-5.59237200	0.28690000	6.04073600

H	-7.22598800	1.49604100	4.56970200	H	5.07053500	-4.59805000	2.89002200
H	-6.88449200	1.54272800	2.08797800	H	4.06528800	-2.38997400	2.28360500
H	-4.83791900	-0.95620300	-2.19396600	H	3.21261100	3.97810200	-1.30667100
H	-6.27725400	-2.72904000	-3.22237300	H	4.26023100	3.18550900	-2.54402000
H	-8.13405100	-3.76728600	-1.88370500	H	3.60310700	2.23745400	-1.18330600
H	-8.56303300	-2.99496900	0.46381600	H	1.62605400	4.81347700	-3.16950700
H	-7.15924000	-1.18490600	1.46891500	H	1.12510700	3.69237600	-4.47346300
H	4.45647100	-3.90300900	-0.56775400	H	2.85011700	4.10378700	-4.26728000
H	4.70765200	-5.22103700	-1.76658900	H	3.32211300	1.56171700	-4.19216700
H	3.88893100	-5.55907300	-0.19875800	H	1.56958600	1.14644900	-4.20080500
H	1.95258100	-3.21654300	-3.32192100	H	2.61352800	0.57822300	-2.86369500
H	3.67546100	-3.69964500	-3.42564400	H	-0.16079700	2.38480300	-4.73373400
H	3.15780100	-2.43685900	-2.25367800	H	-1.91005900	2.45436000	-5.11015800
H	1.88352700	-6.53932000	-1.52276900	H	-1.24002700	1.06919900	-4.18900100
H	2.70978600	-6.16105600	-3.07252600	H	-3.04711600	1.44254300	-2.49913900
H	1.04661700	-5.54305100	-2.74375600	H	-3.62758400	2.90252600	-3.37308100
H	-1.02617100	-4.36971900	3.31167600	H	-3.18790000	3.00840300	-1.64542800
H	-0.40652300	-3.55042600	4.78090100	H	-1.76456900	4.92201300	-2.26605100
H	0.63381300	-4.71115300	3.88557600	H	-2.12499400	4.73769500	-4.01969600
H	2.46539600	-2.97416200	3.66814000	H	-0.42747100	4.80356600	-3.44255300
H	1.46679300	-1.80016200	4.59171700	H	-0.22745900	7.75258000	1.42986100
H	2.10897800	-1.35168100	2.97406000	H	1.01762800	8.71969800	0.55854400
H	6.81060900	1.96490600	0.12069600	H	1.51196300	7.42422200	1.70923700
H	7.85182700	2.88099500	-1.96499500	H	-0.25390300	6.48093400	-2.16200000
H	7.37281100	1.81359400	-4.18456900	H	-0.12299500	8.16594700	-1.56344600
H	5.84805700	-0.18069100	-4.31063200	H	-1.32066700	7.04449200	-0.83707800
H	4.78203900	-1.07231800	-2.22790200	H	2.92411600	6.30772800	-0.13834500
H	3.69920700	2.25667100	1.32413100	H	2.44535900	7.65253800	-1.22640000
H	4.24660200	3.90488500	3.10098100	H	2.18062900	5.95012800	-1.72723000
H	6.11858400	3.43342500	4.73038100	H	-2.44774900	2.63587100	2.81383200
H	7.44021800	1.31077100	4.52798200	H	-1.83975800	1.33348000	3.87939900
H	6.91603400	-0.32821500	2.70750800	H	-1.63118300	1.21286400	2.10350800
H	7.40168100	-1.58543000	-0.37609000	H	0.91379200	0.95434200	2.28269200
H	8.38353700	-3.81989800	0.18649900	H	0.77456100	0.96527700	4.07018500
H	7.22659000	-5.32855500	1.82229300	H	1.87215400	2.11617000	3.24357800

H	0.69267000	4.03213800	4.49394300	H	-1.08164800	4.24905800	4.33878600
H	-0.42625500	2.85361800	5.26911700				

4.5 References

- 1 K. B. Dillon, F. Mathey, J. F. Nixon, *Phosphorus: The Carbon Copy*, Wiley, Chichester, **1998**.
- 2 Reviews on Diphosphacyclobutadiene Complexes: a) A. Chirila, R. Wolf, J. C. Slootweg, K. Lammertsma, *Coord. Chem. Rev.* **2014**, 270-271, 57; b) F. Mathey, *Angew. Chem. Int. Ed.* **2003**, 42, 1578–1604; c) M. Regitz, *Chem. Rev.* **1990**, 90, 191–213; d) M. Regitz, P. Binger, *Angew. Chem. Int. Ed. Engl.* **1988**, 27, 1484–1508; e) J. F. Nixon, *Chem. Rev.* **1988**, 88, 1327–1362.
- 3 a) M. T. Nguyen, L. Landuyt, L. G. Vanquickenborne, *J. Org. Chem.* **1993**, 58, 2817–2821; b) S. Creve, M. T. Nguyen, L. G. Vanquickenborne, *Eur. J. Inorg. Chem.* **1999**, 1999, 1281–1289; c) T. Höltzl, D. Szieberth, M. T. Nguyen, T. Veszprémi, *Chem. Eur. J.* **2006**, 12, 8044–8055.
- 4 Selected examples for 1,3-diphosphacyclobutadiene complexes: a) P. Binger, R. Milczarek, R. Mynott, M. Regitz, W. Rösch, *Angew. Chem.* **1986**, 98, 645–646; *Angew. Chem. Int. Ed. Engl.* **1986**, 25, 644–645; b) P. B. Hitchcock, M. J. Maah, J. F. Nixon, *J. Chem. Soc., Chem. Commun.* **1986**, 737–738; c) P. Binger, R. Milczarek, R. Mynott, C. Krüger, Y. H. Tsay, E. Raabe, M. Regitz, *Chem. Ber.* **1988**, 121, 637–645; d) P. Binger, B. Biedenbach, R. Schneider, M. Regitz, *Synthesis* **1989**, 960–961.
- 5 a) Analogous rhodium(I) and iridium(I) compounds [$\text{CpM}(\eta^4\text{-P}_2\text{C}_2\text{tBu}_2)$] (M = Rh, Ir) and coordination compounds of [$\text{CpCo}(\eta^4\text{-P}_2\text{C}_2\text{tBu}_2)$]: a) P. Binger, B. Biedenbach, R. Mynott, C. Krüger, P. Betz, M. Regitz, *Angew. Chem.* **1988**, 100, 1219–1221; *Angew. Chem. Int. Ed. Engl.* **1988**, 27, 1157–1158; b) P. Binger, B. Biedenbach, R. Mynott, R. Benn, A. Ruffínska, P. Betz, C. Krüger, *J. Chem. Soc., Dalton Trans.* **1990**, 1771–1777; c) P. B. Hitchcock, M. J. Maah, J. F. Nixon, *Heteroatom. Chem.* **1991**, 2, 253–264; d) A. G. Avent, F. G. N. Cloke, K. R. Flower, P. B. Hitchcock, J. F. Nixon, D. M. Vickers, *Angew. Chem.* **1994**, 106, 2406–2408; *Angew. Chem. Int. Ed. Engl.* **1994**, 33, 2330–2332; e) D. Böhm, F. Knoch, S. Kummer, U. Schmidt, U. Zenneck, *Angew. Chem.* **1995**, 107, 251–254; *Angew. Chem. Int. Ed. Engl.* **1995**, 34, 198–201; f) P. A. Arnold, F. G. N. Cloke, P. B. Hitchcock, J. F. Nixon, *J. Am. Chem. Soc.* **1996**, 118, 7630–7631; g) M. Scheer, J. Krug, *Z. Anorg. Allg. Chem.* **1998**, 624, 399–405; h) F. W. Heinemann, S. Kummer, U. Seiss-Brandl, U. Zenneck, *Organometallics* **1999**, 18, 2021–2029; i) F. G. N. Cloke, P. B. Hitchcock, J. F. Nixon, D. M. Vickers, *J. Organomet. Chem.* **2001**, 635, 212–221; h) A. D. Burrows, A. Dransfeld, M. Green, J. C. Jeffery, C. Jones, J. M. Lyman, M. T. Nguyen, *Angew. Chem.* **2001**, 113, 3321–3324; *Angew. Chem. Int. Ed.* **2001**, 40, 3221–3224; j) C. Topf, T. Clark, F. W. Heinemann, M. Hennemann, S. Kummer, H. Pritzkow, U. Zenneck, *Angew. Chem.* **2002**, 114, 4221–4226; *Angew. Chem. Int. Ed.* **2002**, 41, 4047–4052; k) D. Himmel, M. Seitz, M. Scheer, *Z. Anorg. Allg. Chem.* **2004**, 630, 1220–1228; l) E.-M. Rummel, M. Eckhardt, M. Bodensteiner, E. V. Peresyphkina, W. Kremer, C. Gröger, M. Scheer, *Eur. J. Inorg. Chem.* **2014**, 1625–1637.
- 6 1,2-Diphosphacyclobutadiene complexes: a) P. Binger, G. Glaser, S. Albus, C. Krüger, *Chem. Ber.* **1995**, 128, 1261–1265; b) F. W. Heinemann, S. Kummer, U. Seiss-Brandl, U. Zenneck, *Organometallics* **1999**, 18, 2021–2029; c) P. Kramkowski, M. Scheer, *Eur. J.*

- Inorg. Chem.* **2000**, 1869–1876; d) C. Jones, C. Schulten, A. Stasch, *Dalton Trans.* **2006**, 3733–3735; e) E.-M. Rummel, G. Balazs, V. Heintl, M. Scheer, *Angew. Chem.* **2017**, *129*, 9720–9725; *Angew. Chem. Int. Ed.* **2017**, *56*, 9592–9596.
- 7 a) R. Wolf, A. W. Ehlers, J. C. Slootweg, M. Lutz, D. Gudat, M. Hunger, A. L. Spek, K. Lammertsma, *Angew. Chem.* **2008**, *120*, 4660–4663; *Angew. Chem. Int. Ed.* **2008**, *47*, 4584–4587; b) R. Wolf, J. C. Slootweg, A. W. Ehlers, F. Hartl, B. de Bruin, M. Lutz, A. L. Spek, K. Lammertsma, *Angew. Chem.* **2009**, *121*, 3150–3153; *Angew. Chem. Int. Ed.* **2009**, *48*, 3104–3107; c) R. Wolf, E.-M. Schnöckelborg, *Chem. Commun.* **2010**, *46*, 2832–2834, d) R. Wolf, A. W. Ehlers, M. M. Khusniyarov, F. Hartl, B. de Bruin, G. J. Long, F. Grandjean, F. M. Schappacher, R. Pöttgen, J. C. Slootweg, M. Lutz, A. L. Spek, K. Lammertsma, *Chem. Eur. J.* **2010**, *16*, 14322–14334.
- 8 a) W. W. Brennessel, J. V. G. Young, J. E. Ellis, *Angew. Chem.* **2002**, *114*, 1259–1263; *Angew. Chem. Int. Ed.* **2002**, *41*, 1211–1215; b) W. W. Brennessel, R. E. Jilek, J. E. Ellis, *Angew. Chem.* **2007**, *119*, 6244–6248; *Angew. Chem. Int. Ed.* **2007**, *46*, 6132–6136; c) W. W. Brennessel, J. E. Ellis, *Inorg. Chem.* **2012**, *51*, 9076–9094.
- 9 a) J. Malberg, T. Wiegand, H. Eckert, M. Bodensteiner, R. Wolf, *Chem. Eur. J.* **2013**, *19*, 2356–2369; b) T. Wiegand, H. Eckert, S. Grimme, J. Malberg, R. Wolf, *Solid State Nucl. Magn. Reson.* **2013**, *53*, 13–19; c) J. Malberg, T. Wiegand, H. Eckert, M. Bodensteiner, R. Wolf, *Eur. J. Inorg. Chem.* **2014**, 1638–1651; d) J. Malberg, M. Bodensteiner, D. Paul, T. Wiegand, H. Eckert, R. Wolf, *Angew. Chem.* **2014**, *126*, 2812–2816; *Angew. Chem. Int. Ed.* **2014**, *53*, 2771–2775.
- 10 C. Rödl, R. Wolf, *Eur. J. Inorg. Chem.* **2016**, *2016*, 736–742.
- 11 a) H. Werner, A. Salzer, *Synthesis and Reactivity in Inorganic and Metal-Organic Chemistry* **1972**, *2*, 239–248; b) A. Salzer, H. Werner, *Angew. Chem. Int. Ed. Engl.* **1972**, *11*, 930–932.
- 12 H. Aktas, J. C. Slootweg, K. Lammertsma, *Angew. Chem.* **2010**, *122*, 2148–2159; *Angew. Chem. Int. Ed.* **2010**, *49*, 2102–2113.
- 13 Reviews on Metallophosphaalkene Complexes: a) L. Weber, *Coord. Chem. Rev.* **2005**, *249*, 741–763; b) L. Weber, *Angew. Chem. Int. Ed. Engl.* **1996**, *35*, 271–288.
- 14 a) E. Niecke, H.-J. Metternich, M. Nieger, D. Gudat, P. Wenderoth, W. Malisch, C. Hahner, W. Reich, *Chem. Ber.* **1993**, *126*, 1299–1309; b) D. Gudat, M. F. Meidine, J. F. Nixon, E. Niecke, *J. Chem. Soc., Chem. Commun.* **1989**, 1206–1208; c) D. Gudat, E. Niecke, *J. Chem. Soc., Chem. Commun.* **1987**, 10–11.
- 15 P. Pyykkö, M. Atsumi, *Chem. Eur. J.* **2009**, *15*, 186–197.
- 16 a) P. Scherl, A. Kruckenberg, S. Mader, H. Wadehohl, L. H. Gade, *Organometallics* **2012**, *31*, 7024–7027; b) J. Baraut, A. Massard, F. Chotard, E. Bodio, M. Picquet, P. Richard, Y. Borguet, F. Nicks, A. Demonceau, P. Le Gendre, *Eur. J. Inorg. Chem.* **2015**, *2015*, 2671–2682; c) S. H. Schlindwein, S. Hänisch, M. Nieger, D. Gudat, *Eur. J. Inorg. Chem.* **2017**, *2017*, 3834–3842.

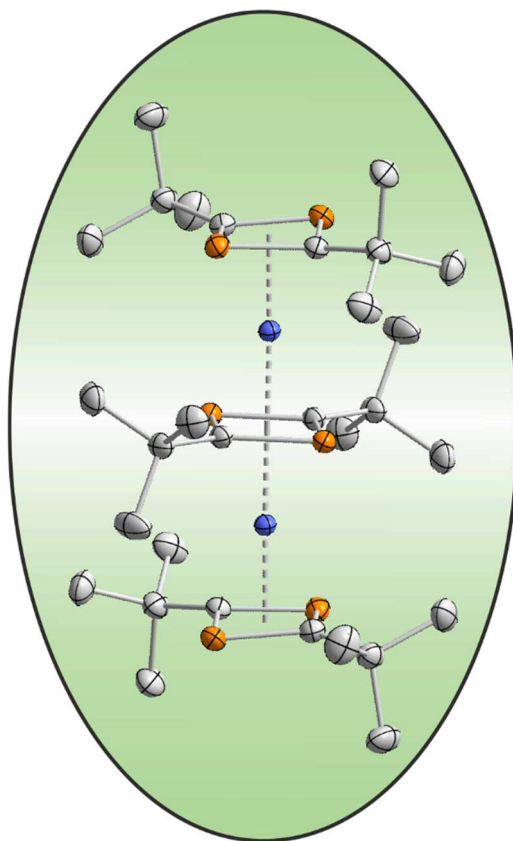
- 17 a) O. J. Scherer, H. Sitzmann, G. Wolmershäuser, *J. Organomet. Chem.* **1984**, 268, C9–C12; b) L. Y. Goh, C. K. Chu, R. C. S. Wong, T. W. Hambley, *J. Chem. Soc., Dalton Trans.* **1989**, 1951–1956; c) M. E. Barr, L. F. Dahl, *Organometallics* **1991**, 10, 3991–3996; d) M. Herberhold, G. Frohmader, W. Milius, *J. Organomet. Chem.* **1996**, 522, 185–196; e) J. Bai, E. Leiner, M. Scheer, *Angew. Chem.* **2002**, 114, 820–823; *Angew. Chem. Int. Ed.* **2002**, 41, 1737–1740; f) C. C. Cummins, *Angew. Chem.* **2006**, 118, 876–884; *Angew. Chem. Int. Ed.* **2006**, 45, 862–870; g) M. Scheer, *Dalton Trans.* **2008**, 4372–4386; h) B. Zarzycki, T. Zell, D. Schmidt, U. Radius, *Eur. J. Inorg. Chem.* **2013**, 2013, 2051–2058; i) M. E. Moussa, B. Attenberger, M. Fleischmann, A. Schreiner, M. Scheer, *Eur. J. Inorg. Chem.* **2016**, 2016, 4538–4541.
- 18 a) W. Trakarnpruk, A. M. Arif, R. D. Ernst, *Organometallics* **1994**, 13, 2423–2429; b) T. Takao, M. Moriya, M. Kajigaya, H. Suzuki, *Organometallics* **2010**, 29, 4770–4773.
- 19 Radius and co-workers synthesized $[\{\text{Ni}(\text{Im}^{\text{iPr}})_2\}_2(\mu:\eta^4:\eta^4\text{-P}_2\text{C}_2\text{tBu}_2)]$ (Im^{iPr} = 1,3-di(iso-propyl)imidazole-2-ylidene) by prolonged heating of the mononuclear complex $[\text{Ni}(\text{Im}^{\text{iPr}})_2(\eta^2\text{-PCtBu})]$ in toluene at 100 °C. The structure of this complex was proposed based on NMR data: T. Schaub, U. Radius, *Z. Anorg. Allg. Chem.* **2006**, 632, 981–984.
- 20 D. Patel, J. McMaster, W. Lewis, A. J. Blake, S. T. Liddle, *Nature Comm.* **2013**, 4, 3323.
- 21 The dicobalt complex $[\{\text{Cp}^{\text{''Co}}\}_2(\mu:\eta^4:\eta^4\text{-P}_2\text{C}_2\text{Me}_2)]$ (**K**, $\text{Cp}^{\text{''Co}}$ = 1,2,4-(*t*Bu)₃C₅H₂) was obtained by Rummel and Scheer via the reaction of $[\{\text{Cp}^{\text{''Co}}\}_2(\mu:\eta^6:\eta^6\text{-C}_7\text{H}_8)]$ (C_7H_8 = toluene) with two equivalents of $\text{MeC}\equiv\text{P}$. This complex appears to be a minor product though (thus, no yield was given); the mononuclear species $[\text{Cp}^{\text{''Co}}(\eta^4\text{-P}_2\text{C}_2\text{Me}_2)]$ was identified as the major product: E.-M. Rummel, *PhD Dissertation*, University of Regensburg., Germany, **2016**.
- 22 The $^{13}\text{C}\{^1\text{H}\}$ NMR spectrum was not informative due to overlap of numerous signals and the observation of very broad resonances. The signals for the quaternary carbon atoms of the P_2C_2 moiety were not detected.
- 23 a) T. Steinke, C. Gemel, M. Winter, R. A. Fischer, *Angew. Chem. Int. Ed.* **2002**, 41, 4761–4763; b) A. M. Williamson, G. R. Owen, D. M. P. Mingos, R. Vilar, A. J. P. White, D. J. Williams, *Dalton Trans.* **2003**, 0, 2526–2532; c) M. Tanabe, N. Ishikawa, M. Chiba, T. Ide, K. Osakada, T. Tanase, *J. Am. Chem. Soc.* **2011**, 133, 18598–18601; d) J. R. Cabrera-Pardo, A. Trowbridge, M. Nappi, K. Ozaki, M. J. Gaunt, *Angew. Chem. Int. Ed.* **2017**, 56, 11958–11962.
- 24 A $J(^{31}\text{P}, ^{31}\text{P})$ coupling constant of less than 5 Hz was assumed for the coupling between the P atoms of the 2,5-diphospha-1-rhodacycle in **G** (see Ref. 5b).
- 25 G. Becker, G. Gresser, W. Uhl, *Z. Naturforsch. B* **1981**, 36, 16–19.
- 26 T. Allspach, M. Regitz, G. Beckerr, W. Becker, *Synthesis* **1986**, 31–36.
- 27 T. Wettling, J. Schneider, O. Wagner, C. G. Kreiter, M. Regitz, *Angew. Chem. Int. Ed. Engl.* **1989**, 28, 1013–1014.

- 28 a) SCALE3ABS, CrysAlisPro, Agilent Technologies Inc., Oxford, GB, **2015**; b) G. M. Sheldrick, SADABS, Bruker AXS, Madison, USA, **2007**.
- 29 G. M. Sheldrick, *Acta Cryst.* **2015**, *A71*, 3.
- 30 G. M. Sheldrick, *Acta Cryst.* **2015**, *C71*, 3.
- 31 Gaussian 09, Revision E.01: M. J. Frisch, G. W. Trucks, H. B. Schlegel, G. E. Scuseria, M. A. Robb, J. R. Cheeseman, G. Scalmani, V. Barone, G. A. Petersson, H. Nakatsuji, X. Li, M. Caricato, A. Marenich, J. Bloino, B. G. Janesko, R. Gomperts, B. Mennucci, H. P. Hratchian, J. V. Ortiz, A. F. Izmaylov, J. L. Sonnenberg, D. Williams-Young, F. Ding, F. Lipparini, F. Egidi, J. Goings, B. Peng, A. Petrone, T. Henderson, D. Ranasinghe, V. G. Zakrzewski, J. Gao, N. Rega, G. Zheng, W. Liang, M. Hada, M. Ehara, K. Toyota, R. Fukuda, J. Hasegawa, M. Ishida, T. Nakajima, Y. Honda, O. Kitao, H. Nakai, T. Vreven, K. Throssell, J. A. Montgomery, Jr., J. E. Peralta, F. Ogliaro, M. Bearpark, J. J. Heyd, E. Brothers, K. N. Kudin, V. N. Staroverov, T. Keith, R. Kobayashi, J. Normand, K. Raghavachari, A. Rendell, J. C. Burant, S. S. Iyengar, J. Tomasi, M. Cossi, J. M. Millam, M. Klene, C. Adamo, R. Cammi, J. W. Ochterski, R. L. Martin, K. Morokuma, O. Farkas, J. B. Foresman, and D. J. Fox, Gaussian, Inc., Wallingford CT, **2016**.
- 32 a) A. D. Becke, *Phys. Rev. A* **1988**, *38*, 3098; b) J. P. Perdew, *Phys. Rev. B* **1986**, *33*, 8822.
- 33 a) A. Schäfer, C. Huber, R. Ahlrichs, *J. Chem. Phys.* **1994**, *100*, 5829; b) F. Weigend, *Phys. Chem. Chem. Phys.* **2006**, *8*, 1057.
- 34 a) S. Grimme, S. Ehrlich, L. Goerigk, *J. Comput. Chem.* **2011**, *32*, 1456. b) S. Grimme, J. Antony, S. Ehrlich, H. Krieg, *J. Chem. Phys.* **2010**, *132*, 154104.
- 35 D. Andrae, U. Häußermann, M. Dolg, H. Stoll, H. Preuß, *Theor. Chim. Acta* **1990**, *77*, 123.
- 36 a) C. Lee, W. Yang, R. G. Parr, *Phys. Rev. B* **1988**, *37*, 785; b) P. J. Stephens, F. J. Devlin, C. F. Chabalowski, M. J. Frisch, *J. Phys. Chem.* **1994**, *98*, 11623.
- 37 GaussView 5.0.9: R. Dennington, T. A. Keith, J. M. Millam, Semicem Inc., Shawnee Mission, KS, **2016**.
- 38 NBO6.0: E. D. Glendening, J. K. Badenhoop, A. E. Reed, J. E. Carpenter, J. A. Bohmann, C. M. Morales, C. R. Landis, and F. Weinhold, Theoretical Chemistry Institute, University of Wisconsin, Madison, **2013**.

5 A HOMOLEPTIC 1,3-DIPHOSPHACYCLOBUTADIENE

TRIPLEDECKER COMPLEX^[a,b]

CHRISTIAN RÖDL AND ROBERT WOLF



[a] Unpublished results.

[b] C. Rödl performed all experiments and theoretical calculations and wrote the manuscript. R. Wolf supervised the project.

5.1 Introduction

Compared to the vast literature on mononuclear sandwich molecules such as ferrocene $[\text{Fe}(\eta^5\text{-C}_5\text{H}_5)_2]$ and its derivatives,¹ related tripledecker complexes have attracted comparatively less attention. According to the classic definition, a tripledecker complex features two metal atoms and three π -coordinated π -hydrocarbon ligands with the middle-deck atoms equally bonding to both metal atoms.^{2,3} Such species are of special interest because the two metal atoms are connected by π -coordinated ligand which should enable a strong electronic interaction. The first tripledecker, $[\text{Ni}_2\text{Cp}_3]^+$ (**A**, Cp = $\eta^5\text{-C}_5\text{H}_5$, Figure 1) was reported by Werner and Salzer in 1972,² i.e. twenty years after the ferrocene was first described.¹ The tripledecker family has grown since then, nonetheless, the number of examples is still dwindling compared to the countless derivatives of ferrocene and related sandwich molecules. Figure 1 shows a few selected milestones in the area, which include the first tripledecker complex with a bridging benzene ring, $[(\text{CpV})_2\{\mu\text{:}\eta^6\text{:}\eta^6\text{-C}_6\text{H}_6\}]$ (**B**) described by Jonas and co-workers,⁴ borole complexes (**C** and **D**) developed by the groups of Russel and Siebert,^{5,6} and complexes with polyphosphorus ligands as the middle-deck such as **E** and **F** reported by Scherer and co-workers.^{7,8}

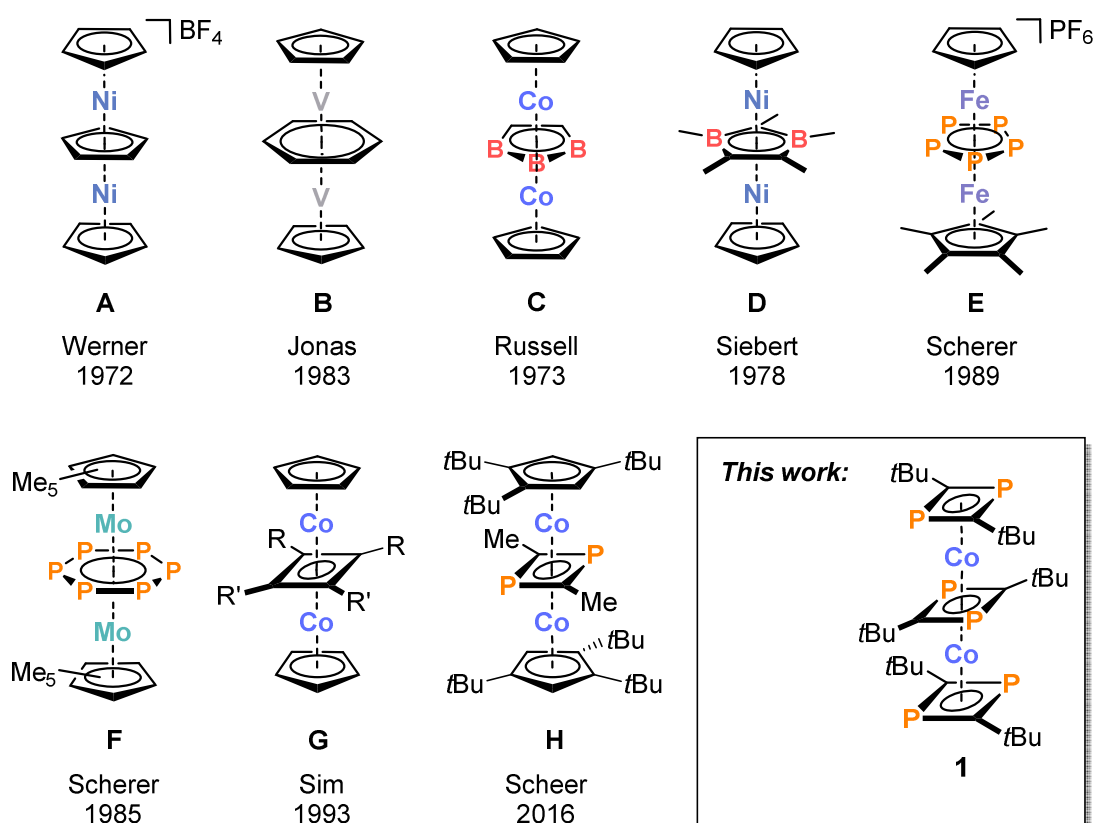


Figure 1. Selected examples of tripledecker complexes; for **G**: R = R' = Et and R = Me, R' = *n*Pr.

Tripledecker compounds with a cyclobutadiene middle-deck are rare and limited to two (thermally unstable) complexes of type **G**,⁹ which have not been structurally characterized though, and the structurally characterized 1,3-diphosphacyclobutadiene complex **H** reported by

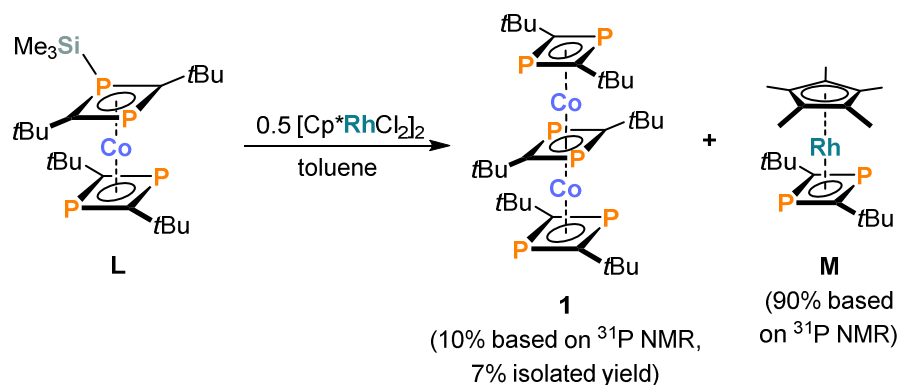
Rummel and Scheer.¹⁰ The latter complex was only partially characterized by X-ray analysis and mass spectrometry as it is a minor product of the reaction of $[\{\text{Cp}^{\text{III}}\text{Co}\}_2(\mu\text{:}\eta^6\text{:}\eta^6\text{-C}_7\text{H}_8)]$ (C_7H_8 = toluene) with two equivalents of $\text{Me-C}\equiv\text{P}$ with mononuclear $[\text{Cp}^{\text{III}}\text{Co}(\eta^4\text{-P}_2\text{C}_2\text{Me}_2)]$ formed as the major product. Finally, two related examples with an “inverted sandwich” structure containing a 1,3-diphosphacyclobutadiene middle-deck are noteworthy:

$[\{\text{Ni}(\text{Im}^{\text{iPr}})_2\}_2(\mu\text{:}\eta^4\text{:}\eta^4\text{-P}_2\text{C}_2\text{tBu}_2)]$ (Im^{iPr} = 1,3-di(*iso*-propyl)imidazolin-2-ylidene)¹¹ and $([\{\text{U}(\text{Ts}^{\text{Tol}})\}_2(\mu\text{:}\eta^4\text{:}\eta^4\text{-P}_2\text{C}_2\text{tBu}_2)]$ (Ts^{Tol} = tris(*N*-tolyl-amidodimethylsilyl)methane)¹² do not formally represent tripledecker complexes according to the definition outlined above, but they also contain a bridging and π -coordinated 1,3-diphosphacyclobutadiene ligand prepared by metal-mediated phosphalkyne dimerization from *t*Bu-C \equiv P and nickel(0) and uranium(III) precursors.

The above-mentioned literature indicates that the structural variety of tripledecker molecules is still small even after decades of research. Indeed, Werner’s classic complex **A** still remains the single example of a tripledecker complex containing just one type of ligand. This paucity of *homoleptic* tripledecker complexes motivated the present investigation of the synthesis of further homoleptic 1,3-diphosphacyclobutadiene tripledecker complexes using the $[\text{Co}(\eta^4\text{-P}_2\text{C}_2\text{tBu}_2)_2]^-$ sandwich anion¹³⁻¹⁵ as a building block (see chapters 1 and 4 for further studies into the coordination chemistry of this anion). Here, we report the synthesis of the first homoleptic diphosphacyclobutadiene tripledecker compound, $[\text{Co}_2(\eta^4\text{-P}_2\text{C}_2\text{tBu}_2)_2(\mu\text{:}\eta^4\text{:}\eta^4\text{-P}_2\text{C}_2\text{tBu}_2)]$ (**1**, Figure 1), via an unexpected pathway from $[\text{Co}(\eta^4\text{-P}_2\text{C}_2\text{tBu}_2\text{SiMe}_3)(\eta^4\text{-P}_2\text{C}_2\text{tBu}_2)]$ (**L**)¹⁶ with $[\text{Cp}^*\text{RhCl}_2]_2$ (0.5 equivalents). We describe the structural and spectroscopic characterization of **1** as well as electrochemical properties (ascertained by cyclic voltammetry), and we analyze its electronic structure by DFT calculations.

5.2 Results and Discussion

Reaction of $[\text{Co}(\eta^4\text{-P}_2\text{C}_2\text{tBu}_2\text{SiMe}_3)(\eta^4\text{-P}_2\text{C}_2\text{tBu}_2)]$ (**L**, see chapter 2 of this thesis) with $[\text{Cp}^*\text{RhCl}_2]_2$ (0.5 equivalents, Scheme 1) in toluene affords a forest-green reaction mixture which contains two species according to $^{31}\text{P}\{^1\text{H}\}$ NMR spectroscopic monitoring (in C_6D_6): $[\text{Cp}^*\text{Rh}(\text{P}_2\text{C}_2\text{tBu}_2)]$ (**M**)¹⁷ can be identified as the major species by a singlet at 39.5 ppm and **1** as the minor species by a set of two singlets at $\delta = 55.7$ and 111.1 ppm in a 2:1 ratio. The complexes are present in 9:1 ratio according to $^{31}\text{P}\{^1\text{H}\}$ NMR integration. Whereas it proved to be impossible to separate the two compounds by fractional crystallization due to their very similar solubilities (both compounds are soluble in *n*-hexane, diethyl ether, benzene, toluene, and THF), they could be separated by column chromatography over Alumina N and *n*-hexane as eluent (see the Supporting Information for details), which afforded a forest-green solid as raw product.

Scheme 1. Synthesis of **1**.

Crystalline **1** was isolated by recrystallization from *n*-pentane at $-35\text{ }^\circ\text{C}$ as an NMR spectroscopically pure compound in a yield of 7%. Single-crystal X-ray diffraction (XRD) studies revealed the molecular structure of **1** (Figure 2). Each molecule of **1** resides on a crystallographic inversion center. A dicobalt complex bearing two terminal η^4 -1,3-diphosphacyclobutadienes and one $\mu:\eta^4:\eta^4$ -bridging 1,3-diphosphacyclobutadiene ligand is observed. Structural parameters of the rhombic P_2C_2 core of these ligands are overall similar, but the P–C bond lengths of the bridging P_2C_2 ring are slightly elongated as a result of the coordination to two metal atoms with an average bond length of 1.860(4) Å, whereas the terminal P–C bonds show an average of 1.787(8) Å. This is typical for an inverted sandwich complex with a bridging 1,3-diphosphacyclobutadiene ligand, cf. for the molecular structures of $[\{\text{Ni}(\text{Im}^{i\text{Pr}})_2\}_2(\mu:\eta^4:\eta^4\text{-P}_2\text{C}_2\text{tBu}_2)]$ ($\text{Im}^{i\text{Pr}} = 1,3\text{-di}(\textit{iso}\text{-propyl})\text{imidazolin-2-ylidene}$),¹¹ $[\{\text{U}(\text{Ts}^{\text{Tot}})\}_2(\mu:\eta^4:\eta^4\text{-P}_2\text{C}_2\text{tBu}_2)]$ ($\text{Ts}^{\text{Tot}} = \text{tris}(\textit{N}\text{-tolyl-amidodimethylsilyl})\text{methane}$),¹² and $[\{\text{Cp}^{\text{III}}\text{Co}\}_2(\mu:\eta^4:\eta^4\text{-P}_2\text{C}_2\text{Me}_2)]$ (**H**, $\text{Cp}^{\text{III}} = 1,2,4\text{-}(\textit{tBu})_3\text{-C}_5\text{H}_2$, Figure 1).¹⁰

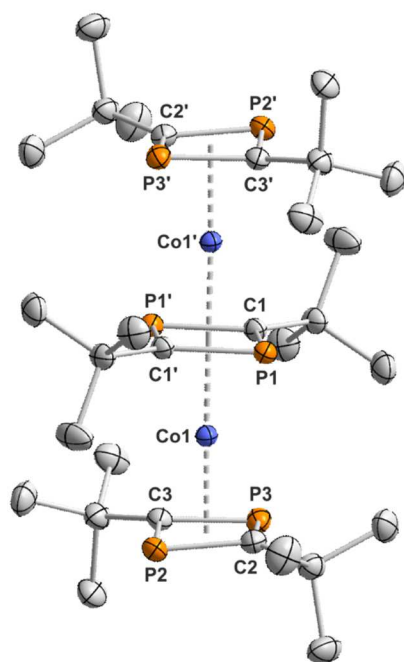


Figure 2. Solid-state molecular structures of **1**. The hydrogen atoms are omitted for clarity. Thermal ellipsoids are drawn at the 50% probability level. Selected bond lengths [Å] and angles [°]: Co1–P1 2.2856(7), Co1–P1' 2.2864(6), Co1–C1 2.141(2), Co1–C1' 2.160(2), Co1–P2 2.2956(7), Co1–P3 2.2715(7), P1–C1 1.861(2), P1–C1' 1.858(2), P2–C2 1.781(2), P2–C3 1.786(2), P3–C2 1.790(2), P3–C3 1.790(2), P2–C3–P3/P3–C2–P2 8.5.

Multinuclear NMR data of **1** in $[D_8]$ THF is in line with the molecular structure determined by X-ray crystallography. The ^1H and $^{13}\text{C}\{^1\text{H}\}$ NMR spectra confirm the presence of two chemically inequivalent two *tert*-butyl groups in the molecule. Moreover, the ^{13}C NMR signal for the quaternary carbon atoms of the terminal and the bridging P_2C_2 rings were detected at $\delta = 114.2$ and 117.7 ppm, respectively. These chemical shifts are in the similar to those of other diphosphacyclobutadiene ligands in cobalt complexes.¹³⁻¹⁵ The $^{31}\text{P}\{^1\text{H}\}$ NMR spectrum of **1** shows two singlets at $\delta = 55.9$ and 111.3 ppm in a 2:1 ratio. As such, the signal at $\delta = 55.9$ ppm is assigned to the terminal ligands, whereas the signal at $\delta = 111.3$ ppm arises from the bridging ligand.

The valence electron count of diamagnetic **1** is 30 in line with empirical and theoretical predictions showing that tripledecker complexes containing 30 or 34 valence electrons are particularly stable structures,¹⁸ while the optimal valence electron count strongly depends on metal atomic number in homobimetallic tripledecker complexes and amounts to 30 for dicobalt complexes.¹⁹ In order to investigate the electronic structure of **1** in more detail, DFT calculations were performed at the BP86-D3BJ/def2-TZVP level.²⁰⁻²² An inspection of the Kohn-Sham molecular orbitals shown in Figure 3 reveals that several of the highest occupied molecular orbitals (HOMOs) are metal-centered, including the HOMO, HOMO–1, and HOMO–3, while the HOMO–2 and HOMO–4 have pronounced P lone pair character. The lowest unoccupied

molecular orbital (LUMO) and the LUMO+1 are also mainly ligand-based, but they also clearly show an antibonding interaction between the bridging ligand and the two metal centers. In line with this, the cyclic voltammogram of **1** (THF/[*n*Bu₄N]PF₆, Figure S5) indicates that a fragmentation reaction occurs upon reduction as indicated by an irreversible reduction process at $E_{pc} = -1.69$ V vs. Fc/Fc⁺, which leads to the formation of the [Co(P₂C₂*t*Bu₂)₂]⁻ sandwich anion. The latter can be identified by a reversible redox wave observed at $E_{1/2} = -0.73$ V vs. Fc/Fc⁺.²³ Finally, TD-DFT calculations have been performed at the B3LYP/def2-TZVP²⁴⁻²² level to analyze the experimental UV/Vis spectrum of **1**, which show two main bands at 403 and 635 nm and a shoulder at 502 nm (see Figure S4 and S6 as well as Table S2). The calculations reproduced the experimental spectrum rather well, but also highlight the composed nature of the observed absorptions. The dominant band at 403 nm is composed of transitions from the HOMO-6 to the LUMO and the HOMO-4 to the LUMO+1 with minor contributions from the HOMO to LUMO transitions. These transitions essentially correspond to MLCT and ILCT type processes. The band at 635 nm mainly originates from transitions from HOMO-9, HOMO-8 HOMO-5 and the HOMO into the LUMO (see Table S2 for further details), which to a first approximation correspond to MLCT transitions. However, it should be noted that clear-cut assignment of the nature of the UV/Vis absorptions is not easily possible in this case, which perhaps illustrates the general limits of the DFT method for the analysis of electronic transitions in such organometallic molecules. Thus, these results should stimulate further theoretical investigations into the electronic structure of **1** using high-level (post Hartree-Fock) calculations.

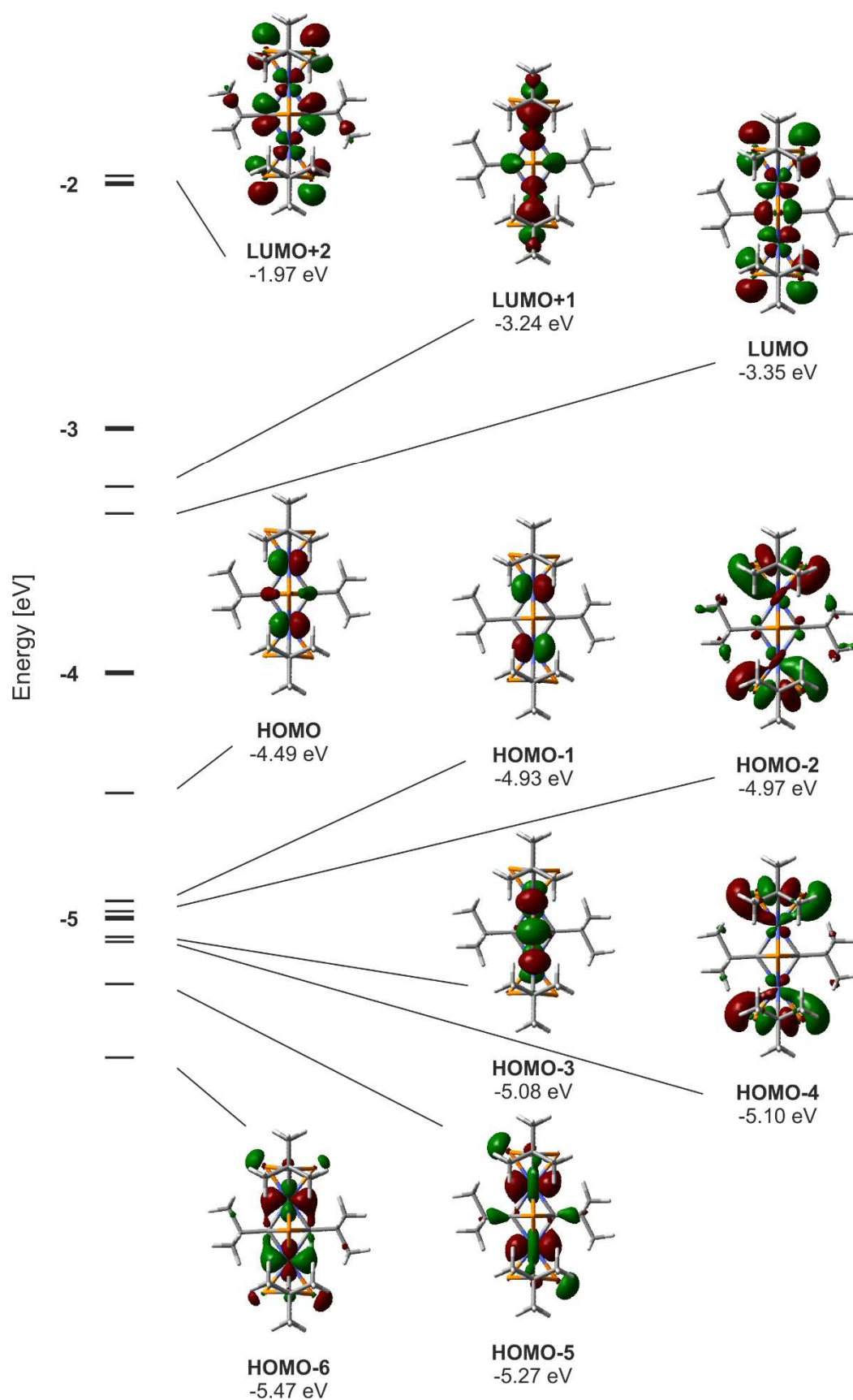


Figure 3. Kohn-Sham frontier orbitals of **1** calculated at the BP86-D3BJ/def2-TZVP level of theory.

5.3 Conclusion

Reaction of the silylated bis(1,3-diphosphacyclobutadiene) cobalt complex $[\text{Co}(\eta^4\text{-P}_2\text{C}_2\text{tBu}_2\text{SiMe}_3)(\eta^4\text{-P}_2\text{C}_2\text{tBu}_2)]$ (**L**, see chapter 2 of this thesis) with a Rh(III) complex affords an unprecedented 1,3-diphosphacyclobutadiene complex **1**, which to our knowledge is the first homoleptic tripledecker complex devoid of cyclopentadienyl ligands. The mechanism of the formation of **1** is currently unclear, but the concomitant formation of the known complex $[\text{Cp}^*\text{Rh}(\text{P}_2\text{C}_2\text{tBu}_2)]$ (**M**) suggest that a 1,3-diphosphacyclobutadiene ligand transfer reaction occurs that might provide a pathway for coordinatively unsaturated 1,3-diphosphacyclobutadiene cobalt intermediates. The molecular structure of **1** highlights the ability of 1,3-diphosphacyclobutadiene sandwich anions to form π -complexes with transition metal centers (see also chapter 4). The results of this study should stimulate further investigations into similar tripledecker complexes. In particular, the analogous diiron species (which should have 28 valence electrons) is a very attractive target in order to investigate how a 1,3-diphosphacyclobutadiene bridge mediates the magnetic coupling between two paramagnetic metal centers.

5.4 Supporting Information

5.4.1 General Procedures

All experiments were performed under an atmosphere of dry argon using standard Schlenk techniques or a MBraun UniLab glovebox. Solvents were dried and degassed with a MBraun SPS800 solvent purification system. THF and toluene were stored over molecular sieves (3 Å). *n*-Hexane and *n*-pentane were stored over a potassium mirror. NMR spectra were recorded on an Avance 400 spectrometer at 300 K and internally referenced to residual solvent resonances. The UV/Vis spectrum was recorded on an Ocean Optics Flame Spectrometer. Mass spectrometry was performed by the analytical department of Regensburg University. $[\text{Co}(\text{P}_2\text{C}_2t\text{Bu}_2\text{SiMe}_3)(\text{P}_2\text{C}_2t\text{Bu}_2)]$ (**L**) was synthesized according to the very recently reported literature procedure.¹⁶ $[\text{Cp}^*\text{RhCl}_2]_2$ was purchased from Sigma Aldrich and used as received.

5.4.2 Synthesis and Characterization

A solution of $[\text{Cp}^*\text{RhCl}_2]_2$ (0.18 g, 0.30 mmol, 0.5 eq) in toluene (6 mL) was added to a solution of $[\text{Co}(\eta^4\text{-P}_2\text{C}_2t\text{Bu}_2\text{SiMe}_3)(\eta^4\text{-P}_2\text{C}_2t\text{Bu}_2)]$ (0.32 g, 0.60 mmol, 1.0 eq) in toluene (10 mL). The reaction mixture was stirred overnight whereupon the color changed from dark-red to forest-green. The solvent was removed *in vacuo*. The residue was purified by column chromatography (20 x 2 cm²) with pre-dried Alumina N and *n*-hexane as eluent. The green band was collected and recrystallized from *n*-pentane at -35 °C. Crystals suitable for X-ray diffraction were obtained by slow evaporation of an *n*-hexane solution. Yield 29 mg (7%); ¹H NMR (400.13 MHz, [D₈]THF, 300 K,) δ /ppm = 1.33 (s, 18H, *t*Bu), 1.37 (s, 36H, *t*Bu); ¹³C{¹H} NMR (100.61 MHz, [D₈]THF, 300 K) δ /ppm = 32.0 (s, C(CH₃)₃), 37.2 (t, ²J_{C,P} = 7.3 Hz, C(CH₃)₃), 38.5 (br, C(CH₃)₃), 40.5 (s, C(CH₃)₃), 114.2 (t, ¹J_{C,P} = 55.1 Hz, terminal C₂P₂), 117.7 (br, bridging C₂P₂); ³¹P{¹H} NMR (161.98 MHz, [D₈]THF, 300 K) δ /ppm = 55.9 (s, 4P), 111.3 (s, 2P); UV/Vis (THF, λ_{max} /nm, (ε_{max} /L·mol⁻¹·cm⁻¹): 403 (67700), 502 (shoulder), 635 (3300).

5.4.3 NMR Data of 1

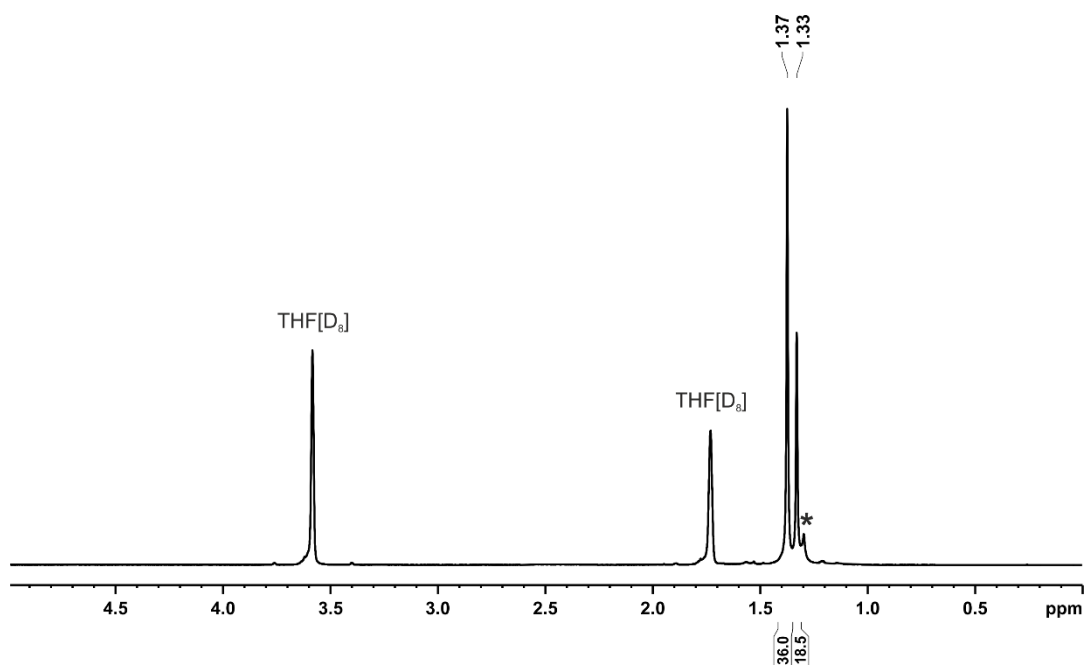


Figure S1. ^1H -NMR spectrum (400.13 MHz, $[\text{D}_8]\text{THF}$, 300 K) of $[\text{Co}_2(\text{P}_2\text{C}_2\text{tBu}_2)_3]$ (**1**). The asterisk marks an unidentified species.

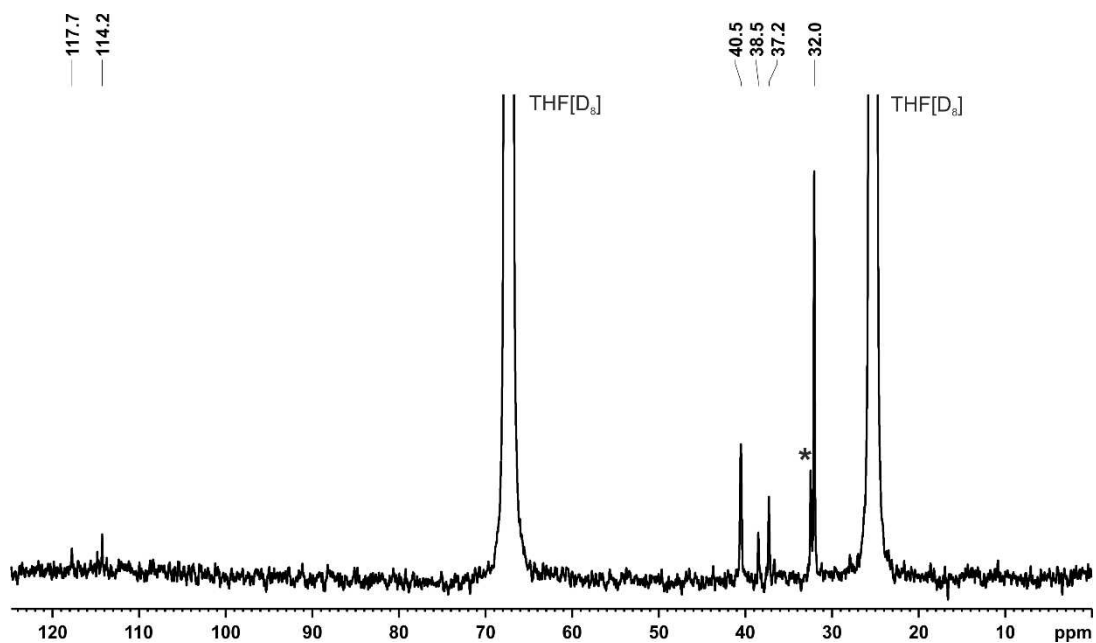


Figure S2. $^{13}\text{C}\{^1\text{H}\}$ -NMR spectrum (100.61 MHz, $[\text{D}_8]\text{THF}$, 300 K) of $[\text{Co}_2(\text{P}_2\text{C}_2\text{tBu}_2)_3]$ (**1**). The asterisk marks an unidentified species.

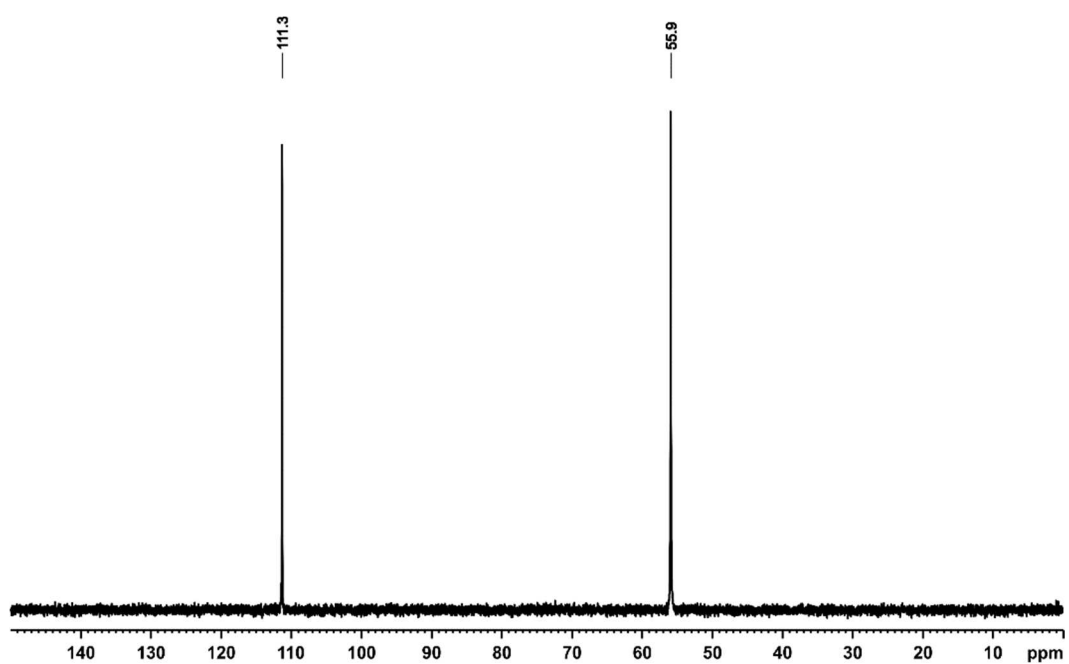


Figure S3. $^{31}\text{P}\{^1\text{H}\}$ -NMR spectrum (161.98 MHz, $[\text{D}_8]\text{THF}$, 300 K) of $[\text{Co}_2(\text{P}_2\text{C}_2\text{tBu}_2)_3]$ (**1**).

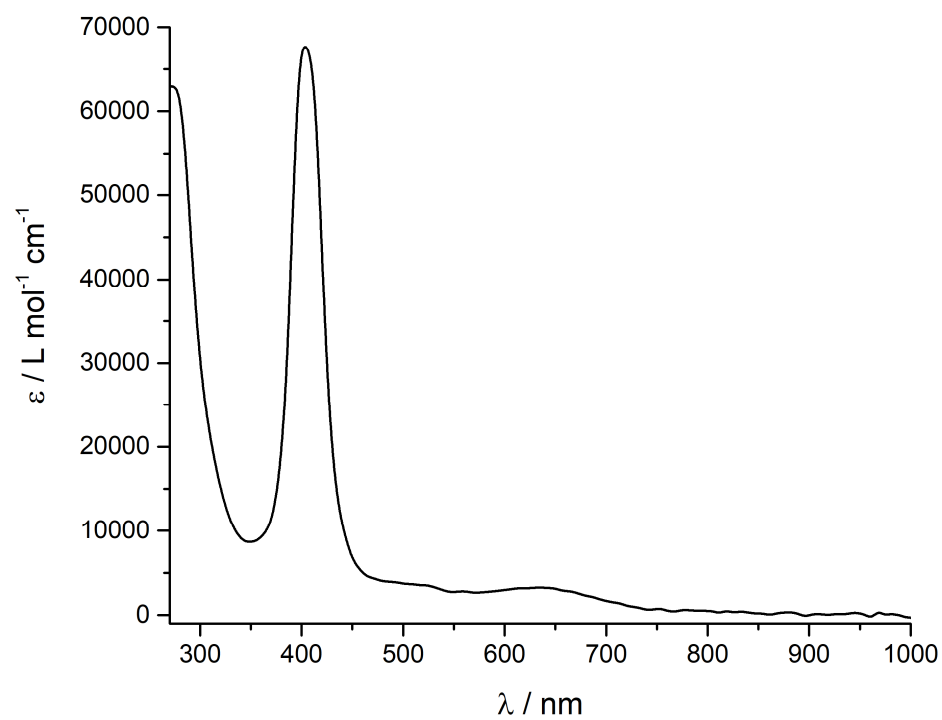
5.4.4 X-ray Crystallography

The single crystal X-ray diffraction data was recorded on an Agilent Technologies SuperNova diffractometer with Cu K α radiation ($\lambda = 1.54184 \text{ \AA}$). Semi-empirical multi-scan absorption corrections²⁵ were applied to the data. The structures were solved with SHELXT²⁶ and least-square refinements on F^2 were carried out with SHELXL²⁷.

Table S1. Crystal and structure refinement data of **1**.

Compound	1
Empirical formula	C ₃₀ H ₅₄ Co ₂ P ₆
Formula weight	718.41
Temperature [K]	123(1)
Crystal system	monoclinic
Space group	<i>P</i> 2 ₁ / <i>n</i>
a [Å]	9.9927(3)
b [Å]	17.6107(5)
c [Å]	10.2590(3)
α [°]	90
β [°]	108.105(4)
γ [°]	90
Volume [Å ³]	1716.0(1)
Z	2
ρ _{calc} [g/cm ³]	1.390
μ [mm ⁻¹]	10.351
F(000)	756.0
Crystal size [mm ³]	0.169 × 0.081 × 0.036
Radiation	CuK _α (λ = 1.54184)
2θ range for data collection [°]	10.046 to 149.084
Index ranges	-12 ≤ h ≤ 12, -22 ≤ k ≤ 21, -8 ≤ l ≤ 12
Reflections collected	21151
Independent reflections	3481 [R _{int} = 0.0485, R _{sigma} = 0.0294]
Data / restraints / parameters	3841 / 0 / 181
Goodness-of-fit on F ²	1.122
Final R indexes [I ≥ 2σ (I)]	R ₁ = 0.0339, wR ₂ = 0.0879
Final R indexes [all data]	R ₁ = 0.0366, wR ₂ = 0.0898
Largest diff. peak/hole [e Å ⁻³]	0.55/-0.27

5.4.5 UV/Vis Spectrum

Figure S4. UV/Vis spectrum of **1** in THF.

5.4.6 Cyclic Voltammetry

Cyclic voltammetry experiments were performed in a single-compartment cell inside a nitrogen-filled glovebox using a CH Instruments CHI600E potentiostat. The cell was equipped with a platinum disc working electrode (2 mm diameter) polished with 0.05 μm alumina paste, a platinum wire counter electrode and a silver/silver nitrate reference electrode. The supporting electrolyte, tetra-*n*-butylammonium hexafluorophosphate, was dried in vacuo at 110 $^{\circ}\text{C}$ for three days. All redox potentials are reported versus the ferrocene/ferrocenium (Fc/Fc^+) couple. The scan rate is $\nu = 100 \text{ mV s}^{-1}$.

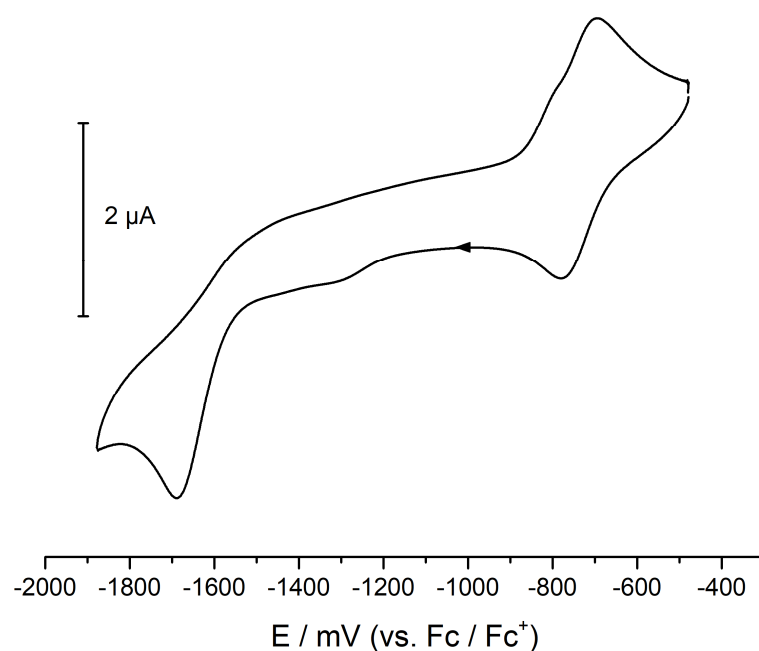


Figure S5. Cyclic voltammogram of **1** recorded in THF/[*n*Bu₄N]PF₆ with a platinum disc working electrode, a platinum wire as counter electrode, and silver/silver nitrate as reference electrode. $\nu = 100 \text{ mV/s}$; potentials are referenced to the Fc/Fc^+ couple.

5.4.7 Theoretical Calculations

Geometry optimization of **1** was performed with the Gaussian09 program package (Revision E.01).²⁸ The BP86 density functional²⁰ and the Ahlrichs def2-TZVP basis set²² were employed for all atoms. Atom-pairwise dispersion correction to the DFT energy with Becke–Johnson damping (D3BJ) was applied.²¹ The nature of the stationary points was verified by numerical frequency analyses. TD-DFT calculations at the B3LYP/def2-TZVP^{24,22} level were carried out using the xyz coordinates of the optimized structure. Tetrahydrofuran solvent effects were considered by applying the SCRF method as implemented in Gaussian.²⁹ Molecular orbitals were visualized with the program GaussView5.³⁰ The isosurface value is set to 0.05 for all figures.

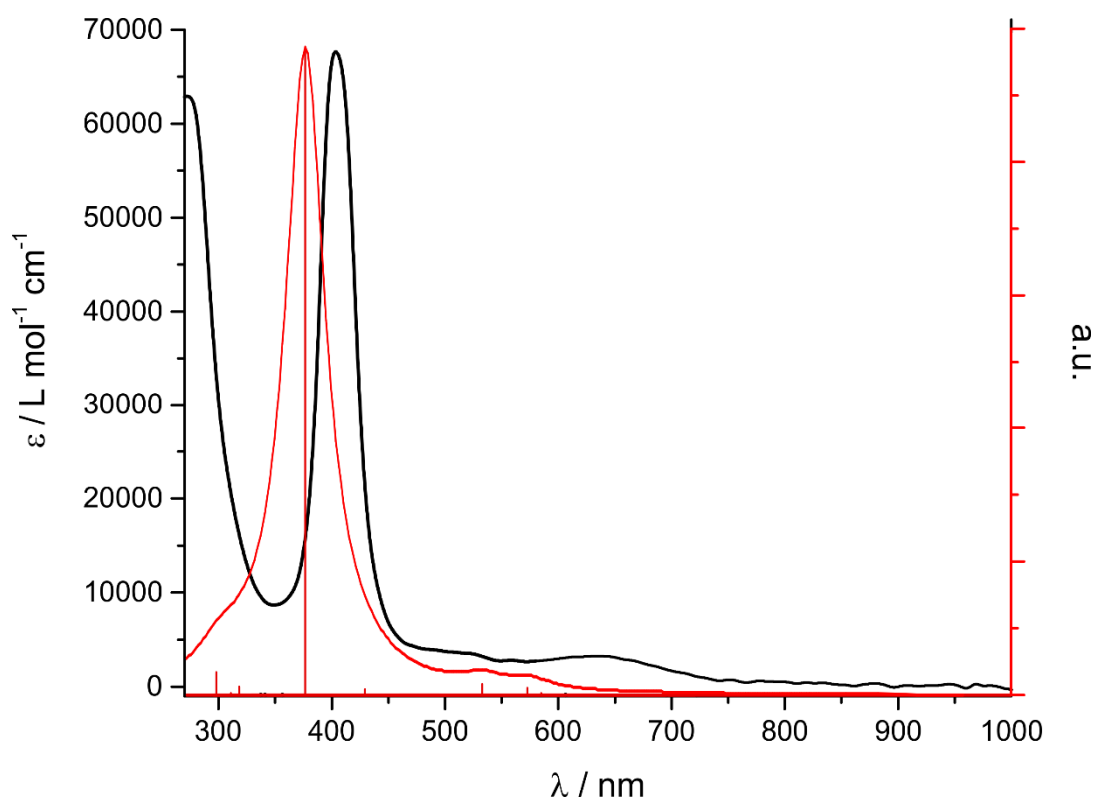


Figure S6. Experimental (black) and calculated (red) UV/vis spectrum of **1** in THF (a.u. = arbitrary units).

Table S2. Calculated electronic transitions of **1** on the B3LYP/def2-TZVP level of theory. The corresponding molecular orbitals are shown in Figure 3.

#	ν [nm]	f	%	Transition	Exp. ν [nm]
1	572	0.011	20	HOMO-9 \rightarrow LUMO+2	635
			45	HOMO-8 \rightarrow LUMO	
			29	HOMO \rightarrow LUMO	
2	532	0.014	19	HOMO-5 \rightarrow LUMO	635
			62	HOMO \rightarrow LUMO	
3	375	0.876	40	HOMO-6 \rightarrow LUMO	403
			39	HOMO-4 \rightarrow LUMO+1	
			15	HOMO \rightarrow LUMO	

5.5 References

- 1 a) T. J. Kealy, P. L. Pauson, *Nature* **1951**, *168*, 1039–1040; b) S. A. Miller, J. A. Tebboth, J. F. Tremaine, *J. Chem. Soc.* **1952**, 632–635; c) G. Wilkinson, M. Rosenblum, M. C. Whiting, R. B. Woodward, *J. Am. Chem. Soc.* **1952**, *74*, 2125–2126; d) E. O. Fischer, W. Pfab, *Z. Naturforsch. B* **1952**, *7*, 377–379.
- 2 a) H. Werner, A. Salzer, *Synth. Inorg. Met.-Org. Chem.* **1972**, *2*, 239–248; b) A. Salzer, H. Werner, *Angew. Chem. Int. Ed. Engl.* **1972**, *11*, 930–932.
- 3 V. Beck, D. O'Hare, *J. Organomet. Chem.* **2004**, *689*, 3920–3938.
- 4 A. W. Duff, K. Jonas, R. Goddard, H.-J. Kraus, C. Krüger, *J. Am. Chem. Soc.* **1983**, *105*, 5479.
- 5 Selected examples of tripledecker complexes with borole, cyclocarborane, and thiadiborolene as bridging ligand: a) G. E. Herberich, J. Hengersbach, U. Kölle, G. Huttner, A. Frank, *Angew. Chem. Int. Ed. Engl.* **1976**, *15*, 433; b) D. C. Beer, V. R. Miller, L. G. Sneddon, R. N. Grimes, M. Mathew, G. J. Palenik, *J. Am. Chem. Soc.* **1973**, *95*, 3046; c) W. M. Maxwell, V. R. Miller, R. N. Grimes, *Inorg. Chem.* **1976**, *15*, 1343; d) W. Siebert, K. Kinberger, *Angew. Chem.* **1976**, *88*, 451; *Angew. Chem. Int. Ed. Engl.* **1976**, *15*, 434; e) W. Siebert, T. Renk, K. Kinberger, M. Bochmann, C. Krüger, *Angew. Chem.* **1976**, *88*, 850; *Angew. Chem. Int. Ed. Engl.* **1976**, *15*, 779; f) W. Siebert, W. Rothermel, *Angew. Chem.* **1977**, *89*, 346; *Angew. Chem. Int. Ed. Engl.* **1977**, *16*, 333; g) W. Siebert, J. Edwin, M. Bochmann, *Angew. Chem.* **1978**, *90*, 917; *Angew. Chem. Int. Ed. Engl.* **1978**, *17*, 868.
- 6 Reviews on tripledecker complexes with boron containing ligands: a) R. N. Grimes, *Coord. Chem. Rev.* **1979**, *28*, 47–96; b) R. N. Grimes, *Chem. Rev.* **1992**, *92*, 251–268.
- 7 O. J. Scherer, H. Sitzmann, G. Wolmershäuser, *Angew. Chem.* **1985**, *97*, 358; *Angew. Chem. Int. Ed. Engl.* **1985**, *24*, 351.
- 8 O. J. Scherer, T. Brück, G. Wolmershäuser, *Chem. Ber.* **1989**, *122*, 2049–2054.
- 9 J. K. Uhm, W. S. Lee, S. B. Kim, J. S. Cha, H. S. Lee, D. H. Lee, H. S. Kim, S. C. Sim, *J. Kor. Chem. Soc.* **1993**, *37*, 832.
- 10 E.-M. Rummel, *PhD Dissertation*, University of Regensburg., Germany, **2016**.
- 11 Radius and co-workers synthesized $[\{\text{Ni}(\text{Im}^{\text{iPr}})_2\}_2(\mu\text{:}\eta^4\text{:}\eta^4\text{-P}_2\text{C}_2\text{tBu}_2)]$ (Im^{iPr} = 1,3-di(isopropyl)imidazole-2-ylidene) by prolonged heating of the mononuclear complex $[\text{Ni}(\text{Im}^{\text{iPr}})_2(\eta^2\text{-PCtBu})]$ in toluene at 100 °C. The structure of this complex was proposed based on NMR data: T. Schaub, U. Radius, *Z. Anorg. Allg. Chem.* **2006**, *632*, 981–984.
- 12 D. Patel, J. McMaster, W. Lewis, A. J. Blake, S. T. Liddle, *Nature Comm.* **2013**, *4*, 3323.
- 13 a) R. Wolf, A. W. Ehlers, J. C. Slootweg, M. Lutz, D. Gudat, M. Hunger, A. L. Spek, K. Lammertsma, *Angew. Chem.* **2008**, *120*, 4660–4663; *Angew. Chem. Int. Ed.* **2008**, *47*, 4584–4587; b) R. Wolf, J. C. Slootweg, A. W. Ehlers, F. Hartl, B. de Bruin, M. Lutz, A. L. Spek, K. Lammertsma, *Angew. Chem.* **2009**, *121*, 3150–3153; *Angew. Chem. Int. Ed.* **2009**, *48*, 3104–3107; c) R. Wolf, A. W. Ehlers, M. M. Khusniyarov, F. Hartl, B. de Bruin, G. J.

- Long, F. Grandjean, F. M. Schappacher, R. Pöttgen, J. C. Sloodweg, M. Lutz, A. L. Spek, K. Lammertsma, *Chem. Eur. J.* **2010**, *16*, 14322–14334.
- 14 a) J. Malberg, T. Wiegand, H. Eckert, M. Bodensteiner, R. Wolf, *Chem. Eur. J.* **2013**, *19*, 2356–2369; b) J. Malberg, M. Bodensteiner, D. Paul, T. Wiegand, H. Eckert, R. Wolf, *Angew. Chem. Int. Ed.* **2014**, *53*, 2771–2775; c) J. Malberg, T. Wiegand, H. Eckert, M. Bodensteiner, R. Wolf, *Eur. J. Inorg. Chem.* **2014**, *2014*, 1638–1651.
- 15 a) C. Rödl, R. Wolf, *Eur. J. Inorg. Chem.* **2016**, *2016*, 736–742; b) C. Rödl, R. Wolf, *manuscript accepted*; DOI: 10.1002/chem.201901061.
- 16 C. Rödl, J. Bissmeyer neè Malberg, R. Wolf, *Z. Naturforsch. B* **2018**, *76*, 895.
- 17 P. B. Hitchcock, M. J. Maah, J. F. Nixon, *J. Chem. Soc., Chem. Commun.* **1986**, 737–738.
- 18 J. W. Lauher, M. Elian, R. H. Summerville, R. Hoffmann, *J. Am. Chem. Soc.* **1976**, *98*, 3219–3224.
- 19 O. J. Scherer, J. Schwalb, H. Swarowsky, G. Wolmershäuser, W. Kaim, R. Gross, *Chem. Ber.* **1988**, *121*, 443–449.
- 20 a) A. D. Becke, *Phys. Rev. A* **1988**, *38*, 3098; b) J. P. Perdew, *Phys. Rev. B* **1986**, *33*, 8822.
- 21 a) S. Grimme, S. Ehrlich, L. Goerigk, *J. Comput. Chem.* **2011**, *32*, 1456. b) S. Grimme, J. Antony, S. Ehrlich, H. Krieg, *J. Chem. Phys.* **2010**, *132*, 154104.
- 22 a) A. Schäfer, C. Huber, R. Ahlrichs, *J. Chem. Phys.* **1994**, *100*, 5829; b) F. Weigend, *Phys. Chem. Chem. Phys.* **2006**, *8*, 1057.
- 23 Electrochemical measurements and preparative studies have shown that $[\text{Co}(\eta^4\text{-P}_2\text{C}_2\text{tBu}_2)]^-$ is readily oxidized to neutral $[\text{Co}(\eta^4\text{-P}_2\text{C}_2\text{tBu}_2)_2]$. A half-wave potential of $E_{1/2} = -0.73$ V vs. Fc/Fc^+ was determined for this process by cyclic voltammetry, see ref. 13c.
- 24 a) C. Lee, W. Yang, R. G. Parr, *Phys. Rev. B* **1988**, *37*, 785; b) P. J. Stephens, F. J. Devlin, C. F. Chabalowski, M. J. Frisch, *J. Phys. Chem.* **1994**, *98*, 11623–11627.
- 25 a) *SCALE3ABS*, *CrysAlis^{Pro}*, Agilent Technologies Inc., Oxford, GB, **2012**, b) G. M. Sheldrick, *SADABS*, Bruker AXS, Madison, USA, **2007**.
- 26 G. M. Sheldrick, *Acta Cryst.* **2015**, *A71*, 3–8.
- 27 G. M. Sheldrick, *Acta Cryst.* **2015**, *C71*, 3–8.
- 28 Gaussian 09, Revision E.01: M. J. Frisch, G. W. Trucks, H. B. Schlegel, G. E. Scuseria, M. A. Robb, J. R. Cheeseman, G. Scalmani, V. Barone, G. A. Petersson, H. Nakatsuji, X. Li, M. Caricato, A. Marenich, J. Bloino, B. G. Janesko, R. Gomperts, B. Mennucci, H. P. Hratchian, J. V. Ortiz, A. F. Izmaylov, J. L. Sonnenberg, D. Williams-Young, F. Ding, F. Lipparini, F. Egidi, J. Goings, B. Peng, A. Petrone, T. Henderson, D. Ranasinghe, V. G. Zakrzewski, J. Gao, N. Rega, G. Zheng, W. Liang, M. Hada, M. Ehara, K. Toyota, R. Fukuda, J. Hasegawa, M. Ishida, T. Nakajima, Y. Honda, O. Kitao, H. Nakai, T. Vreven, K. Throssell, J. A. Montgomery, Jr., J. E. Peralta, F. Ogliaro, M. Bearpark, J. J. Heyd, E. Brothers, K. N. Kudin, V. N. Staroverov, T. Keith, R. Kobayashi, J. Normand, K. Raghavachari, A. Rendell, J. C. Burant, S. S. Iyengar, J. Tomasi, M. Cossi, J. M. Millam, M. Klene, C. Adamo, R. Cammi,

- J. W. Ochterski, R. L. Martin, K. Morokuma, O. Farkas, J. B. Foresman, and D. J. Fox, Gaussian, Inc., Wallingford CT, **2016**.
- 29 J. Tomasi, B. Menucci, R. Cammi, *Chem. Rev.* **2005**, *105*, 2999-3093.
- 30 GaussView 5.0.9: R. Dennington, T. A. Keith, J. M. Millam, Semichem Inc., Shawnee Mission, KS, **2016**.

6 PHOSPHAORGANOMETALLIC COBALT COMPLEXES AS POTENTIAL PRECURSORS FOR THE GENERATION OF THIN INORGANIC FILMS^[a,b]

FALKO ABELS, DANIEL LÖFFLER, HAGEN WILMER,

CHRISTIAN RÖDL, PHILIPP BÜSCHELBERGER,

AND ROBERT WOLF

[a] The results of this chapter were published as a patent: F. Abels, D. Löffler, H. Wilmer, R. Wolf, C. Rödl, P. Büschelberger, *Process for the Generation of Thin Inorganic Films*, **2017**, WO/2017/129440.

[b] F. Abels, D. Löffler, and H. Wilmer (all BASF SE, Ludwigshafen) supervised the project and provided the thermogravimetric analyses. R. Wolf supervised the project. P. Büschelberger synthesized and analyzed compounds **1–5**. C. Rödl synthesized and characterized all remaining compounds and wrote the manuscript.

6.1 Introduction

Atomic layer deposition (ALD) has emerged as a very powerful technique for the growth of thin films for numerous industrial applications.¹ One of the most expanding areas of application nowadays is the field of microelectronics. A major driving force is the current industrial desire to scale down microelectronic devices. ALD is a special modification of chemical vapor deposition (CVD) with benefits in depositing films in a cyclic manner. This is based on the subsequent use of self-terminating gas-solid reactions and includes four steps each for a reaction cycle (Figure 1): (1) reaction of the first reactant **A** with the surface/substrate; (2) removal of the unreacted residues by purging or evacuation; (3) treatment of the first reactant **A** in order to activate the surface for the next step – or – reaction with another reactant **B**; (4) purge or evacuation step.

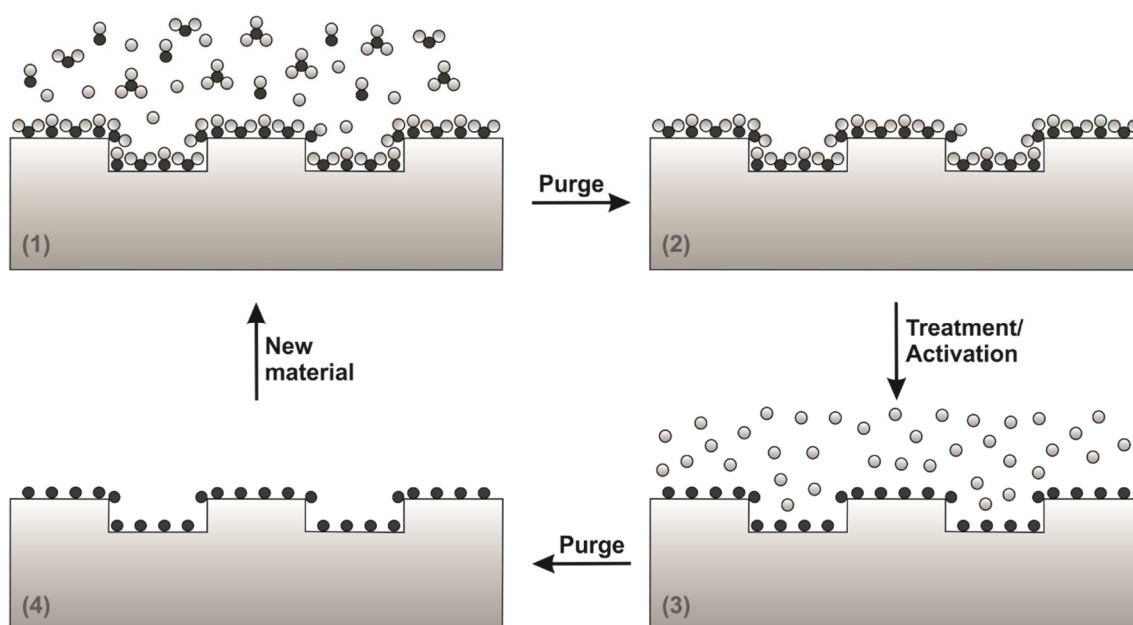


Figure 1. Schematic illustration of one reaction cycle during the ALD process.

The ALD process was developed under the name “atomic layer epitaxy” (ALE) by Suntola *et al.* according to the more commonly acknowledged origin.² They demonstrated ALD growth of ZnS, SnO₂, and GaP by elemental precursors. Independently, the group of Aleskovskii described the growth of TiO₂ and GeO₂ starting from TiCl₄/H₂O and GeCl₄/H₂O, respectively.³ The development of ALD over the past decades was reviewed by several groups.⁴

The ALD process involves some demands on the reactant. It has to be volatile at low temperature, i.e. at ambient or elevated temperatures, but may not decompose during the deposition process. Furthermore, the reactant has to feature self-terminating growth properties. Taking into account these requirements, there is much room for tuning the properties by using different metal atoms as well as different ligand systems. The most common ligand systems are halides,^{3,5} alkyls,⁶ cyclopentadienyls,⁷ alkoxides,⁸ β -diketonates,^{8d,9} amides,¹⁰ and amidinates.¹¹

The metal atoms of complexes with these ligands display variable oxidation states. Consequently, redox processes occur during the deposition, which require the use of reducing or oxidizing co-reactants. In order to accomplish the cleavage of the ligand and the reduction or the oxidation of the corresponding metal atom a number of co-reactants can be utilized: (i) O_2 , O_3 , (ii) H_2 , (iii) O_2 , O_3 or H_2O followed by H_2 , (iv) hydrosilanes, hydroboranes or hydroalanes, (v) amines, hydrazines, (vi) formaldehyde, glyoxylic acid, formic acid, and alcohols, (vii) Zn metal, (viii) $ZnEt_3$, (ix) $AlMe_3$.¹²

ALD is initiated by adsorption of the precursor on the surface. Depending on the strength of the interactions between the solid surface and the deposited molecule the adsorption can be divided into two different types: Physisorption and chemisorption.¹³ Physisorption, also called van-der-Waals adsorption, implies only small changes in electronic configuration, which arise from weak interactions. By contrast, chemisorption involves an activation energy together with changes in the electronic state. Moreover, breaking and formation of covalent bonds leads to either exothermic or endothermic irreversible reactions. Chemisorption, however, is limited in space due to the steric hindrance of the ligands as well as a limited number of bonding sites at the surface of the reactant. Hence, chemisorption occurs in monolayers while physisorption preferably occurs in multilayers. In an ideal process, the growth of one full two-dimensional monolayer per cycle would be achieved. Indeed, several growth modes exist (Figure 2).^{4h} The Frank-van-der-Merwe growth describes the two-dimensional growth mode in which each layer is deposited on the top of the prior deposited film (layer-by-layer, Figure 2, left). In contrast, the Volmer-Weber growth characterizes an island growth in which the new material is preferably deposited on the grown material (Figure 2, middle). A combination of both, two-dimensional and island growth, is called Stranski-Krastanov growth. Usually, the first layer grows in a two-dimensional manner while the consecutive layers grow in an island fashion (Figure 2, right).

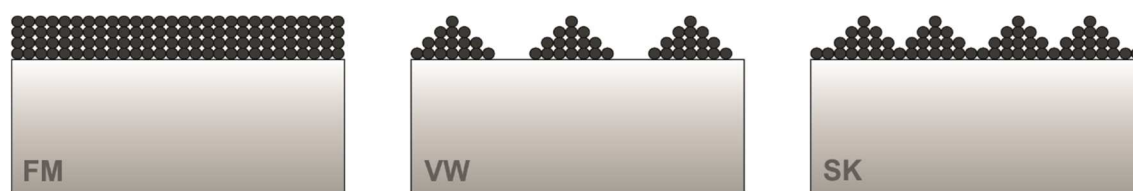


Figure 2. Illustration of the most common modes of thin-film growth at a solid surface: Frank-van-der-Merwe (FM, layer-by-layer, left), Volmer-Weber (VW, island formation, middle), Stranski-Krastanov (SK, layer and island, right).

Especially in the microelectronics industry, transition metal-silicide films are required as contact layers in order to provide low contact resistance and good compatibility with silicon processing for device scaling.¹⁴ Several silicide materials have already been applied in deposition processes, i.e. WSi_2 ,¹⁵ $TaSi_2$,¹⁶ $MoSi_2$ ¹⁷ as well as $TiSi_x$, $NiCoSi_x$, and $PtSi_x$.¹⁸ A disadvantage of these silicides is that they are difficult to grow by direct reaction with silicon. Therefore, precursor compounds with improved properties are urgently needed. In addition, cobalt silicide ($CoSi_x$) is a

highly attractive contact material for microelectronic devices due to its wider silicidation window compared to TiSi_2 , for example, and its higher thermal and chemical stability. Furthermore, the low resistivity and the similarity of the crystal lattice (mismatch of $\sim 1.2\%$ at room temperature) are highly interesting properties, which make CoSi_2 an excellent material for the application as a contact layer in microelectronic devices.¹⁹ Challenges are the reproducibility and the conformability of the resulting films.⁴ⁱ Consequently, deposition of highly pure cobalt monolayers for the generation of CoSi_2 contact layers is essential in microelectronics. Therefore, there is still need for suitable precursors affording cobalt monolayers that feature self-terminating growth properties at the same time.

In summary, precursor design plays a vital role in ALD processes. The precursor compounds should possess adequate volatility and a sufficiently large temperature window between evaporation and decomposition for deposition. It was the objective of this PhD thesis to investigate the potential utility of cobalt complexes bearing phosphanes, phosphalkynes, 1,3-diphosphacyclobutadienes, or phospholes in their structural framework for ALD of nickel and cobalt films. The presented work was performed in collaboration with the BASF SE company.

6.2 Results and Discussion

In order to assess the applicability of neutral cobalt complexes with phosphorus containing ligands in their structural framework we tested different ligand systems, in particular monophosphanes, phosphalkynes, 1,3-diphosphacyclobutadienes, and phospholes. The thermal properties of the resulting complexes were investigated by thermogravimetric analyses and vapor pressure measurements. Long-term stability tests were performed in order to get first insights into the behavior of these complexes under thermal stress. One complex was found to be a potential precursor for ALD. Thus, preliminary ALD tests were performed at TU Dresden (in cooperation with BASF SE) with this precursor featuring promising thermal properties (*vide infra*).

6.2.1 Synthesis, Characterization and Thermal Properties of Monophosphane Complexes

Transition metal phosphane complexes have previously been used as precursors for chemical vapor deposition (CVD) processes.²⁰ In order to test the applicability of phosphane complexes in ALD processes, we utilized a series of five known cobalt and nickel phosphane complexes. They were synthesized according to literature procedures reported by Klein and Ittel (Figure 3).²¹ Complexes **1** and **2** were prepared by reduction of CoCl_2 with Mg in presence of the corresponding olefin in good yields of 84% and 71%, respectively. The anthracene complex **3** was obtained by substitution of cyclopentene of **2** by anthracene in moderate yield of 55%. Compound **4** was synthesized by reduction of CoCl_2 with Mg and subsequent treating with an excess of PMe_3 , whereas **5** was prepared by treating $[\text{Ni}(\eta^4\text{-1,5-cod})_2]$ with four equivalents of PMe_3 in 80% yield. Compounds **1–5** were characterized by ^1H NMR spectroscopy (except **4** due to its paramagnetic properties) and elemental analysis.

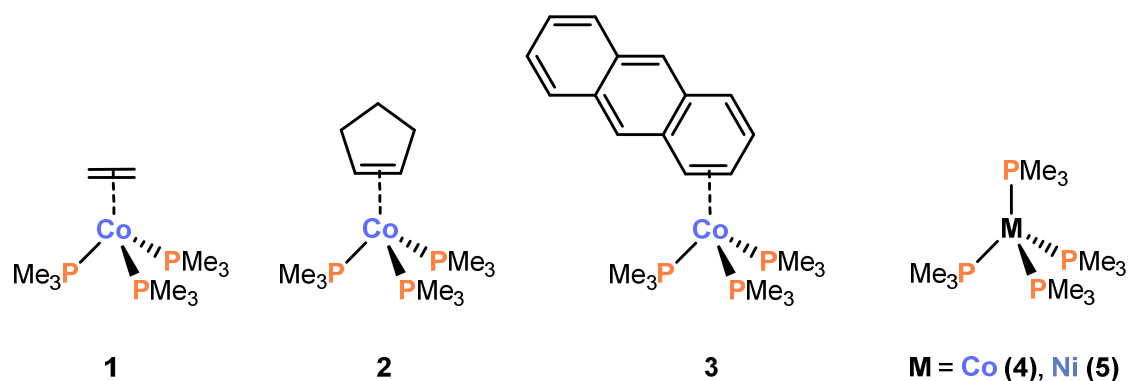


Figure 3. Investigated cobalt and nickel phosphane complexes.

Compounds **1–3** are heteroleptic tris(trimethylphosphane)cobalt complexes of the type $\text{Co}(\text{L})(\text{PMe}_3)_3$ with a labile π -coordinated ligand L, i.e. ethylene (**1**), cyclopentene (**2**), and anthracene (**3**). Compounds **4** and **5** are homoleptic tetrakis(trimethylphosphane) complexes. As a rough estimation of the suitability in ALD processes, the long-term stability of **1–5** in the gas phase was tested by controlled heating of samples in sealed glass tubes at 10^{-1} mbar for a certain

period of time (see the Supporting Information for further details). While complexes **4** and **5** were stable up to 120 °C and 130 °C, respectively, complexes **1–3** decomposed above 90 °C. Furthermore, **4** and **5** are sublimable at mild conditions (10^{-1} mbar/80 °C), whereas **1–3** are not sublimable at a laboratory scale. In sealed glass tubes, however, **1** and **2** sublimed at 10^{-1} mbar/60 °C. In order to transfer the desired compound in the gas phase from the repository to the substrate within a certain period of time it has to provide a certain vapor pressure. Nevertheless, the desired vapor pressure of 1 mbar was determined to 120 °C for **4** and 240 °C for **5**, respectively. In addition, thermogravimetric analysis showed that **4** decomposes with a maximum decomposition rate of 11.4%/min at 191 °C (Figure S6). A residual mass of 14.3% (Co content 16.2%) at 500 °C, in fact, is promising. However, the decline of the curve is continuous indicating a permanent decomposition process instead of generating metallic cobalt. In conclusion, complexes **1–5** are not suitable for the application in ALD processes. In particular, heteroleptic phosphane complexes **1–3** are thermally unstable at temperatures above 90 °C and are not sublimable. Whilst the homoleptic complexes **4** and **5** are thermally more stable and also sublimable at mild conditions, the thermogravimetric analysis of $[\text{Co}(\text{PMe}_3)_4]$ (**4**) revealed decomposition at temperatures required for ALD.

6.2.2 Synthesis, Characterization and Thermal Properties of Phosphaalkyne Complexes

Dicobalt hexacarbonyl *tert*-butylacetylene (CCTBA) is an excellent precursor for the low-temperature ALD of Co_3O_4 films.²¹ However, thermal decomposition of CCTBA and subsequent oxidation by ozone is described as the dominant process. We synthesized the analogous phosphorus-containing compounds, i.e. dicobalt hexacarbonyl phosphaalkyne complexes according to a literature procedure reported by Nixon.³¹ Due to the light-sensitivity of the products, all manipulations were performed with exclusion of light. Treatment of dicobalt octacarbonyl (one equiv.) with a little excess of phosphaalkyne (1.1 equiv.) gave complexes **6** and **7** in high yields. However, compound **6** could only be isolated in low purity of about 70% (^1H NMR analysis). Both compounds were characterized by ^1H and $^{31}\text{P}\{^1\text{H}\}$ NMR and IR spectroscopy.

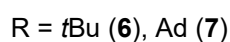
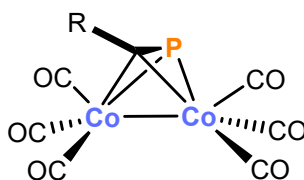


Figure 4. Cobalt hexacarbonyl phosphaalkyne complexes.

In analogy to CCTBA, the molecular structures of **6** and **7** comprises a phosphaalkyne molecule bridging two cobalt atoms of the dicobalt hexacarbonyl unit (Figure 4). The compounds are very

difficult to handle due to their light-sensitivity and their waxy state. **6** and **7** decompose when stored at 100 °C for 12 hours. Furthermore, they showed poor sublimation properties. Thermogravimetric analysis of **6** showed only one continuous decrease which is indicative for decomposition rather than stepwise dissociation of ligands, i.e. carbon monoxide or phosphalkyne. Consequently, complexes **6** and **7** cannot be applied in ALD processes.

6.2.3 Synthesis, Characterization and Thermal Properties of 1,3-Diphosphacyclobutadiene Complexes

Wolf, Lammertsma and co-workers have shown that homoleptic bis(1,3-diphosphacyclobutadiene)metalates **C** and **D** can be synthesized by treating bis(anthracene)metalates **A** and **B** (Figure 5)²⁴ with four equivalents of phosphalkyne (see section 1.2).^{25,26} **D** can be oxidized to the neutral complex **8** and it reacts with electrophiles such as HCl, MeI, and Me₃SiCl to form further neutral derivatives **9–11**.^{25a}

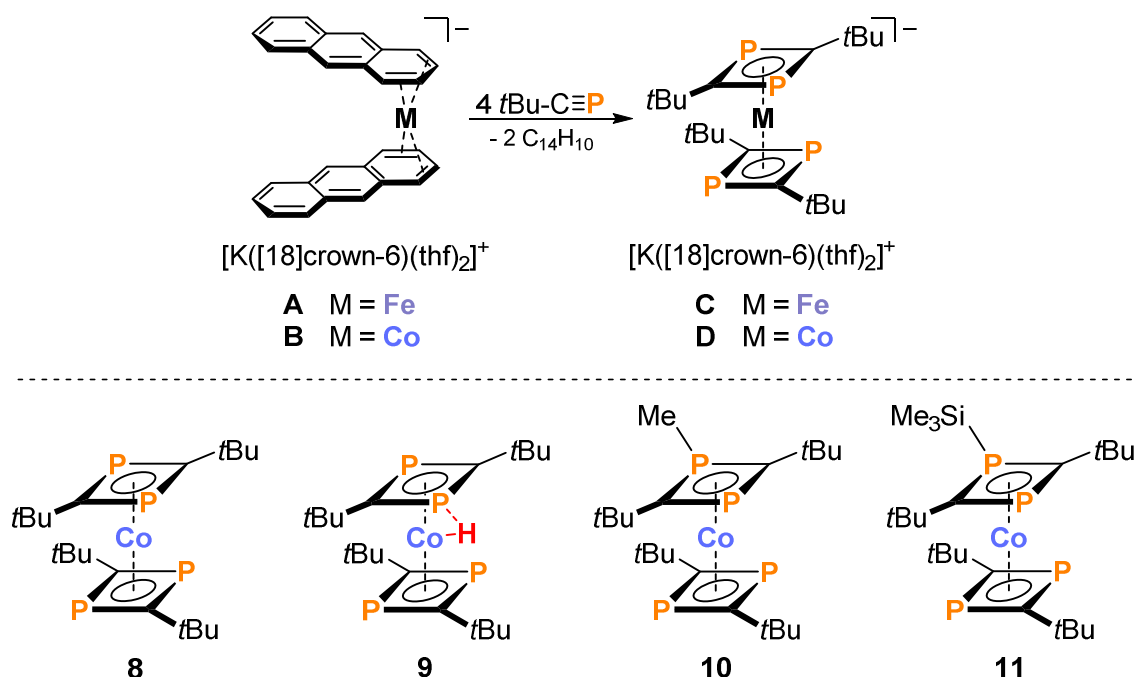


Figure 5. Top: Synthesis of bis(1,3-diphosphacyclobutadiene)metalate anions; bottom: Symmetric (**8**) and asymmetric (**9–11**) diphosphacyclobutadiene complexes.

We wondered whether complexes such as **8–11** could be used as ALD precursors. Although the melting or decomposition points had been described,^{25,26} further insights into thermal properties and vapor pressure were not reported. In order to get information on the suitability of complexes **8–11**, we performed long-term stability tests in sealed glass tubes as well as thermogravimetric measurements (see the Supporting Information for further details, Table S1 and Figure S7). The long-term stability test of compound **8** showed that sublimation at reduced pressure (10^{-1} mbar) in a sealed glass tube at 140 °C comes along with decomposition (see the Supporting Information for further details). Unfortunately, the substituted complexes **9–11** have similarly unfavorable

sublimation (130 °C) and decomposition (140 °C) temperatures. The thermogravimetric analysis confirmed that complexes **8–11** are unsuitable precursors for the deposition of CoSi₂ films. In particular, the TG/DTG plot of **8** (Figure S7) shows one sharp peak at 200 °C and a residual mass of 27.34% (cobalt content of **8**: 12.83%) at 500 °C as is similar for compound **9**. The TG/DTG graph of **9** displays a maximum decrease rate of 12%/min at 206 °C and a residual mass of 37.05% at 500 °C. Moreover, introduction of sterically more demanding Me (complex **10**) or SiMe₃ groups (complex **11**) does not improve the thermal properties as suggested by the long-term stability tests. The TG/DTG curve of **11** shows a maximum rate of 6.6%/min at 229 °C and a residual mass of 22.80% at 500 °C (cobalt content 11.07%). In summary, bis(diphosphacyclobutadiene)cobalt complexes show poor stability at reduced pressure under thermal stress which cannot be improved by introducing methyl or trimethylsilyl substituents. Hence, this type of complex cannot be applied in an ALD process.

6.2.4 Synthesis, Characterization and Thermal Properties of Phosphole Complexes

In the past decade there was large effort in exploring effective precursor compounds for the growth of thin cobalt films. In addition to CCTBA,²¹ cyclopentadienylcobalt dicarbonyl was found to be a highly attractive precursor for the application in ALD processes.²⁸ However, a disadvantage of both types of compounds is the high carbon contamination of the films during the deposition process due to the high content of carbon in their molecular framework. In order to reduce the amount of carbon in the cyclopentadienyl moiety, we substituted one CH group by a P atom (Figure 6).

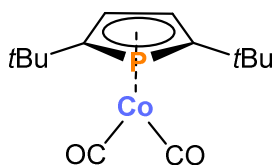


Figure 6. Molecular structure of [Co(PC₄tBu₂H₂)(CO)₂] (**12**).

Compound **12** was synthesized in quantitative yield and high purity via a modified procedure by Mathey and co-workers by refluxing Co₂(CO)₈ in *n*-heptane with the biphosphole for four days.²⁹ Long-term stability tests revealed high stability upon thermal stress (see the Supporting Information for further details). This is demonstrated by partial decomposition (black particles precipitated) only after storing a sample for seven days at 170 °C in a sealed ampule at 10⁻¹ mbar. Vapor pressure measurements revealed that this compound has a sufficient vapor pressure of 1 mbar at approximately 105 °C and 10 mbar at approximately 135 °C, respectively (Figure S5). Thermogravimetric analysis of **12** showed an exponential mass change between 120 °C and 200 °C and a residual mass of 11.58% at 500 °C (Co content 19.00%, see Figure S8). Hence, complex **12** was submitted for tests as potential precursor for an ALD process. The tests were performed by Shashank Shukla at TU Dresden as part of his masters' thesis.³⁰ The precursor was

tested with several co-reactants such as diethanolamine (DEA), formic acid, NH_3/H_2 , H_2 , trimethylalane (TMA), and air at a substrate temperature of 180–210 °C. A CVD component (precursor only dosing) was found at these temperatures (30–50%) which increased with rising temperature (80% at 227 °C). Thus, the precursor was also tested in CVD mode using a parallel dosing of precursor and H_2 at 250 °C substrate temperature. The films grown by CVD contain significant amounts of carbon and phosphorus. However, XPS measurements revealed that metallic cobalt is the main component in the 2p region, although conductivity measurements were not fully conclusive.

6.3 Conclusion

In summary, we have synthesized cobalt(0) complexes bearing different ligand classes, i.e. phosphanes, phosphalkynes, 1,3-diphosphacyclobutadienes or phospholes, in their structural framework. We explored their thermal properties and investigated their potential suitability in ALD applications. We learned that neither cobalt phosphane complexes nor dicobalt phosphalkyne complexes nor 1,3-diphosphacyclobutadiene cobalt complexes can be applied in ALD processes due to their low decomposition temperature (phosphane and 1,3-diphosphacyclobutadiene complexes) or their very poor sublimation properties (phosphalkyne complexes). The cobalt(dicarbonyl)(phosphole) complex **12**, however, seems to be a good starting point for further investigations of this ligand class due to the wide thermal window (range between sublimation temperature and decomposition temperature) and a sufficient vapor pressure. Nevertheless, there is much effort needed to overcome the problem of high carbon contamination in the generated thin film. Moreover, tuning of the thermal properties could be achieved by changing the substituents of the phosphole ligand or even substitution of the carbonyl ligands by more labile olefin ligands such as 1,5-cyclooctadiene.

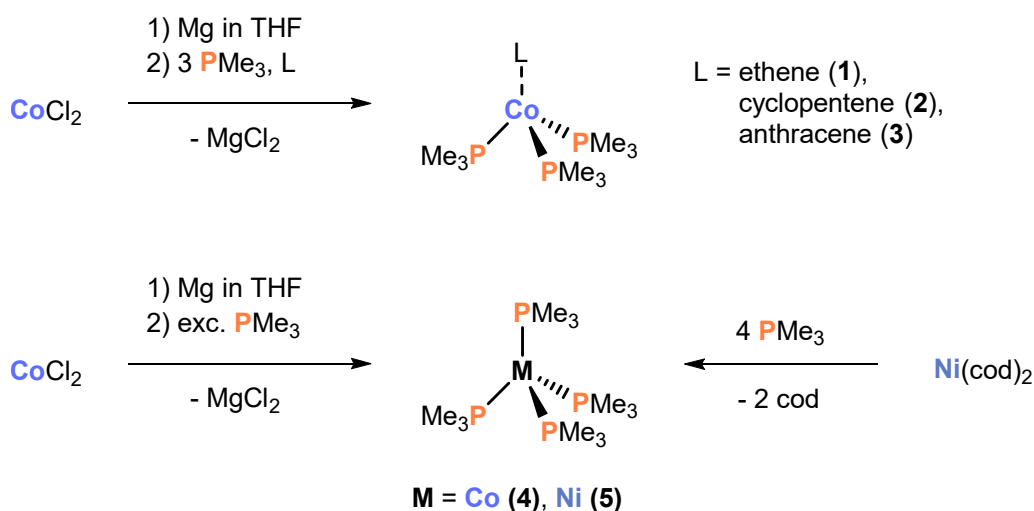
6.4 Supporting Information

6.4.1 General Procedures

All manipulations were performed under an atmosphere of dry argon using standard Schlenk line techniques or a MBraun UniLab glovebox. Solvents were dried and degassed with a MBraun SPS800 solvent purification system. Tetrahydrofuran, toluene, and diethyl ether were stored over molecular sieves (3 Å). *n*-Hexane was stored over a potassium mirror. NMR spectra were recorded on Bruker Avance 300 and Avance 400 spectrometers at 300 K and internally referenced to residual solvent resonances. Elemental analyses were determined by the analytical department of Regensburg University.

6.4.2 Synthesis and Characterization of Phosphane Complexes 1–5

[Co(C₂H₄)(PMe₃)₃] (**1**), [Co(C₅H₈)(PMe₃)₃] (**2**), [Co(C₁₀H₁₄)(PMe₃)₃] (**3**), [Co(PMe₃)₄] (**4**), and [Ni(PMe₃)₄] (**5**) were prepared according to literature procedures.²¹



Scheme S1. Synthesis of phosphane complexes 1–5.

Characterizations of compounds 1–5:

1: Yield 1.32 g (84%); elemental analysis calcd. for C₁₁H₃₁P₃Co (M = 315.22): C 41.91, H 9.91, found: C 41.87, H 9.69.

2: Yield 2.54 g (71%); elemental analysis calcd. for C₁₄H₃₅P₃Co (M = 355.29): C 47.33, H 9.93, found: C 46.88, H 9.72.

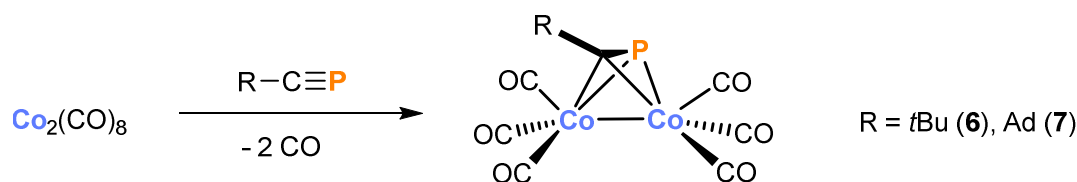
3: Yield 0.51 g (55%); elemental analysis calcd. for C₂₃H₃₇P₃Co (M = 465.40): C 59.36, H 8.01, found: C 59.39, H 8.03.

4: Yield 0.78 g (54%); elemental analysis calcd. for C₁₂H₃₆P₃Co (M = 363.25): C 39.68, H 9.99, found: C 39.87, H 9.96.

5: Yield 1.58 g (80%); ^1H NMR (300.13 MHz, C_6D_6 , 300 K,) δ /ppm = 1.16 (s, 36H, PMe_3); $^{31}\text{P}\{^1\text{H}\}$ NMR (121.49 MHz, C_6D_6 , 300 K,) δ /ppm = -17.2 (s, 4P, PMe_3).

6.4.3 Synthesis and Characterization of Phosphaalkyne Complexes **6** and **7**

$[\text{Co}_2(\text{CO})_6(t\text{BuCP})]$ (**6**) was synthesized according to the literature procedure.³¹ Yield 300 mg (80%); ^1H NMR (300.13 MHz, C_6D_6 , 300 K) δ /ppm = 1.12 (s, 9H, $t\text{Bu}$); $^{31}\text{P}\{^1\text{H}\}$ (121.49 MHz, C_6D_6 , 300 K) δ /ppm = -66.5 (br, $\nu_{\text{FWHM}} = 55$ Hz, 1P); IR/ATR: $\tilde{\nu} = 1480$ (vs), 2030 (s), 2050 (s) cm^{-1} .



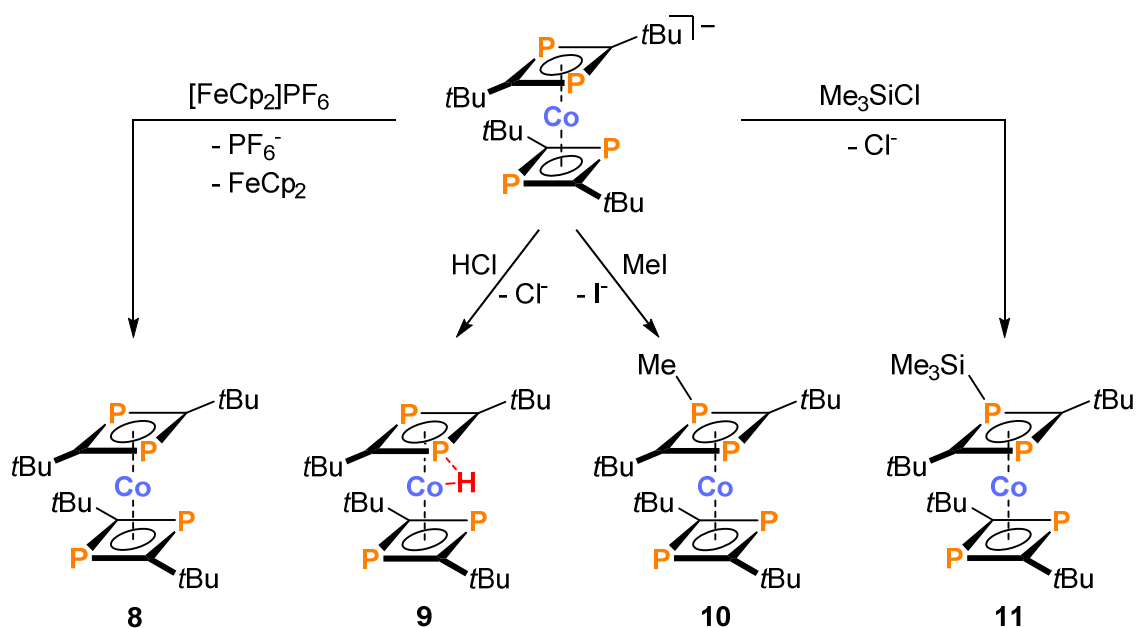
Scheme S2. Synthesis of phosphaalkyne complexes **6** and **7**.

A modified procedure was applied for the synthesis of $[\text{Co}_2(\text{CO})_6(\text{AdCP})]$ (**7**):

A solution of AdCP (356 mg, 2.00 mmol, 1.0 eq) in *n*-pentane (5 mL) was added to a solution of $\text{Co}_2(\text{CO})_8$ (684 mg, 2.00 mmol, 1.0 eq) in *n*-pentane (15 mL) via syringe. Upon stirring the reaction mixture gas evolution was observed and the color changed from yellow to dark red. After stirring overnight the solvent was removed *in vacuo* and the residue was dried for several hours. Compound **7** was isolated as dark-red waxy solid. Yield 880 mg (95%); ^1H NMR (300.13 MHz, C_6D_6 , 300 K) δ /ppm = 1.32–2.23 (m, 15H, Ad); $^{31}\text{P}\{^1\text{H}\}$ NMR (121.49 MHz, C_6D_6 , 300 K) δ /ppm = -69.5 (s, 1P).

6.4.4 Synthesis and Characterization of 1,3-Diphosphacyclobutadiene Complexes **8**–**11**

$[\text{Co}(\text{P}_2\text{C}_2t\text{Bu}_2)_2]$ (**8**), $[\text{Co}(\text{P}_2\text{C}_2t\text{Bu}_2)_2\text{H}]$ (**9**), $[\text{Co}(\text{P}_2\text{C}_2t\text{Bu}_2\text{Me})(\text{P}_2\text{C}_2t\text{Bu}_2)]$ (**10**), and $[\text{Co}(\text{P}_2\text{C}_2t\text{Bu}_2\text{SiMe}_3)(\text{P}_2\text{C}_2t\text{Bu}_2)]$ (**11**) were prepared according to literature procedures (Scheme S3).²⁴

Scheme S3. Synthesis of 1,3-diphosphacyclobutadiene complexes **8–11**.**Characterizations of compounds 8–11:**

8: Yield 0.12 g (46%); M.p. 193-194 °C (dark oil);²⁶ 1H NMR (300.13 MHz, C_6D_6 , 300 K) δ /ppm = -2.6 (very br, *t*Bu).

9: Yield 0.60 g (58%); M.p. 185-186 °C (dark oil);^{25a} 1H NMR (300.13 MHz, C_6D_6 , 300 K) δ /ppm = -4.47 (quintet, $J_{H,P}$ = 16.4 Hz, 1H), 1.13 (s, 36H, *t*Bu); $^{31}P\{^1H\}$ NMR (121.49 MHz, C_6D_6 , 300 K) δ /ppm = -4.7 (very br).

10: Yield 0.96 g (70%); M.p. 196-197 °C (dark oil);^{25a} 1H NMR (300.13 MHz, C_6D_6 , 300 K) δ /ppm = 1.15 (s, 18H, *t*Bu), 1.23 (s, 9H, *t*Bu), 1.32 (s, 9H, *t*Bu), 1.50 (d, $^2J_{H,P}$ = 13.8 Hz, 3H, Me); $^{31}P\{^1H\}$ NMR (121.49 MHz, C_6D_6 , 300 K) δ /ppm = -50.2 (d, $^2J_{P,P}$ = 14 Hz, 1P), 25.9 (s, 2P), 42.4 (br, ν_{FWHM} = 35 Hz, 1P).

11: Yield 0.32 g (77%); M.p. 135-136 °C (dark oil); 1H NMR (300.13 MHz, C_6D_6 , 300 K) δ /ppm = 0.28 (d, $^3J_{H,P}$ = 7 Hz, 9H, SiMe₃), 1.24 (s, 18H, *t*Bu), 1.30 (s, 18H, *t*Bu); ^{29}Si DEPT NMR (79.49 MHz, C_6D_6 , 300 K) δ /ppm = 12.0; $^{31}P\{^1H\}$ NMR (121.49 MHz, C_6D_6 , 300 K) δ /ppm = -1.7 (s, 1P), 19.2 (s, 1P), 21.7 (s, 2P).

6.4.5 Synthesis and Characterization of Phosphole Complex 12

The ligand 2,2',5,5'-tetra-(*tert*-butyl)-1,1'-biphosphole was synthesized according to literature procedures and provided by the BASF SE group.³²

Complex **12** was prepared by a modified procedure of Mathey *et al.*:²⁹

A solution of $Co_2(CO)_8$ (3.420 g, 10.00 mmol) and 2,2',5,5'-tetra-(*tert*-butyl)-1,1'-biphosphole (3.905 g, 10.00 mmol) in toluene (120 mL) was heated to reflux for four days. Subsequently, the

solvent was removed *in vacuo*. The red-orange oil was isolated in quantitative yield. The NMR spectroscopic data of **12** are in accordance with the values reported in literature.²⁹

12: Yield 6.10 g (98%); ¹H NMR (300.13 MHz, C₆D₆, 300 K) δ /ppm = 1.05 (s, 18H, *t*Bu), 5.08 (d, ³J_{H,P} = 4 Hz, 2H, PC₄*t*Bu₂H₂); ³¹P{¹H}NMR (121.49 MHz, C₆D₆, 300 K) δ /ppm = -9.4 (s, 1P).



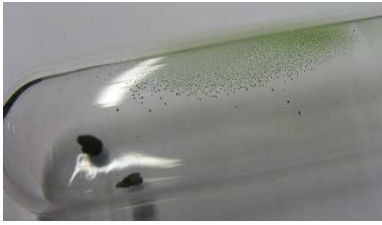






6.4.6 Long-Term Stability Tests







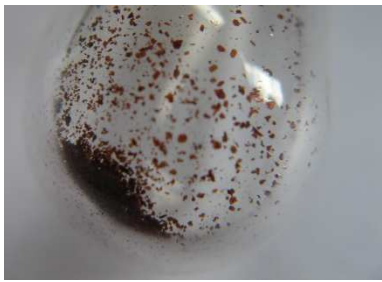



In order to determine the potential suitability of compounds **1–12** for the application in ALD processes we performed long-term stability tests. Glass ampoules were filled with the respective compound (20–30 mg) and sealed with an internal pressure of 10⁻¹ mbar. They were stored in an oven with temperature-control for at least 24 h starting from 60 °C. Afterwards, the temperature was raised in steps of 10 °C. This procedure was continued for each compound until obvious decomposition occurred (indicated by the formation of a metallic mirror or black particles). Preliminary sublimation and decomposition temperatures under reduced pressure were recorded by this procedure.



Figure S1. Representation of a compound sealed in a glass tube at an internal pressure of 10⁻¹ mbar for long-term stability tests at different temperatures.

Table S1. Selected pictures of 1–12 in sealed ampoules demonstrating sublimation and decomposition.

Com- pound	Sublimation	T [°]	Decomposition	T [°]
1		60		100
2		60		100
3	not sublimable			100
4		80		120
5		60		130
6	not sublimable		not performed	

Compound	Sublimation	T [°]	Decomposition	T [°]
7	not sublimable		not performed	
8		130		140
9		130		150
10		130		160
11		130		140
12		130		200

6.4.7 Vapor Pressure Measurements

Measurements of the vapor pressure of selected complexes were performed by the BASF SE company. Selected examples (compounds **2–4**, and **12**) are shown in Figures S2–S5. The graphs demonstrate that the investigated phosphane complexes are not able to generate high vapor pressures. A satisfactory vapor pressure (>100 mbar) is required for maintaining enough substance in the gas phase for subsequent film growth. This could not be achieved with **2–4**, but for compound **12** (Figure S5).

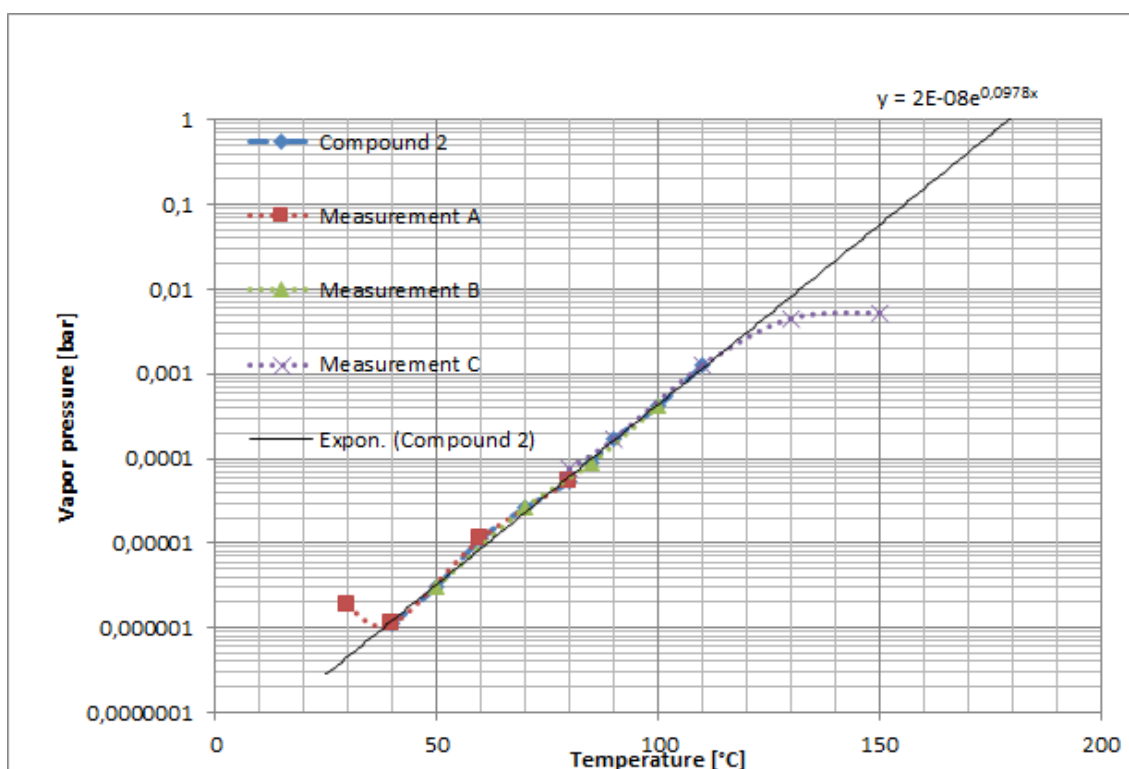


Figure S2. Graphical illustration of the vapor pressure of **2**.

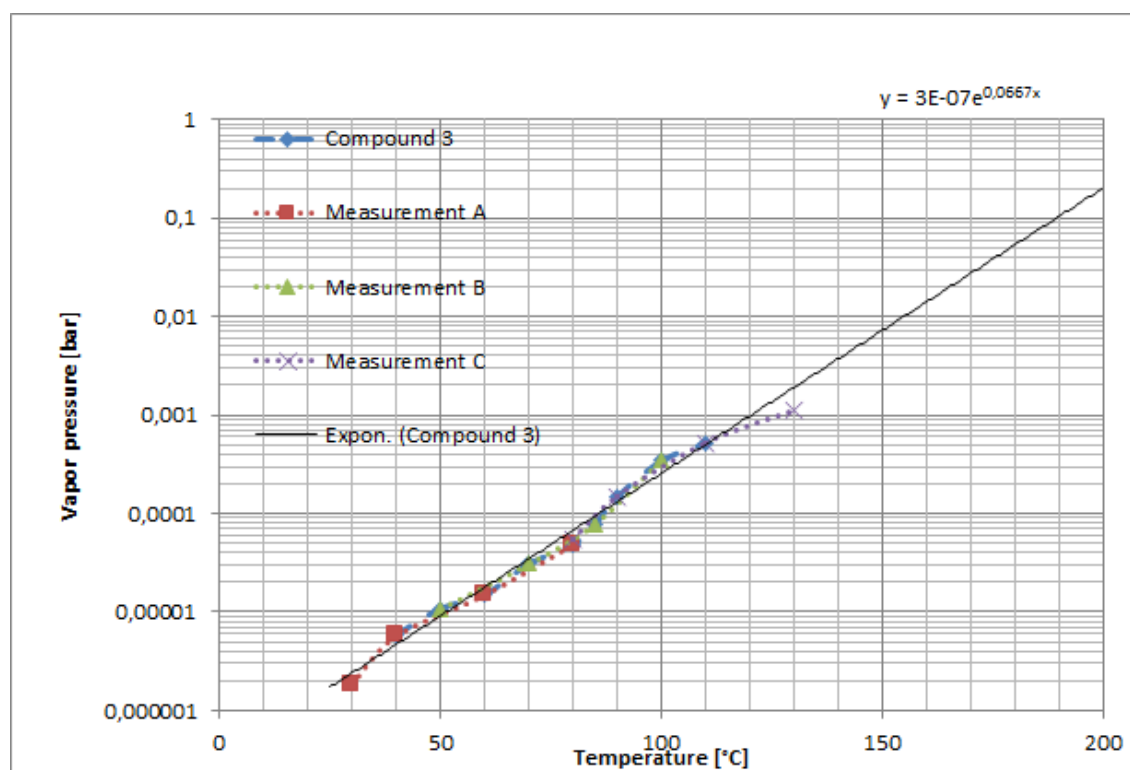


Figure S3. Graphical illustration of the vapor pressure of 3.

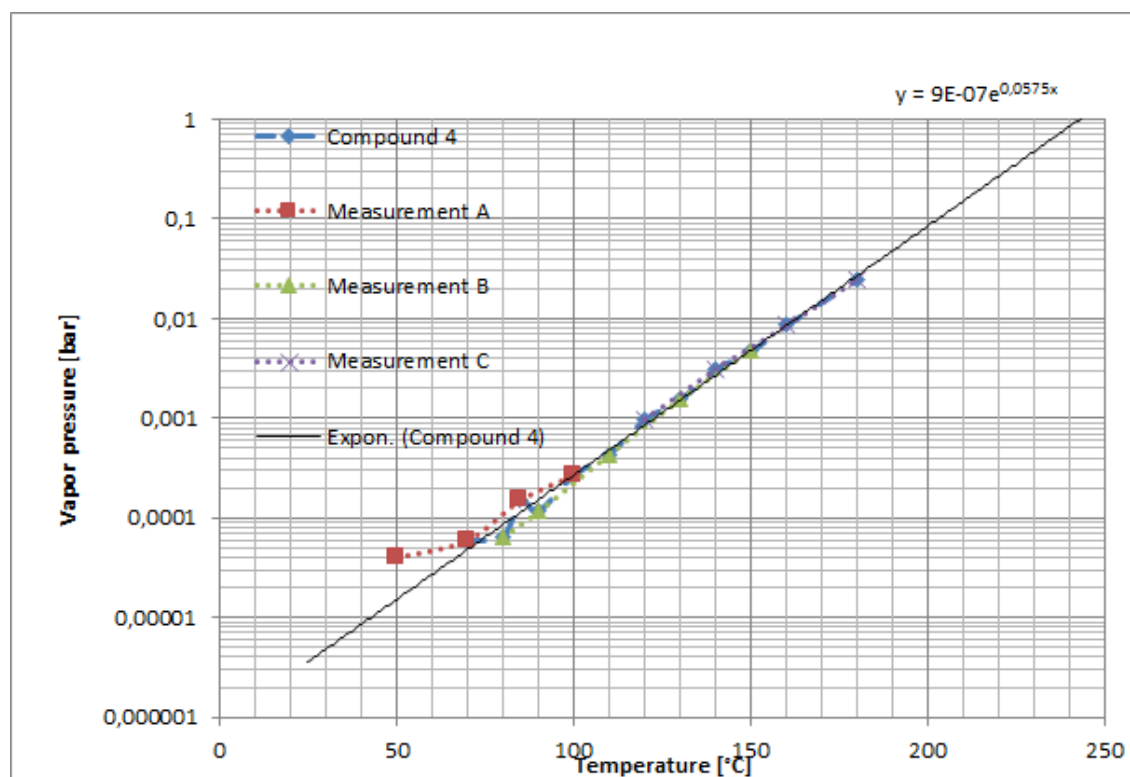


Figure S4. Graphical illustration of the vapor pressure of 4.

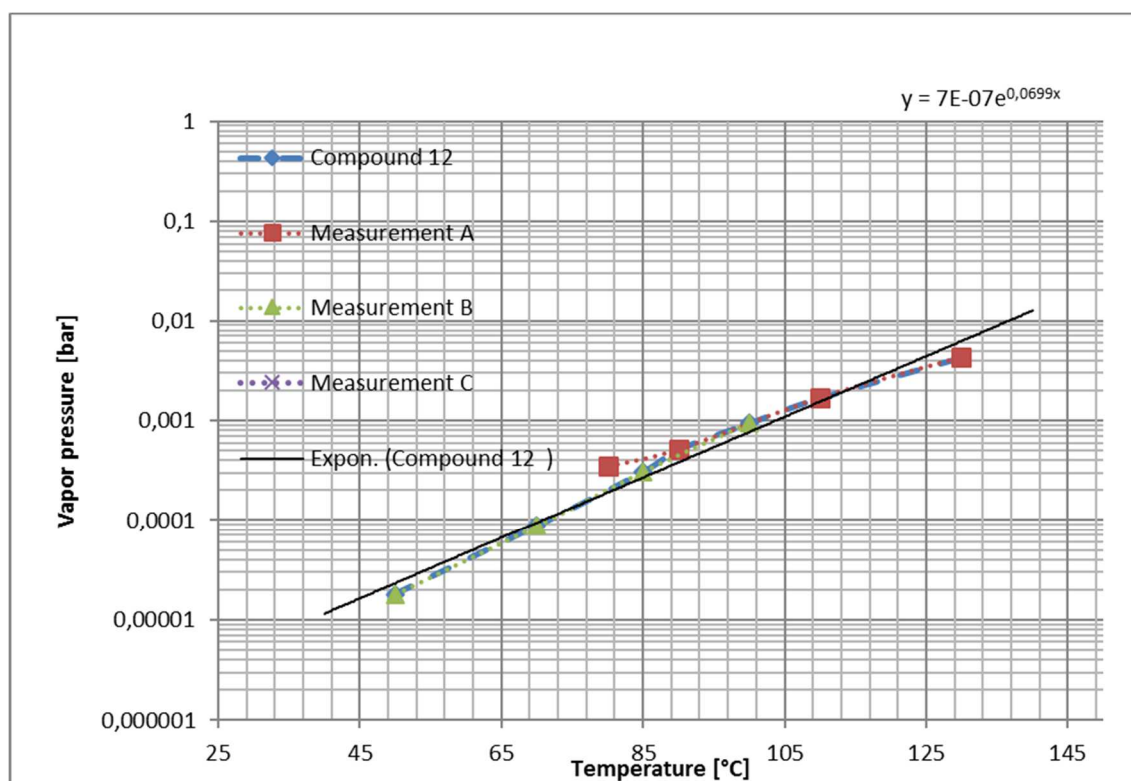


Figure S5. Graphical illustration of the vapor pressure of 12.

6.4.8 Thermogravimetric Analysis

TG/DTG analyses were performed on a Netzsch TG 209F1 Libra unit. Samples of 20–30 mg were heated to 550 °C with a constant heating rate of 5 °C/min.

Table S2 summarizes characteristic thermal properties of **1–12**, sorted by their corresponding ligand system (phosphanes: **1–5**; phosphalkynes: **6, 7**; 1,3-diphosphacyclobutadiene: **8–11**; phosphole: **12**). Neither phosphalkynes nor 1,3-diphosphacyclobutadienes are interesting ligand systems for the generation of cobalt thin films due to their poor thermogravimetric results, i.e. there is more residual mass left at 500 °C than the cobalt content in these compounds. Hence, it is reasonable to assume that there is a high carbon and phosphorus content in the residue. By contrast, homoleptic phosphane complexes **4** and **5** as well as the phosphole complex **12** show a lower residual mass than the calculated metal content of these compounds. Nevertheless, only **12** was utilized for tests as potential precursor for an ALD process because phosphane complexes were previously used in CVD methods.

Table S2. Comparison of characteristic thermal parameters of compounds **1–12**.^a

	M (g/mol)	Mp (°C)	T_{exo} (°C)	Subl (°C)	Amount of metal (%)	Residual mass (%)
1	315.22	100 ^b	-	60	18.70	-
2	355.29	126 ^b	171	60	16.59	21.38
3	465.40	114 ^b	160	-	12.66	19.54
4	363.25	180 ^b	191	80	16.22	14.31
5	363.01	198	176	60	16.17	10.79
6	386.03	100 ^c	171	-	30.53	38.86
7	464.14	100 ^c	-	-	25.39	-
8	459.34	193 ^b	200	>90 ^d /130	12.83	27.34
9	460.34	185 ^b	211	>90 ^d /130	12.80	37
10	474.37	196 ^b	-	100 ^d /130	12.42	38
11	532.53	193 ^b	229	>80 ^d /130	11.07	22.80
12	310.22	180 ^b	184	130	19.00	11.58

^aLeft to right: molecular mass; melting point (derived from literature); onset temperature of decomposition (derived from TG/DTG); sublimation temperature (at 10⁻¹ mbar); amount of the metal in the respective complex; residual mass at 500 °C (derived from TG/DTG); ^bDecomposition temperature; ^cDerived from long-term stability test in sealed glass tube; ^dat 10⁻¹ mbar.

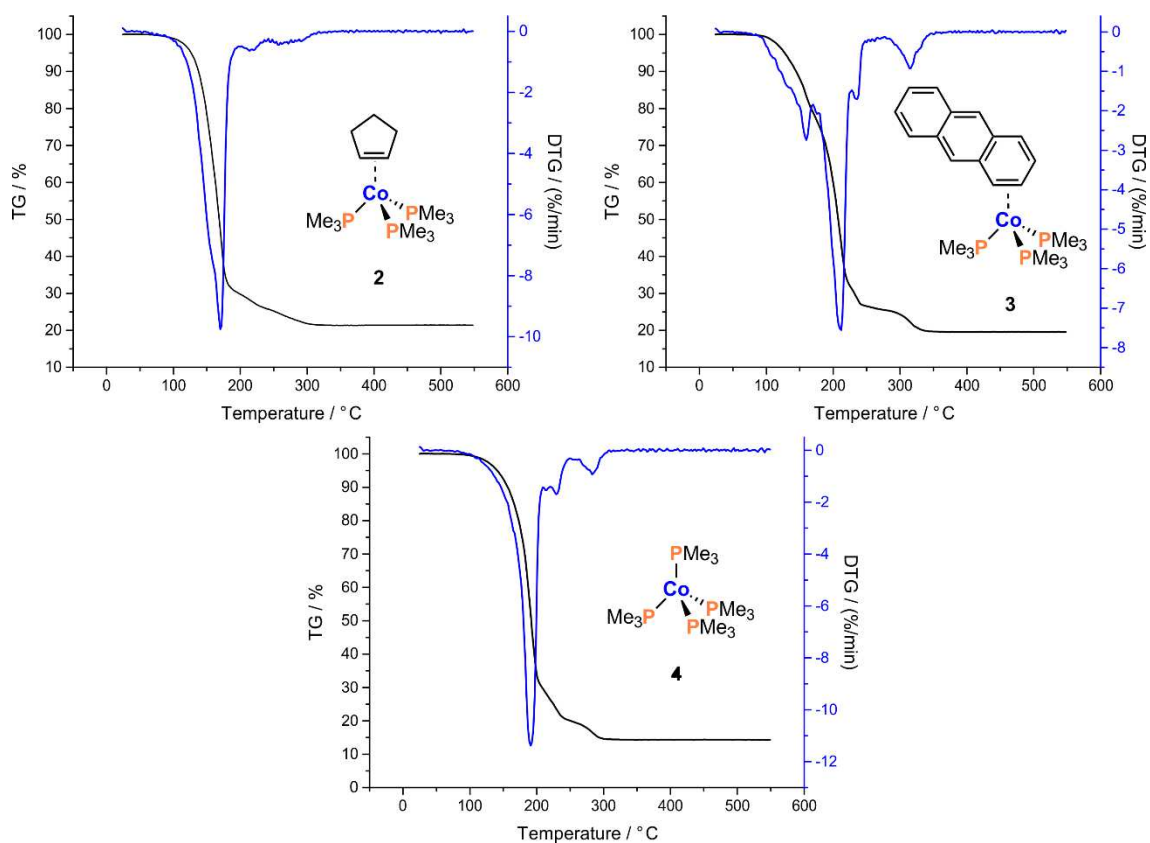


Figure S6. TG/DTG plots of compounds 2–4.

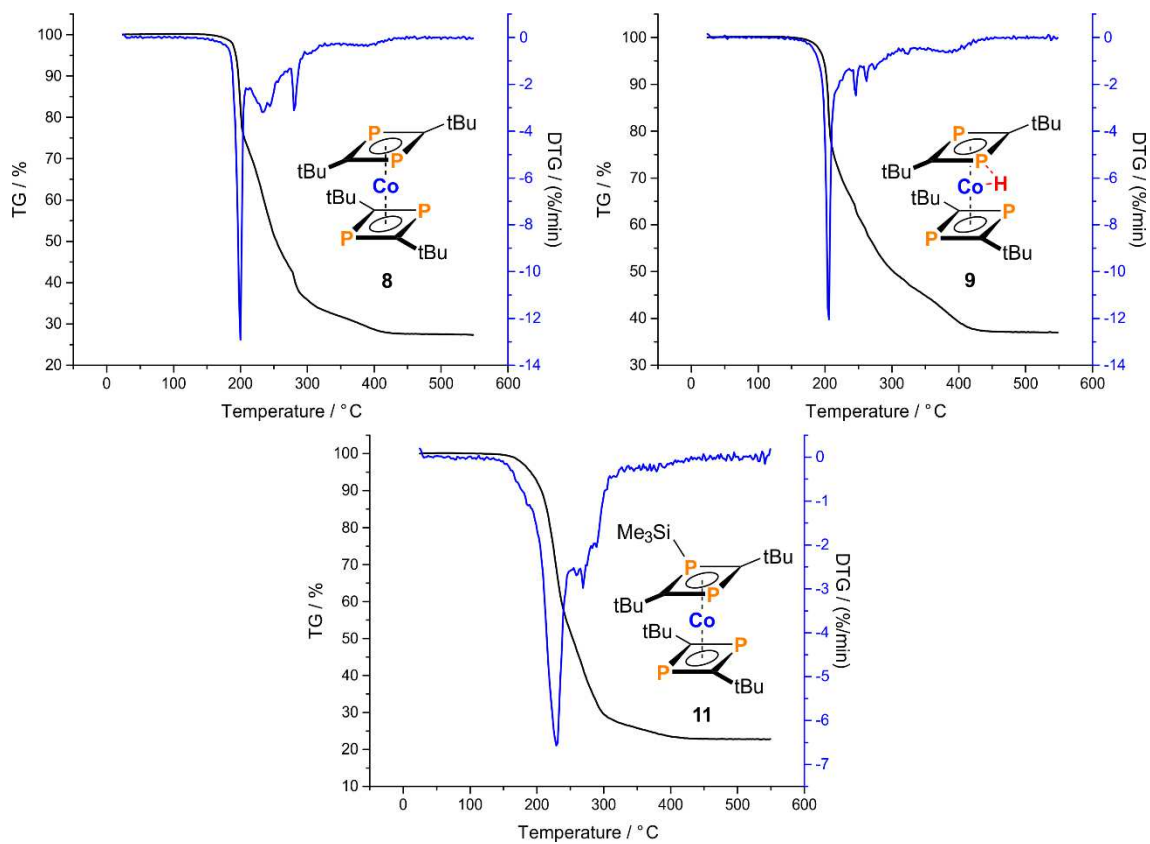


Figure S7. TG/DTG plots of compounds 8, 9, and 11.

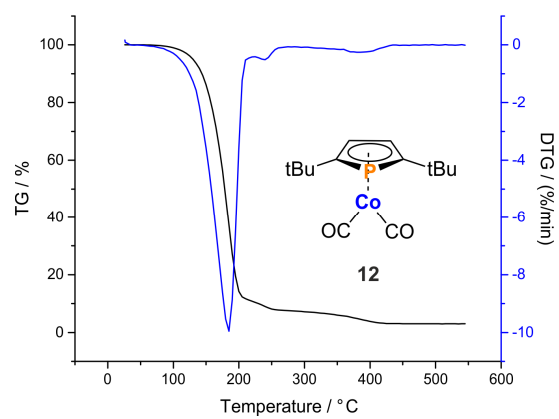


Figure S8. TG/DTG plot of compound **12**.

6.5 References

- 1 M. Ritala, M. Leskelä, in *Handbook of Thin Films* (Ed.: H.S. Nalwa), Academic Press, Burlington, **2002**, pp. 103–159.
- 2 T. Suntola, J. Antson, *U.S. Patent 4058430*, **1977**.
- 3 A. M. Shevjakov, G. N. Kuznetsova, V. B. Aleskovskii, *Chemistry of High Temperature Materials*, Nauka, Leningrad. **1967**, 149–155 (in Russian).
- 4 a) M. Ritala, M. Leskelä, in *Handbook of Thin Film Materials*, **2002**, 103–159; b) C. H. L. Goodman, M. V. Pessa, *J. Appl. Phys.* **1986**, *60*, R65; c) T. Suntola, *Mater. Sci. Rep.* **1989**, *4*, 261; d) L. Niinistö, M. Ritala, M. Leskelä, *Mater. Sci. Eng. B* **1996**, *41*, 23–29; e) S. M. George, A. W. Ott, J. W. Klaus, *J. Phys. Chem.* **1996**, *100*, 13121–13131; f) T. Suntola, *Appl. Surf. Sci.* **1996**, *100/101*, 391–398; g) M. Leskelä, M. Ritala, *Angew. Chem. Int. Ed.* **2003**, *42*, 5548–5554; h) R. L. Puurunen, *J. Appl. Phys.* **2005**, *97*, 121301; i) S. M. George, *Chem. Rev.* **2010**, *110*, 111–131.
- 5 a) T. S. Suntola, A. J. Pakkala, S. G. Lindfors, *U.S. Patent 4413022*, **1977**; b) M. Pessa, R. Mäkelä, T. Suntola, *Appl. Phys. Lett.* **1981**, *38*, 131–132.
- 6 a) J. Nishizawa, H. Abe, T. Kurabayashi, *J. Electrochem. Soc.* **1985**, *132*, 1197–1200; b) S. M. Bedair, M. A. Tischler, T. Katsuyama, N. A. El-Masry, *Appl. Phys. Lett.* **1985**, *47*, 51–53; c) A. Doi, Y. Aoyagi, S. Namba, *Appl. Phys. Lett.* **1986**, *49*, 785–787; d) M. A. Tischler, S. M. Bedair, *Appl. Phys. Lett.* **1986**, *48*, 1681–1683; e) M. A. Tischler, N. G. Anderson, S. M. Bedair, *Appl. Phys. Lett.* **1986**, *49*, 1199–1200; f) R. Huang, A. H. Kitai, *Appl. Phys. Lett.* **1992**, *61*, 1450–1452.
- 7 a) R. Huang, A. H. Kitai, *J. Electron. Mater.* **1993**, *22*, 215–220; b) R. Huang, A. H. Kitai, *J Mater Sci Lett* **1993**, *12*, 1444–1446; c) K. Kim, K. Lee, S. Han, T. Park, Y. Lee, J. Kim, S. Yeom, H. Jeon, *Jpn. J. Appl. Phys.* **2007**, *46*, L173.
- 8 a) L. Hiltunen, H. Kattelus, M. Leskelä, M. Mäkelä, L. Niinistö, E. Nykänen, P. Soininen, M. Tiittad, *Mater. Chem. Phys.* **1991**, *28*, 379–388; b) H. Döring, K. Hashimoto, A. Fujushima, *Ber. Bunsenges. Phys. Chem.* **1992**, *96*, 620–622; c) M. Ritala, M. Leskelä, E. Rauhala, *Chem. Mater.* **1994**, *6*, 556–561; d) E. Nykänen, J. Laine-Ylijoki, P. Soininen, L. Niinistö, M. Leskelä, L. G. Hubert-Pfalzgraf, *J. Mater. Chem.* **1994**, *4*, 1409–1412; e) K. Kukli, M. Ritala, M. Leskelä, *J. Electrochem. Soc.* **1995**, *142*, 1670–1675.
- 9 a) M. Leskelä, L. Niinistö, P. Niemela, E. Nykänen, P. Soininen, M. Tiitta, J. Vähäkangas, *Vacuum* **1990**, *41*, 1457–1459; b) J. Aarik, A. Aidla, A. Jaek, M. Leskelä, L. Niinistö, *Appl. Surf. Sci.* **1994**, *75*, 33–38; c) J. Rautanen, M. Leskelä, L. Niinistö, E. Nykänen, P. Soininen, M. Utriainen, *Appl. Surf. Sci.* **1994**, *82–83*, 553–558; d) P. Soininen, L. Niinistö, E. Nykänen, M. Leskelä, *Appl. Surf. Sci.* **1994**, *75*, 99–105; e) M. Ylilampi, T. Ranta-aho, *J. Electrochem. Soc.* **1994**, *141*, 1278–1284; f) H. Mölsä, L. Niinistö, M. Utriainen, *Adv. Mater. Opt. Electron.* **2004**, *4*, 389–400.
- 10 a) J.-S. Min, Y.-W. Son, W.-G. Kang, S.-S. Chun, S.-W. Kang, *Jpn. J. Appl. Phys.* **1998**, *37*, 4999; b) J.-S. Min, H.-S. Park, S.-W. Kang, *Appl. Phys. Lett.* **1999**, *75*, 1521–1523; c)

- J.-W. Lim, J.-S. Park, S.-W. Kang, *J. Appl. Phys.* **2000**, *87*, 4632–4634; d) R. G. Gordon, J. Becker, D. Hausmann, S. Suh, *Chem. Mater.* **2001**, *13*, 2463–2464; e) J.-S. Park, M.-J. Lee, C.-S. Lee, S.-W. Kang, *Electrochem. Solid-State Lett.* **2001**, *4*, C17–C19; f) D. M. Hausmann, E. Kim, J. Becker, R. G. Gordon, *Chem. Mater.* **2002**, *14*, 4350–4358.
- 11 a) B. S. Lim, A. Rahtu, R. G. Gordon, *Nat. Mater.* **2003**, *2*, 749–754; b) B. S. Lim, A. Rahtu, J.-S. Park, R. G. Gordon, *Inorg. Chem.* **2003**, *42*, 7951–7958; c) Q. Guo, Z. Guo, J. Shi, W. Xiong, H. Zhang, Q. Chen, Z. Liu, X. Wang, *ACS Appl. Mater. Int.* **2018**, *10*, 8384–8390.
- 12 D. J. H. Emslie, P. Chadha, J. S. Price, *Coord. Chem. Rev.* **2013**, *257*, 3282–3296; and references therein.
- 13 D. H. Everett, *Pure Appl. Chem.* **1972**, *31*, 579.
- 14 H. Kim, *Microelectron. Eng.* **2013**, *106*, 69–75.
- 15 a) S. G. Telford, M. Eizenberg, M. Chang, A. K. Sinha, T. R. Gow, *J. Electrochem. Soc.* **1993**, *140*, 3689–3701; b) G. S. Sandhu, *U.S. Patent 5231056*, **1993**; c) S. H. Jung, *U.S. Patent 5726096*, **1998**; d) C. A. van der Jeugd, *U.S. Patent 6335280*, **2002**; e) T. Saito, K. Oshima, Y. Shimogaki, Y. Egashira, K. Sugawara, K. Takahiro, S. Nagata, S. Y. H. Komiyama, *Chem. Eng. Sci.* **2007**, *62*, 6403–6411; f) G. J. Leusink, E. P. Guidotti, *U.S. Pat. Appl. Publ. 0087550*, **2009**; g) C. E. Sveen, Y. Shi, *Thin Solid Films* **2011**, *519*, 4447–4450.
- 16 a) A. E. Widmer, R. Fehlmann, *Thin Solid Films* **1986**, *138*, 131–140; b) C. Milanese, V. Buscaglia, F. Maglia, U. Anselmi-Tamburini, *J. Phys. Chem. B* **2002**, *106*, 5859–5863; c) A. M. Lemonds, T. Bolom, W. J. Ahearn, D. C. Gay, J. M. White, J. G. Ekerdt, *Thin Solid Films* **2005**, *488*, 9–14.
- 17 a) T. C. Chou, T. G. Nieh, *Thin Solid Films* **1992**, *214*, 48–57; b) S. Madhukar, S. Aggarwal, A. M. Dhote, R. Ramesh, S. B. Samavedam, S. Choopun, R. P. Sharma, *J. Mater. Res.* **1999**, *14*, 940–947.
- 18 J. G. Lee, C.-W. Lee, S.-W. Lee, S.-W. Lee, K.-H. Hwang, J.-H. Park, E.-J. Jung, *U.S. Pat. Appl. Publ. 0189846*, **2011**.
- 19 a) S. L. Hsia, T. Y. Tan, P. Smith, G. E. McGuire, *J. Appl. Phys.* **1992**, *72*, 1864–1873; b) S. Bocelli, G. Guizzetti, F. Marabelli, G. Thungström, C. S. Petersson, *Appl. Surf. Sci.* **1995**, *91*, 30–33; c) M. C. Poon, F. Deng, H. Wong, M. Wong, J. K. O. Sin, S. S. Lan, C. H. Ho, P. G. Han, in *1997 IEEE Hong Kong Proceedings Electron Devices Meeting*, **1997**, pp. 65–68; d) J. Chen, J.-P. Colinge, D. Flandre, R. Gillon, J. P. Raskin, D. Vanhoenacker, *J. Electrochem. Soc.* **1997**, *144*, 2437–2442; e) A. R. Ivanova, G. Nuesca, X. Chen, C. Goldberg, A. E. Kaloyeros, B. Arkles, J. J. Sullivan, *J. Electrochem. Soc.* **1999**, *146*, 2139–2145; f) R. Lindsay, A. Lauwers, M. de Potter, N. Roelandts, C. Vrancken, K. Maex, *Microelectron. Eng.* **2001**, *55*, 157–162; g) T.-H. Lin, T. Margossian, L.-Q. Zheng, S. Kumar, I. Marozau, O. Sereda, D. Zemlyanov, C.-J. Shih, R. Zenobi, D. Baudouin, G. de Micheli, P. Gaillardon, C. Copéret, *Chem. Mater.* **2018**, *30*, 2168–2173.

- 20 a) D. A. Edwards, R. M. Harker, M. F. Mahon, K. C. Molloy, *J. Mater. Chem.* **1999**, *9*, 1771–1780; b) N. Roth, A. Jakob, T. Waechtler, S. E. Schulz, T. Gessner, H. Lang, *Surf. Coat. Technol.* **2007**, *201*, 9089–9094; c) M. Shahid, Imtiaz-ud-Din, M. Mazhar, K. C. Molloy, *Inorg. Chim. Acta* **2009**, *362*, 3069–3072; d) L. B. Henderson, J. G. Ekerdt, *Electrochem. Solid-State Lett.* **2009**, *12*, D36–D38; e) L. B. Henderson, J. H. Rivers, D. E. Bost, R. A. Jones, J. G. Ekerdt, *J. Vac. Sci. Technol., A* **2010**, *28*, 54–60.
- 21 a) H.-F. Klein, G. Lull, B. Rodenhäuser, G. Cordier, H. Paulus, *Z. Naturforsch. B.* **1988**, *43*, 1256–1262; b) H.-F. Klein, K. Ellrich, S. Lamac, G. Lull, L. Zsolnai, G. Huttner, *Z. Naturforsch. B.* **1985**, *40*, 1377–1382; c) H.-F. Klein, H. H. Karsch, *Chem. Ber.* **1975**, *108*, 944–955; d) S. D. Ittel, *Inorg. Synth.* **1990**, *28*, 99–104.
- 22 a) H.-S. Kim, G.-H. Choi, S.-B. Kang, W.-H. Sohn, J.-H. Yun, K.-J. Moon, *U.S. Patent 7172967*, **2007**; b) B. Han, K. H. Choi, K. Park, W. S. Han, W.-J. Lee, *Electrochem. Solid-State Lett.* **2012**, *15*, D14–D17.
- 23 a) K. B. Dillon, F. Mathey, J. F. Nixon, *Phosphorus: The Carbon Copy*, Wiley, Chichester, **1998**; b) J. F. Nixon, *Chem. Rev.* **1988**, *88*, 1327–1362; c) J. F. Nixon, *Endeavour* **1991**, *15*, 49–57; d) J. F. Nixon, *Chem. Soc. Rev.* **1995**, *24*, 319–328; e) J. F. Nixon, *Coord. Chem. Rev.* **1995**, *145*, 201–258; f) A. Chirila, R. Wolf, J. Chris Slootweg, K. Lammertsma, *Coord. Chem. Rev.* **2014**, *270–271*, 57–74.
- 24 a) W. W. Brennessel, J. Young Victor G., J. E. Ellis, *Angew. Chem. Int. Ed.* **2002**, *41*, 1211–1215; b) W. W. Brennessel, R. E. Jilek, J. E. Ellis, *Angew. Chem. Int. Ed.* **2007**, *46*, 6132–6136.
- 25 a) R. Wolf, A. W. Ehlers, J. C. Slootweg, M. Lutz, D. Gudat, M. Hunger, A. L. Spek, K. Lammertsma, *Angew. Chem. Int. Ed.* **2008**, *47*, 4584–4587; b) R. Wolf, J. C. Slootweg, A. W. Ehlers, F. Hartl, B. de Bruin, M. Lutz, A. L. Spek, K. Lammertsma, *Angew. Chem. Int. Ed.* **2009**, *48*, 3104–3107.
- 26 a) R. Wolf, A. W. Ehlers, M. M. Khusniyarov, F. Hartl, B. de Bruin, G. J. Long, F. Grandjean, F. M. Schappacher, R. Pöttgen, J. C. Slootweg, M. Lutz, A. L. Spek, K. Lammertsma, *Chem. Eur. J.* **2010**, *16*, 14322–14334.
- 27 J. Malberg, *Dissertation* **2013**, University of Regensburg.
- 28 a) E. P. Marsh, *U.S. Pat. Appl. Publ. 0032365*, **2005**; b) E. P. Marsh, *U.S. Pat. Appl. Publ. 0157863*, **2006**; c) H.-B.-R. Lee, H. Kim, *Electrochem. Solid-State Lett.* **2006**, *9*, G323–G325; d) K. Kim, K. Lee, S. Han, T. Park, Y. Lee, J. Kim, S. Yeom, H. Jeon, *Jpn. J. Appl. Phys.* **2007**, *46*, L173–L176; e) S. Ganguli, S. S. Chu, M. Chang, S.-H. Yu, K. Moraes, S.-E. Phan, *U.S. Pat. Appl. Publ. 0202254*, **2007**; f) B. Han, K. Ha Choi, J. Min Park, J. Woo Park, J. Jung, W.-J. Lee, *J. Vac. Sci. Technol., A* **2012**, *31*, 01A145.
- 29 A. J. M. Caffyn, D. Carmichael, F. Mathey, L. Ricard, *Organometallics* **1997**, *16*, 2049–2054.
- 30 S. Shukla, *Masters Thesis* **2016**, TU Dresden.

- 31 J. C. T. R. B.-S. Laurent, P. B. Hitchcock, H. W. Kroto, J. F. Nixon, *J. Chem. Soc., Chem. Commun.* **1981**, 1141–1143.
- 32 D. Carmichael, L. Ricard, F. Mathey, *J. Chem. Soc., Chem. Commun.* **1994**, 1167–1168.

7 SUMMARY

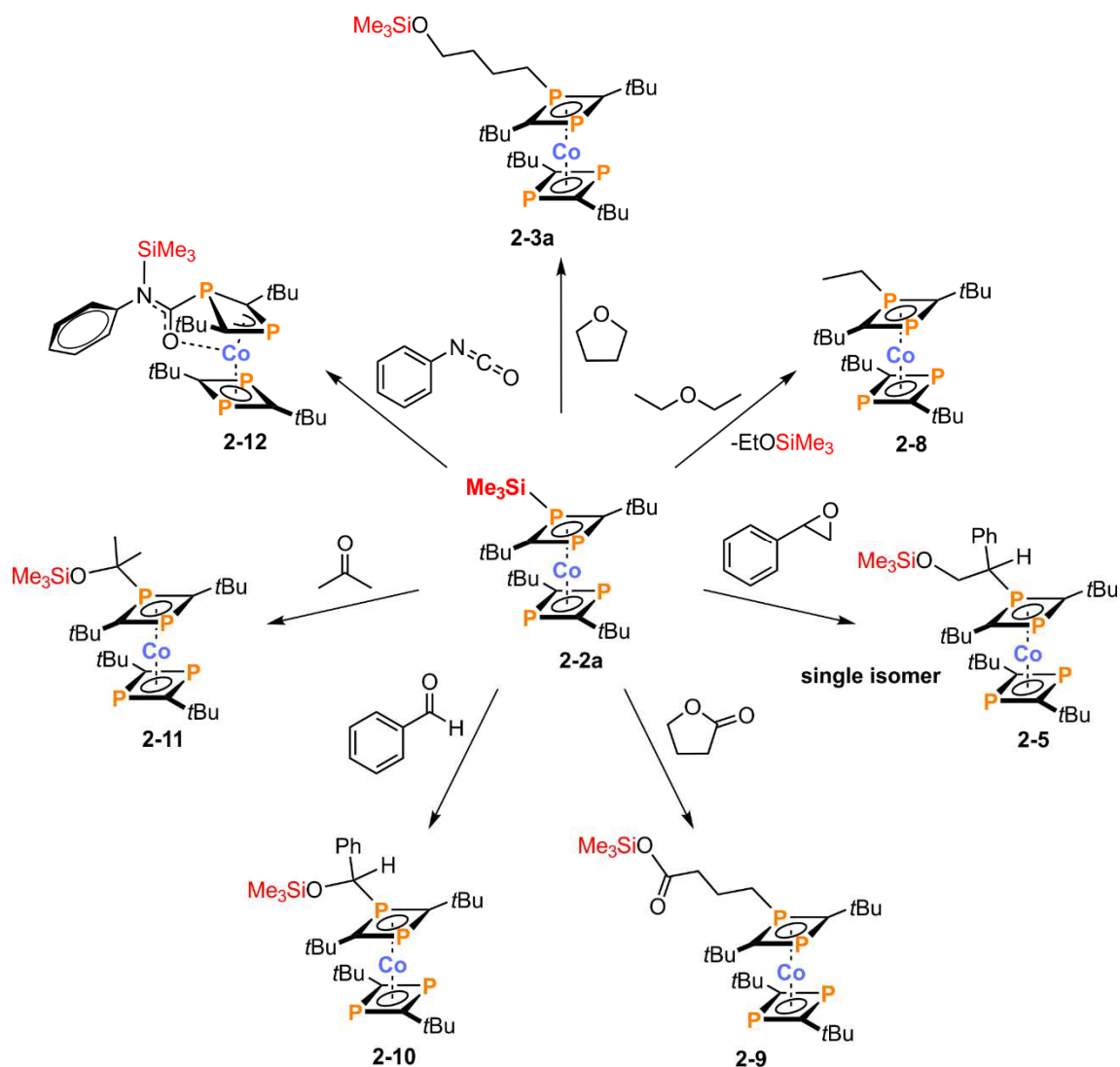
Chapter 1. The Chemistry of Phosphaalkyne and Diphosphacyclobutadiene Complexes

This introductory chapter briefly reviews the chemistry of phosphaalkynes and complexes derived therefrom. The aim of this chapter is to point out the importance of the development of phosphaalkynes for organometallic chemistry and to highlight their ability to form several phosphorus-containing ligands in the coordination sphere of transition metals. Besides the structural motifs of these ligands, this chapter covers previously reported oligonuclear compounds bearing diphosphacyclobutadienes in their structural framework. Finally, more recent results reported by our group are described.

Chapter 2. Functionalization of 1,3-Diphosphacyclobutadiene Cobalt Complexes via Si–P Bond Insertion¹

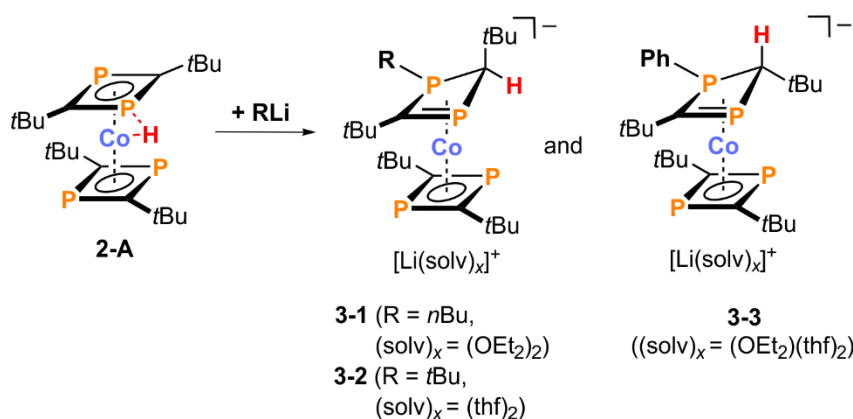
The main goal of this thesis was to further explore the reactivity of the previously described, anionic, homoleptic $[\text{Co}(\text{P}_2\text{C}_2\text{tBu}_2)_2]^-$ sandwich compound and to synthesize and characterize new oligonuclear diphosphacyclobutadiene complexes in order to understand its coordination behavior. The results are summarized in Schemes 1–6.

Complexes **2-3a–2-12** were synthesized according to Scheme 1 by reacting the new trimethylsilylated complex **2-2a** with ethers, epoxides, esters, aldehydes, ketones, and phenyl isocyanate to afford functionalized 1,3-diphosphacyclobutadiene complexes. Besides, complex **2-2a** was obtained by treating the THF-free salt $[\text{K}(\text{tol})_2\{\text{Co}(\text{P}_2\text{C}_2\text{tBu}_2)_2\}]$ with Me_3SiCl . In an initial study we found that reacting $[\text{K}(\text{thf})_2\{\text{Co}(\text{P}_2\text{C}_2\text{tBu}_2)_2\}]$ with Me_3SiCl gives **2-3a** in quantitative yield according to $^{31}\text{P}\{^1\text{H}\}$ NMR spectroscopy. Reaction of **2-2a** with acyclic ethers resulted in alkylation of the diphosphacyclobutadiene ligand through elimination of EtOSiMe_3 (complex type **2-8**). Cleavage of a C–O bond of styrene oxide was observed in the reaction with **2-2a** giving complex **2-5** as the single regioisomer. Insertions have also been observed using lactones, aldehydes, and ketones as substrates (complexes **2-9–2-11**). Nevertheless, the insertion of epoxides, aldehydes, and ketones is limited as it resulted in unselective reactions and the formation of certain amounts of the known hydride complex $[\text{Co}(\text{P}_2\text{C}_2\text{tBu}_2)_2\text{H}]$ (**2-A**). Interestingly, the reaction of **2-2a** with phenyl isocyanate afforded the C–N inserted complex **2-12** instead of the C–O inserted species. An interaction between the isocyanate oxygen atom and the cobalt atom was also observed (Co–O 2.037(1) Å), which leads to a severely tilted η^3 -coordinated 1,3-diphosphacyclobutene-2-yl ligand showing a dihedral angle between the C1–P2–C2/C2–P1–C1 planes of 38.3°.

Scheme 1. Synthesis of functionalized 1,3-diphosphacyclobutadiene complexes **2-2a–2-12**.

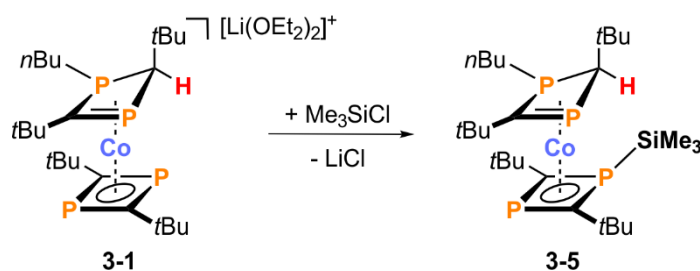
Chapter 3. 1,3-Diphosphacyclobutene Cobalt Complexes²

In a similar study, we were interested in the reactivity of the above-mentioned hydride complex [Co(P₂C₂tBu₂)₂H] (**2-A**). We found that treatment of **2-A** with lithium organyls RLi gives novel functionalized 1,3-diphosphacyclobutene complexes **3-1–3-3** (Scheme 2). Remarkably, depending on the substituent R we observed primarily the *endo*-H isomer (**3-1**, R = *n*Bu; **3-2**, R = *t*Bu) or the *exo*-H isomer (**3-3**, R = Ph). In the latter one the formation of **3-*exo*-H-3** proceeds via **3-*endo*-H-3** as demonstrated by ³¹P NMR monitoring at different temperatures. In comparison, only trace amounts of the corresponding **3-*exo*-H-1** compound could be observed whereas **3-*exo*-H-2** was not formed even at elevated temperature, although DFT calculations (in the gas phase) have shown that the *exo*-H isomers are thermodynamically favored in all three cases.



Scheme 2. Synthesis of novel functionalized 1,3-diphosphacyclobutene complexes **3-1**–**3-3**.

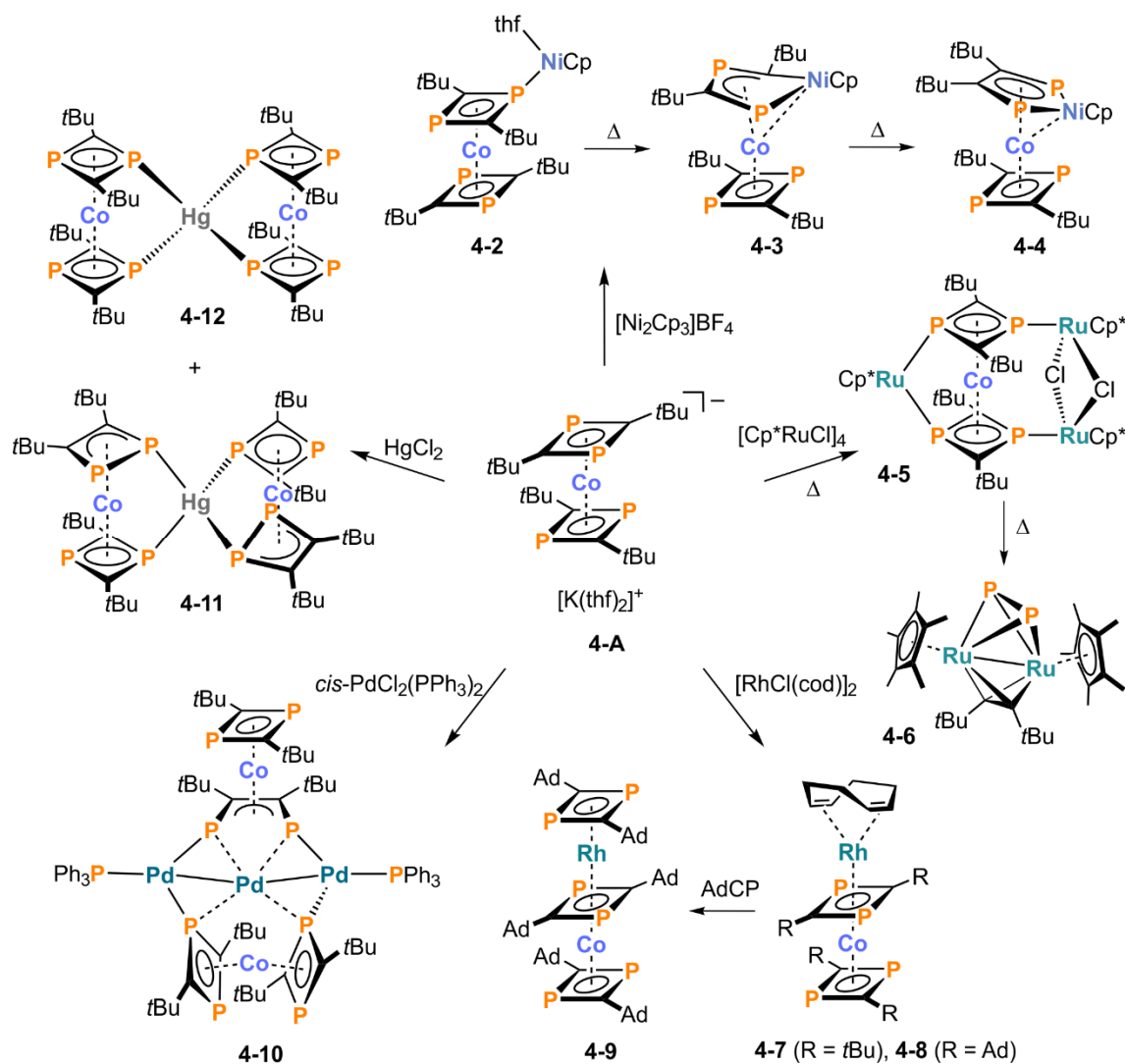
We further studied the reactivity of these anionic species, as exemplified by the reaction of **3-1** with Me₃SiCl (Scheme 3). The most intriguing aspect of compound **3-5** is the *endo*-position of the SiMe₃ group pointing in the direction of the cobalt atom. This may result from template effects of the lithium cation in **3-1**, although the actual reason is presently unclear. By contrast, the silyl substituent of **2-2a** points away from the central metal atom. Another feature of complex **3-5** is that both P₂C₂ ligands are functionalized by different substituents. Following this procedure with other nucleophiles and electrophiles is expected to yield diverse bis-functionalized complexes of type **3-5** which could be the focus of future investigations.



Scheme 3. Functionalization of 1,3-diphosphacyclobutene complex **3-1** with Me₃SiCl.

Chapter 4. Flexidentate Coordination Behavior and Chemical Non-Innocence of a Bis(1,3-diphosphacyclobutadiene) Sandwich Anion³

In extension to our reactivity studies demonstrated on [Co(P₂C₂*t*Bu₂SiMe₃)(P₂C₂*t*Bu₂)] (**2-2a**) and [Co(P₂C₂*t*Bu₂)₂H] (**2-A**) we were keen to investigate the coordination behavior of our homoleptic [Co(P₂C₂*t*Bu₂)₂][−] sandwich anion (**4-A**) toward transition metal cations, i.e. Ru(II), Ni(II), Rh(I), Pd(II), and Hg(II). We found that the anionic sandwich complex **4-A** can be utilized as a flexidentate ligand displaying a variety of coordination modes. The results are summarized in Scheme 4.



Scheme 4. Synthesis of di-, tri-, tetra-, and pentanuclear 1,3-diphosphacyclobutadiene complexes 4-2-4-12.

Transmetalation of **4-A** with $[Ni_2Cp_3]BF_4$ at low temperature gave the dinuclear complex **4-2** showing the well-known σ -coordination mode. This reaction is followed by insertion of the $CpNi^+$ fragment into one of the 1,3-diphosphacyclobutadiene ligands to afford complex **4-3**. Interestingly, an insertion process of a transition metal fragment into an intact P_2C_2 ligand had never previously been observed. Only the reaction with the main group electrophile PPh_2^+ had resulted in insertion into a C–P bond of a P_2C_2 ligand moiety. Prolonged stirring of a THF solution at ambient temperature or heating to 60 °C for nine hours yielded the isomerization product **4-4**. Compounds **4-3** and **4-4** show remarkably downfield shifted signals in the ^{31}P NMR spectra due to the coordination to nickel ($\delta = +492$ ppm for **4-3**, $\delta = +459$ ppm for **4-4**).

Heating a THF solution of **4-A** and 0.75 equivalents of $[Cp^*RuCl]_4$ to reflux for four hours yielded the tetranuclear complex **4-5** which displays the $Co(P_2C_2tBu)_2$ fragment in an eclipsed conformation. When the same reaction mixture was heated to reflux for 30 hours decomposition obviously occurred giving the dinuclear diruthenium complex **4-6** as the main product. An

intriguing aspect of this species is the presence of both a bridging P_2^{2-} and a bridging alkyne which, to the best of our knowledge, has never been observed before. The P_2^{2-} fragment gives rise to a broad signal in the ^{31}P NMR spectrum at $\delta = +128$ ppm.

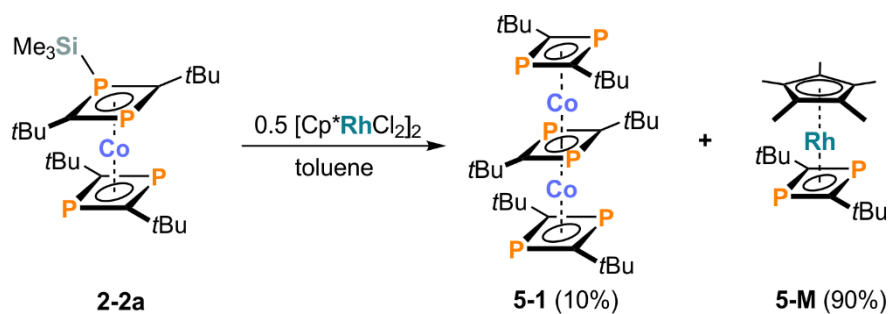
A highly interesting result was obtained when **4-A** was reacted with 0.5 equivalents of $[RhCl(cod)]_2$. The complex **4-7** formed in this reaction shows a rare example of a 1,3-diphosphacyclobutadiene ligand acting as a π -ligand to two metal atoms simultaneously by adopting a bridging position. When the related adamantyl substituted compound **4-8** was reacted with two equivalents of $AdC\equiv P$ at low temperature we observed characteristic $^{31}P\{^1H\}$ NMR signals which indicate the formation of the first tripledecker complex bearing only 1,3-diphosphacyclobutadiene ligands. Only the solid-state molecular structure remains unknown as the crystals obtained from *n*-pentane had too bad quality to be investigated by XRD studies. Nevertheless, the presumed dinuclear cobalt-rhodium complex **4-9** demonstrates that tripledecker complexes featuring exclusively P_2C_2 ligands might be accessible through stepwise synthesis starting from treatment of $[K(thf)_2\{Co(P_2C_2Ad)_2\}]$ with a suitable Rh(I) precursor and subsequent addition of phosphalkyne.

Transmetalation of $[K(thf)_2\{Co(P_2C_2tBu)_2\}]$ (**4-A**) with *cis*- $PdCl_2(PPh_3)_2$ (3:2 stoichiometry) gave complex **4-10** as the main product. This pentanuclear compound features a Pd_3 chain which is stabilized by two $Co(P_2C_2tBu)_2$ moieties. One cobaltate fragment coordinates as a chelating ligand similar to complex **4-5**. However, the most remarkable feature of the molecular structure of **4-10** is the presence of a 1,4-diphospha-2-butene ligand which presumably forms upon isomerization of one 1,3-diphosphacyclobutadiene unit to the 1,2-isomer (as also observed for the rearrangement of **4-3** to **4-4**), followed by an oxidative addition of the resulting P–P bond on palladium.

Partly motivated by the presumed tripledecker complex **4-9** another goal of this thesis was to explore whether tetradeccker complexes of the type $[M\{Co(P_2C_2tBu)_2\}_2]$ (M = transition metal) are accessible. Hence, we reacted **4-A** with $HgCl_2$ (2:1 stoichiometry). Single-crystal X-ray diffraction studies, however, revealed two isomeric complexes **4-11** and **4-12**. The molecular structures of both compounds show the sandwich anion $[Co(P_2C_2tBu)_2]^-$ acting as chelating ligand to mercury. The molecular structure of **4-11** also exhibits an isomerization of one 1,3-diphosphacyclobutadiene ligand of each $Co(P_2C_2tBu)_2$ fragment to its 1,2-derivative.

Chapter 5. A Homoleptic 1,3-Diphosphacyclobutadiene Tripledecker Complex

During our investigations of the coordination behavior of $[Co(P_2C_2tBu)_2]^-$ we found that the trimethylsilated complex **2-2a** is a good precursor for the one-pot synthesis of the tripledecker complex **5-1** (Scheme 5). This complex is the first homodinuclear tripledecker which exhibits



Scheme 5. Synthesis of tripledecker complex 5-1.

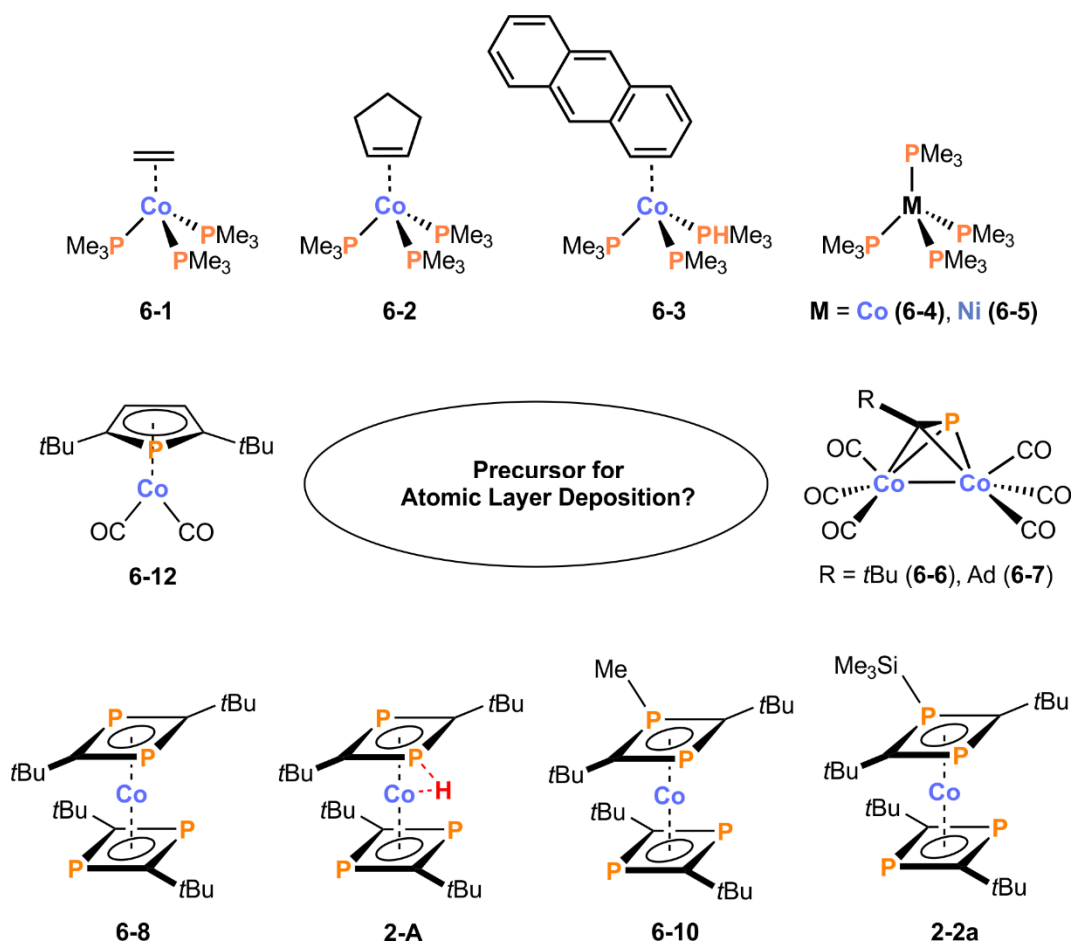
only 1,3-diphosphacyclobutadiene ligands in its structural framework. The known $[\text{Cp}^*\text{Rh}(\text{P}_2\text{C}_2\text{tBu})]$ (**5-M**) was identified as the main product by ^{31}P NMR spectroscopy giving a doublet at $\delta = +39$ ppm. This protocol suggests a possible route to the analogous diiron-tripledecker complex which is expected to be an interesting compound due to its paramagnetic properties. This should allow for the exploration of whether the bridging 1,3-diphosphacyclobutadiene ligand enables the presumed (anti)ferromagnetic coupling between the iron centers or if it behaves as coupling barrier.

Chapter 6. Phosphaorganometallic Cobalt Complexes as Potential Precursors for the Generation of Thin Inorganic Films⁴

In chapter 6 we describe the potential application of neutral cobalt complexes with phosphorus containing ligands such as monophosphanes, phosphalkynes, 1,3-diphosphacyclobutadienes, and phospholes as precursors in atomic layer deposition (ALD) processes (Scheme 6).

Compounds **28–39** have been characterized by different methods, i.e. NMR (**6-6–6-12**) and IR spectroscopy (**6-6**, **6-7**, **6-12**), and elemental analysis (**6-1–6-5**). In order to determine if they are suitable precursors for the application in ALD processes, compounds **6-1–6-12** have been thoroughly analyzed by their sublimation properties and their long-term stability upon thermal stress, and by vapor pressure and thermogravimetric measurements.

We found that neither cobalt phosphane complexes nor dicobalt phosphalkyne complexes nor 1,3-diphosphacyclobutadiene cobalt complexes can be applied in ALD processes due to their low decomposition temperature or their very poor sublimation properties. However, the cobalt phosphole complex **6-12** seems to be a good starting point for further studies as it revealed a wide thermal window (range between sublimation temperature and decomposition temperature) and a sufficiently high vapor pressure. Nevertheless, generated thin films showed high carbon contamination which should be avoided in order to obtain cobalt monolayers. Future investigations could focus on improving the thermal properties by changing the substituents or substitution of the carbonyl ligands by more labile ligands like olefins.



Scheme 6. Neutral cobalt complexes 6-1–6-12 featuring monophosphanes, phosphalkynes, 1,3-diphosphacyclobutadienes or phospholes as potential precursor for ALD applications.

References

- 1 C. Rödl, J. Bissmeyer, R. Wolf, *Z. Naturforsch. B* **2018**, 73, 895.
- 2 C. Rödl, K. Schwedtmann, J. J. Weigand, R. Wolf, *Chem. Eur. J.* **2019**, 25, 6180.
- 3 C. Rödl, R. Wolf, *Chem. Eur. J.* **2019**, DOI: 10.1002/chem.201901061.
- 4 F. Abels, D. Löffler, H. Wilmer, R. Wolf, C. Rödl, P. Büschelberger, *Process for the Generation of Thin Inorganic Films*, **2017**, WO/2017/129440.

8 ACKNOWLEDGEMENT

Zuletzt möchte ich mich bei folgenden Personen bedanken:

- Ganz besonders bei Prof. Dr. Robert Wolf für die hervorragende Betreuung, die interessante Aufgabenstellung, die anregenden Diskussionen, die exzellenten Arbeitsbedingungen und der großen Freiheit bei meiner Forschung.
- Prof. Dr. Manfred Scheer (Zweitgutachter), Prof. Dr. Frank-Michael Matysik (Drittprüfer) und Prof. Dr. Alkwin Slenzka (Vorsitz) für die Bereitschaft, die Plätze der Prüfungskommission zu besetzen.
- Dr. Michael Bodensteiner, Dr. Stefanie Gärtner und Prof. Dr. Robert Wolf für die Unterstützung und Lösung von Problemfällen bei der Einkristallstrukturanalyse.
- Den Mitarbeitern der zentralen Analytik und Werkstätten, insbesondere: Sabine Stempfhuber und Katharina Beier (Röntgenstrukturanalyse), Annette Schramm, Georgine Stühler und Fritz Kastner (NMR-Abteilung), Barbara Baumann und Helmut Schüller (Elementaranalyse), Markus Lindner (Glasbläserei), Peter Fuchs (Elektronikwerkstatt).
- Meinen Kooperationspartnern Prof. Dr. Jan J. Weigand und Dr. Kai Schwedtmann (TU Dresden) für ihren wertvollen Beitrag, ihr hohes Engagement und die interessanten Diskussionen.
- Meinen lieben Nachbarn auf dem Gang des 2. Stockwerks sowie auf den Stockwerken ober- und unterhalb, den Mitarbeitern der Arbeitskreise: Díaz-Díaz, Fleischer, Garcia Mancheño, Jacobi von Wangelin, für die wunderbaren Kaffeepausen, Grillabende (als sie noch erlaubt waren ☺), Weihnachtsfeiern, Konferenzen, oder einfach für's Zuhören und Quatschen.
- Dem AK Weigand: Felix Hengersdorf, Rene Panzer, Chris Sala, Kathleen Schnaars, Robin Schoemaker, Stephen Schulz, Kai Schwedtmann, Fabian Watt, Jan J. Weigand und Sivathmeehan Yogendra für sehr schöne und unterhaltsame Konferenztage sowie die herzliche Aufnahme ins AK-Geschehen bei meinem Besuch im November 2016.
- Den aktuellen und früheren Arbeitskreismitgliedern: Anup Adhikari, Percia Beatrice Arockiam, Philipp Büschelberger, Uttam „Der Uttinger“ Chakraborty, Dirk Herrmann, Gabi Hierlmeier, Christian Hoidn, John Kelly, Helge Lange, Julia Leitl, Ulrich Lennert, Thomas Maier, Matt Margeson, Julia Märsch, Bernd Mühldorf, Stefan Pelties, Veronica Scheidler, Daniel Scott, Marion Till, Robert Wolf, Christoph Ziegler für die einmalige Stimmung im Arbeitskreis, die sehr kollegiale Atmosphäre, die motivierende nach-dem-Labor-trinkma-no-a-Halbe, die musikalischen Mottotage, die eingeschlafene Planung einer Probe unserer Band *Organometallica*, die Lasertag-Besuche sowie die AK-Ausflüge.

- All meinen Freunden aus Regensburg und der Heimat sowie meiner Familie: Brigitte und Gerhard, Simone und Franz, Alexander sowie Petra, Wolfgang, Dennis und meiner Oma Renate für euer großes Verständnis und die Unterstützung in vielerlei Hinsicht.
- Meinen Schwiegereltern Inge und Helmut und bei meinen Schwagern und Schwägerinnen und den Kindern für ihr stetiges Interesse und den Aufmunterungen, die wesentlich zum Erfolg beigetragen haben.

Unendlich dankbar bin ich meiner Frau, Susi, für ihre Geduld und ihren Rückhalt während meiner gesamten Studien- und Promotionszeit, sowie für ihre grenzenlose Unterstützung, die sie mir tagtäglich entgegenbringt.

9 CURRICULUM VITAE

Education

Since Jan. 2015	Ph.D. at the University of Regensburg, Germany (Institute of Inorganic Chemistry) in the group of Prof. Dr. R. Wolf: “Reactivity and Coordination Studies of Diphosphacyclobutadiene Sandwich Anions”
Dec. 2012 – Nov. 2014	Master of Science in Chemistry at the University of Regensburg, Germany Master Thesis in the group of Prof. Dr. R. Wolf (Institute of Inorganic Chemistry): “Synthese und Charakterisierung von mehrkernigen Metallkomplexen mit 1,3-Diphosphacyclobutadien-Liganden”
Oct. 2009 – Nov. 2012	Bachelor of Science in Chemistry at the University of Regensburg, Germany Bachelor Thesis in the group of Prof. Dr. R. Wolf (Institute of Inorganic Chemistry): “Eisen(II)-Arylkomplexe: Synthese, Charakterisierung und Reaktivität gegenüber Alkylelektrophilen”
Juni 2008	Abitur at the Maximilian-von-Montgelas Gymnasium, Vilsbiburg

Presentations

08. – 13.07.2018	Talk – 22 nd International Conference on Phosphorus Chemistry (ICPC) in Budapest, Hungary
11. – 13.03.2018	Poster – 14 th Koordinationschemie-Treffen in Heidelberg
10. – 14.09.2017	Poster – Wissenschaftsforum Chemie – Jubiläumskongress „GDCh – 150 Jahre“ in Berlin, Germany
09. – 13.07.2017	Poster – 22 nd EuCOMC in Amsterdam, The Netherlands
20. – 22.03.2017	Talk – 14 th European Workshop on Phosphorus Chemistry (EWPC) in Cluj-Napoca, Romania
19. – 21.02.2017	Talk – 15 th Ferrocene Colloquium in Mainz, Germany
26. – 28.09.2016	Poster – 18 th Vortragstagung der Wöhler-Vereinigung für Anorganische Chemie in Berlin, Germany
05. – 10.06.2016	Talk – 21 st International Conference on Phosphorus Chemistry (ICPC) in Kazan, Russia
07. – 09.03.2016	Poster - 13 th European Workshop on Phosphorus Chemistry (EWPC) in Berlin, Germany
23. – 28.08.2015	Talk – Wissenschaftliches Kolloquium von Arbeitsgruppen für Anorganische Chemie 2015 in Hirschegg, Austria
26. – 31.07.2015	Poster – 14 th International Symposium on Inorganic Ring Systems (IRIS) in Regensburg, Germany
16. – 18.03.2015	Poster - 12 th European Workshop on Phosphorus Chemistry (EWPC) in Kassel, Germany
22. – 24.02.2015	Poster – 13 th Ferrocene Colloquium in Leipzig, Germany

10 LIST OF PUBLICATIONS

- 1) C. Rödl, R. Wolf, *Eur. J. Inorg. Chem.* **2016**, 2016, 736–742, “Cobalt(I) and Nickel(II) Complexes of Bis(1,3-diphosphacyclobutadiene) Sandwich Anions”
- 2) F. Abels, D. Loeffler, H. Wilmer, R. Wolf, C. Roedl, P. Büschelberger, *Process for the Generation of Thin Inorganic Films*, **2017**, WO/2017/129440
- 3) P. Coburger, S. Demeshko, C. Rödl, E. Hey-Hawkins, R. Wolf, *Angew. Chem. Int. Ed.* **2017**, 56, 15871–15875, “Oxidative P-P Bond Addition to Cobalt(-I): Formation of a Low-Spin Cobalt(III) Phosphanido Complex”
- 4) D. Herrmann, C. Rödl, B. de Bruin, F. Hartl, R. Wolf, *Dalton Trans.* **2018**, Vol, Page, “Synthesis, electronic structure and redox properties of the diruthenium sandwich complexes $[Cp^*Ru(\mu-C_{10}H_8)RuCp^*]^x$ ($x = 0, 1+$; $Cp^* = C_5Me_5$; $C_{10}H_8 = naphthalene$)”
- 5) C. Rödl, J. Bissmeyer, R. Wolf, *Z. Naturforsch. B* **2018**, 73, 895–909, “Functionalization of 1,3-Diphosphacyclobutadiene Cobalt Complexes via Si-P Bond Insertion”
- 6) P. Büschelberger, C. Rödl, R. Wolf, *Inorg. Synth.* **2018**, 37, 72–76, “Bis(1,2-dimethoxyethane)potassium bis(1,2,3,4- η^4 -anthracene)cobaltate $[K(dme)_2[Co(\eta^4-C_{14}H_{10})_2]]$ ”
- 7) C. M. Hoidn, C. Rödl, M. L. McCrea-Hendrick, T. Block, R. Pöttgen, A. W. Ehlers, P. Power, R. Wolf, *J. Am. Chem. Soc.* **2018**, 140, 13195–13199, “Synthesis of a Cyclic Co_2Sn_2 Cluster Using a Co^- Synthone”
- 8) C. Rödl, K. Schwedtmann, J. J. Weigand, R. Wolf, *Chem. Eur. J.* **2019**, 25, 6180–6188, “1,3-Diphosphacyclobutene Cobalt Complexes”
- 9) C. Rödl, R. Wolf, *Chem. Eur. J.* **2019**, 25, 8332–8343, “Flexidentate Coordination Behavior and Chemical Non-Innocence of a Bis(1,3-diphosphacyclo-butadiene) Sandwich Anion”

Eidesstattliche Erklärung

Ich erkläre hiermit an Eides statt, dass ich die vorliegende Arbeit ohne unzulässige Hilfe Dritter und ohne Benutzung anderer als der angegebenen Hilfsmittel angefertigt habe; die aus anderen Quellen direkt oder indirekt übernommenen Daten und Konzepte sind unter Angabe des Literaturzitats gekennzeichnet. Die Arbeit wurde bisher weder im In- noch im Ausland in gleicher oder ähnlicher Form einer anderen Prüfungsbehörde vorgelegt.

Christian Rödl

